universität wien

DISSERTATION

A detailed abundance analysis of early-type stars in open clusters: constraints to diffusion models

Luca Fossati

angestrebter akademischer Grad
Doktor der Naturwissenschaften (Dr.rer.nat)

Wien, im April 2009

Studienkennzahl lt. Studienblatt:	A 091 413
Dissertationsgebiet lt. Studienblatt:	Astronomie
Betreuer:	Prof.Dr. Werner W. Weiss

Declaration

Part of the material present in this thesis is taken from the following publications:

Bagnulo, S., Landstreet, J. D., Mason, E., Andretta, V., Silaj, J., Wade, G. A. 2006, A&A, 450, 777 - Fig. 1.1

Fossati, L., Bagnulo, S., Monier, R., Khan, S. A., Kochukhov, O., Landstreet, J.,Wade, G. & Weiss, W. 2007, A&A, 476, 911 - part of text, tables and figures

Fossati, L., Bagnulo, S., Monier, R., Khan, S. A., Kochukhov, O., Landstreet, J.,Wade, G. & Weiss, W. 2008, Contributions of the Astronomical Observatory Skalnate Pleso, 38, 2, 123 - part of text, tables and figures

Fossati, L., Bagnulo, S., Landstreet, J, Wade, G., Kochukhov, O., Monier, R., Weiss, W., Gebran, M. 2008, A&A, 483, 891 - part of text, tables and figures

Fossati, L., Ryabchikova, T., Bagnulo, S., Alecian, E., Grunhut, J., Kochukhov, O., Wade, G. 2009, A&A, in press - part of the text and two figures

Kharchenko, N. V., Piskunov, A. E., Röser, S., Schilbach, E., Scholz, R.-D. 2005, A&A, 438, 1163 - Fig. 4.1

In Appendix A there are the copyright permissions to reproduce text, figures and tables present in the papers above.

In Appendix B there is a copy of these papers ,if already published, of which I am the first author. Here there is also a description of the work I performed for each of these papers.

Zusammenfassung

Die Untersuchung der Atmosphäre von "early-type" Sternen spielt eine bedeutende Rolle in der stellaren Astrophysik. Die Atmosphären solcher Sterne zeigen eine Vielfalt verschiedener Phänomene wie etwa die Anwesenheit starker Magnetfelder, ausgeprägte Oberflächenkonvektion, Pulsation sowie Diffusion chemischer Elemente. Um die tiefere Bedeutung dieser Phänomene vollständig zu verstehen ist es notwendig Bedingungen aus den Beobachtungen abzuleiten und vor allem eine grosse Anzahl von Sternen unterschiedlichen Alters und Typs zu untersuchen.

Sterne offener Haufen sind aus zwei Gründen besonders interessant: 1) Man kann annehmen, dass alle Mitglieder eines Haufens in etwa ähnliches Alter und chemische Zusammensetzung haben. 2) Das Alter von Sternen offener Haufen ist wesentlich genauer bestimmbar als jenes von Feldsternen.

Unter Verwendung modernster Instrumente (inkl. FLAMES der ESO VLT) erhielt ich hochqualitative Spektren einer grossen Anzahl altersmässig gleichverteilter "early-type" Sterne in zehn offenen Haufen. Hier präsentiere ich die Resultate für die Sterne zweier Haufen (NGC 5460 und Praesepe). Untersucht wurde der Zusammenhang zwischen der Elementenhäufigkeit und den Sternparametern im Hinblick auf Bedingungen an das Diffusionsmodell. Die Bestimmung der Parameter und der LTE Elementenhäufigkeit erfolgte mittels eines neuen Modells für Atmosphäre und Synthese welches verschiedene spektroskopische Parameter einbezieht. Die Schwankungen der Elementenhäufigkeiten wurden dabei exakt berücksichtigt.

Die Stichprobe besteht aus 54 chemisch unauffälligen "early-type" Sternen, drei heissen He-armen Sternen und neun Am Sternen. Der wesentliche neue Beitrag meiner Arbeit ist die Erkenntnis, dass die Elementenhäufigkeit bestimmter Elemente zwischen 7000 K und 10500 K mit der Temperatur zunimmt und zwischen 10500 K und 13000 K wieder abnimmt. Für chemisch unauffällige Sterne wurde kein Zusammenhang zwischen Elementenhäufigkeit und $\upsilon \sin i$ gefunden. Hingegen fand ich eine starke Korrelation zwischen der chemischen Ausprägung von Am Sternen und $\upsilon \sin i$, nämlich dahingehend, dass diese Ausprägung mit zunehmendem $\upsilon \sin i$ abnahm.

Abstract

In stellar astrophysics, the study of the atmospheres of early-type stars plays a very special role. The atmospheres of these stars display a variety of different phenomena, such as the presence of large magnetic fields, strong surface convection, pulsation, diffusion of chemical elements. To fully understand the actual role of all these physical phenomena, it is important to seek constraints from the observations, in particular to perform a detailed study of a large number of stars of different ages and peculiarity types.

Open cluster stars are particularly interesting for two reasons: 1) it is possible to assume that all cluster members have approximately the same original chemical composition and age; 2) the age of stars belonging to open clusters can be determined with much higher accuracy than for field stars.

Using advanced available instrumentation (including FLAMES of the ESO VLT) I obtained high-quality spectra of a large number of early-type stars in ten open clusters, uniformly distributed in age. Here I present the results obtained for the stars observed in two clusters (NGC 5460 and Praesepe), searching for correlations between abundances and stellar parameters and to provide constraints to the models of diffusion theory.

Parameter determination and LTE abundance analysis were performed with new generation model atmosphere and synthesis codes, taking into account different spectroscopic parameter indicators. A rigorous treatment of the abundance uncertainties was performed.

The sample is composed of 54 chemically normal early-type stars, three hot He-weak stars and nine Am stars. The original main contribution of this work is the finding that the abundance of several elements increases with temperature between 7000 K and 10500 K and decreases from 10500 K to 13000 K. No correlation between abundance and $\upsilon \sin i$ was found for chemically normal stars, while I found a strong correlation between the peculiarity of Am stars and $\upsilon \sin i$, in particular that chemical peculiarity decreases with $\upsilon \sin i$.

Contents

Chapter 1

Introduction

In stellar astrophysics, the study of the atmospheres of A- and B-type stars plays a very special role. The atmospheres of these stars display a variety of different phenomena, such as the presence of large and relatively simple magnetic fields, strong surface convection, pulsation, diffusion of chemical elements, and various kinds of mixing processes from small-scale turbulence to global circulation currents. These general physical processes are almost certainly active in the atmospheres (and interiors) of stars other than the main sequence A- and B-type stars, but in more subtle ways. Because of the easily visible effects found in A- and B-type stars, these stars provide a unique access to the invisible interior processes. To fully understand the actual role of all these physical phenomena, it is very important to seek constraints from the observations, in particular to perform a detailed study of a large number of stars of different ages and peculiarity types.

The variety of phenomena present in A- and B-type stars is shown also by the large amount of different stellar typologies present in this region of the main sequence, such as: *i*) ApBp displaying a wide range of chemical peculiarities and an organised magnetic field. *ii*) HgMn stars that present large overabundances of Hg and possibly of Mn. *iii*) AmFm stars that display underabundances of C, N, O, Ca, Sc and overabundances of Fe-peak and rare-earths elements (see Preston 1974, for a better characterisation of these three types of chemically peculiar stars). *iv*) roAp stars that display all the peculiarities of Ap stars together with the presence of a rapid oscillation of the order of ten minutes (Kochukhov 2008). *v*) Pulsating Am stars that display pulsation together with the characteristic abundance pattern of Am stars (Kurtz 1989). *vi*) λ Boo stars for which the abundance pattern is characterised by strong underabundances of elements heavier than oxygen (Kamp et al. 2008). *vii*) Be stars that exhibit or exhibited emission lines in the photospheric spectrum (Zorec 2004). *viii*) δ Sct stars that display luminosity variations up to one magnitude with a typical period of few hours (Breger 2000). *ix*) γ Dor stars displaying non-radial pulsation with a period of the order of one day (Balona et al. 1994). *x*) γ Dor-δ Sct hybrids that present pulsational signals typical of both γ Dor and δ Sct stars (Handler & Shobbrook 2002; Handler et al. 2002).

The chemical peculiarities of both the peculiar and the normal A- and late B-type stars certainly reveal the action of a number of hydrodynamic processes occurring inside the stars. The details of most of these processes, and how they interact with one another, are far from clear, although some reasonably successful semi-empirical models are being produced (e.g. Richer et al. 2000; Talon et al. 2006). These processes are almost certainly operating in the atmospheres of all stars, but due to competing effects are difficult or impossible to detect and study. Therefore it is important to study the atmospheres of A- and B-type stars in order to understand this general physics. Observations can support the necessary theoretical work by providing information about how the symptoms of these processes (chemical anomalies, slow rotation, etc.) appear on individual stars, and how these symptoms depend on stellar mass and age. Because of the easily visible effects found in A- and B-type stars, these stars provide a unique access to the invisible interior processes.

In recent years, also the so-called normal early-type stars started to receive attention, and detailed abundance determinations have been performed for a few tens of them. An example is the whole series of papers based on the analysis of spectra obtained at the Dominon Astrophysical Observatory (DAO) and led by Saul Adelman[1]. Another example is Erspamer & North (2003), who analysed a large sample of spectra of F- and A-type stars present in the archive of the ELODIE spectrograph[2].

This project is intended to study, for the first time, the correlation between the element abundances of early-type stars and the stellar evolution state. Up to now there are not such studies, besides few analysis of small samples of early-type stars in open clusters, of which Varenne & Monier (1999) was probably the precursor. Other analysis of cluster early-type stars were for example performed by Stütz et al. (2006) and Folsom et al. (2007), but the sample of studied stars was always quite small and the analysis of several cluster stars was never performed, up to now, in a consistent way.

For this project, it is very interesting to study stars that are cluster members, rather then selecting targets in the field, because of two very compelling reasons. First, it is possible to assume that all cluster members have approximately the same original chemical composition and age. Therefore, when the analysis of chemical abundances of stars belonging to the same cluster is performed, it is possible to assume that the studied objects are different only by their initial mass, rotational velocity, magnetic field strength and binarity. Second, the age of stars belonging to open clusters can be determined with much higher accuracy then for objects in the field, especially for stars that are young enough that less then half of their life on the main sequence has elapsed. Figure 1.1, taken from Bagnulo et al. (2006),

[1] Adelman (1988), Adelman (1991a), Adelman et al. (1991b), Pintado & Adelman (1993), Adelman (1994), Adelman (1996), Ryabchikova et al. (1996), Adelman et al. (1997), Caliskan & Adelman (1997), Adelman (1998), Adelman et al. (1998), Adelman & Albayrak (1998), Adelman (1999), Adelman et al. (2000), Adelman et al. (2001), Caliskan et al. (2002) and Kocer et al. (2003)

[2] http://atlas.obs-hp.fr/elodie/

shows why this occurs. The left panel shows the position of four stars on the

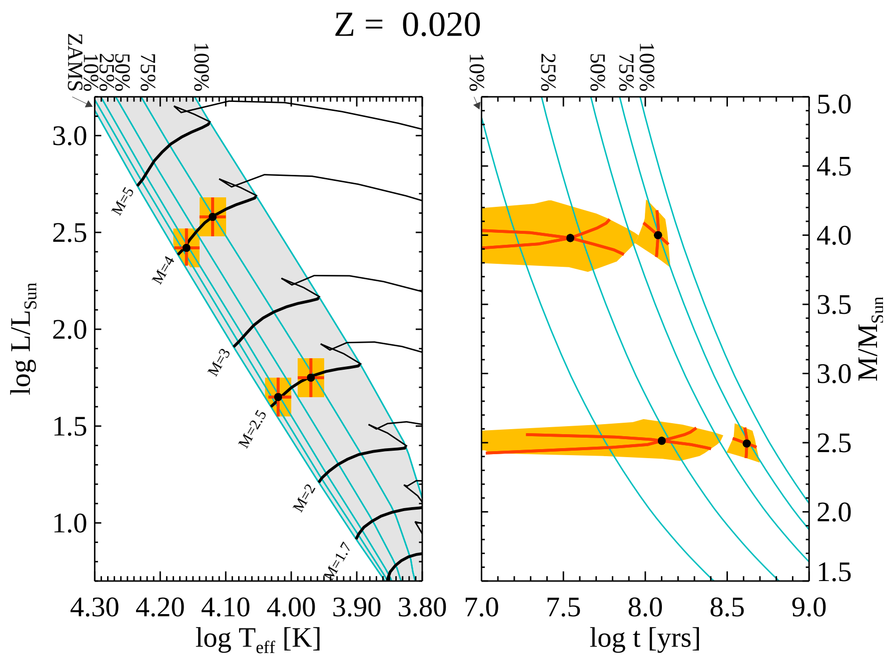

Figure 1.1: Left panel: position of four stars, with uncertainties on $T_{\rm eff}$ and $\log L/L_\odot$ of 5% and 0.1 dex respectively, in the Hertzsprung-Russell diagram. Right panel: position of the same four stars in an age-mass diagram. The transformation uses evolution tracks for Z = 0.020 from Schaller et al. (1992). This Figure is taken from Bagnulo et al. (2006).

Hertzsprung-Russell diagram, while the right panel shows the position of the same four stars on an age-mass diagram, assuming an uncertainty of 5% on $T_{\rm eff}$ and of 0.1 dex on $\log L/L_\odot$. The transformation uses evolutionary tracks with Z = 0.020 from Schaller et al. (1992). Figure 1.1 clearly shows that when transforming the typical uncertainties on $T_{\rm eff}$ and $\log L/L_\odot$ on the age-mass diagram, the uncertainty on the age determination is smaller for stars that has already elapsed at least half of their main sequence lifetime.

The work presented in this thesis makes part of a bigger project for which two large observational campaigns were carried out with FORS1 at the ESO/VLT and with ESPaDOnS at the Canada-France-Hawaii Telescope (CHFT). The survey consists of polarimetric observations of magnetic A- and B-type stars in open clusters, to search for links between magnetic fields and stellar evolution. These stars present a large variety of chemical peculiarities such as large overabundances of Cr, Sr and Eu, of Si, etc. The project intends as well to study the evolution of the chemical peculiarities of magnetic A- and B-type stars. The results of the campaign concerning the measurement of magnetic fields in chemically peculiar cluster A- and B-type stars are presented in Bagnulo et al. (2006); Landstreet et al. (2007, 2008).

Another part of the bigger project consists of a multicolor photometrical survey of magnetic A- and B-type stars in open clusters to obtain high precision light curves to determine stellar rotational periods. This part of the project will allow to search for correlations between rotational period, amplitude of the light curve and magnetic field strength, as well as to check whether angular momentum loss still occurs during the main sequence phase.

In the framework of these observational campaigns, high-resolution spectroscopy of a large number of early-type stars in about ten open clusters of different ages was obtained. The clusters are approximately uniformly distributed in logarithmic age from $\log t = 6.8$ to $\log t = 8.9$, and the spectra have been obtained using five different spectrographs: FLAMES the multi-object spectrograph at the ESO/VLT, FIES the high resolution spectrograph at the Nordic Optical Telescope (NOT), ELODIE and SOPHIE the mid and high resolution spectrographs at the Observatoire de Haute-Provence (OHP) and ESPaDOnS the high resolution spectropolarimeter at the CFHT. All these instruments, except FIES, is described in Chapter 2. Table 1.1 shows the clusters selected and observed for this project, the indication of the instrument adopted to observe them, their age and distance modulus.

Table 1.1: Open clusters observed for the survey. The second and third columns give the distance modulus, in magnitudes, and age of the cluster, in $\log t$. The last column shows which instrument (and telescope) were adopted to obtain the spectra of the stars.

Cluster	Distance Modulus [mag]	$\log t$ [dex]	Instrument
NGC 6193	11.8	6.8	FLAMES (VLT)
NGC 6383	10.9	6.9	FLAMES (VLT)
NGC 6250	10.8	7.4	FLAMES (VLT)
IC 4665	8.3	7.6	FIES (NOT)
NGC 6405	8.9	8.0	FLAMES (VLT)
NGC 3114	10.0	8.1	FLAMES (VLT)
NGC 5460	9.4	8.2	FLAMES (VLT)
NGC 7092	7.6	8.4	FIES (NOT)
NGC 6633	8.4	8.6	FLAMES (VLT)
M 44 / Praesepe	6.4	8.9	SOPHIE & ELODIE (OHP) ESPaDOnS (CFHT)

Figure 1.2 shows the distance modulus as a function of the logarithmic age for all the clusters present in the WEBDA database (Mermilliod & Paunzen 2003). This plot illustrates why the use of observations with a large telescope, such as the ESO/VLT, were necessary. With the use of small and mid-size telescopes it would have been impossible to obtain high signal to noise ratio (SNR) spectra for a large

number of stars (mainly for the younger open clusters) within a reasonable amount of telescope time.

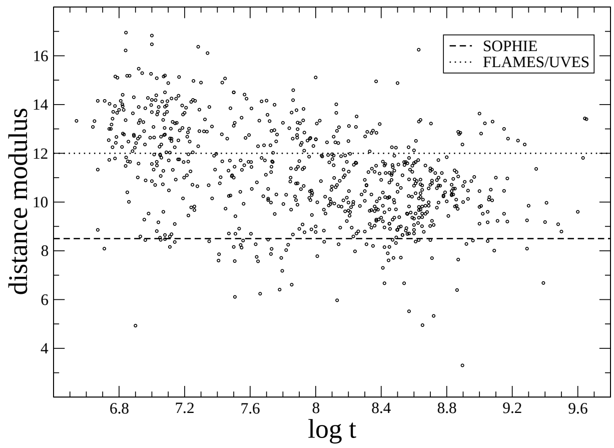

Figure 1.2: Cluster distance modulus as a function of logarithmic age for all the open clusters present in the WEBDA database (Mermilliod & Paunzen 2003). The dotted and dashed lines correspond to the magnitude limit that it is possible to reach with FLAMES/UVES and SOPHIE respectively, assuming a SNR of 200 and 30 minutes of exposure time.

The spectra collected for this project have a quality, in terms of SNR and resolution, similar to the one presented by other authors that studied chemical abundances of early-type stars. The big advantage of the sample of stars presented here is its extension and the fact that for each star the age is well determined. As a matter of fact, I am here looking for very small effects, smaller then the uncertainties associated with the derived abundances, even for chemically normal slowly rotating stars analysed with very high quality spectra (see Fossati et al. 2009b). For this reason it was necessary to obtain an extremely large sample of stars and to analyse them in a consistent way. The methodology followed to perform the fundamental parameter determination and the abundance analysis is described in Chapter 3.

The project described above will give several important results concerning different topics. It will allow to better constrain open cluster parameters (such as age and metallicity) and membership of cluster stars. Due to the very large sample, this survey will allow to address the distribution of angular velocities in stars of various masses along the main sequence, important to investigate the distribution and evolution of angular momentum among the objects in which the transition between radiative and convective envelopes occurs (such data exist for only a very few bright open clusters). Within the collected sample of observed open clusters there are some very young objects in which there are several pre-main sequence stars (including pulsating pre-main sequence stars), for which important information on the fundamental parameters and chemical composition will be extracted.

In this thesis (Chapters 4 and 5) I present the results obtained for the stars observed in NGC 5460 and in the Praesepe cluster. This thesis is concentrated on the analysis of the obtained abundances in the context of diffusion, looking for correlations between the abundances of the chemical elements and other stellar parameters, such as the effective temperature (T_{eff}) and the projected rotational velocity ($\upsilon \sin i$).

NGC 5460 is an intermediate age open cluster ($\log t = 8.20 \pm 0.20$, Ahumada & Lapasset 2007) that includes a large number of early-type stars, covering a large range in stellar mass. NGC 5460, observed with FLAMES at the ESO/VLT, gives the possibility to test the quality of the observations performed with this instrument. NGC 5460 is also an almost completely unknown open cluster on the spectroscopic point of view, except for few polarimetric observations Bagnulo et al. (2006). This allows to discover much more of this open cluster, not only on the point of view of the cluster parameters (such as the metallicity that was previously unknown), but also on the single objects in the cluster field of view. NGC 5460 contains also three chemically peculiar stars (He-weak stars) that are here spectroscopically analysed for the first time.

Praesepe (M 44, NGC 2632), a nearby intermediate age open cluster ($\log t = 8.85 \pm 0.15$, González-García et al. 2006), is an especially interesting target because it includes a large number of A-type stars, among which are many Am stars. Furthermore, because of the cluster is relatively close to the sun (d = 180 ± 10 pc, Robichon et al. 1999), many of the member A-type stars are bright enough to allow to obtain high resolution spectra with intermediate class telescopes. As mentioned, this cluster is particularly interesting for the very large number of cluster member Am stars. In particular, Praesepe is probably the know open cluster containing the largest number of Am stars. This allows for the first time to characterise this type of stellar peculiarity on a statistically relevant and consistent sample giving an important contribution to the development of diffusion models.

In conclusion the aim of the project is to give fundamental observational constraints to the modelling of diffusion processes present in the envelopes of early-type stars.

1.1 Target selection

The target selection performed for this thesis is divided essentially into two parts: the selection of the clusters and the selection of the cluster stars.

The cluster selection was based on an age, visibility and ”interest” criteria. For the project it was necessary to have clusters more or less uniformly distributed in age. It was of course necessary that the clusters were visible at the time and place from where observations were performed. What I have here called ”interest” criterium consists in the fact that the open clusters were chosen taking into account also the number of ”interesting” objects (such as chemically peculiar stars) in the cluster. Although this thesis is mainly based on a consistent analysis of chemically normal stars, the observational interest on clusters containing magnetic stars clearly appears considering the whole project behind this thesis. High resolution spectroscopy of magnetic stars, analysed in Bagnulo et al. (2006), Landstreet et al. (2007) and Landstreet et al. (2008) is extremely valuable for the prosecution of the project.

In the past, the spectroscopic analysis of a large amount of cluster stars was not possible due to the difficulty given by the determination of the cluster membership. Recently, several catalogs of memberships in open cluster stars were published, thanks also to the data provided by space missions such as HIPPARCOS and TYCHO. These catalogs provided the necessary information to be able to determine with an acceptable accuracy the cluster membership of a large number of stars in a cluster's field of view.

The first step of the target selection of cluster stars was to recognise the most probable cluster member chemically peculiar stars (Am, Ap, HgMn stars) in a way to assign them the highest priority. A high priority was assigned also to stars known as slow rotators (typically $\upsilon \sin i < 50\ \mathrm{km\,s^{-1}}$) since there are good chances that also these objects display chemical peculiarity (if not, they would provide anyway high precision abundances for several elements). For this purpose I designed a standard procedure followed to select the stars to observe and to assign their priority.

The first step of the procedure consists in identifying the most probable cluster members by checking the membership probabilities given by several authors. For this operation, the most useful works to check are: Robichon et al. (1999) and Baumgardt et al. (2000) based on HIPPARCOS data, Kharchenko et al. (2004) and Dias et al. (2006). In particular I considered as probable members of the cluster every star with a kinematic and photometric membership probability higher than 0.14 (Kharchenko, private communication) in the case of the Kharchenko et al. (2004) catalogue, or a membership probability higher than 10% for the Dias et al. (2006) catalogue. For some clusters there are publications of photometric data where stellar memberships are assigned, but not always these information are accessible in electronic form, so that sometimes there was not the possibility to carefully check all of them.

There is a catalog that deserves a special place in the description of the target selection. The catalog recently published by van Leeuwen (2007) provides probably the best kinematic membership probabilities ever published for a number of cluster stars. van Leeuwen (2007) shows the results of a new reduction of the HIPPARCOS data performed with a much better understanding of the satellite movements. The outcome is that the uncertainties of the HIPPARCOS data here published are very much reduced. Unfortunately the catalog became available only after that most of the target selection was performed.

I searched then for information about the spectral type, magnitude, colors, $\upsilon \sin i$, binarity, variability, chemical peculiarities, magnetic field and radial velocity for each star considered a probable member of the cluster. I collected information from SIMBAD[3] (scanning also the different references mentioned therein), VIZIER[4] (using a combination of several keywords – binaries: cataclysmic, binaries: eclipsing, binaries: spectroscopic, multiple_ stars, open_ clusters, positional_ data, proper_ motions, rotational_ velocities, spectral_ classification, spectrophotometry, spectroscopy, stars: early-type, stars: late-type, stars: peculiar, stars: variable – in a range of 10 arcsec around the position of each star) and the WEBDA[5] database (Mermilliod & Paunzen 2003). The WEBDA database is also particularly useful for the presence of tasks that allow to plot the color-magnitude and color-color diagram of the available clusters, so that it is possible to make a further check of the adopted stellar memberships. I looked also for additional information about each star in articles by Glebocki & Stawikowski (2000) and Royer et al. (2002a,b, 2007) for $\upsilon \sin i$ measurements, Rodríguez et al. (2000) for δSct pulsations, the SB9 catalogue (Pourbaix et al. 2004) for information about a possible binarity and Renson et al. (1991) for chemical peculiarities.

The mentioned publications and catalogs deserve further comments. I have found them probably to be up to now the best and more complete data source in their field, but some of them do not cover very large sky regions. The tools of the Virtual Observatory (VO) are very useful to show the cover of the sky given by each catalog. The SB9 catalog provides a very good example. It is probably the most complete and easily accessible existing catalog on spectroscopic binaries (SB), but it covers only very small and selected regions of the sky, as shown in Fig. 1.3. Each dot, visible in Fig. 1.3, displays the position of a spectroscopic binary present in the SB9 catalog. There are clearly huge regions of the sky where there are no information at all even about the presence or not of SB stars.

Other catalogs such as Glebocki & Stawikowski (2000) (Fig. 1.4, upper panel) and Royer et al. (2002a,b, 2007) (Fig. 1.4 lower panel) cover the sky in a much more complete way.

I searched then for high resolution spectra in several archives (e.g. the ESO archive[6] and the ELODIE archive[7]), in order to avoid a duplication of observational effort, in case some stars had already been observed with high resolution spectroscopy. The presence of archives of stellar spectra, only recently available, gave an important contribution in the collection of the large sample of observed cluster stars here presented. A clear example of this contribution is given by the ELODIE archive that provided the spectra of four of the eight Am stars analysed in the Praesepe cluster.

Of the sample of stars obtained with this procedure for a given cluster, I kept only the stars with spectral types between early F5 (to avoid too long an exposure time on a single object) and B5 (to avoid strong stellar winds), giving a higher rank to peculiar stars and slow rotators. From the sample I removed stars already known

[3]`http://simbad.u-strasbg.fr/simbad/sim-fid`
[4]`http://vizier.u-strasbg.fr/viz-bin/VizieR`
[5]`http://www.univie.ac.at/webda/`
[6]`http://archive.eso.org/`
[7]`http://atlas.obs-hp.fr/elodie/`

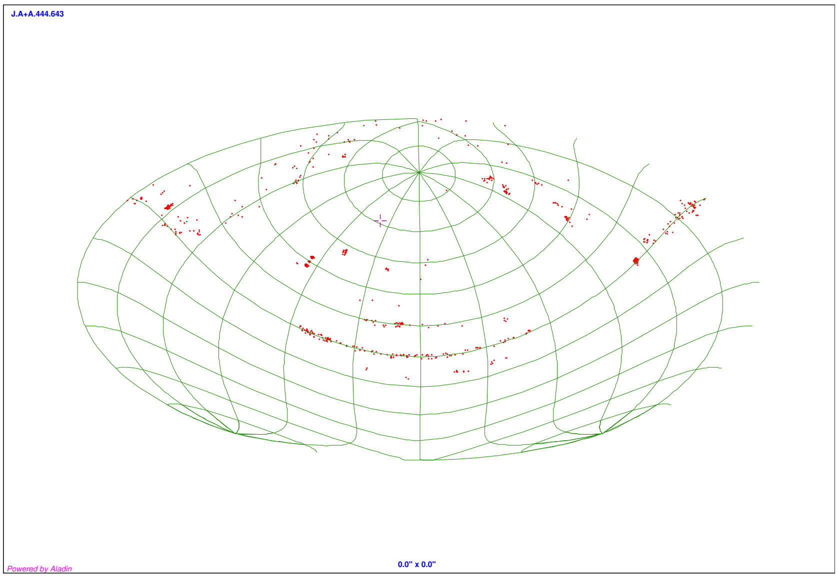

Figure 1.3: Position in the sky of the objects cataloged in the SB9 catalog. The dots show the position of the spectroscopic binary stars. The pole visible at the top of the plot is the north celestial pole.

to be SB2 (double line spectroscopic binary) systems, unless they had already been extensively observed using high resolution spectroscopy. In the list of target stars I included also some G-type star to be able to recover the cluster original metallicity. This kind of stars have a rather deep convective zone and are not too faint to obtain enough signal to noise ratio for an abundance analysis.

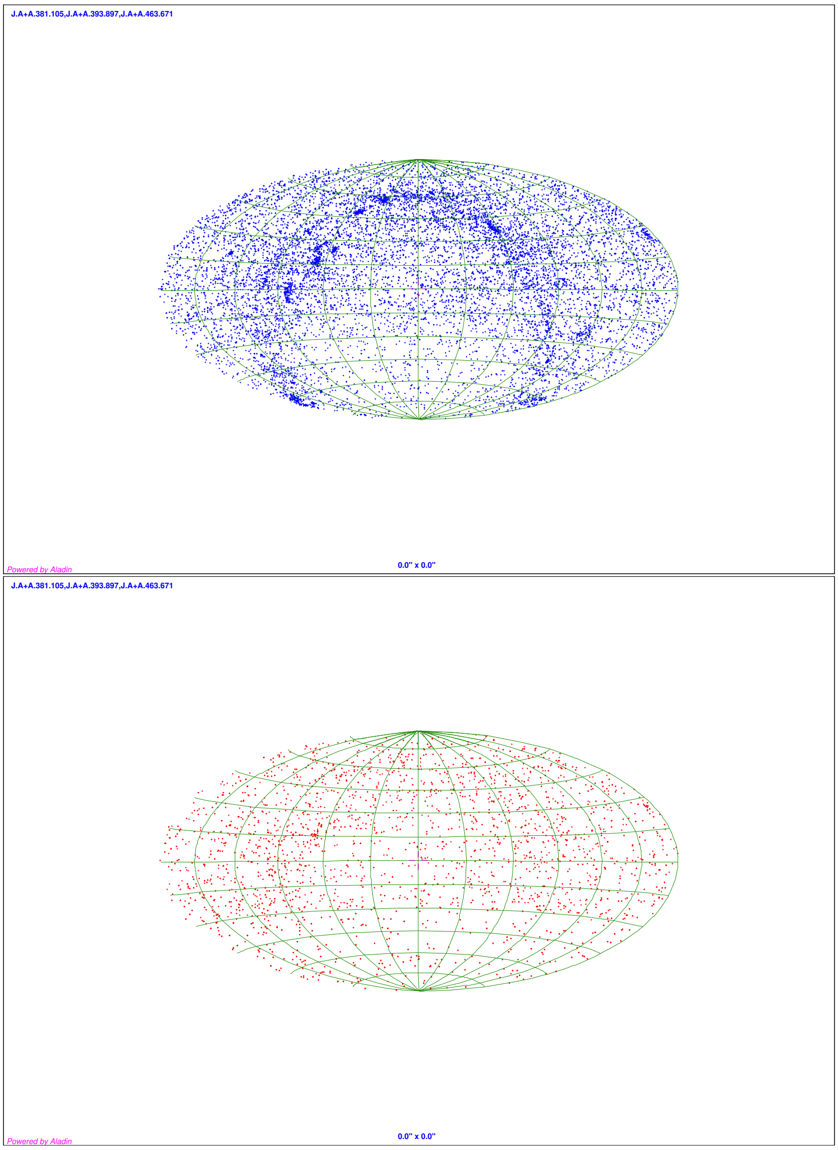

Figure 1.4: Position in the sky of the objects cataloged in Glebocki & Stawikowski (2000) (upper panel) and Royer et al. (2002a,b, 2007) (lower panel). Each dot correspond to the position of a star for which there is a cataloged $\upsilon \sin i$ measurement.

Chapter 2

Instruments, telescopes and data reduction

This thesis is based on observations obtained with four different instruments: FLAMES at the European Southern Observatory (ESO/VLT), ESPaDOnS at the Canada-France-Hawaii Telescope (CFHT), ELODIE and SOPHIE at the Observatoire de Haute Provence (OHP).

The choice of the instruments was crucial since it was necessary at the same time high resolution (for the few slowly rotating stars) and high signal to noise ratio, together with high efficiency and large wavelength coverage when possible. This was necessary because I had to derive abundances for as many elements as possible for each star, considering that the adopted methodology requires large amount of measured spectral lines. At same time I had to observe a large number of stars in a reasonable amount of telescope time. Almost all the adopted instruments fulfill all these conditions.

Here I aim to describe the instruments and telescopes employed for the observations of the cluster stars, together with the applied data reduction. The normalisation procedure will be then described in Sect. 3. At the end of the chapter I will show a comparison among some of the instruments, employing spectra of a "reference" star (HD 73666 belonging to the Praesepe cluster). This star was already used as a comparison star by Ryabchikova et al. (2008). At last I show a comparison of the exposure times necessary to reach a signal to noise ratio (SNR) per pixel of 200 with each adopted instrument, given a certain stellar magnitude, instrument settings and airmass.

2.1 FLAMES@ESO VLT

FLAMES is the multi-object low, intermediate and high resolution spectrograph that is mounted at UT2 telescope of the ESO/VLT and can access targets over a large field of view of 25 arcmin of diameter. UT2 at the ESO/VLT is one of the four 8.2 m telescopes at Cerro Paranal in Chile. Each telescope provides two

Nasmyth and one Cassegrain focus station.

FLAMES consists of three main components:

1. A Fiber Positioner (OzPoz) composed by two plates: while the observation is performed with one plate, the other one is set up for the subsequent observation. In this way the dead time between two observations is limited to less than 15 minutes, including the telescope preset and the field acquisition.

2. A low, medium and high resolution optical spectrograph, FLAMES/GIRAFFE, with three types of feeding fiber systems: MEDUSA (stellar objects), IFU and ARGUS (extended objects). In this work I have used only MEDUSA fibers.

3. The UVES high resolution spectrograph (Red Arm) fed via 8 single fibers.

Thanks to a special observing software (FLAMES OS) it is possible to acquire simultaneously and independently FLAMES/GIRAFFE and FLAMES/UVES observations. FLAMES is mounted at the Nasmyth A platform of UT2, while UVES at the Nasmyth B platform, on the other side of the telescope relative to the A platform.

Together with Dr. S. Bagnulo, PI of the proposal with title ”Observing the chemical evolution of early-type stars in open clusters” we obtained 14 hours of telescope time with FLAMES at the ESO/VLT to carry out in service mode observations of early-type stars in seven open clusters.

2.1.1 MEDUSA and the fiber positioner system

MEDUSA is one of the three fiber systems (the other two IFU and ARGUS are used for integral field spectroscopy) that feeds FLAMES/GIRAFFE and FLAMES/UVES and the only one available for stellar objects. MEDUSA fibers can observe simultaneously up to 132 separate objects. The core of the system is the fiber positioner system (OzPoz) that is equipped with four plates, but only two are currently used. These plates are metallic disks on which the magnetic buttons, holding the fibers, are attached. The curvature of each plate is of 3950 mm to match the curvature of the corrector of the focal plane. In this way all fibers can receive the full telescope beam, apart from their position on the plate. The plates are hold by a trolley that is able to rotate, to exchange the plates, and to approach or retract the Nasmyth focus of the telescope.

Each fiber is connected to a retractor that maintains the fiber in constant traction. The parking position of the fibers is just outside the plate. A number is assigned to each fiber to be able to distinguish them. Each even-numbered fiber is a MEDUSA fiber, while each odd-numbered fiber is an IFU fiber (ARGUS fibers are parked at the center of the plate).

OzPoz (the fiber positioner) is also equipped with a calibration box hosting an optical system which redirects the light both from a W lamp and from a Th-Ar lamp, and from a Ne lamp into a fiber, to obtain a wavelength calibrations both for FLAMES/GIRAFFE and FLAMES/UVES. For FLAMES/GIRAFFE there are four additional fibers for the calibration lamp, while for FLAMES/UVES one of the eight fibers has to be kept for the wavelength calibration.

For combined observations, the exposure times for FLAMES/UVES and FLAMES/GIRAFFE do not need to be the same. This allows to increase considerably the SNR of the spectra of the stars observed with FLAMES/GIRAFFE (the total exposure time is controlled by FLAMES/UVES, since it is the instrument that requires more time to obtain the necessary SNR). FLAMES/GIRAFFE does not provide both large wavelength coverage and high resolution, but has an exceptional efficiency that allows to obtain high quality spectra for very faint stars within few seconds of exposure time. It is anyway not possible to observe simultaneously in two FLAMES/GIRAFFE modes, or to observe the same target simultaneously with the two spectrographs (FLAMES/GIRAFFE and FLAMES/UVES). For this reason the target selection and the observing strategy, especially for the observations carried out with FLAMES, were real crucial procedures.

Four particular magnetic buttons are equipped with a system of 19 coherent fibers each. This set of fibers is used to obtain images of four "fiducial" or "reference" stars (FACB). These stars are continuously observed during the whole observation and their images are recorded on a technical CCD. A separate computer computes the centroids and calculates the proper offsets to be applied to the telescope to keep the fiducial stars in the center of the bundle of fibers. These four stars represent the link between the sky and the plate coordinates, for this reason it is essential that these objects are very carefully chosen. They have to be sufficiently isolated, bright (R <15 mag) and with a low proper motion. Due to the low dynamical range of the technical CCD, the magnitude of the four FACB stars should lay within a range of 3 mag. For obvious reasons it is very important to have accurate coordinates for all the observed stars and in particular of the four FACB stars. I used the UCAC2 catalogue (Zacharias et al. 2004) as coordinate source, as also suggested in the FLAMES user manual[1].

The Fiber Positioning System Software (FPOSS) controls the fiber crossing during each movement to their final position on the plate and determines also the button movement sequence configuration to the next one. This is an important part of MEDUSA since more than four fibers cannot cross in the same place, as well as no fibers can pass too close to other buttons. All these rules are implemented in the FPOSS that, given a certain observing sample of stars, creates the best observing configuration of the fibers. It tries to maximise the number of observed stars, giving the possibility to set priorities to each star (in my case, the ones that should be observed with the FLAMES/UVES fibers had a higher priority as well as slowly rotating stars).

Figure 2.1 shows the plate configuration for the observation of NGC 5460. The FACB stars are identified by the green fibers, while the red and gray fibers cor-

[1]http://www.eso.org/sci/facilities/paranal/instruments/flames/doc/

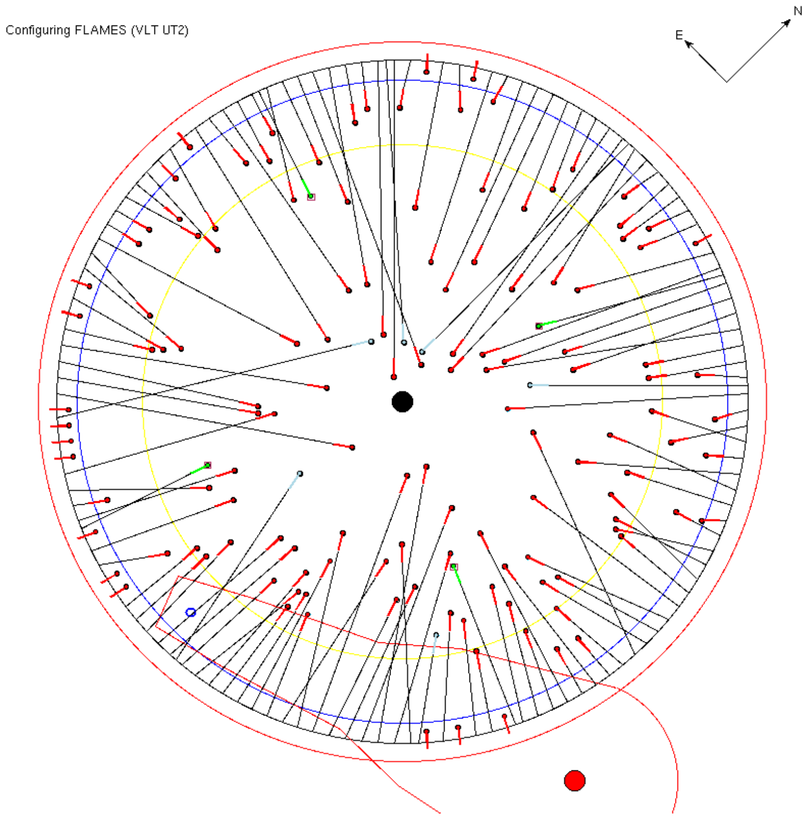

Figure 2.1: Configuration of the plate for the observation of NGC 5460. See the text for a description of symbols and colors.

respond to the fibers that feed FLAMES/GIRAFFE and FLAMES/UVES respectively. The black spot in the center identifies the hole where the fibers of ARGUS lay. All the observable objects must lay inside the blue ring. FPOSS requires as input file the coordinates of the center of the plate and of each star, together with their magnitudes and observational priority. The small blue circle is connected with the red structure visible at the bottom of the figure. It consists of an arm that lays over the plate and is locked on a further reference star. No star that lays behind this arm can be observed.

Differential atmospheric effects

An important problem that cannot be neglected when performing multi-object spectroscopy in a large field, is the atmosphere differential refraction. This is a differential effect in the sense that the atmospheric refraction index, and hence the direction of propagation of the light from a given star, changes with the wavelength and the distance from the zenith. There are two important consequences for astronomical observations:

- A chromatic effect where the refraction index changes with wavelength. The red and the blue part of the spectrum do not hit the fiber at the same position, therefore part of the stellar spectrum can fall outside the entrance of the fiber. This effect is actually important only when observing over a wide spectral range, especially in the blue.

- An achromatic effect where the refraction index at a given wavelength changes with the zenith distance in a non-linear way. This is very important when observing large fields, because stars in different positions can have significantly different distances from the zenith so that they do not move in a coherent way across the sky during the exposure time, making it impossible to guide on the whole field.

The achromatic effect (dependent on the zenith distance) cannot be compensated, since it has a differential character across the field and it is strongly dependent on the zenith distance. It was therefore extremely important to be aware of its amplitude with different observing conditions, in order to plan the observations in the correct way. The problem, when observing a large field of view, is that an object placed at the corner of the field will have a zenith distance (z') different from the one at the center of the field (z). In this way the observed position of the stars placed at the field corner will show a displacement respect to their "real" position, by a different quantity. The size of this difference is then proportional to tan(z)-tan(z'), varying non-linearly with the distance of the whole field from the zenith. Since the telescope is guided with respect to the center of the field, this effect leads to distortions at the field corners, that are time dependent, since the observed field moves across the sky. The maximum size of this effect can be of few arcsec in the blue on the field of view of FLAMES since due to the dependence of the refraction index upon wavelength, the effect would be significantly smaller in the red.

The central wavelength of each observation is given as input of the acquisition template, to allow the telescope to guide at the same wavelength. Due to the chromatic effect, different spectral regions will be displaced with respect to the central one and for large displacements they could fall outside the entrance of the fiber. Figure 2.2 illustrates this displacement between a central wavelength at 4000 Å and four other wavelengths for a typical FLAMES/GIRAFFE spectrum, covering a wavelength range of 600 Å (Figure taken form the FLAMES user manual).

The FLAMES Fiber Positioner Software is able to calculate the mean position of each object during the exposure, based on the coordinates of the field and the time of the observation. Extremely rapid airmass variations could cause a dramatic change of the position of an object close to the field edge. This change could be of the order of 2 arcsec in one hour exposure. For this reason, it is important to avoid high airmass observations. The risk is that some or the whole stellar flux goes lost due to the fact that objects placed far from the center of the field could move away

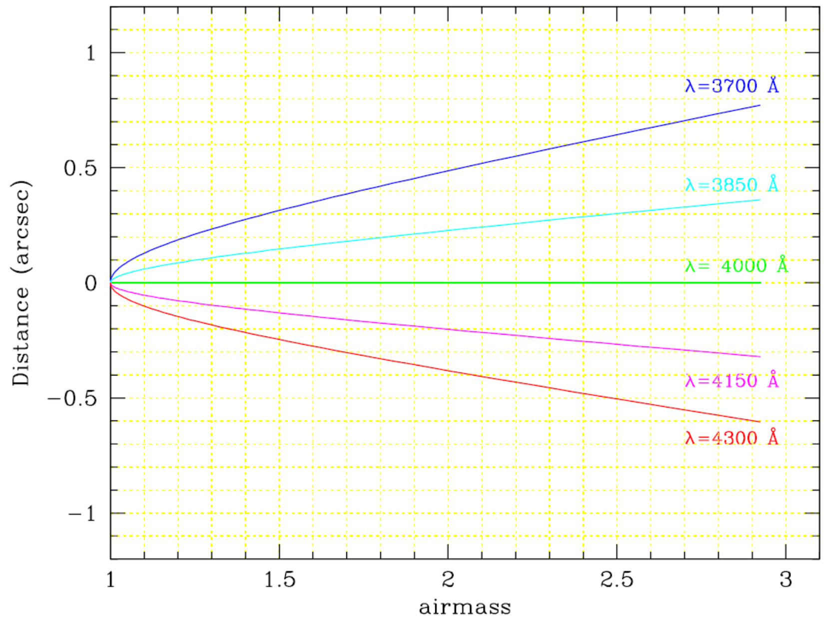

Figure 2.2: Relative displacement between the central wavelength at 4000 Å and nearby wavelengths covered by typical FLAMES/GIRAFFE gratings (FLAMES user manual).

from the position of their fiber during long exposures. For this reason I decided to divide each exposure into three or four subexposures.

At the time when I prepared the observing blocks for FLAMES no detailed description of the differential atmospheric effects was available in the FLAMES user manual. For this reason I used the results obtained for the Keck Observatory, taking roughly into account the difference in altitude above the sea level of about 2000 m between Cerro Paranal and Mauna Kea.

FLAMES/UVES and in particular FLMANES/GIRAFFE allow to chose among a large number of settings. This gave the possibility to chose the best wavelength regions to observe, but paying always attention to the presence of the chromatic and achromatic atmospheric effects. For example, observations of both Hα and Hβ would be extremely valuable for a solid determination of the fundamental parameters, but some stellar flux could be lost if observations are performed with a high airmass. A detailed description of the selection of the settings and of the adopted observation strategy for FLAMES is given in Sect. 4.1.

2.1.2 FLAMES/GIRAFFE

FLAMES/GIRAFFE is a low and medium resolution (R=7500–30000) spectrograph in the visible range 3700–9000 Å and it is suited for observations of single and extended objects in regions of the sky with a high stellar density such as open and globular clusters and clusters of galaxies.

FLAMES/GIRAFFE uses filters to select the required spectral range and each object is observed in a single echelle order at once. The light, coming from one of the 6 available slits, passes through the order sorting filter, to be then reflected into a double pass collimator (the light passes though the collimator again after being dispersed). Afterwords the light goes to the gratings (high or low resolution) and finally to the CCD. The list of available filters, gratings and correlated resolutions for FLAMES/GIRAFFE and FLAMES/UVES is given in Table 2.1. For a given filter and grating, the spectral resolution is very uniform along the CCD.

FLAMES/GIRAFFE is equipped with an EEV CCD with an exceptionally good quantum efficiency in the blue and UV domain. It is not possible to change the CCD readout characteristics, such as windowing, variable readout speed and binning. The CCD saturates at about 60000 ADU.

FLAMES/GIRAFFE has an online pipeline that automatically reduces the acquired spectra. The online reduction pipelines performs a very high quality data reduction so that no further manual reduction was necessary.

2.1.3 FLAMES/UVES

UVES is the high resolution spectrograph of the ESO/VLT and is able to work both in long slit mode and in fiber mode on its Red Arm. FLAMES employs the fiber mode of UVES. The fibers are injected just before the slit through a projector, which changes the F/3 fiber exit to the F/10 UVES aperture of the long slit mode.

Each positioner plate has 8 fibers connected to the Red Arm of UVES. The resolving power of the spectrograph in fiber mode is R=47 000. As shown in Table 2.1 only three standard UVES setups are offered, with central wavelengths of 5200 Å, 5800 Å and 8600 Å. In addition to the 8 fibers per plate, an extra fiber is available for the simultaneous wavelength calibration. Due to the large UVES interorder separation, only 7 fibers can be devoted to astronomical objects when the simultaneous calibration fiber is used. With certain settings, as the one I adopted, it is required that one or two fibers are devoted to record the sky contribution.

The detector placed in the red arm consists of a mosaic of one EEV (CCD 44-82) and one MIT-LL (CCID-20) 4kx2k CCD; this optimises the detector response as a function of wavelength, reducing the fringing at far-red wavelengths. The gap between the two CCDs is 0.96 mm implying the loss of one spectral order (~5170-5230 Å). This gap and the non-perfect alignment of the two chips require a separate extraction of the spectra recorded on each of the two chips. The CCD control system reads the mosaic as a single image with 100 artificial pixels between the two CCDs so that the file has to be split before reduction. As for the CCD of FLAMES/GIRAFFE, windowing or binning of the two CCDs is not allowed. The saturation of the EEV and MIT-LL CCDs is about 65000 and 40000 ADU, respectively. The efficiency of the RED arm of UVES in fiber mode is about 40% lower than UVES in long slit mode for observations of a single point source. It is however rather difficult to accurately predict the real differences between the two modes because they will be function both of the seeing and of how accurate the fiber centering has been performed.

FLAMES/UVES has a reduction pipeline that automatically reduces the acquired spectra. Unfortunately the data I obtained from the pipeline were of very low quality. What probably happened during the automatic reduction was that the pipeline lost the tracing of the spectral orders, generating only noise spectra. For this reason I performed a manual reduction of the spectra with the MIDAS tools provided by ESO. The manual reduction revealed the origin of the problem at the stage of the application of the order definition frame. The only difference between the online pipeline and the manual one was the setting of the P5 parameter for the FMSTA/FLAMES task. This parameter sets the rotation of the CCDs around a fixed reference point. The original setting is P5=0,0, while the best order definition is obtained with P5=12,-33. It could probably happened that the UVES red arm CCDs were unmounted for technical reasons and then remounted with a different angle that was then not recovered in the online reduction pipeline.

In spite of the very high pressure to obtain telescope time at the ESO/VLT, in particular at UT2[2], within 14 hours of awarded telescope time FLAMES allowed to collect very high quality spectra of about 1400 stars. The available database contains probably the largest amount of photons ever collected for early-type stars in open clusters.

2.2 ESPaDOnS@CFHT

ESPaDOnS is a high resolution echelle spectrograph and spectropolarimeter of the CFHT that is fiber fed from a Cassegrain module that includes calibration, guiding facilities and an optional polarisation analyser. The instrument is able to obtain a spectrum of the optical region 3700–10500 Å with a single exposure with resolving power of R=68 000 up to R=81 000, dependent on the adopted setting. The efficiency provided by the fiber link is of about 40–45%. ESPaDOnS is mounted at the 3.6 m telescope of the CFHT, located at the summit of Mauna Kea, on the island of Hawaii, USA.

The polarimeter includes one quarter-wave and two half-wave Fresnel rhombs coupled to a Wollaston prism, providing a very achromatic polarisation analysis of the stellar light.

The instrument provides three different configurations: a spectropolarimetric mode, a first spectroscopic mode called "object+sky" and a second spectroscopic mode called "object only". In spectropolarimetric mode both ordinary and extraordinary beams are recorded and all four Stokes parameters (I, V, Q and U) are obtained along the whole wavelength range with a mean resolving power of about R=68 000. In first spectroscopic mode both the stellar and the sky spectra are ob-

[2]This is due to the presence, at the time of the submitted proposal, of three very much requested instruments mounted at the same telescope: FORS1, UVES and FLAMES.

tained with a mean resolution of R=68 000, while in second spectroscopic mode only the star is observed giving the possibility to reach a resolution of R=81 000. To switch between two observing modes takes about 10–15 minutes, including the refocusing of the spectrograph.

The CCD is an EEV with a size of 2kx4.5k square pixel with the possibility of four different readout speeds, usually not offered by other instruments. This gives the possibility to perfectly tune the readout mode on the brightness of the observed object. The CCD saturates at about 65000 ADU for each readout speed but the fastest, for which the saturation is reached at 58000 ADU. Unfortunately, if illuminated with infrared light, the CCD shows severe fringing, but this effect is well reproduced by the flat fields, giving in this way the possibility to remove it during the reduction process. The only left signature of fringing is a variation of the error bars of the reduced spectrum up to 25%.

In polarimetric mode, to minimise errors due to waveplates imperfections and to minimise the crosstalk between circular and linear polarisation (Bagnulo et al. 2009), observations are carried out in series of four subexposures, each taken with a different waveplate configuration. The polarisation signal is then obtained by processing the complete series of four subexposures, while the unpolarised signal by processing separately each of the subexposures.

ESPaDOnS spectra are reduced automatically by the available reduction pipeline called Libre-ESpRIT and described in detail in Donati et al. (1997). The reduction pipeline is not openly available and can be used only at the CFHT observatory or under agreement of the author. When observations are carried out in spectropolarimetric mode (as done for the stars observed for this work) Libre-ESpRIT gives two files as output: a ".out" file containing the spectra and a ".s" file containing the log produced by the reduction pipeline. The file containing the spectra presents six columns: wavelength in nanometers, normalised intensity, normalised Stokes V, error bars associated to intensity and Stokes V, and N spectrum. The normalisation of the intensity spectrum is not optimal and cannot be used for an abundance analysis. A definition of the N spectrum together with its meaning can be found in Bagnulo et al. (2009). The file containing the log of the reduction procedure contains important information like the number and place of the rejected pixels for each order and the χ^2 relative to the fit of the wavelength calibration. At the very end of this file other important information are present such as the coordinates of the observed object, total exposure time, heliocentric correction and the SNR at the center of each order in a bin of 2 pixels.

ESPaDOnS provides both a larger wavelength coverage in the red (very important because it is the only region where for example lithium and nitrogen lines are visible in early-type stars), the polarimetric mode and a high resolution. All these benefits are strengthened by a high efficiency, as shown in Table 2.2. Together with FLAMES, ESPaDOnS represents probably the prototype of the perfect instrument for this project, but both are very much requested by the community.

2.3 ELODIE & SOPHIE@OHP

2.3.1 ELODIE

ELODIE is a cross-dispersed echelle spectrograph fed by a pair of optical fibers from the Cassegrain focus of the 1.93 m telescope at OHP. This instrument was decommissioned in mid-August 2006. One fiber was used for the starlight, while the other one for the sky background or the wavelength calibration lamp, but there was also the possibility to mask it. The spectra (67 spectral orders) cover the optical wavelength range 3850–6800 Å with a spectral resolution of about R=42 000. Only this configuration of the instrument was available.

At the Cassegrain adapter two lamps were mounted, a Tungsten lamp for flat fields and a Thorium lamp for the wavelength calibration. The instrument was designed for high precision radial velocity measurements and it was able to reach precisions up to 6 $\mathrm{m\,s^{-1}}$, with simultaneous observation of the Thorium calibration lamp.

The CCD was a thinned, back-illuminated, anti-reflection coated Tektronix 1kx1k square pixel with a saturation level at about 64000 ADU.

The spectra were automatically reduced by an online pipeline able to perform a localisation of all orders on the frame, optimal order extraction, cosmic-ray rejection and wavelength calibration. After the automatic reduction of the spectra there was the possibility to continue with the determination of the radial velocity by numerical cross-correlation with the use of different available masks, adapted for several stellar spectral types.

All the spectra obtained with the ELODIE spectrograph can be retrieved from the ELODIE archive: `http://atlas.obs-hp.fr/elodie/`.

If ELODIE would have been still mounted at the OHP, probably it would have not been selected for observations for this project, mainly because the observed stars are rather faint for the efficiency of the instrument, leading to rather long exposures. The ELODIE archive gave/gives the possibility to increase the number of available spectra without any extra-observing time, but some of the spectra did not have an optimal quality.

2.3.2 SOPHIE

The successor of ELODIE at the 1.93 m telescope at the OHP is SOPHIE, a cross-dispersed echelle spectrograph that had first light on August 2006. The spectrograph is fed from the Cassegrain focus through one of two separate optical fiber sets, yielding two different spectral resolutions called high efficiency (HE) and high resolution (HR) mode. The spectra cover the optical wavelength range 3870–6940 Å.

The spectrograph is fed by two pairs of optical fibers, each of 100 micron of diameter. Within one pair, one fiber (fiber A) is normally used for the target, while the other one (fiber B) can be used for the sky spectrum or for a simultaneous observation of the Thorium wavelength calibration lamp. One pair of fibers is used for the high resolution mode leading to a spectral resolution of R=75 000, the other one for the high efficiency mode with a spectral resolution of R=40 000.

The difference between the HE and the HR modes is a factor of 2.5 (1 magnitude), for this reason the HE mode is particularly useful for low magnitude objects. Switching between the two modes involves moving the fiber heads in the adapter, which takes about 3 minutes plus the observation of a complete set of calibrations (bias, flat fields, wavelength calibration lamp) since the reduction pipeline takes as input the last observed set.

The gain in efficiency with SOPHIE in the V band has been determined to be about 3 magnitudes in HE mode relative to the previous ELODIE spectrograph and consequently of 2 magnitudes in HR mode. These values where obtained comparing SNR values for the same object, wavelength and spectral bin with the two spectrographs. Another gain was reached in the accuracy of the radial velocity measurements that is about 50 cms^{-1} in HR mode.

The CCD is a thinned, back-illuminated, anti-reflection coated E2V44-82 chip with 4096x2048 pixels. The chip can be read out using three different settings: fast, medium and slow. For fast and medium readout mode the saturation is reached at 177000 ADU, while in slow readout mode at 44560 ADU.

The data reduction is performed automatically after each exposure and the pipeline takes automatically as calibrations the last obtained set. The pipeline was adapted from the one of the HARPS spectrograph placed at ESO/LaSilla and performs localisation of the orders on the frame, optimal order extraction, cosmic-ray rejection and wavelength calibration. The obtained spectrum for each order is stored in a multidimensional fits file. The orders are then reconnected after correction for the blaze function (derived from the flat field), yielding a one dimensional fits file, which includes the barycentric correction.

I was PI of an accepted proposal with title ”Chemical composition of A-type stars in the Praesepe cluster: a clue to their evolutionary status” that brought to the observation of 15 A- and F-type stars member of the Praesepe cluster and 7 field δ Sct stars in 4 nights, 1.5 of them lost for bad weather and technical problems. I personally carried out the observations. SOPHIE has a much higher efficiency compared to ELODIE making this instrument suitable for the project, with the bonus to be more easily accessible since it is not far from Vienna.

2.4 Comparison of characteristics and performances of the different instruments

Since this work is based on spectra obtained with different instruments, it was important to compare them to be able to assure that the obtained results are not instrument dependent. For a future employment of one of these instruments, for a work similar to the one here presented, it is useful to compare their performances and to know which of them can be operated in service mode. In this way, it will result easier to chose the instrument to be employed.

Figure 2.3 shows the comparison among the spectra of HD 73666 obtained with ESPaDOnS, ELODIE and SOPHIE. No significant differences are visible apart the ones due to the spectral resolution. I was not able to find FLAMES/UVES spectra of this star because it was never observed with it.

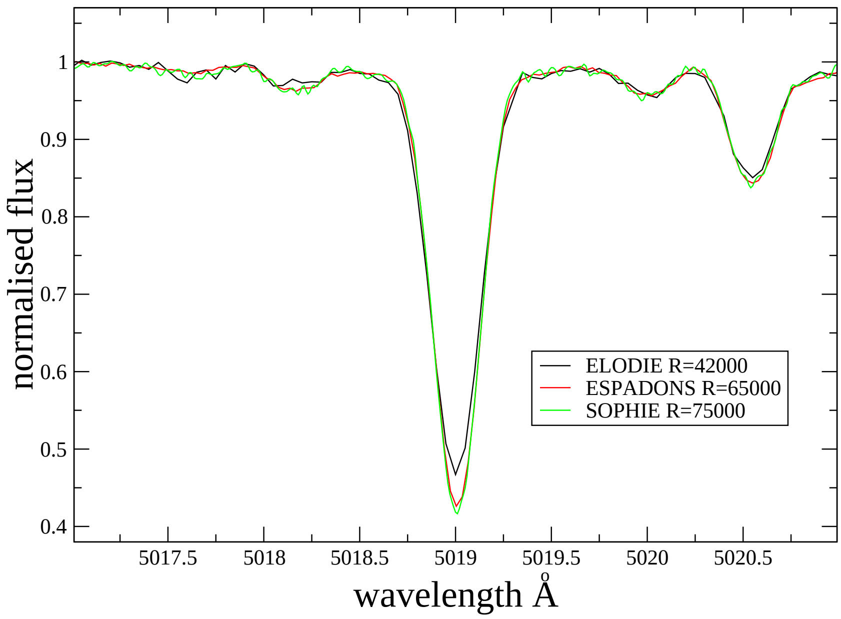

Figure 2.3: Comparison between the spectra of HD 73666 obtained with ELODIE@OHP, black line - R=42 000), ESPaDOnS (red line - R=65 000) and SOPHIE (green line - R=75 000).

The good agreement among the spectra obtained with these different instruments allows to compare results obtained with them for different stars. Possible undetected differences could be due to small disagreements with the wavelength calibration and with an undetected straylight. The disagreements in wavelength calibration should not be anyway larger than the typical error bar given for the radial velocity (the majority of the analysed stars are fast rotators - $\upsilon \sin i \geq 50\,\mathrm{km\,s^{-1}}$ - for which the $\sigma_{\upsilon_\mathrm{r}}$ is larger than $2\,\mathrm{km\,s^{-1}}$). Straylight is generally negligible for all the described spectrographs. As a check of a possible wavelength dependent (dependent on the position on the CCD) straylight, for each star, I have always looked for any clear correlation between the obtained line abundance and wavelength for a certain element/ion, without having found any.

Table 2.2 shows the comparison of the exposure time required to reach a SNR per pixel of 200 at ~5000 Å for each of the instrument described above. The values given in Table 2.2 do not take into account the difference in pixel size among each instrument.

Table 2.2 shows clearly the low efficiency of the ELODIE spectrograph. I have to mention here that this instrument was anyway not designed to reach high SNR, but to reach high precision radial velocity measurements with the use of a cross-correlation technique, that does not require high SNR.

Another important issue to take into account when choosing the instrument to employ for a certain kind of observation is the possibility or not to use the instrument in service mode. Without taking into account ELODIE, already decommissioned, all the adopted instruments, but ESPaDOnS, can be operated in service mode. Service mode gives the big opportunity to obtain time resolved spectra or to make use of instruments with high competition (the observations can be performed anytime the possibility is given), such as the ESO/VLT. The big issue of observing in service mode is the planning of the observations, since the exposure times have to be optimal for any kind of sky condition. In other words the exposure time has to be both long enough to be able to obtain the necessary amount of photons and short enough to avoid saturation of the CCD. It is very important to keep this into account mainly when observing with SOPHIE in service mode since the weather is highly unstable and often thin clouds are present. The solution I adopted to set up the observing time for observations in service mode is the following. I calculated the optimal observing time to obtain the requested SNR, with almost the worse weather condition, and then split the given exposure time in several subexposures. The analysed spectrum was then the sum or the median of the single obtained spectra.

Table 2.1: Filters, grisms and spectral resolutions available for FLAMES (GIRAFFE+UVES). $\lambda 1$ and $\lambda 2$ correspond to the starting and ending wavelengths, respecively. The ”B” settings have a lower efficiency than the ”A” settings. The resolution correesponds to the resolution of MEDUSA. In **bold face** the filters and grisms used to for my observations.

Instrument	Filer & Grism p2pp/ETC	$\lambda 1$ [nm]	$\lambda 2$ [nm]	Resolution
FLAMES/GIRAFFE (HR)	H379.0/HR1	370.0	386.7	22 500
	H395.8/HR2	385.4	404.9	19 600
	H412.4/HR3	403.3	420.1	24 800
	H429.7/HR4	418.8	439.2	20 350
	H447.1A/HR5A	434.0	458.7	18 470
	H447.1B/HR5B	437.6	455.2	26 000
	H465.6/HR6	453.8	475.9	20 350
	H484.5A/HR7A	470.0	497.4	18 529
	H484.5B/HR7B	474.2	493.2	26 700
	H504.8/HR8	491.7	516.3	20 000
	H525.8A/HR9A	509.5	540.4	17 750
	H525.8B/HR9B	514.3	535.6	25 900
	H548.8/HR10	533.9	561.9	19 800
	H572.8/HR11	559.7	584.0	24 200
	H599.3/HR12	582.1	614.6	18 700
	H627.3/HR13	612.0	640.5	22 500
	H651.5A/HR14A	630.8	670.1	17 740
	H651.5B/HR14B	638.3	662.6	28 800
	H665.0/HR15N	647.0	679.0	17 000
	H679.7/HR15	660.7	696.5	19 300
	H710.5/HR16	693.7	725.0	23 900
	H737.0A/HR17A	712.9	758.7	17 425
	H737.0B/HR17B	722.5	749.0	30 200
	H769.1/HR18	746.8	788.9	18 400
	H805.3A/HR19A	774.5	833.5	13 867
	H805.3B/HR19B	785.6	822.5	22 200
	H836.6A/HR20A	807.3	863.2	16 036
	H836.6B/HR20B	819.5	850.9	28 600
	H875.7/HR21	848.4	900.1	16 200
	H920.5A/HR22A	881.6	956.5	11 642
	H920.5B/HR22B	896.0	941.9	19 000
FLAMES/GIRAFFE (LR)	L385.7/LR1	362.0	408.1	12 800
	L427.2/LR2	396.4	456.7	10 200
	L479.7/LR3	450.1	507.8	12 000
	L543.1/LR4	501.5	583.1	9 600
	L614.2/LR5	574.1	652.4	11 800
	L682.2/LR6	643.8	718.4	13 700
	L773.4/LR7	710.2	834.3	8 900
	L881.7/LR8	820.6	940.0	10 400
FLAMES/UVES	**SHP700-520**	414.0	621.0	47 000
	SHP700-580	476.0	684.0	47 000
	OG590-860	660.0	1060.0	47 000

Table 2.2: Comparison of the exposure time needed for each described insturment to reach a SNR per pixel of 200 at about 5000 Å. The exposure times are calculated with the exposure time calculator available for each intrument, for a A0 star of 7th magnitude in V band. An airmass of 1.6 and a seeing of 0.8 arcsec was taken into account. For GIRAFFE the exposure time is calculated with no fiber displacement. These values do not take into account the difference in pixel size among each instrument.

Instrument	Setting	SNR	Exp.time (Sec)
GIRAFFE	HR 525.8B	200	30
GIRAFFE	LR 479.7	200	6.6
UVES	580	200	60
ESPaDOnS	polarimetric mode	200	100
ELODIE		200	3600
SOPHIE	high efficiency	200	600

Chapter 3

Abundance analysis

In this chapter I aim to describe the way in which the continuum normalisation and the abundance analysis were performed. I decided to put these two topics together because nowadays several reduction pipelines (such as Libre-ESpRIT for ESPaDOnS) perform already a continuum normalisation, but usually not enough precise for an abundance analysis. For this reason the continuum normalisation belongs more to the spectral analysis than to the spectra reduction. In this chapter, I describe in detail certain tools adopted to manage and visualise spectra because there is no literature on them, while I provide the references for all the other tools that were already previously described by other authors.

3.1 Continuum normalisation

The continuum normalisation was performed with an IDL tool (called ”dvd2”) developed and maintained by Dr. O. Kochukhov. The layout of this tool is shown in Fig. 3.1. It provides all the facilities given also by the widely used *continuum* task of iraf, but with the advantage of a much better visualisation of the spectrum, leading to a general more precise continuum setting.

The adopted tool gives the possibility to select between a polynomial and a spline for the continuum description. When the polynomial function is selected it is possible to change the polynomial order, while for the spline the smoothing parameter. In general it is better to use low order polynomials as well as rather high smoothing parameters (around 10^4-10^5), but this is strongly dependent on the instrument and on the performed spectral reduction.

Both polynomial and spline continuum fitting make the following sequence of operations:

- fitting through the spectrum of a smooth line (polynomial of a given degree or spline of a given smoothing parameter);

- computation of the standard deviation of the fit;

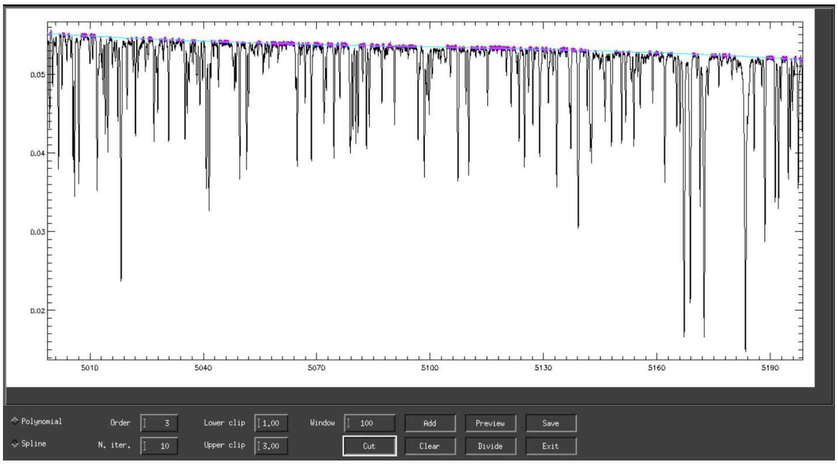

Figure 3.1: Layout of the dvd2 normalisation tool. The bright blue line shows the fitting line, the black line the spectrum and the violet dots correspond to the rejected spectral points. The colors were here inverted for visualisation reasons.

- rejection of the points above and below the clipping thresholds.

This three-steps sequence constitutes one iteration. Since the upper and lower clipping thresholds are asymmetric (by default 3 sigma upper and 1 sigma lower clipping), more points lying below the fitting line are rejected. In this way, an increase of the number of iterations will move gradually upwards the fitting line. This gives the possibility, together with a tuning of the lower and upper clip, to set the best possible continuum with a rather high precision.

The parameter in Fig. 3.1 indicated as ”Window”, if below 100, gives the possibility to horizonthaly zoom the spectrum and watch it with a scrolling bar that automatically appears. There is also the ”Cut” option that allows to remove portions of spectra from the fitting. The removed spectral ranges will not be normalised and saved in the output. It is important to remember that to save the normalised spectrum it is necessary to click first the ”Divide” button and then the ”Save” button, otherwise the code will save the unnormalised spectrum.

Since most of the reduction pipelines provide spectra with unmerged single echelle orders, I always normalised each order separately. The next step was to cut the high noise inter-order overlapping regions and merge the orders to get the whole normalised spectrum. For the normalisation of the hydrogen lines of stars between spectral type F and B this method cannot usually be applied since the lines are broader than the wavelength range of one echelle order (in the case that the center of the hydrogen line lays in the center of the spectral order). In this case I first merged the unnormalised orders containing the hydrogen lines, normalising then the merged spectrum. This operation was not performed in general for all spectral regions because it is much more time consuming. This is because there are often systematic vertical shifts between two adjacent orders that have to be manually removed. The continuum normalisation of the single orders removes automatically all these systematic shifts.

In the case of SOPHIE spectra, the output of the reduction pipeline is a single spectrum, since the orders are already merged by the pipeline (see Fig. 1 of Fossati et al. 2008b) and for this reason the continuum normalisation was performed in a slightly different way. I divided the whole spectrum in ranges of about 300–400 Å long, with a small overlap among them. I then normalised each of these section and merged them.

The normalisation of the hydrogen lines deserves further discussion since it is of crucial importance for the fundamental parameters determination. The continuum normalisation of hydrogen lines should be performed fitting a very low order polynomial (between 1 and 3) between carefully selected continuum points at the outer limits of the hydrogen line wings. The problem usually is the determination of these continuum points. In many cases photometry or even spectral classification give a first idea of the fundamental parameters, in particular of the $T_{\rm eff}$, that can be used to synthesise an hydrogen line profile to check where the synthetic profile moves away from the continuum. These two regions are not changing within a certain temperature range; for example the continuum points will be the same for profiles obtained from models with $T_{\rm eff}$ = 8000 K and $T_{\rm eff}$ = 9000 K. In this way it is possible to know, before the normalisation, where the continuum lays with a good approximation.

3.2 Tools for the visualisation and treatment of spectra

In Vienna two IDL tools for the spectral visualisation and treatment are available. One is called "binmag" and the other one "rotate_MG.csh". Both codes are quite similar in the spectral visualisation, but have different features for the spectral treatment, so that for the abundance analysis of each star both tools were used.

Figure 3.2 and 3.3 show the layout of binmag and rotate_MG.csh respectively, when an observation and a synthetic spectrum are plotted.

For the purposes of this thesis it is not necessary to describe both codes in details so I will mention only the features that make them a kind of "unique" codes.

Binmag was written by Dr. O. Kochukhov and is freely available on his web site: `http://www.astro.uu.se/~oleg/`. As for dvd2, there is the possibility to horizonthaly zoom the spectrum and to scroll it with a bar. The code allows to display at the same time a maximum of two synthetic spectra and one observation. The features that distinguish binmag from the other tool are mainly the possibility to deal with spectroscopic binary stars and the automatic fitting of various parameters, such as $\upsilon_{\rm r}$ and $\upsilon \sin i$. When two synthetic spectra are displayed there is the possibility to introduce the ratio between the radius of the two stars and the code produces the synthetic spectrum of the whole binary system. Of course, $\upsilon_{\rm r}$, $\upsilon \sin i$ and $\upsilon_{\rm macro}$ can be separately set for the two synthetic spectra. The code gives

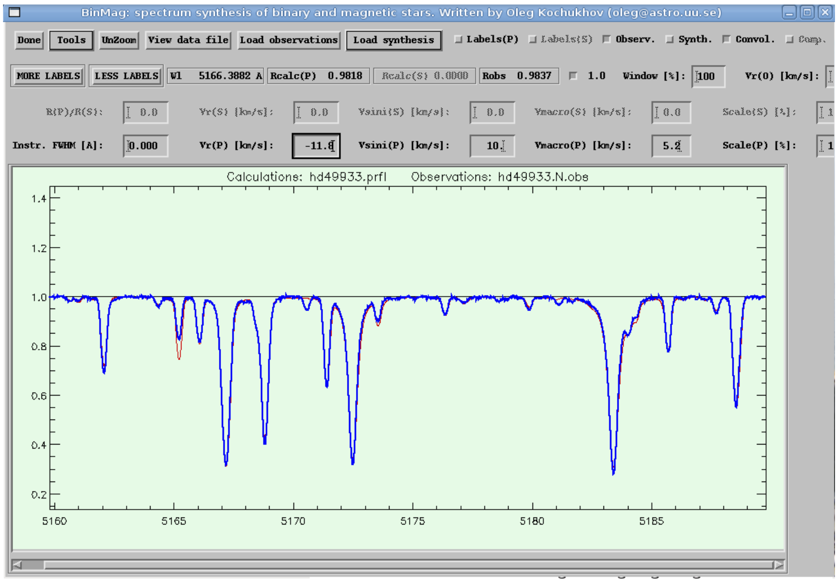

Figure 3.2: Layout of binmag. The blue line corresponds to the observed spectrum, while the red line to the synthetic spectrum.

also the possibility to fit υ_r and $\upsilon \sin i$ at the same time or separately in a selected wavelength region. One of the other main feature is the calculation of equivalent widths with two different methods: direct integration and profile fitting. The direct integration is very useful and precise in case of unblended lines and high SNR spectra. The profile fitting gives the possibility to derive the equivalent width also for lines in simple blends. The fitting of the line profile can be performed both with a Gaussian profile, setting previously the instrumental resolution, or with a Doppler profile, setting previously the $\upsilon \sin i$. The Gaussian profile represents better spectral lines of slowly rotating stars, up to $\upsilon \sin i \sim 10\,\mathrm{km\,s^{-1}}$. The Doppler profile represents better spectral lines of fast rotators. For stars with a $\upsilon \sin i$ between 10 and $20\,\mathrm{km\,s^{-1}}$ both profiles do not perfectly represent the line shape. The Gaussian profile will give a higher equivalent width, while the Doppler profile a lower equivalent width, compared to the one measured with direct integration. The best would be a compromise between the two profiles: a Doppler line core profile with Gaussian wings. This feature is already implemented in the new version of binmag which is still under construction.

Rotate_MG.csh (written by Mag. M. Gruberbauer) is still under construction and aims to put into one code all the features present in the older versions of rotate and in binmag, but the goal is not yet reached. The main feature of this tool is the possibility to load an arbitrary number of observations and synthetic spectra. This characteristic is very useful for example for the determination of fundamental parameters with hydrogen line fitting, since it is performed by comparison of

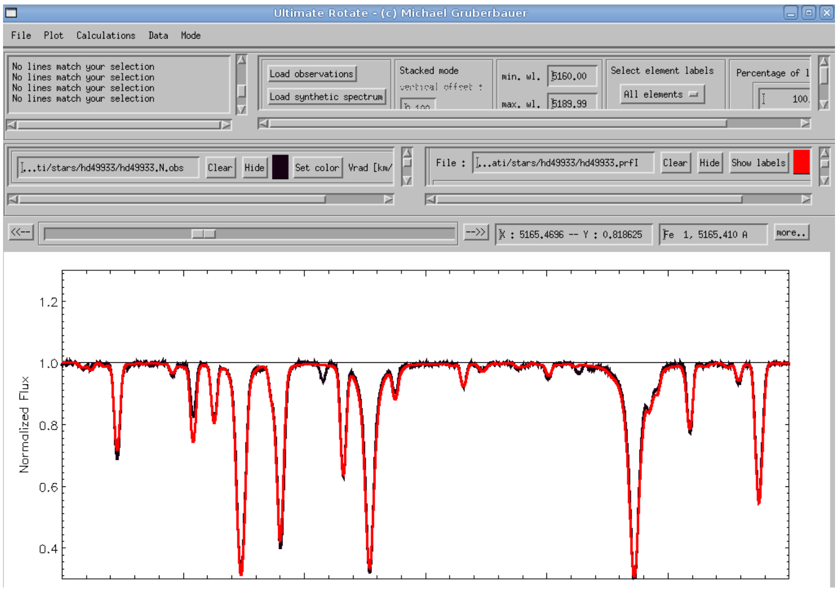

Figure 3.3: Layout of rotate_MG.csh. The black line corresponds to the observed spectrum, while the red line to the synthetic spectrum.

several synthetic profiles with the observation. As for binmag, rotate_MG.csh allows to calculate equivalent widths from a multigaussian fit, but this procedure in rotate_MG.csh, is operationally slightly longer than in binmag. For this reason equivalent widths were always calculated with binmag. Rotate_MG.csh provides also a very nice visualisation of the spectra that does not require an unzoom to switch between two a spectral regions, allowing to scroll always the whole spectrum wherever the zoom was previously made. In rotate_MG.csh there is also the possibility to mark the lines selected for the abundance analysis and to save the line parameters in a file.

3.3 Model atmospheres

The stellar atmosphere is the region of the star that does not have its own energy sources and where spectral lines are formed. Stellar model atmospheres are self-consistent mathematical models of stellar atmospheres containing information about the distribution of the main physical stellar quantities, such as temperature and pressure with a geometric depth, counting from a setted zero-level inside the star up to the stellar surface. Self-consistent means that having a set of free parameters the code provides a unique solution.

For stellar model atmosphere codes the following can be assumed:

- the total amount of radiative energy coming from the inner part of the star is the same anywhere throughout the atmosphere ($div(F_{\rm rad}) = 0$, $F_{\rm rad}$ is the stellar flux);

- plane-parallel geometry ($r_{\rm atm} \ll R_{\rm star}$). All the physical quantities depend only on geometrical depth h;
- homogeneous abundances;
- hydrostatic equilibrium (no large-scale motions);
- the atmosphere is time-independent (statistical equilibrium);
- there are no sources or sinks of energy;
- energy transport takes place only by radiation and convection (no heat conduction, acoustic waves, MHD waves, etc.);
- the free electrons as well as the free heavier particles obey the Maxwell distribution with local kinetic temperature $T_{\rm e}$;
- Local Thermodynamical Equilibrium (LTE) is assumed.

A stellar atmosphere can be treated in LTE when the electron and ion populations follow the thermal Boltzmann distribution:

$$\frac{n_i}{n_j} = \frac{g_i}{g_j} \exp(-\frac{E_j - E_i}{kT}), \tag{3.1}$$

where $\frac{n_i}{n_j}$ represents the ratio of populations in two levels i and j with statistical factors g_i and g_j. In this thesis LTE is assumed for both model atmosphere calculation and abundance determination.

Model atmospheres were calculated with the LTE code LLmodels, which uses direct sampling of the line opacity (Shulyak et al. 2004) and allows the computation of model atmospheres with individualised (not scaled to the solar) abundance patterns. This allows to compute self-consistent model atmospheres that match the actual abundances and to thereby minimise systematic errors (Khan & Shulyak 2007).

LLmodels uses the VALD database (see Sect. 3.4) as a source of spectral line data, including lines that originate from predicted levels. A preselection procedure is applied automatically to eliminate those lines that do not contribute significantly to the line opacity. The preselection is performed on the basis of precomputed ATLAS9 (Kurucz 1993a) model atmospheres with fundamental parameters corresponding to the one of the star to model. The line selection criterion required that the line-to-continuum opacity ratio at the center of each line, at any atmospheric depth, to be greater than 0.05%.

The stellar atmosphere is described by a logarithmic Rosseland optical depth ($\log \tau_{\rm ross}$) spanning from +2 to -6.875 and subdivided into 72 layers. The opacity sampling has a spacing of 0.1 Å.

Convection in general was not particularly important due to the temperature of the analysed stars, but it was always treated according to the Canuto-Mazzitelli (CM) approach (Canuto & Mazzitelli 1992). Figure 3.4 shows the difference of the temperature structure between a model calculated without convection and one with the treatment of convection according to the adopted CM approach, for a star of $T_{\text{eff}} \sim 7700$ K. No visible differences are present in the main line forming

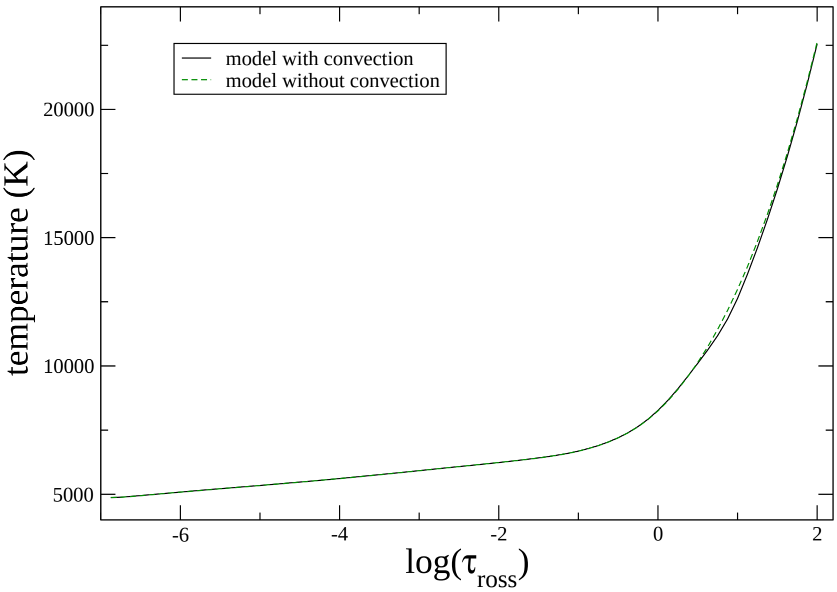

Figure 3.4: The solid line shows the temperature structure of a $T_{\text{eff}} \sim 7700$ K star modeled with the convection treated according to the CM approach, while the dashed line is calculated without any convection treatment.

region, between $\log \tau_{\text{ross}}$ -2 and 0. The analysis of the same object with the two models reveals differences of less than 0.01 dex, clearly within the error bars of the analysis.

I will go back to the importance of using models with individualised abundances later in Sect. 3.5.

3.4 Vienna Atomic Line Database (VALD)

The Vienna Atomic Line Database (VALD) is a collection of atomic line parameters of astrophysical interest and provides tools to select subsets of lines for typical astrophysical applications, such as line identification, chemical composition, radial velocity measurements and model atmosphere calculations. VALD is available online at `http://ams.astro.univie.ac.at/~vald/` or `http://www.astro.uu.se/~vald/` or `http://vald.inasan.ru/~vald/`. The three web sites are completely identical mirror sites.

Four kind of requests are possible: show line, extract all, extract element and extract stellar. *Show line* extracts from the database all the available information about spectral lines of the same species in a small wavelength region. *Extract all* extracts the best atomic parameters for all spectral lines in a given wavelength region. *Extract element* does the same as *extract all*, but for a specific element/ion. *Extract stellar* extracts all spectral lines, with their best parameters, which produce significant absorption in a stellar atmosphere with a given set of fundamental parameters. Since there are several sources for the same parameters, VALD provides the possibility to decide which source to adopt for each extracted parameter, implemented in a configuration file given by default in VALD and that can be changed anytime according to the user's wish. Once the user has created his own configuration file, it is duty of the user to keep track of the changes in the database and update the personal configuration file. All the changes in the database are clearly announced on the main web page. A more detailed description of the database can be found on each of the mentioned web sites or in Piskunov et al. (1995), Kupka et al. (1999) and Ryabchikova et al. (1999).

The presence of a VALD server in Vienna was of great help in dealing with a manual abundance analysis of a large number of stars. The extraction of data from the database was done in few seconds, directly from the source files, without the use of the web interface, and without any restriction in wavelength range. It gave also the possibility to make requests anytime a change in abundance was made (dozens of times for each star) during the analysis of each star, leading to a general decrease of possible small inaccuracies due to an inappropriate line selection caused by the abundance changes.

For the data extraction I always used the most recent and updated configuration file available at that time. Along the three years of work, two major changes in the VALD database occurred. They concerned the data regarding silicon and chromium. For both elements, no difference can be present between the analysis performed before and after the update, since it concerned lines for which the line parameters (in particular wavelengths and $\log gf$ values) were clearly incorrect. As a consequence neither these lines nor lines in their wings were ever used for the abundance analysis before the update.

3.5 Abundance analysis

Here I intend to give a short description of the physics at the basis of the adopted spectrum synthesis code and a detailed explanation of the procedure followed for both parameter determination and abundance analysis.

Passing through the gas of the atmosphere, the radiation is absorbed, re-emitted and scattered many times. The description of these mechanisms defines the way in which the radiation at each frequency is transferred from the bottom of the atmosphere up to the surface. The intensity I_ν is defined as

$[I_\nu] = erg\,cm^{-2}\,s^{-1}\,Hz^{-1}\,sterad^{-1}$:

$$I_\nu = \frac{dE_\nu}{\cos\theta d\sigma d\nu d\omega dt}, \quad (3.2)$$

that can be rewritten as:

$$\mu\frac{dI_\nu}{d\tau_\nu} = I_\nu - S_\nu, \quad (3.3)$$

with $\mu = \cos\theta$. This equation is called radiative transfer equation (RTE). $S_\nu = \frac{\eta_\nu}{\kappa_\nu}$ is called source function, where η_ν denotes the emission and κ_ν the absorption per volume element as a function of the frequency ν, and $d\tau_\nu = -\kappa_\nu\rho ds$ is the optical depth.

On the physical point of view this thesis aims to obtain a solution of the RTE for each of the analysed stars deriving the set of stellar atmospheric parameters and abundances that best fit the observed spectrum.

The formal solution of the RTE is:

$$I_\nu(\mu) = -e^{\tau_\nu/\mu}\int_c^{\tau_\nu} S_\nu e^{-t/\mu}\frac{dt}{\mu}. \quad (3.4)$$

$I_\nu(\mu)$ is the intensity of the radiation emitted outwards from a certain depth defined by the lower limit of the integration (c). Knowing the form of the source function it is possible to solve the RTE, thus to find the solution of the problem.

Often the source function is assumed to be equal to the Plank function:

$$S_\nu = B_\nu(T) = \frac{2h\nu^3}{c^2}\frac{1}{e^{h\nu/kT} - 1}, \quad (3.5)$$

but more generally the source function is assumed to have this form:

$$S_\nu = \frac{\kappa_\nu B_\nu(T) + \sigma_\nu J_\nu}{\kappa_\nu + \sigma_\nu}, \quad (3.6)$$

where σ_ν denotes the scattering and J_ν is called mean intensity and represents the energy emitted by unit of surface area in any direction:

$$J_\nu = \frac{1}{4\pi}\int I_\nu d\omega. \quad (3.7)$$

Without taking into account the scattering the source function in Eq. 3.6 takes the form of the Plank function shown in Eq. 3.5.

From Eq. 3.3 it comes that to solve the RTE it is necessary to know the source function S_ν which also depends on the solution of the RTE itself due to a scattering term $\sigma_\nu J_\nu$ (see Eq. 3.6), but with the use of Eq. 3.3, 3.6 and 3.7 it is then possible to solve the RTE, thus find the solution of our problem.

To describe more in detail the characteristics of the spectral lines it is useful first to separate the source function in the contribution of the continuum (e.g. $\eta_{\nu/C}$) and of the spectral lines (e.g. $\eta_{\nu/L}$). This operation allows to substitute the continuum source function with the Plank function (B_ν) obtaining:

$$\eta_\nu = \eta_{\nu/C} + \eta_{\nu/L}, \qquad \kappa_\nu = \kappa_{\nu/C} + \kappa_{\nu/L}, \tag{3.8}$$

so that

$$S_\nu = \frac{\kappa_{\nu/L}}{\kappa_\nu} S_{\nu/L} + \frac{\kappa_{\nu/C}}{\kappa_\nu} B_\nu. \tag{3.9}$$

Now, being Φ_ν the line absorption profile, Ψ_ν the line emission profile[1], A_{ji} the probability of spontaneous emission (j→i), B_{ij} the absorption coefficient (j→i) and B_{ji} the probability of induced absorption (i→j)[2] it is possible to write the source function that describes spectral lines as follows:

$$S_{\nu/L} = S_\nu = \frac{\eta_\nu}{\kappa_\nu} = \frac{h\nu A_{ji} n_j \Psi_\nu}{h\nu(B_{ij}n_i - B_{ji}n_j)\Phi_\nu}. \tag{3.10}$$

With the use of the basic relations on A_{ji}, B_{ij} and B_{ji}:

$$g_i B_{ij} = g_j B_{ji}, \qquad A_{ji} = \frac{2h\nu^3}{c^2} B_{ji} \tag{3.11}$$

it is possible to rewrite Eq. 3.10 as follows:

$$S_\nu = \frac{2h\nu^3}{c^2} \frac{1}{\frac{n_i g_j}{n_j g_i} - 1} \frac{\Psi_\nu}{\Phi_\nu}. \tag{3.12}$$

We consider now only the line absorption κ_ν that, from Eq 3.10, depends only on the absorption coefficient B_{ij} and on the absorption profile Φ_ν in this way:

$$\kappa_\nu = h\nu B_{ij}(n_i - n_j \frac{g_i}{g_j})\Phi_\nu, \tag{3.13}$$

showing also that the general shape of the absorption profiles does not vary much from line to line.

With the presence of no external effects such as magnetic field, rotation, microturbulence velocity, etc. spectral lines are broadened by thermal Doppler effect (λ_D), radiative damping (γ_{rad}) and collisional damping (Stark effect - γ_{st} and Van der Waals - γ_{vw}). The thermal Doppler broadening is due to the Doppler effect induced by the thermal agitation of the particles and is described as:

$$\lambda_D = \frac{\lambda_L}{c} \sqrt{\frac{2kT}{m_n} + v_{micro}^2} \tag{3.14}$$

[1] Φ_ν and Ψ_ν are normalised as follows: $\int \Phi_\nu d\nu = 1$ and $\int \Psi_\nu d\nu = 1$.

[2] A_{ji}, B_{ij} and B_{ji} are called Einstein coefficients. They describe the probabilities for emission and absorption between an upper atomic level j and a lower atomic level i.

where λ_L is the central wavelength of the spectral line and m_n the mass of the atom or ion. The radiative damping is described as:

$$\gamma_{rad} = \sum_{l<i} \frac{1}{\tau_{il}} + \sum_{l<j} \frac{1}{\tau_{jl}}, \tag{3.15}$$

where the transition takes place between two excited levels i and j with lifetimes τ_i and τ_j respectively, while l is a running index. The Stark effect is due to the collision with other ions and electrons. The line broadening is proportional to the inverse of the square root of the Stark constant (hydrogen and helium) or to $\frac{1}{\gamma_{st}^4}$ (called quadratic Stark effect). The line broadening due to the Van der Waals effect (collisions with neutral atoms) is proportional to $\frac{1}{\gamma_{vw}^6}$. Usually radiative and collisional dampings are combined in one damping constant γ:

$$\gamma = \gamma_{rad} + \gamma_{st} + \gamma_{vw}. \tag{3.16}$$

Assuming the case of a photon absorbed by an atom, the absorption probability depends not only on the energetic difference between the atomic levels (ΔE_{ij}), but also on the velocity and direction of motion of the atoms. The absorption profile around the line center (small $\Delta\nu_D$) can be written as:

$$\Phi(\Delta\nu) = \frac{1}{\sqrt{\pi}\Delta\nu_D} e^{-\frac{\Delta\nu}{\Delta\nu_D}^2} + terms\ of\ higher\ order \tag{3.17}$$

This equation is obtained assuming a Maxwellian velocity distribution, the normalisation of the absorption profile Φ_ν ($\int \Phi_\nu d\nu = 1$), a Voigt function and $a = \frac{\gamma}{\Delta\nu_D} \ll 1$. For the line wings (large $\Delta\nu_D$) the absorption profile is:

$$\Phi(\Delta\nu) = \frac{a\Delta\nu_D}{\pi(\Delta\nu)^2} + ... = \frac{\gamma}{\pi(\Delta\nu)^2} + ... \tag{3.18}$$

On the classical point of view with the equations here shown it is possible to describe absorption line profiles, but the classical equations are not enough since they do not take into account the quantum mechanics that rules the atomic transitions. For this reason the oscillator strength f_{ij}, different for each line, was introduced with this definition:

$$f_{ij} = \frac{m_n h\nu}{\pi e^2} B_{ij}. \tag{3.19}$$

The line absorption (κ_{nu}) is directly proportional to f_{ij}.

The VALD database provides f_{ij}, γ_{rad}, γ_{st} and γ_{vw} almost for each line. In particular f_{ij} is given for every line, while all three damping constants are not always present in the database for each line. When this occurs the database returns a default value of 99.000.

As already mentioned, synthetic spectra were calculated with Synth3 (Kochukhov 2007), that is able to calculate synthetic spectra on the basis of models of any $T_{\rm eff}$ and with also the presence of molecules. The code is maintained by Dr.

O. Kochukhov and regularly updated (the main updates regard partition functions). Both LLmodels and SYNTH3 assume the source function to be of form given in Eq. 3.6. The derivation of the abundances from equivalent widths was performed using a modified version (Tsymbal 1996) of the WIDTH9 code (Kurucz 1993a). Both codes use as input files model atmospheres in the ATLAS9 format and line lists in the format given by the *extract stellar* request of VALD.

When approaching an abundance analysis the first and probably most important step to do is the determination of the fundamental parameters: $T_{\rm eff}$, $\log g$ and $\upsilon_{\rm mic}$. For several objects a correct parameter determination is strictly connected with the determination of the abundances.

For the general discussion on the derivation of fundamental parameters and abundances I will use mainly as example two chemically normal slowly rotating field stars: HD 49933 and 21 Peg. HD 49933 is a solar-type star, while 21 Peg is a late B-type star. HD 49933 and 21 Peg are analysed in very much detail in Ryabchikova et al. (2009) and Fossati et al. (2009b), respectively. I decided to use these two objects because of their non-chemical peculiarity, slow rotation and difference in temperature, that help a clear description of the adopted methodology for the analysis of cluster stars from early G- up to late B-type.

3.5.1 Determination of the fundamental stellar atmosphere parameters

A first good guess of the fundamental parameters is given by photometric indicators. A further spectroscopic derivation of the fundamental parameters is then necessary since different photometries and calibrations give different parameters. Only a deep spectroscopic analysis will clarify which is the best final set of parameters not only for an abundance analysis, but also for any other kind of analysis such as Doppler imaging or line identification.

Parameters from photometry

Photometry gives a description of the stellar flux. The smaller is the photometric band, the finer is the description. With the use of a grid of precomputed stellar model atmospheres it is possible to associate the observed colors to a set of fundamental parameters. An easy example is given taking into account Johnson photometry and main sequence stars. If $B - V$ is equal to 0, the star has spectral type A0 and the $T_{\rm eff}$ is about 10000 K. With the use of more colors, it is possible to constrain also gravity and sometimes metallicity. The photometric calibrations differ according to the stellar spectral type and are strongly dependent on the model atmosphere adopted to build the grid that gives the references for the calibration.

In literature there exist calibrations to obtain $T_{\rm eff}$, $\log g$ and sometimes also metallicity from both broad-band and narrow-band photometry. The most used are Johnson photometry among the broad bands and Strömgren and Geneva photometry among the narrow bands. For these three photometric systems there exist several calibrations each providing a different set of fundamental parameters. In this way it is possible to have an idea of the error bars introduced by the calibration. This uncertainty has to be added to the uncertainty relative to the photometric measurements. Usual error bars for chemically normal stars of spectral types between F and B are 300 K in $T_{\rm eff}$ and 0.2 dex in $\log g$, in case of narrow band photometry. For chemically peculiar stars the error bars increase to at least 500 K in $T_{\rm eff}$ and 0.4 dex in $\log g$. If a broad band photometry is used to derive the fundamental parameters the error bars increase at least to the double of the given values, since this kind of photometry describes much less in detail the characteristics of the stellar flux.

I used always narrow band photometry taken from the Hauck & Mermilliod (1998) catalogue, for the Strömgren photometry, or Rufener (1988) catalogue for the Geneva photometry. When no photometry was available, I took as starting point the typical $T_{\rm eff}$ and $\log g$ corresponding to the spectral type of the star. The adopted calibrations for Strömgren photometry were by Moon & Dworetsky (1985) and Napiwotzki et al. (1993). Regarding Geneva photometry I adopted calibrations by North & Nicolet (1990), Kobi & North (1990), Hauck & North (1993) and Kunzli et al. (1997) according to the expected $T_{\rm eff}$ and chemical peculiarity of the star to analyse.

Parameters from spectroscopy

Hydrogen lines Hydrogen line wings are optimal parameter indicators because they promptly react to variations of at least one fundamental parameter ($T_{\rm eff}$ or $\log g$) and are not affected by non-LTE effects (Mihalas 1978). The only problems that could be encountered when fitting hydrogen line wings for parameter determination concerns a wrong continuum normalisation or the use of a model atmosphere calculated with a wrong metallicity.

Figure 3.5 shows the variation of the Hβ line profile as a function of $T_{\rm eff}$ (top plot) and $\log g$ (bottom plot). Hydrogen lines reach their maximum depth at $T_{\rm eff} \sim$ 8000 K, where they are most sensitive to both temperature and $\log g$ variations. At lower temperatures they react more on temperature, while at higher temperatures on gravity variations. This is due to the fact that at high temperatures hydrogen is almost completely ionised and it cannot react anymore on temperature variations, but just on pressure variations. This effect can also be observed in the last raw of the top plot of Fig. 3.5, where the variation of the hydrogen line profile is not so large as in the other two raws.

With the use of the hydrogen line fitting it is also possible to derive a realistic error bar on the fundamental parameters, that takes into account also the quality of the observed spectrum and of the normalisation, if more than one hydrogen line is available. Figure 3.6 shows the Hβ line profile for 21 Peg in comparison with the synthetic profiles calculated with the adopted stellar parameters. In Fig. 3.6 I added also the synthetic line profiles calculated with 1 σ error bar on $T_{\rm eff}$ ($\pm$ 200 K; top spectrum) and $\log g$ ($\pm$ 0.1 dex; bottom spectrum). The error bars on $T_{\rm eff}$ and

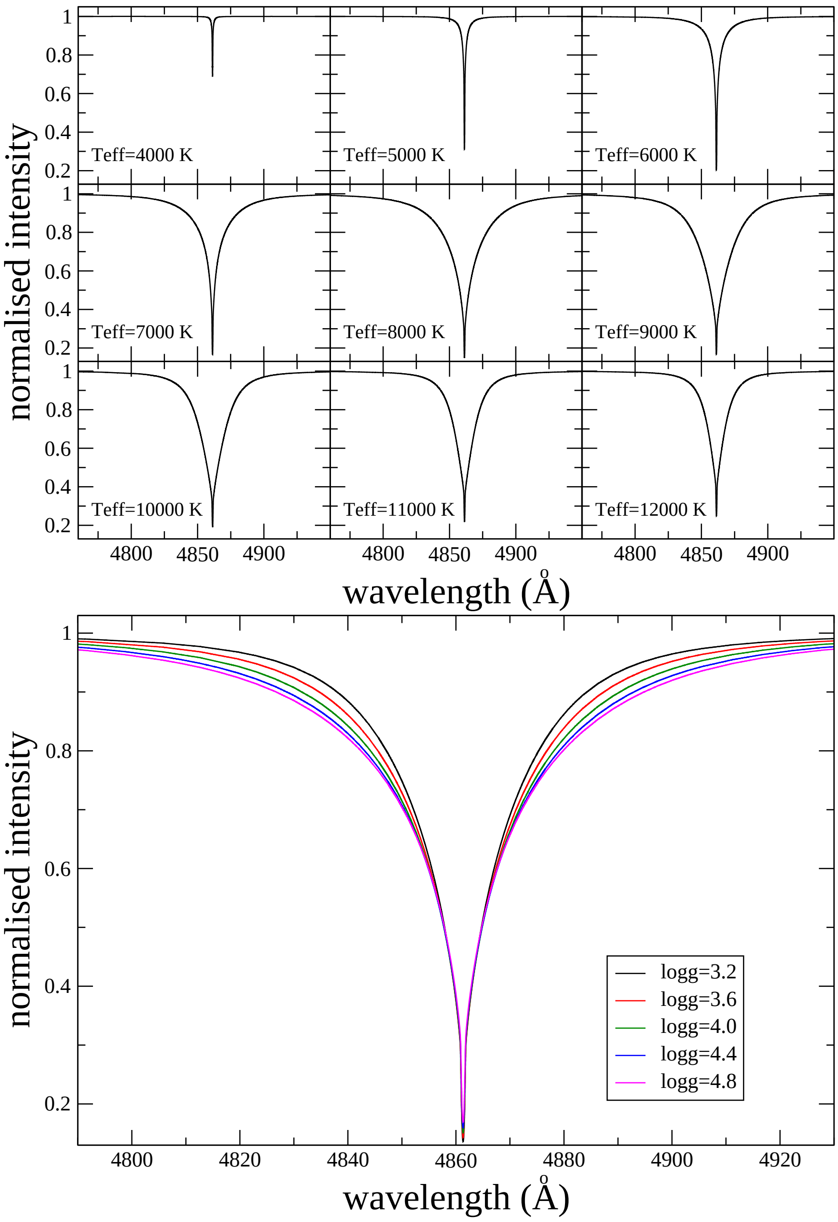

Figure 3.5: Variation of the Hβ line profile as a function of $T_{\rm eff}$ (top plot) and $\log g$ (bottom plot). For both plots the $\upsilon \sin i$ is $0\,{\rm km\,s^{-1}}$ and $\upsilon_{\rm mic}$ is $2.0\,{\rm km\,s^{-1}}$. For the top plot $\log g$ is set to 4.0, while for the bottom plot $T_{\rm eff}$ is set to 8000 K.

$\log g$ obtained from hydrogen line fitting change according to $T_{\rm eff}$. For example at $T_{\rm eff} \sim 6000$ K typical error bars are of the order of 50 K, due to the high sensitivity of the hydrogen lines to $T_{\rm eff}$, but on the other side the error bars on $\log g$ increases drastically, even up to 0.5 dex or more. For this reason other parameter indicators have to be used in such cases.

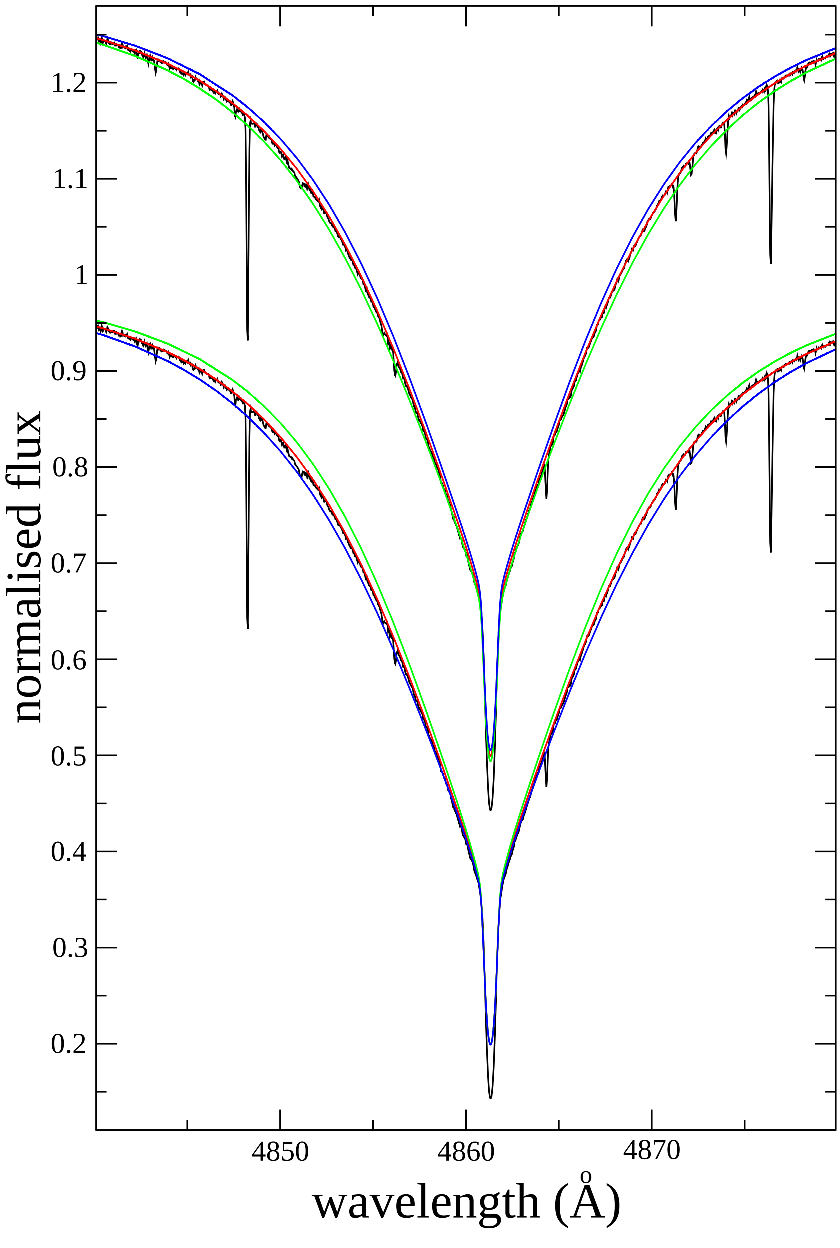

Figure 3.6: Observed Hβ line profile for 21 Peg (black solid line), compared to synthetic profiles (red blue and green lines). The red solid lines were obtained assuming the best $T_{\rm eff}$ and $\log g$ values ($T_{\rm eff}$ = 10400 K, $\log g$ = 3.55). The blue lines show the synthetic profile by increasing $T_{\rm eff}$ by 200 K (top spectrum) or $\log g$ by 0.1 dex (bottom spectrum). The green lines show the synthetic profile by decreasing $T_{\rm eff}$ by 200 K (top spectrum) or $\log g$ by 0.1 dex (bottom spectrum).

The core of hydrogen lines cannot in general be fitted in LTE, since non-LTE effects are rather strong in that region. Only in case of very low resolution, as in my case was for FLAMES/GIRAFFE observations, it is possible to fit also the line core. This is rather useful because, as already mentioned, also the depth of the hydrogen line depends on the $T_{\rm eff}$ and the fit of the line core helped with the temperature determination.

As shown extensively in Khan & Shulyak (2007) non-solar abundances lead to a different atmospheric structure that is then reflected on the determination of the fundamental parameters with any spectroscopic method. For early-type stars an even small overabundance of He is clearly visible in the hydrogen line profiles. At $T_{\rm eff} \sim 15000$ K a helium overabundance of 0.2 dex corresponds to an increase of 0.1 dex in $\log g$, since a helium overabundance acts as pressure. This means that if He is overabundant of 0.2 dex the final adopted $\log g$ has to be 0.1 dex lower than the one derived with models with solar He abundance. On the contrary an underabundance of He of 0.2 dex does not produce any effect in the model structure, at the same temperature.

A clear example of the importance of using the correct abundances for the model calculation is given by the analysis of the hydrogen lines of HD 49933. The star shows a moderate underabundance (up to 0.5 dex) of almost all the analysed elements (Ryabchikova et al. 2009). The $T_{\rm eff}$ determination made with solar abundances lead to a $T_{\rm eff}$ = 6550±50 K. With this temperature I derived then the abundances and used them to calculate a new model to rederive $T_{\rm eff}$. The $T_{\rm eff}$ obtained with the model with the revised abundances was then $T_{\rm eff}$ = 6450±50 K. This new $T_{\rm eff}$ was then used to rederive the abundances and then $T_{\rm eff}$, till convergence. This example shows how an underabundance of 0.5 dex, that sometimes is considered almost trascurable, clearly affects the determination of the fundamental parameters. Also for stars considered chemically ”normal”, such as HD 49933 or π Cet (see Fossati et al. 2009b). In conclusion even small non-solar abundances play an important role in the model structure calculation, that is reflected then in the parameter determination.

The model structure is modified not only by non-solar abundances, but also by the presence of magnetic field or stratification. This should be kept in mind whenever dealing with chemically peculiar (CP) stars.

Metallic lines The analysis of the metallic lines provides useful constraints on the atmospheric parameters, besides being the only way to determine the $\upsilon_{\rm mic}$. The minimisation of the correlation between individual line abundances and excitation potential, for a certain element/ion, will lead to the determination of the $T_{\rm eff}$. If no deviation from LTE is expected, then the balance between different ionisation stages of the same element will provide a value for $\log g$ (ionisation equilibrium). The microturbulent velocity ($\upsilon_{\rm mic}$) is then determined by minimising the correlation between individual line abundances and equivalent widths for a certain element/ion.

The ionisation equilibrium, imposed to derive the $\log g$ value, has its physical basis on the Saha equation that describes the ratio of the ion numbers:

$$\frac{n_I}{n_J} = \frac{2}{n_e}\frac{g_I}{g_J}(\frac{2\pi/mkT}{h^2})^{3/2}\exp(-\frac{E_J - E_I}{kT}). \quad (3.20)$$

Similarly to the Eq. 3.1, the ratio $\frac{n_I}{n_J}$ corresponds to the ratio of the number of atoms in two different ionisation stages. For example $\frac{n_1}{n_0}$ is the ratio of ionic to neutral number of atoms. The information regarding the element abundances enters in Eq. 3.1 and Eq. 3.20.

Figure 3.7 displays the abundance of more than 400 measured FeII lines for 21 Peg as a function of the excitation potential. The abundances were calculated on the basis of two models, one with $T_{\rm eff}$ = 10000 K and the second with $T_{\rm eff}$ = 11000 K, both adopting $\log g$ = 3.55 and $\upsilon_{\rm mic}$ = 0.5 km s^{-1} (the final adopted $T_{\rm eff}$ is 10400 K Fossati et al. 2009b).

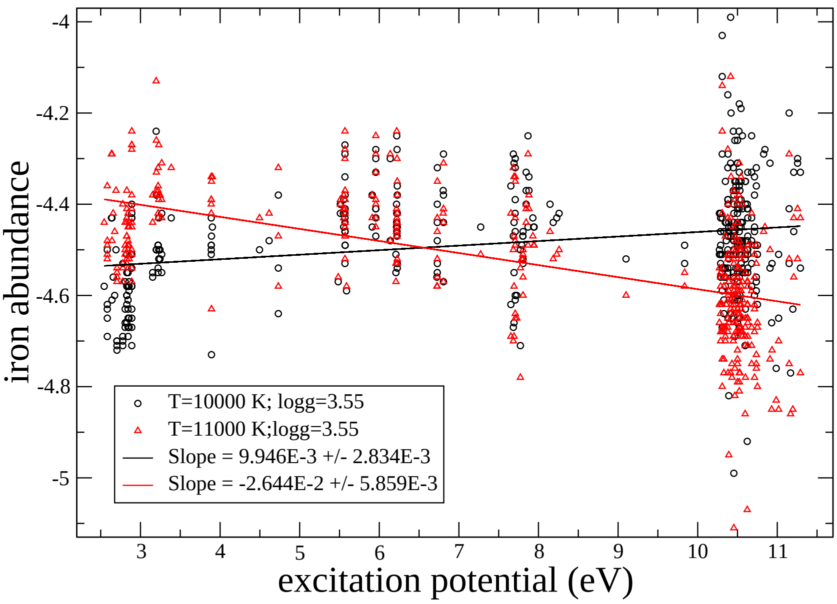

Figure 3.7: FeII line abundance vs. excitation potential adopting two different $T_{\rm eff}$ of 10000 K (black circles) and 11000 K (red triangles). The lines represent the linear fit.

With a plot of the correlations obtained for a $T_{\rm eff}$ lower and higher than expected, as a function of $T_{\rm eff}$itself, it is possible to quickly estimate $T_{\rm eff}$, as shown in Fig. 3.8. According to this plot the effective temperature derived from the FeII lines is a little less than 10300. Lines of different elements/ions will give little different results for $T_{\rm eff}$. One solution would be to obtain as many $T_{\rm eff}$ values as the number of analysed elements/ions and then adopt the average. I always proceed in this way, when possible, only with the difference that I adopted not the simple average, but the weighted mean with the number of lines as weight.

Figure 3.8 assumes a linear variation of the slope with $T_{\rm eff}$. Linearity is assured within a small range in $T_{\rm eff}$. A deep analysis of the linearity together with other details regarding the parameter determination from metallic lines is still in progress and will be shown in future papers. Preliminary results of this study are published in Stütz et al. (2008).

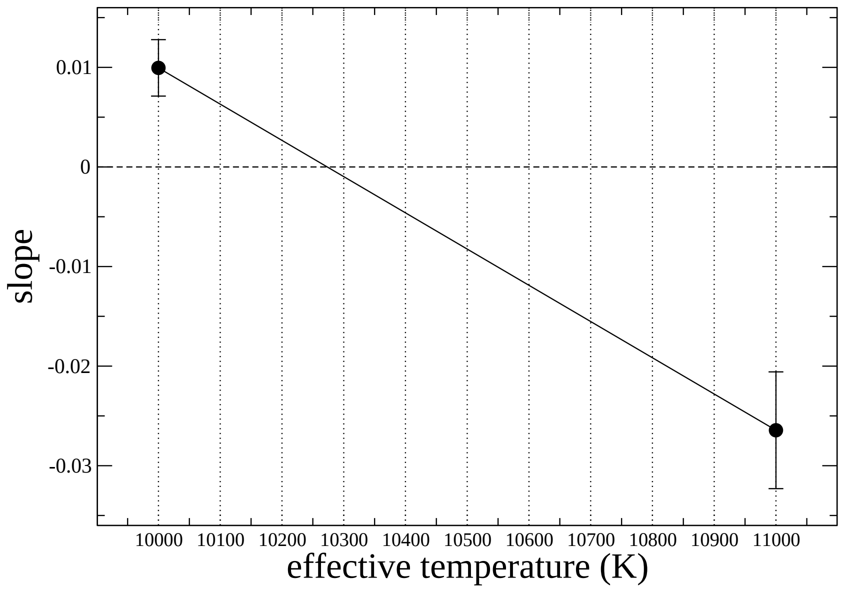

Figure 3.8: Value of the slopes derived from Fig. 3.7, with their error bar, as a function of $T_{\rm eff}$. The $T_{\rm eff}$ for which the slope is 0 is the value to adopt.

Figure 3.9 shows the mean abundance and standard deviation of measured FeI, FeII and FeIII lines for 21 Peg as a function of $\log g$. The abundances were calculated on the basis of two models, one with $\log g = 3.35$ and the second with $\log g = 3.75$, assuming $T_{\rm eff} = 10400$ K and $\upsilon_{\rm mic} = 0.5$ km s^{-1}(the final adopted $\log g$ is 3.55 Fossati et al. 2009b). As for the determination of $T_{\rm eff}$, the plot in Fig. 3.9 allows to derive the best $\log g$ value for a certain element. As for $T_{\rm eff}$ I always used several elements, if possible, and adopted the weighted mean.

Figure 3.10 displays the correlation between the abundances of FeII lines and the measured equivalent widths for 21 Peg. The $\upsilon_{\rm mic}$ value to adopt is found when no correlation is present. It is important to notice that a variation in $\upsilon_{\rm mic}$ leads to a variation in abundance, mainly for the strong lines. For this reason, with the use of the only shallow lines, it is possible to derive rather correct abundances even without knowing the correct $\upsilon_{\rm mic}$.

There are other methods to obtain $\upsilon_{\rm mic}$, such as using Blackwell diagrams, but all of them are based on the same principle, already explained.

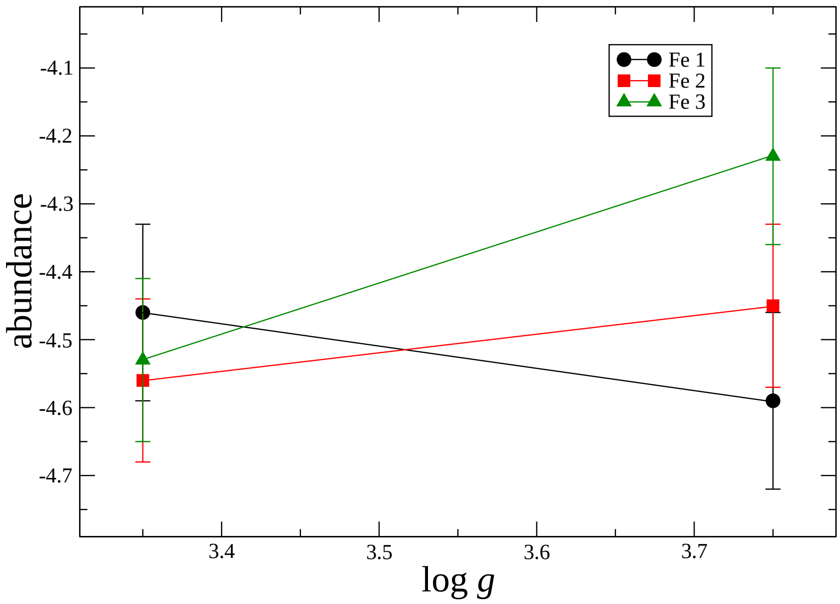

Figure 3.9: Iron mean abundance and standard deviation as a function of $\log g$. The black circles correspond to the FeI, red squares to FeII and green triangles to FeIII abundances.

υ_{mic} can be measured just with the analysis of metallic lines, but T_{eff} and $\log g$ can be determined in other ways, such as hydrogen lines fitting and spectrophotometry. For this reason the determination of T_{eff} and $\log g$ should be done only with metallic lines just when nothing else is available, otherwise it should be left as a check. Actually, the derivation of T_{eff} and $\log g$ only through the analysis of the metallic lines could lead to an incorrect set of parameters. For example, the ionisation equilibrium for several elements is very often not reached, due to different non-LTE effects for different ions. Another danger comes from the adopted $\log gf$ values that for some lines are not correct or accurate enough, leading to wrong slopes or abundances, mainly when a small number of lines is available. The latter is the reason for which it is better always to have as many measured lines as possible, meaning large spectral wavelength coverage.

A good indicator for T_{eff} for cool stars is the balance between two ionisation stages of elements for which the abundance of only one of the two ions reacts very fast on a T_{eff} variation. Such elements are for example Ti and V. Having a rather good value for $\log g$, the correct T_{eff} is obtained when the equilibrium, for example, between TiI and TiII is present. As a matter of fact, the abundance derived from the TiII lines will not change much with a temperature variation, while the one of TiI will change very fast. It is important to remember that for hot stars the ionisation equilibrium is more sensitive to $\log g$ variations, while for cool stars it is more sensitive to T_{eff} variations.

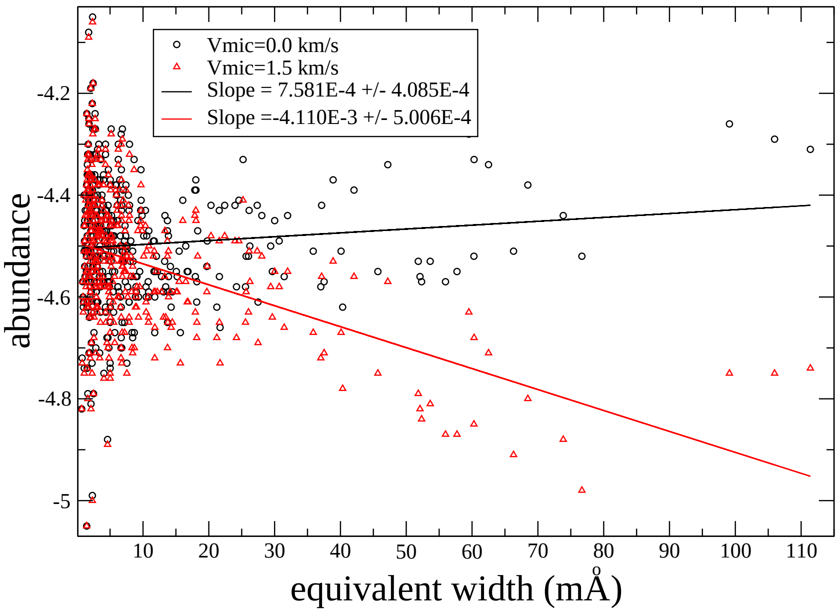

Figure 3.10: FeII line abundance vs. equivalent width adopting two different $\upsilon_{\rm mic}$ of 0.0 km s^{-1} (black circles) and 1.5 km s^{-1}(red triangles). The lines represent the linear fit.

A very good $\log g$ indicator for cool stars is given by the fitting of line wings of MgI lines with developed wings. Such lines in the visible are at $\lambda\lambda$ 5167, 5172 and 5183 Å. The method, described in details in Fuhrmann et al. (1997), consists in the derivation of the Mg abundance from other MgI lines with no developed wings, such as $\lambda\lambda$ 4571, 4730, 5528 and 5711 Å, and then fit the wings of the other three mentioned lines tuning $\log g$. To apply this method, it is necessary to have very accurate $\log gf$ values and Van der Waals damping constants. Comparison with several cool stars shows that the values given by Fuhrmann et al. (1997) are of very high quality and better than the ones currently present in VALD (Barklem et al. 2000). Fuhrmann et al. (1997) gives the Van de Waals damping constants in a different format than present in VALD. The conversion between the two formats can be done using this simple formula: $\log C_6 = 2.5 \log \gamma - 12.32$, where $\log C_6$ is the format given by Fuhrmann et al. (1997) and $\log \gamma$ the one present in VALD. This method was used also for the derivation of $\log g$ for HD 49933, as shown in detail in Ryabchikova et al. (2009).

In case the parameters are obtained only from the analysis of metallic lines, as it happens often with automatic tools for abundance analysis, the obtained parameters might be very different from the real ones. An example is well illustrated in Ryabchikova et al. (2009). HD 49933 was analysed with an automatic abundance analysis tool called VWA (Bruntt et al. 2008) that led to $T_{\rm eff}$ = 6780±130 K and $\log g$ = 4.24±0.13. This set of parameters does not fit at all the hydrogen line profiles of the star. The use of the hydrogen lines and of the wings of some MgI lines allow to determine a much ”safer” set of parameters, as actually confirmed from the analysis of the other metallic lines. In other words, the surface in the $T_{\rm eff}$ - $\log g$ plane has probably more than one minimum; the use of the hydrogen lines and MgI lines avoids often to fall in the wrong one, as happened to Bruntt et al. (2008).

Spectrophotometry For a complete self-consistent analysis of any star one should reproduce the stellar spectral energy distribution with the adopted parameters and abundances for model atmospheres. The most adopted source of spectrophotometry were Adelman et al. (1989), Breger (1976), IUE satellite spectra and Clampitt & Burstein (1997). Other good source of spectrophotometry are the TD-1 satellite (Jamar et al. 1976) and spectra coming from the STIS instrument mounted on the HST. In particular, STIS provides well calibrated spectra, from the near ultraviolet up to the near infrared.

Figure 3.11 shows the comparison between the measured flux distributions and the model fluxes calculated with the adopted atmospheric parameters for 21 Peg and π Cet (Fossati et al. 2009b). The optical spectrophotometry was taken from Adelman et al. (1989) and Breger (1976). All flux measurements were normalised to the flux value at 5000 Å.

For 21 Peg there is the presence of a small discrepancy in the near infrared. This often happens with the optical spectrophotometry, as shown in Figure 1 of Adelman et al. (2002). It can be that this effect is due to the fact that the interstellar reddening is not taken into account since its uncertainty is often rather high, but this is just a possibility and I do not have a definite explanation for this effect.

Figure 3.12 shows a comparison of the model fluxes, normalised to the flux at 5560 Å with spectrophotometry from Clampitt & Burstein (1997) for the Praesepe star HD 73345.

On the spectrophotometry an increase of $T_{\rm eff}$ leads to a decrease of the flux in the visible and infrared regions and an increase of the flux in the ultraviolet region. This modifies as well the shape of the Balmer jump, but mainly in hot stars, while for cool stars the Balmer jump is modified mainly by $\log g$ variations. For cool stars, where the hydrogen lines give high quality information almost only for the $T_{\rm eff}$, the spectrophotometry allows to get accurate measurements also of $\log g$. For hot stars it is the opposite. The case of A-type stars is the best one since for them it is possible to measure accurately both $T_{\rm eff}$ and $\log g$ from both hydrogen lines fitting and spectrophotometry. For this reason spectrophotometry is so important in the parameter determination.

LLmodels allows to get not only model atmospheres, but also synthetic fluxes, with a resolution of R=50 000 both in ergs cm^{-2} s^{-1} A^{-1} and ergs cm^{-2} s^{-1} Hz^{-1}. All the adopted spectrophotometries were given in ergs cm^{-2} s^{-1} A^{-1}, so no conversions were needed before the comparison. Anyway a useful place to recover all the units adopted in astronomy for fluxes measurements and how to convert one each other is the PhD thesis of Dr. R. Kurucz (Kurucz 1973).

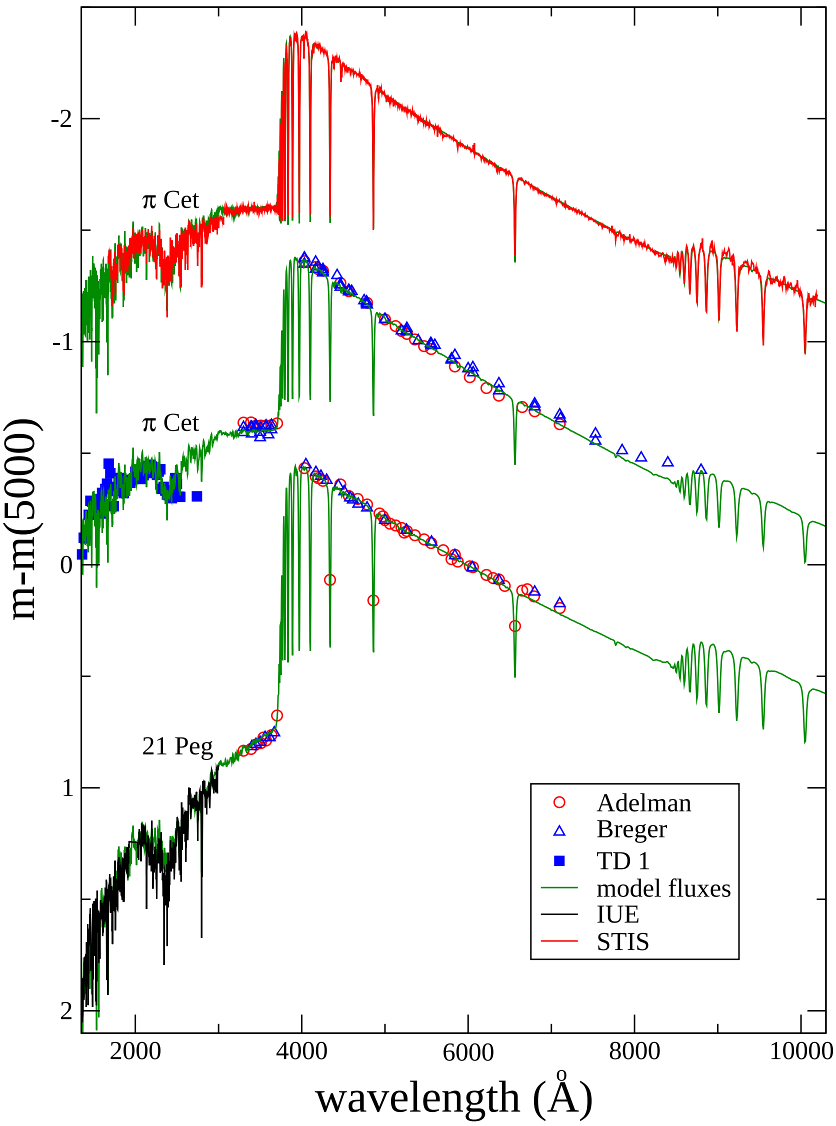

Figure 3.11: Comparison between LLMODELS theoretical fluxes calculated with the fundamental parameters and abundances derived for 21 Peg and π Cet (green solid line) with spectrophotometries by Adelman et al. (1989) (open red circles) and Breger (1976) (open blue triangles), IUE calibrated fluxes (full black line), TD-1 observations (full blue squares) and STIS spectrum (full red line). The model fluxes for 21 Peg and π Cet, shown in the middle of the panel, were convolved to have the same spectral resolution of the IUE fluxes ($R \sim 900$), while the upper of π Cet has a spectral resolution 700, approximately the same of STIS spectra.

To be able to match synthetic fluxes with IUE fluxes it is necessary to correct

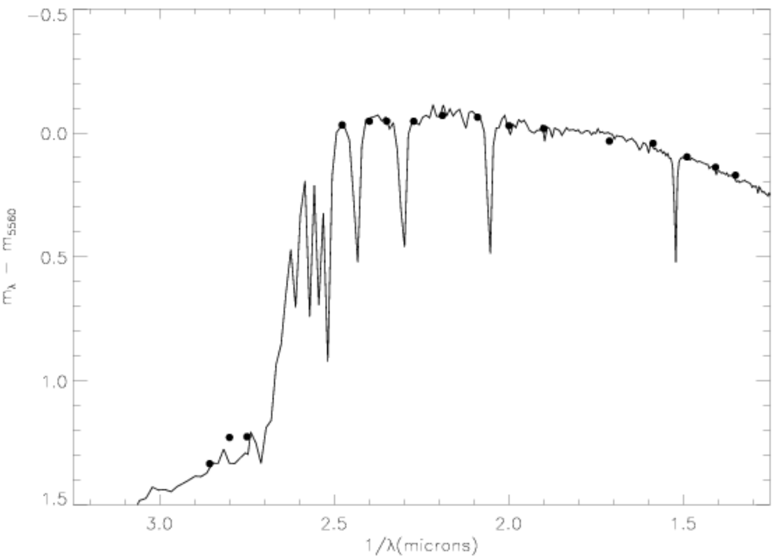

Figure 3.12: Comparison between spectrophotometry from Clampitt & Burstein (1997) and normalised fluxes at 5560 Å with the fundamental parameters adopted for the abundance analysis of the Praesepe star HD 73345.

the synthetic fluxes according to the radius and distance of the star, but this is in general not possible since these two parameters are not known with the necessary accuracy. For this reason the applied correction is usually based on a number that is obtained just matching at best synthetic and observed fluxes.

It is important to mention here that for a physically correct comparison between model fluxes and observed fluxes it is necessary to convolve the model fluxes with the same resolution of the observation(s).

The use of the energy distribution plays a crucial role in adjusting the model atmospheric parameters because it is independent of the photometrical calibrations (different for each author), of the hydrogen line fitting (reduction and normalisation dependent) and of the ionisation equilibria approach (dependent on several effects such as the adopted atomic line data and non-LTE effects).

3.5.2 Derivation of the abundances

In the case that it was possible to measure equivalent widths, a preliminary set of abundances was determined with the already mentioned WIDTH9 code and then the final abundances were obtained through a line by line comparison of the observations with synthetic spectra.

Each spectrum was carefully scanned to select spectral lines with these characteristics: not heavily blended, with a good set of line parameters, with a well established continuum and strong enough to be measurable.

Line parameters of the lines selected for the abundance analysis were checked synthesising those lines and comparing them with the solar spectrum obtained from the National Solar Observatory Atlas[3]. The lines for which I found a clear discrepancy between the observed and synthesised solar spectrum were rejected.

The abundance of each of these selected lines was automatically fitted on the observed spectra in a restricted wavelength range, dependent on the $\upsilon \sin i$ of the star. The adopted code fits only of the selected line abundance, taking into account obviously all the lines of the same element in the selected wavelength range.

The fitting procedure and the abundance determination was performed iteratively for each elements in order to obtain at every iteration a better determination of the abundances in case of blends.

The adopted abundance of an element/ion was defined as the mean of the abundances obtained from each selected line of the same element/ion. The error bar associated with each mean abundance is the standard deviation, and does not take into account the uncertainties on the fundamental parameters.

For all the elements that were not analysed I adopted the solar abundance from Asplund et al. (2005). This fact enters into the model atmosphere computation, and in the normalisation of the results expressed according to the total number of nuclei per unit volume $N_{\rm tot}$.

In the derivation of the abundances I took into account the hyperfine structure for all the elements for which it is present (such as Li, Mn, Cu etc.) and visible due to the low $\upsilon \sin i$ of some of the analysed stars.

3.5.3 Radial velocity and projected rotational velocity ($\upsilon \sin i$)

The radial velocity is a crucial parameter in this work, since it is used, together with the proper motion, to check the cluster membership.

Radial velocity and $\upsilon \sin i$, both in km s^{-1}, were determined in a very similar way, computing the median of the results obtained by synthetic fitting of several individual lines in the observed spectrum. The typical error bars associated with $\upsilon_{\rm r}$ and $\upsilon \sin i$ are dependent on $\upsilon \sin i$. For $\upsilon_{\rm r}$ the uncertainty ranges between 1 and 8 km s^{-1}, while for $\upsilon \sin i$ it is about 5%.

When possible, the fitting of the $\upsilon \sin i$ was made after the determination of the fundamental parameters and of the abundances (obtained from equivalent widths) because the hydrogen line fitting is not strongly dependent on $\upsilon \sin i$ and the equivalent widths are $\upsilon \sin i$ independent.

A set of magnetic null lines on which perform the $\upsilon \sin i$ determination is given by Landstreet (1969). These lines have the property not to be broadened by magnetic field, due to the zero landé factor, giving the possibility to derive a correct $\upsilon \sin i$ value also for well known magnetic stars or stars where the magnetic field strength is unknown.

[3] http://www.coseti.org/natsolar.htm

In case of stars with too much line blending for equivalent width measurements, the fitting of $\upsilon_{\rm r}$ and $\upsilon \sin i$ was performed just after the derivation of the fundamental parameters. Usually these kind of stars do not show abundances very different from the solar ones, allowing a precise $\upsilon \sin i$ determination even adopting slightly inappropriate abundances.

3.5.4 Fast rotating stars

The derivation of $T_{\rm eff}$ and $\log g$ was in principle not affected by a high $\upsilon \sin i$ since I mostly used hydrogen line fitting. The main difference consists in the fact that no equivalent widths measurement was possible, so that the derivation/check of the parameters via analysis of the metallic lines was performed directly with the fit of synthetic spectra, to obtain line abundances.

For such stars it is not possible to derive $\upsilon_{\rm mic}$ in the classical way, so I adopted the following method. I obtained the mean abundance and relative standard deviation for elements, for which a consistent number of lines was selected, adopting different values of the $\upsilon_{\rm mic}$. The next step was to plot the derived standard deviations, from the mean abundance, as a function of $\upsilon_{\rm mic}$. The adopted $\upsilon_{\rm mic}$ value is the one for which the standard deviation is minimum. Four examples of this kind of plot are shown in the upper panels of Fig. 3.16 and 3.17.

The heavy line blending of some of the analysed stars results in a different and smaller selection of lines compared to the line list employed for stars with less blending. I checked if this effect is a source of systematic errors by performing the abundance analysis of two Praesepe stars: HD 73045 ($\upsilon \sin i$ = 10 km s^{-1}) and HD 73746 ($\upsilon \sin i$ = 95 km s^{-1}) adopting the line list used for HD 72757 ($\upsilon \sin i$ = 179 km s^{-1}). The results of this test, illustrated in Fig. 3.13, show that no systematic errors are introduced by the difference in selected lines.

3.5.5 Abundance uncertainties

The first source of abundance uncertainty that I take into account here is due to the continuum normalisation, that for stars with small line blending is also connected with the uncertainty on the equivalent widths measurement.

At first it is important to know which is the minimum measurable equivalent width and as a consequence its uncertainty, given a certain SNR and $\upsilon \sin i$. Taking as example 21 Peg, with a two σ error bar I derived a value of 0.2 mÅ ($\upsilon \sin i$ of 21 Peg is about 3.8 km s^{-1}, and SNR per pixel of the observed spectrum about 700). This value is derived assuming a triangular line with a depth (height of the triangulum) proportional to twice the signal to noise and wide (base of the triangulum) as a single spectral line broadened with the adopted $\upsilon \sin i$. At low $\upsilon \sin i$ the uncertainty is completely driven by the SNR showing the importance of a very high SNR not only for fast rotating stars, but also for slowly rotating stars. This uncertainty includes also the uncertainty due to the continuum normalisation.

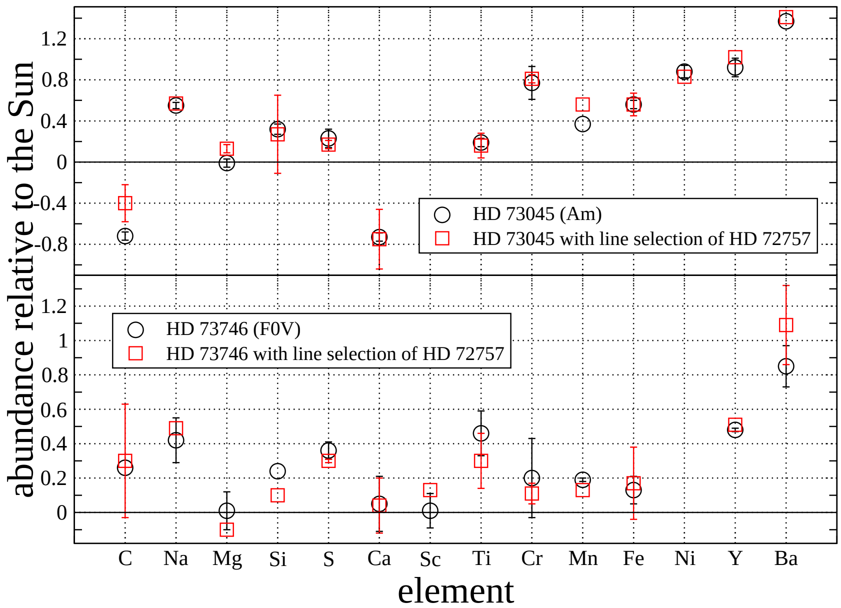

Figure 3.13: Comparison between the abundances derived for HD 73045 ($\upsilon \sin i$ = 10 km s^{-1}- open circles in the upper panel) and HD 73746 ($\upsilon \sin i$ = 95 km s^{-1} - open circles in the lower panel) adopting a proper line selection and the lines used to determine the abundances of HD 72757 ($\upsilon \sin i$ = 179 km s^{-1} - open squares in both panels).

In Fig. 3.14 I plot the error bars in abundance for a certain line as a function of equivalent widths for 21 Peg. To derive the uncertainty in abundance due to the error bar on equivalent widths measurement I took a representative FeII line and derived the abundance of this line on the basis of different values of equivalent widths ranging from 0.3 mÅ to 110 mÅ. I then calculated the difference between the abundance obtained with the equivalent width X and X+δX, where δX is the error bar on the equivalent widths measurement. For equivalent widths greater than 30 mÅ, the abundance error bar tends asymptotically to zero.

Knowing the mean measured equivalent width, with the use of the plot shown in Fig. 3.14, it is possible to derive the mean error bar in abundance due to the uncertainty on the equivalent widths measurement and continuum normalisation. In the case of 21 Peg the mean equivalent width is about 20 mÅ leading to an error bar in abundance of 0.03 dex.

For a sufficiently larger number of lines, it is possible to assume that the internal scatter of each ion takes into account also the error bars due to equivalent widths measurement and continuum normalisation.

Figure 3.15 shows the abundance scatter as a function of the number of measured lines for 21 Peg. For elements for which non-LTE effects are supposed to be important and line dependent, such as Al and S, the internal standard deviation is

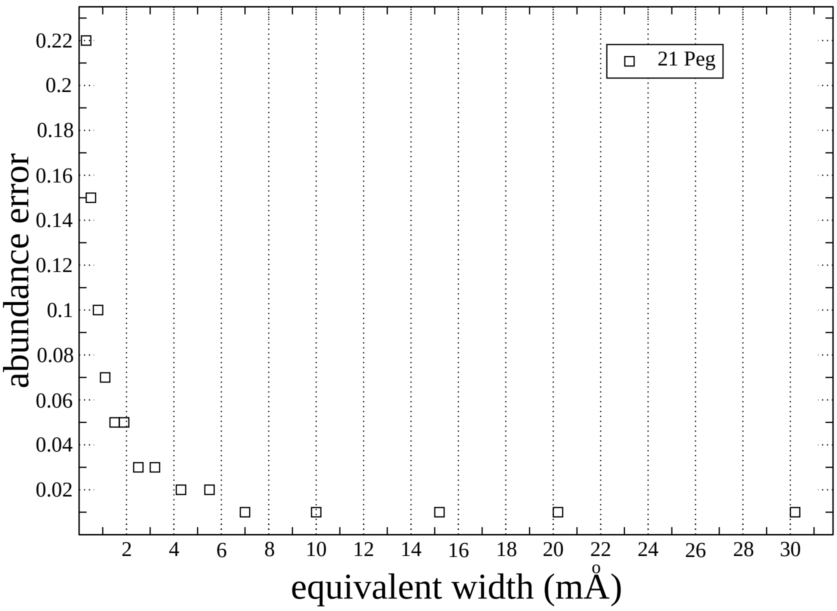

Figure 3.14: Error bar in abundance as a function of equivalent widths 21 Peg. This uncertainty is due to the uncertainty in the equivalent widths measurement and continuum normalisation.

particularly high. The same is found for elements for which the $\log gf$ values are not very accurate due to the complexity of the atomic structure, such as Si. For the other elements, Fig. 3.15 shows that for a sufficiently high number of spectral lines, say $n > 10$, it is reasonable to expect an internal error bar of 0.11 dex.

For fast rotating stars it is not possible to use the method just described, so I performed the following test. I derived the abundance of the FeII line at 5325.6 Å for the Praesepe stars HD 73746 ($\upsilon \sin i$ = 95 km s^{-1}), HD 72757 ($\upsilon \sin i$ = 179 km s^{-1}) and HD 73798 ($\upsilon \sin i$ = 200 km s^{-1}) with the adopted normalised observed spectrum and with the spectrum multiplied / divided by 0.99. In this way I increased / decreased the continuum level of 1%, that I estimate to be a reasonable uncertainty. The difference between the abundances obtained in this way is increasing with $\upsilon \sin i$ from about 0.1 dex for HD 73746, to about 0.2 dex for the two faster rotators.

I believe that in most cases these error bars are upper limits since the line by line abundance analysis method, used in this work, allows a very careful line selection that rejects all the lines for which the continuum level looks uncertain. If for some lines the continuum level is too low, for some others it would be too high, leading to an increase of the dispersion, but not to an abundance variation.

The internal scatter is just a part of the total error bar on the abundance determination, since the uncertainties on the determination of the fundamental parameters have to be taken into account.

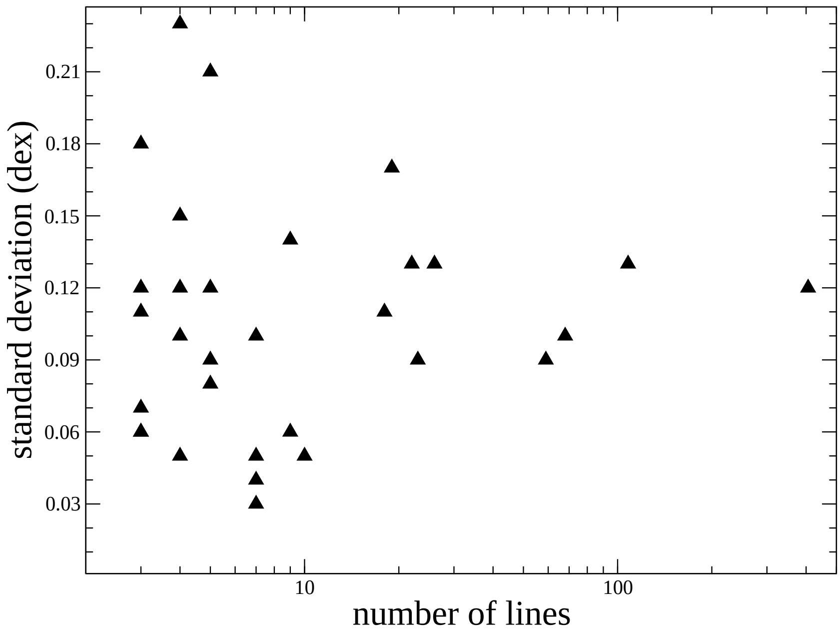

Figure 3.15: Standard deviation of the derived abundances as a function of the the number of lines (shown in logarithmic scale and for a number of lines greater than 2). For visualisation reasons I omitted the standard deviation given by ZrII.

Table 5 of Fossati et al. (2009b) shows the variation in abundance, for each analysed ion of 21 Peg, that was determined when a fundamental parameter is increased of 1σ, keeping fixed all the other parameters. The main source of uncertainty is the error bar on the effective temperature, while the variation due to $\log g$ and in particular to $\upsilon_{\rm mic}$ is almost negligible, although in Fossati et al. (2009b) an uncertainty on $\upsilon_{\rm mic}$ of 2σ is considered.

The last column of Table 5 of Fossati et al. (2009b) shows the final abundance error bar, assuming all sources of uncertainty independent.

For fast rotating stars, the heavy line blending results in a line list dominated by strong and saturated lines. These lines are more sensitive to $\upsilon_{\rm mic}$ variations than shallow lines. For this reason the uncertainties of the adopted $\upsilon_{\rm mic}$ value needs to be reconsidered to obtain a realistic estimate of the error bars associated with the derived element abundances.

To quantify the importance of the error bar on $\upsilon_{\rm mic}$ as a function of $\upsilon \sin i$ and then on the abundances, I performed the following test. For four Praesepe stars with different $\upsilon \sin i$ values (HD 73730, $\upsilon \sin i$ = 29 km s^{-1}- HD 73746, $\upsilon \sin i$ = 95 km s^{-1}- HD 72757, $\upsilon \sin i$ = 179 km s^{-1}- HD 73798, $\upsilon \sin i$ = 200 km s^{-1}) I performed the abundance analysis of selected Fe, Ni, Cr and Ti lines for assumed $\upsilon_{\rm mic}$ varying from 1 to 5 km s^{-1} in steps of 0.1 km s^{-1}. I plotted then in Fig. 3.16 and in Fig. 3.17 the variation of the standard deviation from the mean abundance (upper panel) and the mean abundance itself (lower panel) as a function of $\upsilon_{\rm mic}$.

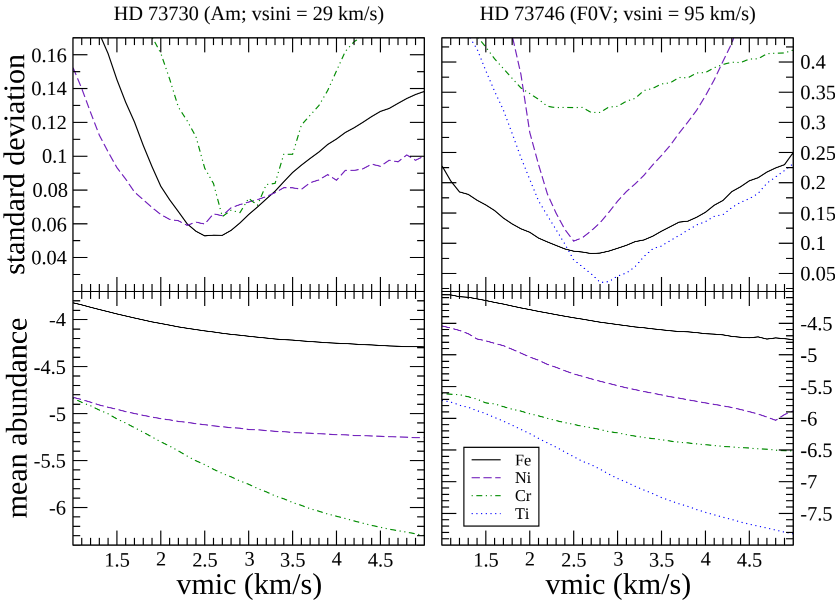

Figure 3.16: The upper panels show the variation of the standard deviation from the mean abundance of Fe, Ni, Cr and Ti as a function of $\upsilon_{\rm mic}$, for HD 73730 ($\upsilon \sin i$ = 29 km s^{-1}) and HD 73746 ($\upsilon \sin i$ = 95 km s^{-1}). The lower panels show the variation of the mean abundance as a function of $\upsilon_{\rm mic}$.

Taking into account the different best $\upsilon_{\rm mic}$ values obtained from different elements, and the dispersion of the standard deviation as a function of $\upsilon_{\rm mic}$, the uncertainty that I assigned to $\upsilon_{\rm mic}$, for the rapid rotators, is 0.7 km s^{-1}. The lower panels of Fig. 3.16 and Fig. 3.17 allow to derive directly the abundance uncertainty given the uncertainty on $\upsilon_{\rm mic}$ for each element. I used Fe as a standard element to derive the abundance standard error bar, since it is the element with the highest number of selected lines. An error bar of 0.7 km s^{-1} in $\upsilon_{\rm mic}$ produces an uncertainty of element abundance increasing from 0.1 dex for the slow rotators, to 0.2 dex for the rapid rotators. The error bar on the element abundance is dominated by the uncertainty of $T_{\rm eff}$ for the slow rotators, while the uncertainty in $\upsilon_{\rm mic}$ becomes increasingly important for larger $\upsilon \sin i$. Assuming that $T_{\rm eff}$ and $\upsilon_{\rm mic}$ are completely uncorrelated, the resultant abundance error bar for the rapidly rotating stars is given by standard error propagation theory, which leads to an uncertainty of about 0.3 dex. In conformity with this analysis, I assumed an abundance error bar increasing linearly with $\upsilon \sin i$ from 0.2 dex to 0.3 dex at a $\upsilon \sin i$ value of 200 km s^{-1}.

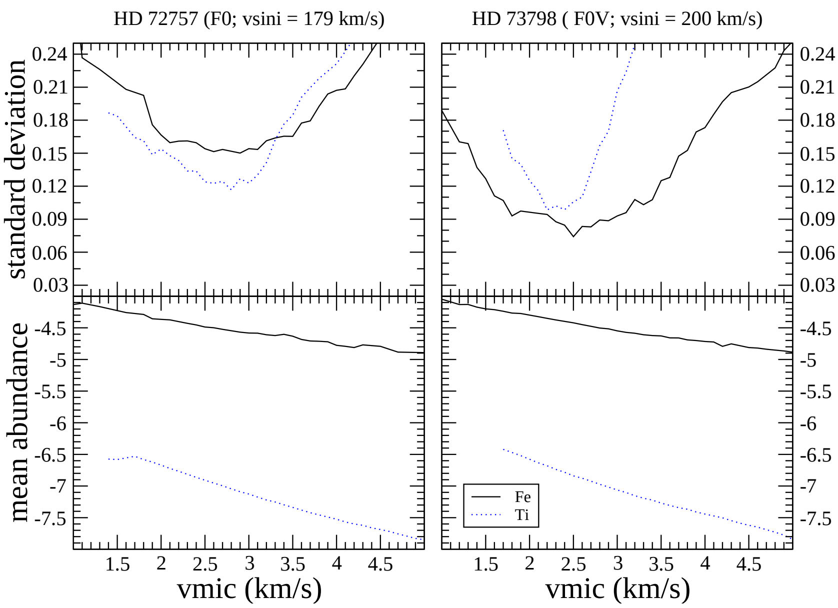

Figure 3.17: As for Fig. 3.16, but for HD 72757 ($\upsilon \sin i$ = 179 $\mathrm{km\,s^{-1}}$) and HD 73798 ($\upsilon \sin i$ = 200 $\mathrm{km\,s^{-1}}$).

3.6 High precision magnetic field search

As already mentioned in Sect. 2, I analysed spectra obtained with the ESPaDOnS spectropolarimeter, in polarimetric mode. This instrument configuration allows to obtain all four Stokes parameters and in particular Stokes *V* was obtained for the observed stars. For these objects it was possible to perform a measurement of the mean longitudinal magnetic field through the Least-Square Deconvolution technique (LSD).

LSD is a cross-correlation technique developed for the detection and measurement of weak polarisation signatures in stellar spectral lines. The method is described in detail in (Donati et al. 1997) and Wade et al. (2000).

Figure 3.18 shows the LSD profile obtained for one of the analysed stars member of the Praesepe cluster: HD 73730. The bottom line corresponds to the intensity LSD profile, while the upper profile to the LSD Stokes *V* profile. No signature is present in the LSD Stokes *V* profile meaning that no magnetic field was detected. For comparison it is possible to see Fig. 2 and Fig. 3 in Alecian et al. (2008) where Stokes *V* profiles of magnetic stars are presented.

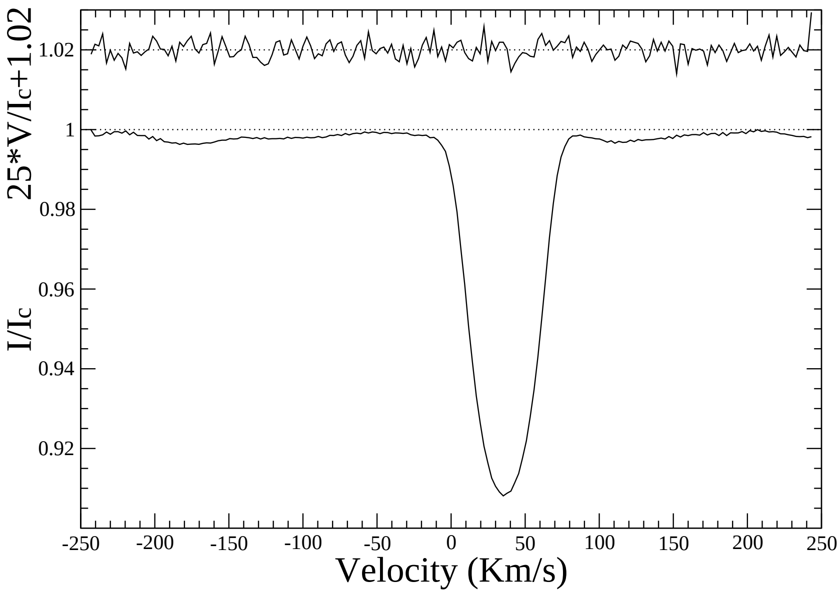

Figure 3.18: LSD profiles for the normalised Stokes *I* and Stokes *V* spectra (from bottom to top) of HD 73430. The Stokes *V* profile is expanded by a factor of 25 and shifted upward of 1.02.

Chapter 4

Results and discussion of the open cluster analysis

In this chapter I aim to describe the results obtained for the two analysed clusters: NGC 5460 and Praesepe (M 44, NGC 2632).

NGC 5460 is an intermediate age open cluster ($\log t = 8.20 \pm 0.20$, Ahumada & Lapasset 2007) including a large number of early-type stars that cover a large part of the upper main sequence. This cluster was observed with with FLAMES at the ESO/VLT. Besides few spectropolarimetric measurements obtained for three stars of the cluster, NGC 5460 is almost completely unknown on the spectroscopic point of view. This allows to get important new information on the cluster parameters, such as metallicity, and of the stars in the cluster field of view.

Praesepe is also a nearby intermediate age open cluster ($\log t = 8.85 \pm 0.15$, González-García et al. 2006) and is an especially interesting target because it includes a large number of A-type stars, among which are many Am stars. Among the known open cluster, Praesepe is probably the one containing the largest number of Am stars. Since Praesepe is relatively close to the sun (d = 180 ± 10 pc, Robichon et al. 1999), many of the member A-type stars are bright enough to allow to obtain high resolution spectra with intermediate class telescopes. This open cluster was observed with ELODIE and SOPHIE at the OHP, and ESPaDOnS at the CFHT.

Several analysed F- and A-type stars lay or could lay in the instability strip so that they could be variables and most likely δ Sct pulsators Breger (2000). Together with other three collaborators, I analysed the possibility for the δ Sct stars to show systematically different abundance patterns compared to the non-pulsating stars of similar spectral type, with negative results (Fossati et al. 2008b). This result allows to treat the abundances of the δ Sct stars and of the stars that could be δ Sct pulsators in the same way as done for the non-pulsating stars.

4.1 NGC 5460

NGC 5460 was photometrically studied primarily by Claria (1971), Claria et al. (1993) and Barrado & Byrne (1995), but it is still spectroscopically almost unknown, except for the few CP stars for which measurements of the longitudinal magnetic field were obtained with FORS1 at the ESO VLT (HD 122983, HD 123183 and HD 123225 by Bagnulo et al. 2006).

4.1.1 Observing strategy

This cluster was observed with FLAMES at the ESO/VLT. FLAMES was described in detail in Chapter 2. Here I intend to describe the observing strategy adopted to maximise the performances of FLAMES in order to obtain the highest possible spectral quality of the largest possible number of cluster member stars.

The observing strategy was based on the selection of the target stars, fundamental to decide the adopted instrument setup.

Selection of the target stars

On the basis of the target selection described in Chapter 1, I divided the whole sample of stars in the field of NGC 5460 according to their properties (as already described in Chapter 2, FPOSS allows to give a decreasing observational priority, from 9 to 1, to the selected targets and to allocate automatically each fiber, following the given priority). At first, I separated the objects members of the cluster to the non-members taking the membership from the available surveys: Robichon et al. (1999), Kharchenko et al. (2004), Kharchenko et al. (2005) and Dias et al. (2006). The membership given for each star was then checked at a further stage (see Sect. 4.1.2). I divided the selected stars according also to their spectral classification; in particular I was interested in stars with spectral type between early G and late B. Within this subsample of stars I separated the stars with the most interesting properties, such as chemical peculiarity, slow rotation, variability, etc. from the others.

I selected about ten stars among the most interested and I gave them the highest observational priority. In this way the four available FLAMES/UVES fibers were automatically positioned on four of these most interesting stars and the other stars of this subsample were observed with FLAMES/GIRAFFE. The remaining fibers of FLAMES/GIRAFFE were then "almost" automatically positioned on the other selected stars according to the given observational priority. I gave a pretty high priority (between 4 and 5) also to the non-member early-type stars present in the field of view. This will allow to analyse in a further stage possible systematic abundance differences between cluster member and non cluster member early-type stars present in the same field of view, but this topic is not touched in this thesis.

Instrument setup

An important decision to take, before observing with FLAMES, regards the settings to adopt, both with FLAMES/UVES and FLAMES/GIRAFFE. Taking into account that for the parameters determination it is very useful to have observations of the hydrogen lines (at least one) and that the number of lines (and elements) increases towards the blue spectral regions, the most adequate FLAMES/UVES setting is the SHP700-520 that covers the wavelength region 4140–6210 Å with a mean resolving power of 47 000.

The choice of the setting has to take into account the atmospheric effects, described in Chapter 2, that play an important role when observing with multifiber spectrographs such as FLAMES.

The telescope was guided at the central wavelength of the adopted FLAMES/UVES setting (5200 Å) because the observations with FLAMES/UVES require the longest exposure time to reach the desired SNR. Given the guiding wavelength, the settings chosen for FLAMES/GIRAFFE could not have a central wavelength too far from 5200 Å due to the mentioned atmospheric effects. For this reason the choice of the H525.8B setting was almost obvious since it has a central wavelength very close to the one of the setting chosen for FLAMES/UVES and a spectral resolution of 25 900, higher than both the H525.8 and H525.8A settings that have the same central wavelength. The total exposure time was controlled by FLAMES/UVES and it was long enough to allow exposures with FLAMES/GIRAFFE with more than one setting. As mentioned, for the abundance analysis it is extremely useful to have available at least one hydrogen line. For the parameters determination with hydrogen line fitting, high resolution is not necessary so I decided to adopt the L479.7 FLAMES/GIRAFFE setting, that covers the whole Hβ line region plus a large wavelength range on the blue of the hydrogen line, allowing the analysis of a larger portion of the stellar spectrum. As third setting for FLAMES/GIRAFFE I decided to take the H572.8 that provides the rather good resolution of 24 200 and the central wavelength lays not too far from the guiding wavelength, allowing to obtain abundances for elements not visible with the other selected settings, such as sodium.

The knowledge of $T_{\rm eff}$ allowed also to perform a spectral classification of each observed star, extremely valuable due to the fact that most of the selected stars were never observed spectroscopically so that no clear spectral classification was available.

Each FLAMES observation was composed by four FLAMES/UVES exposures and two FLAMES/GIRAFFE exposures for each setting. The final analysed spectrum of a star observed with a given instrument/setting was calculated summing the single spectra obtained with each exposure.

4.1.2 Target list

Table 4.1 lists the sample of stars analysed in NGC 5460. This Table does not contain all the stars observed in the cluster field of view since not all of them were directly interesting for this work. I analysed "only" all the stars with spectral type between early G and late B, and denoted as cluster member by Kharchenko et al. (2004) and/or Dias et al. (2006). For several stars, the spectral type was unknown, so that first I quickly derived a rough value for the $T_{\rm eff}$ of each star automatically fitting precomputed synthetic Hβ line profiles on the observed spectra. Based on the so obtained $T_{\rm eff}$, I selected the stars to be analysed in this cluster.

Some stars of the sample are here called with their UCAC2 catalog (Zacharias et al. 2004) name. One star of the sample, HD123201B, is member of a visual double system, while the stars denoted in Table 4.1 as SB2 are newly discovered double line spectroscopic binaries. All the analysed stars were assigned as cluster member by Kharchenko et al. (2004) and/or Dias et al. (2006), but a more detailed discussion of the membership is needed.

The HJD at the middle of the exposure is the same both for the spectra obtained with FLAMES/UVES and FLAMES/GIRAFFE and it is 2454242.096. The total exposure time for the spectra obtained with FLAMES/UVES is 2520 seconds, while for FLAMES/GIRAFFE is 1300 seconds with the H525.8B setting, 900 seconds with the H572.8 setting and 240 seconds with the L479.7 setting.

Cluster membership

Table 4.2 lists the proper motion and their uncertainties for the observed stars given by Dias et al. (2006) and Hog et al. (2000), the membership probabilities given by Dias et al. (2006) and Kharchenko et al. (2004), and stellar identification and membership given by Claria et al. (1993). The mean cluster proper motion given by (Kharchenko et al. 2005) is (-5.70,-3.58) ± (0.27,0.37).

Figure 4.1 shows a comparison between the proper motions published by Kharchenko et al. (2004) and the ones given for the observed stars by Dias et al. (2006) and Hog et al. (2000). Within the cluster chart given by Kharchenko et al. (2004) and shown at the bottom of Fig. 4.1, the middle plot in the lower raw has to be taken into consideration for the comparison of the proper motions given by the other authors.

The upper plots of Fig. 4.1 show clearly how difficult is for this cluster to obtain a precise determination of the cluster membership with only the use of the stellar proper motion. For this reason it was very important to establish the cluster membership the use of the already published photometry. Photometry of almost all the stars here analysed was performed by Claria et al. (1993), who gave cluster memberships as well. For this reason in the end I decided to adopt the cluster membership given by Claria et al. (1993). The final adopted cluster membership for each analysed star is given in Table 4.1. Stars for which no information is given by Claria et al. (1993), for safety reasons, were considered as non cluster members.

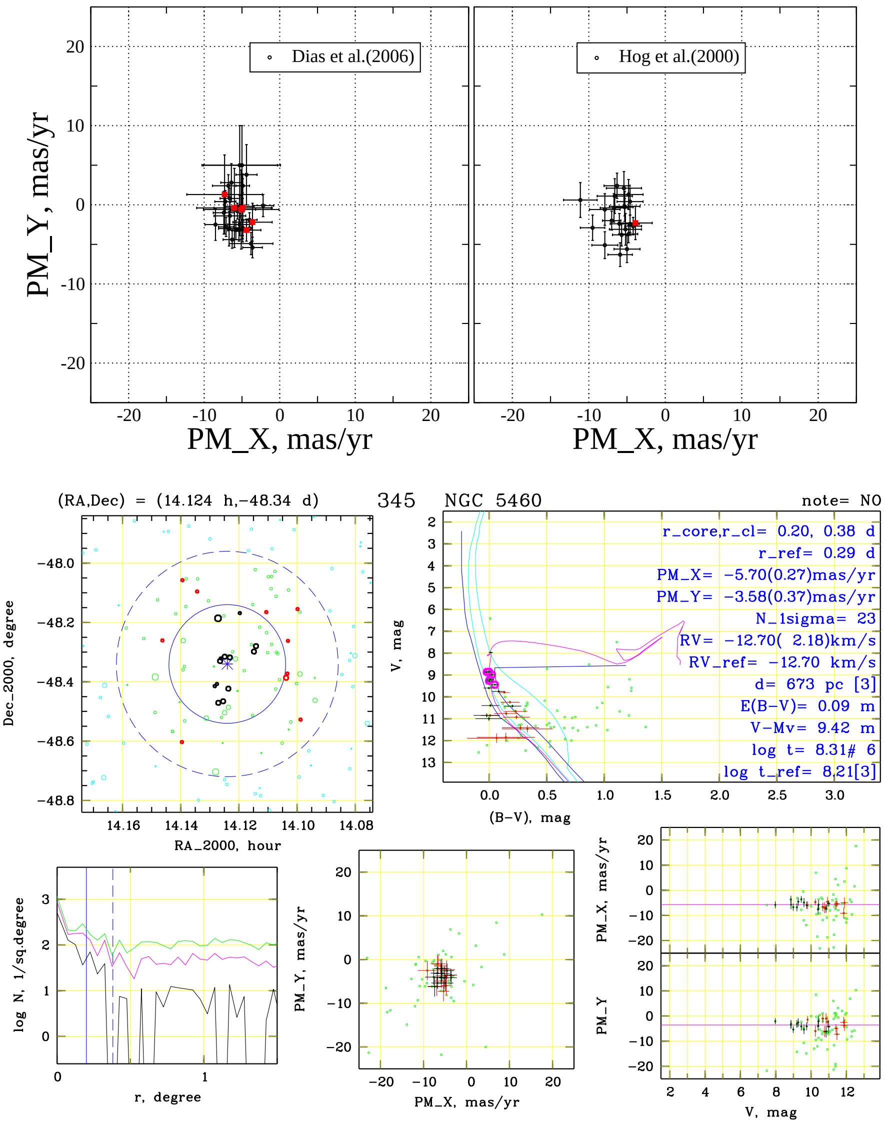

Figure 4.1: The upper row of plots shows the proper motion of the observed stars with the data taken by Dias et al. (2006) and Hog et al. (2000). The red dots indicate the proper motion of the stars considered in the end as not member of the cluster. The lower set of plots reproduces the chart published by Kharchenko et al. (2004).

This work allows to establish as well the mean cluster radial velocity. Without taking into account SB2 stars and non cluster members, the mean radial velocity is: -17.9 ± 5.2 km s^{-1}. The mean cluster radial velocity published by (Kharchenko et al. 2005) is: -12.70 ± 2.18 km s^{-1}. The two values are in good agreement also because the value given by (Kharchenko et al. 2005) is obtained averaging the results obtained for only three stars.

4.1.3 Results of the abundance analysis

Fundamental parameters and abundances of the program stars were obtained as explained in Chapter 3. Table 4.3 lists the fundamental parameters derived for each analysed star in NGC 5460.

For all the SB2 stars, but HD 123225, it was possible to derive only υ_r and $\upsilon \sin i$ values and to roughly estimate $T_{\rm eff}$ and $\log g$. There is the possibility that some of the analysed stars is a single line spectroscopic binary such as maybe HD 123182, but this is impossible to address wit a reasonable accuracy with only one available spectrum and the measured mean cluster υ_r.

The given $\sigma_{\log g}$ for G- and late F-type stars are pretty high due to the fact that the parameters were obtained mainly with hydrogen line fitting and ionisation equilibrium. The fitting of Mg lines with developed wings to determine $\log g$ was not possible due to the low spectral resolution. The ionisation equilibrium gives rather good results in the determination of $\log g$, but it is dependent on possible non-LTE effects and on the obtained abundance dispersion. In the case of G- and late F-type stars the abundance dispersion was rather large due to the large number of heavily blended spectral lines, and to the low spectral resolution and SNR (because these stars are rather faint) of the available spectra.

Figure 4.2 shows a comparison between observed and synthetic Hβ line profiles for seven stars of various $T_{\rm eff}$ observed with FLAMES/GIRAFFE. The fit here shown demonstrates the general high quality of the available spectra and of the adopted fundamental parameters.

The obtained abundances for each analysed star (including the non cluster member stars) are shown from Table 4.4 to Table 4.8

In the following I describe more in detail the results obtained for some particularly interesting individual star.

HD 122983

HD 122983 was observed by Bagnulo et al. (2006) with FORS1, because suspected chemically peculiar, to measure the magnetic field, but no field was detected. The abundance pattern, displayed in Fig. 4.3, shows that HD 122983 is a He-weak chemically peculiar star, but it is not possible to say if the star is a HgMn star or not. Manganese lines are too weak to be measurable and mercury lines are in principle present, but not visible in the spectral region covered by the available spectrum. A spectrum of the blue visible region would be extremely valuable to detect the presence of Hg overabundance (Hubrig & Mathys 1996). I looked for the presence of the overabundance of other elements typically visible in HgMn stars, such as P and Xe, but without success.

HD 123182

The abundance pattern of HD 123182 (see Fig. 4.3) reveals that the star is most likely a mild He-weak star, in particular it could be a hot Am star or a cool HgMn

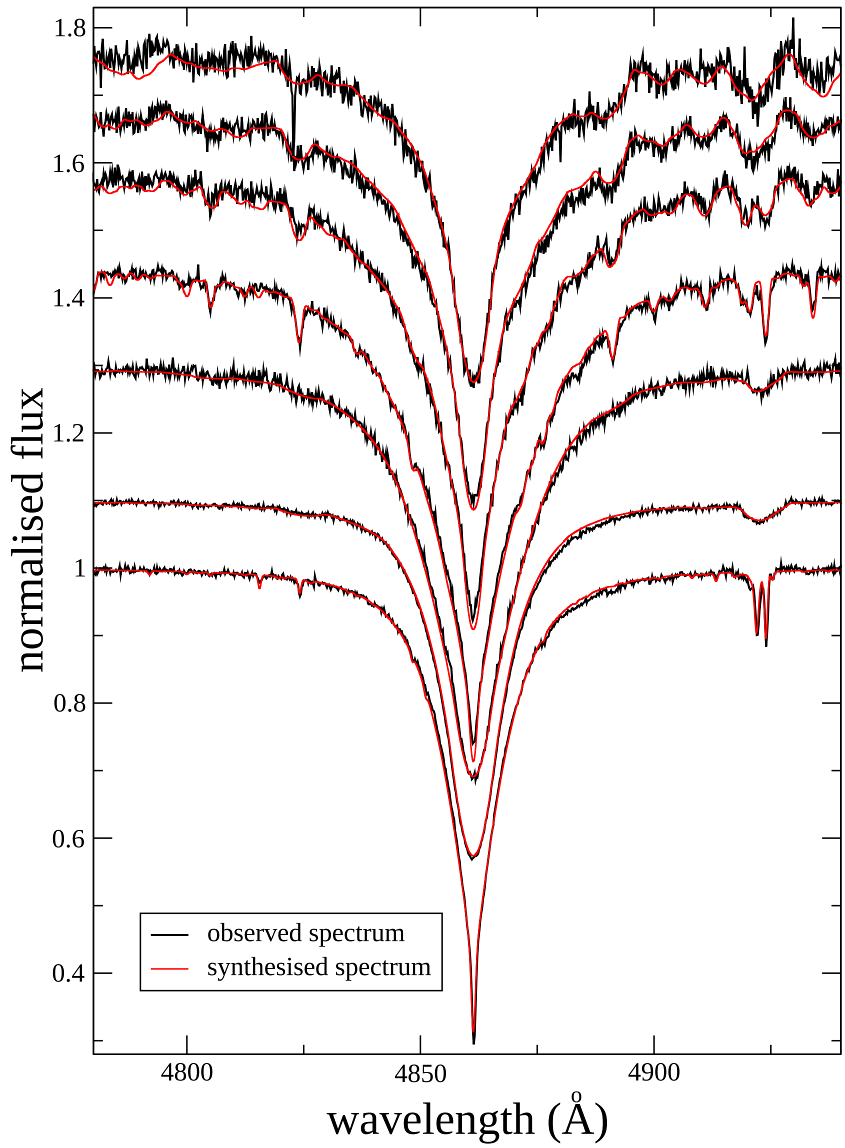

Figure 4.2: Comparison between the observed Hβ line profile (thick black lines) and synthetic line profile (thin red lines) for seven stars observed with FLAMES/GIRAFFE. From top to bottom the stars here displayed are: UCAC 11104969 ($T_{\rm eff}$ = 7050 K), UCAC 11105106 ($T_{\rm eff}$ = 7500 K), UCAC 11105176 ($T_{\rm eff}$ = 8100 K), CPD-47 6385 ($T_{\rm eff}$ = 9350 K), CD-47 8868 ($T_{\rm eff}$ = 10400 K), HD 123202 ($T_{\rm eff}$ = 11400 K) and HD 123226 ($T_{\rm eff}$ = 12400 K). The stars are here shown in order of increasing $T_{\rm eff}$ from top to bottom. For display purposes I applied an arbitrary vertical shift.

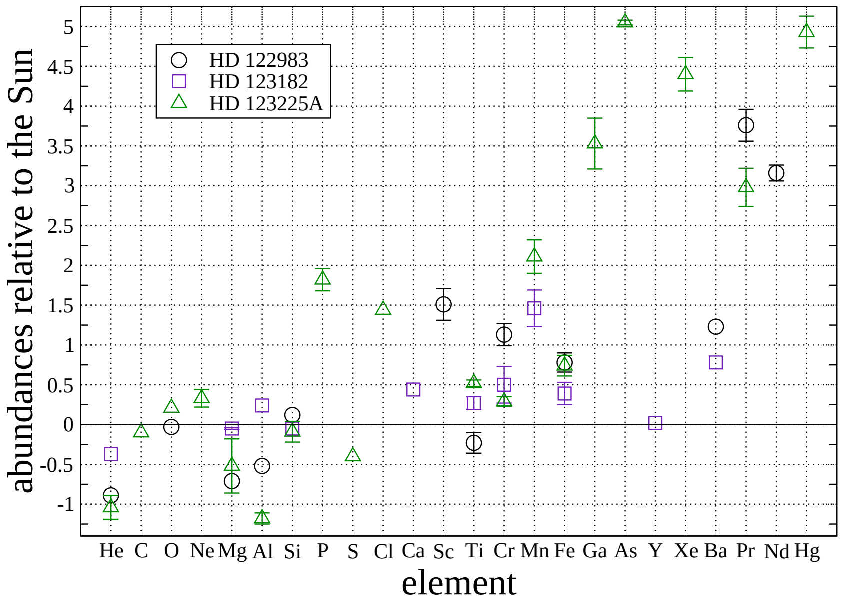

Figure 4.3: Elemental abundances relative to the Sun (Asplund et al. 2005) of HD 122983, HD 123225 and HD 123182. The error bars are the standard deviation from the mean abundance.

star. Sc lines are not measurable from the observed spectrum, so it is not possible to say whether it is underabundant or not. The not extreme overabundance of Cr and Fe (related to the rather high $\upsilon \sin i$), and the fact that Hg, P and Xe are not visible (although lines are present in the observed wavelength range) are in agreement with the Am possible classification. On the other side the clear Mn overabundance would tend more to a HgMn classification. On the basis of the available data I can only conclude that HD 123182 is a He-weak star of an unclear type. As already mentioned this star could also be a single line spectroscopic binary, due to the high measured radial velocity, compared to the other cluster stars.

HD 123183

HD 123183 was observed with FORS1 by Bagnulo et al. (2006) who published a marginal magnetic field detection of $< Bz >$ = -440 ± 146 G. The abundance pattern (see Table 4.6) does not reveal any peculiarity that could strengthen this detection. The very high $\upsilon \sin i$ of 275 ± 14 km s^{-1} goes as well against a classification of this object as chemically peculiar. For this reason I conclude that this object is a ”normal” early-type star.

HD 123225

HD 123225, observed with FLAMES/UVES, is another newly discovered SB2 star. Thanks to the characteristics of Binmag, to the slow rotation of the two components, to the high resolution, to the large wavelength coverage and to the large separation between the spectral lines of the two stars, it was possible to perform a rather accurate parameter determination and abundance analysis of the primary component and a parameter determination of the secondary. The radio ratio that best fits the observed spectrum is $R_{primary}/R_{secondary}$ = 1.32. Figure 4.4 shows the obtained best fit of the observed Hβ line profile. The primary component (the hot-

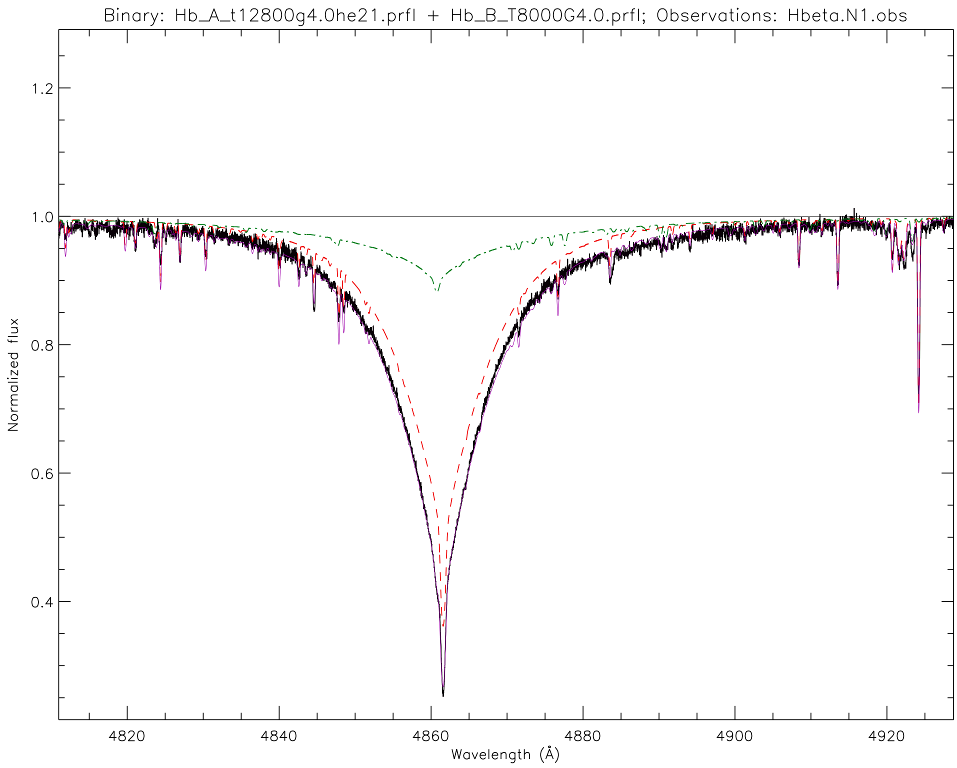

Figure 4.4: Best fit of the observed Hβ line profile for HD 123225. The black solid line is the observed spectrum. The red and the green dashed lines are the spectra of the primary and secondary components respectively scaled according to the given radio ratio. The violet solid line is the synthetic spectrum of the system.

ter star) is a HgMn star, as clearly shown by the abundances pattern displayed in Fig. 4.3. HD 123225 was observed with FORS1 by Bagnulo et al. (2006), but no magnetic field was detected.

The secondary component of this system shows solar abundances, although there is the possibility that this star is an Am star for the following reason. Since the primary component is a low $v \sin i$ HgMn star, it is likely that also the low

$v \sin i$ of the secondary component is due to an intrinsic slow rotation, that at this $T_{\rm eff}$ could lead to the formation of Am peculiarities. Several high resolution spectra of this object would be extremely valuable to explore this possibility, since a system composed by a HgMn star and by an Am star is not common. Remembering that this is a binary system in an open cluster (meaning that extremely accurate parameters and age could be determined), the accurate abundances that could be obtained by this system would be valuable to give constraints to diffusion models both for HgMn and Am stars.

HD 123201B and HD 123184

HD 123201B and HD 123184 are both "normal" early-type stars and join the common property of showing a different $v \sin i$ for the He lines, compared to the other spectral lines. The $v \sin i$ of HD 123201B, measured on not-He lines, is about 202 km s^{-1}, while He lines are best fit with a $v \sin i$ of about 150 km s^{-1}. The same is found with HD 123184 for which $v \sin i$ is about 65 km s^{-1}, but He lines are best fit with a $v \sin i$ of about 50 km s^{-1}. Figure 4.5 shows the comparison between the observed spectrum and two synthetic line profiles with $v \sin i$ = 65 km s^{-1} and 50 km s^{-1} in the region of the FeII line at ~ 5018 Å and of the He multiplet at ~ 5875 Å for HD 123184. This plot shows that for the He multiplet the adopted stellar $v \sin i$ of 65 km s^{-1}is too large, while a $v \sin i$ of 50 km s^{-1} fits better the observation. In comparison there is the plot of the region around the FeII line showing that the adopted stellar $v \sin i$ of 65 km s^{-1} is correct. Both for HD 123201B and HD 123184 the He abundance was measured with the $v \sin i$ proper of the He lines.

This effect is most likely due to the fact that both stars are fast rotators so that, due to their non-spherical geometry, the poles are hotter than the equator. In such stars He lines are mostly produced in regions around the poles, where $v \sin i$ is actually less. This effect should be visible also in other spectral lines with high $\chi_{\rm excit}$, but, besides He, no other lines with high $\chi_{\rm excit}$ were observed.

CD-47 8879

This is a double line spectroscopic binary with a low $v \sin i$ for both components. To solve the binarity, Binmag requests the radio ratio of the system (see Chapter 3). With the parameters given in Table 4.3, the radio ratio ($R_{\rm primary}/R_{\rm secondary}$) that at best fits the observed spectrum is 1.3. Given the $T_{\rm eff}$ (usually chemically "normal" A-type stars are fast rotators) and the $v \sin i$ of the two components, there is the possibility that the orbital plane is very much inclined respect to the line of sight, but if this is not the case and both stars are intrinsically slowly rotating, there is the possibility that they are chemically peculiar (Am, HgMn). A high resolution spectrum or a series of high resolution spectra would allow to check the presence of chemical peculiarity in the atmosphere of these two objects.

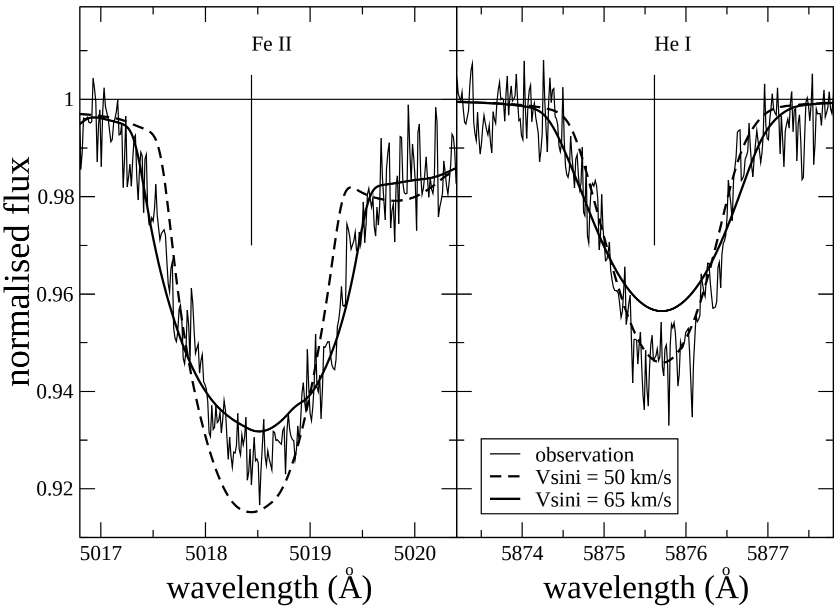

Figure 4.5: Comparison between the observed spectrum (thin line) and synthetic spectra calculated with $\upsilon \sin i = 65\,\mathrm{km\,s^{-1}}$ (thick line) and $\upsilon \sin i = 50\,\mathrm{km\,s^{-1}}$ (thick dashed line) in the region of the FeII line at $\sim$ 5018 Å (left plot) and of the He multiplet at $\sim$ 5875 Å (right plot), for HD 123184.

4.1.4 Abundance patterns in NGC 5460: from F- to B-type stars

Figure 4.6 shows the comparison among the mean abundance pattern obtained for B-, A- and F-type stars considered members of the cluster. The error bars are the standard deviations from the mean abundance. All the G-type stars of the sample were unfortunately not cluster member. In the whole sample, after the assignment of the cluster membership, only three F-type stars were left and of these three objects only one, UCAC 11104969, is a single star with measured abundances, so that the mean abundance of the F-type stars corresponds actually to the abundance pattern of UCAC 11104969.

The mean abundance patterns of the three stellar types are quite similar and concentrated around solar values except for a sulphur overabundance, that cannot be ascribed to non-LTE effects (see Sect. 4.2.10), and for an apparent Am peculiarity of some elements for UCAC 11104969 (Sc underabundance, Y and Ba overabundance). The stars cannot anyway be classified as Am stars since the $\upsilon \sin i$ ($260 \pm 15\,\mathrm{km\,s^{-1}}$) is too high for Am stars because the maximum rotational velocity to let a star evolve Am peculiarities is $90\,\mathrm{km\,s^{-1}}$ (Charbonneau & Michaud 1991). Am stars are also characterised by CNO underabundances and overabundances of the Fe-peak elements, both not present in the obtained abundance pattern.

A very important result of this work is the estimation of the cluster metallic-

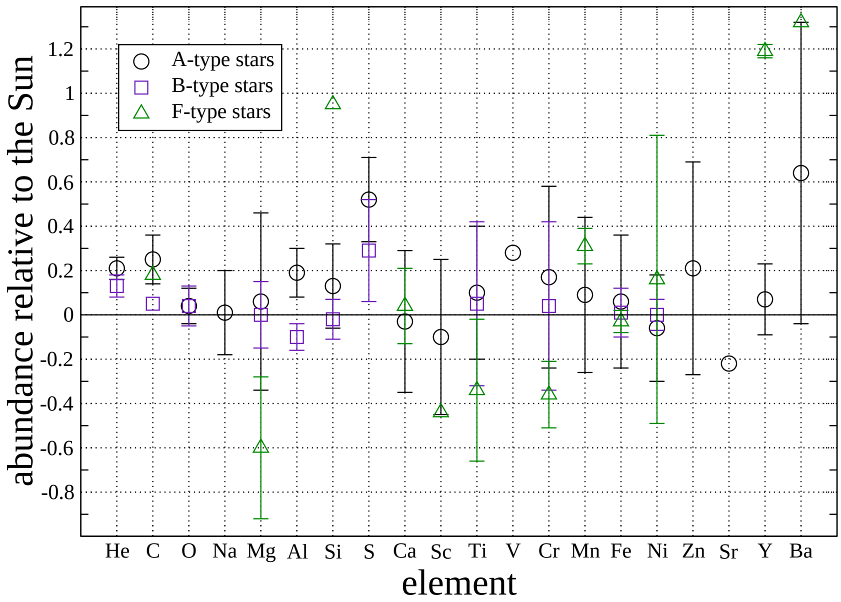

Figure 4.6: Comparison between the mean abundances obtained for B-, A- and F-type stars indicated by an open square, circle and triangle respectively. The error bars are the standard deviations from the calculated mean abundances. The abundance patter of the mean F-type stars is corresponds to the abundance pattern of UCAC 11104969, since it is the only F-type stars of the sample with measured abundances.

ity (Z), unknown up to now. On this point of view, the most important elements are C, O, Si and Fe (without taking into account H and He). For all these five elements there is a fairly good agreement among the three stellar types, excluding the Si abundance of UCAC 11104969[1], that was not taken into account in the determination of Z.

Since the cluster metallicity should be calculated on the basis of the abundances of the cool stars (more mixed) and that only one F-type star is present in the sample, I decided to derive Z from the mean abundance of this one F-type stars and of the cool A-type stars (T_{eff} *leq* 8500 K), that still have a reasonably deep convective zone. In this way I used seven stars of the sample to derive the cluster metallicity Z (I excluded all the SB2s for which no abundances were measured). The Z value I obtained is 0.014±0.003 dex, that has to be compared with the solar value of Z = 0.0122 obtained adopting the solar abundances by Asplund et al. (2005). The obtained cluster Z shows that NGC 5460 has a solar metallicity.

The Z value used to characterise isochrones is calculated with the following

[1]The star shows a $\upsilon \sin i$ of about 260 km s^{-1} and the Si abundance was derived only from one line. This makes the Si abundance determination extremely uncertain.

approximation:

$$Z_{cluster} \simeq 10^{([FE/H]_{\mathrm{F}stars}-[Fe/H]_{\odot})} \cdot Z_{\odot} \, , \qquad (4.1)$$

assuming $Z_{\odot}$=0.019 dex. I recalculated the Z value of NGC 5460, according to this approximation, obtaining Z = 0.011±0.005. This value was derived from the mean Fe abundance of the seven stars taken into account ([Fe/H] = -0.22±0.22 dex).

4.1.5 HR diagram

Using the stellar magnitudes given by Claria et al. (1993), I built the color-magnitude (CM) diagram of the cluster using the stars of the available sample. The CM diagram is shown in Fig. 4.7 together with an isochrone by Girardi et al. (2002) corresponding to an age of $\log t$ = 8.20 and solar metallicity (Z = 0.019). The plot was made considering a distance modulus of 9.44 mag and a reddening of 0.092 mag, both values given in WEBDA.

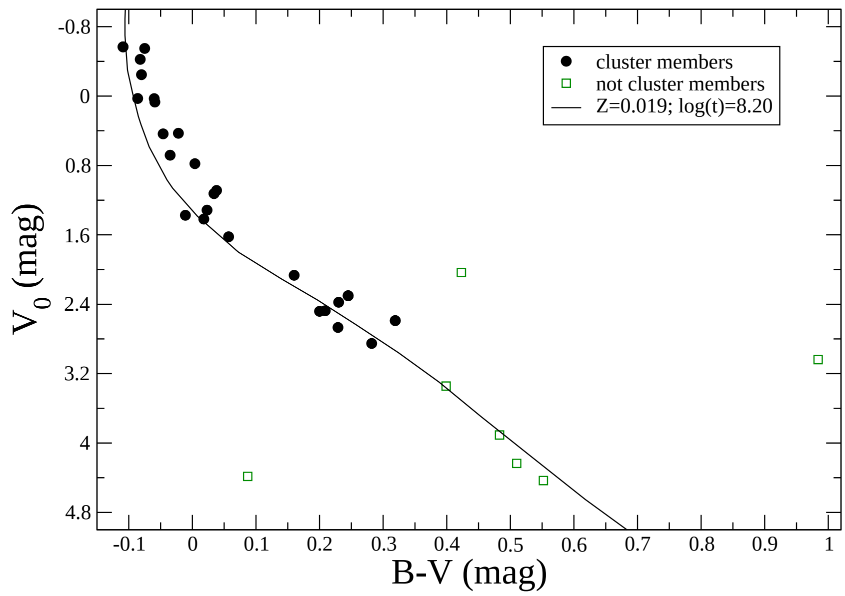

Figure 4.7: Color-magnitude diagram of the cluster produced using the photometry given by Claria et al. (1993). The full circles show the position of the cluster members, while the open squares denote the not cluster members. The full lines corresponds to an isochrone from Girardi et al. (2002) for an age of $\log t$ = 8.20 and solar metallicity.

The CM diagram shows clearly the not membership of three stars, while, for the four stars laying on the isochrone and denoted as non cluster member, the not membership was given from the analysis of the color-color (CC) diagram (Claria et al. 1993).

With the temperatures obtained for the abundance analysis and the magnitudes given by (Claria et al. 1993), I built the HR diagram of the cluster (Fig. 4.8). As already mentioned, to built the HR diagram, I adopted a distance modulus of 9.44 mag, a reddening of 0.092 mag (both values given in WEBDA) and the bolometric correction given by Balona (1994). In Fig. 4.8 I do not show the stars considered not member of the cluster.

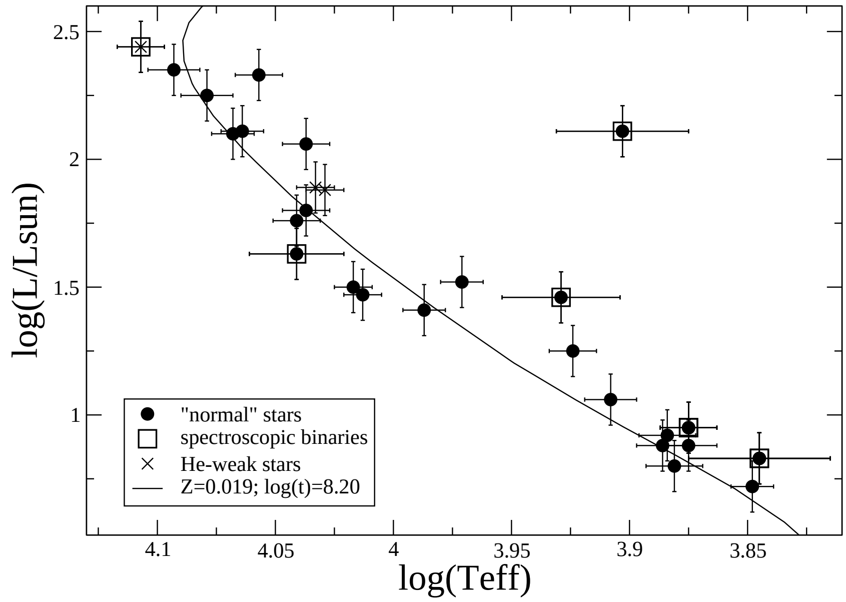

Figure 4.8: Hertzsprung–Russell diagram of NGC 5460. The crosses and filled circles show the position on the HR diagram for the He-weak and normal B-, A- and F-type stars, respectively. The open squares indicate the spectroscopic binaries. I did not correct the luminosity of these stars due to the presence of the companion so that their position on the HR diagram could be very different from how it appears on the plot. The error bar in luminosity is 0.10 dex. The full line shows an isochrone from Girardi et al. (2002) for an age of $\log t$ = 8.20 and solar metallicity (Z = 0.019). The not cluster member stars are not shown.

Luminosities are listed in Table 4.9. With a distance modulus uncertainty of 0.20 mag, an uncertainty in the bolometric correction of about 0.07 mag, and a reddening uncertainty of 0.01 mag, I estimate the typical uncertainty in $M_{\rm bol}$ being about 0.28 mag, corresponding to an uncertainty in $\log L/L_{\odot}$ of about 0.10 dex.

In the HR diagram I separated the chemically normal stars (full circles) and the He-weak stars (crosses) and highlighted the spectroscopic binaries (open squares). I did not correct the luminosities of the spectroscopic binaries so that their real position on the HR diagram could be very different from what it is shown in Fig. 4.8. A clear example is given by the star on the top right of the HR diagram, that is the secondary component of HD 123225. The HR diagram shows that this star should have a V magnitude of about 9.9 mag, 1 mag below what adopted here. The correction of the magnitude on the basis of the derived $T_{\rm eff}$ of each component of the SB2 systems could anyway lead to a wrong placement in the HR diagram creating only confusion for the writer and the reader.

The solar metallicity of NGC 5460, obtained in Sect. 4.1.4 has a very important consequence for the parameter determination of the cluster. It confirms that the metallicity of the isochrones adopted in literature up to now to derive the cluster age was correct. The obvious conclusion is that both the distance modulus of 9.44±0.20 mag and the reddening of 0.092 mag and the age of 8.20±0.20 adopted up to now do not require corrections due to a different cluster metallicity. Anyway, a definitive check of this conclusion could be done only performing and abundance analysis of cluster member late-type stars.

4.1.6 Abundances vs. $T_{\rm eff}$ and $\upsilon \sin i$

From Fig. 4.9 to Fig. 4.11 I display the abundances of the most analysed elements against $T_{\rm eff}$, without taking into consideration the abundances of the not cluster member stars. I divided the sample according to their spectral classification: B-type stars (open squares), A-type stars (open circles), F-type stars (open triangles), He-weak stars (crosses).

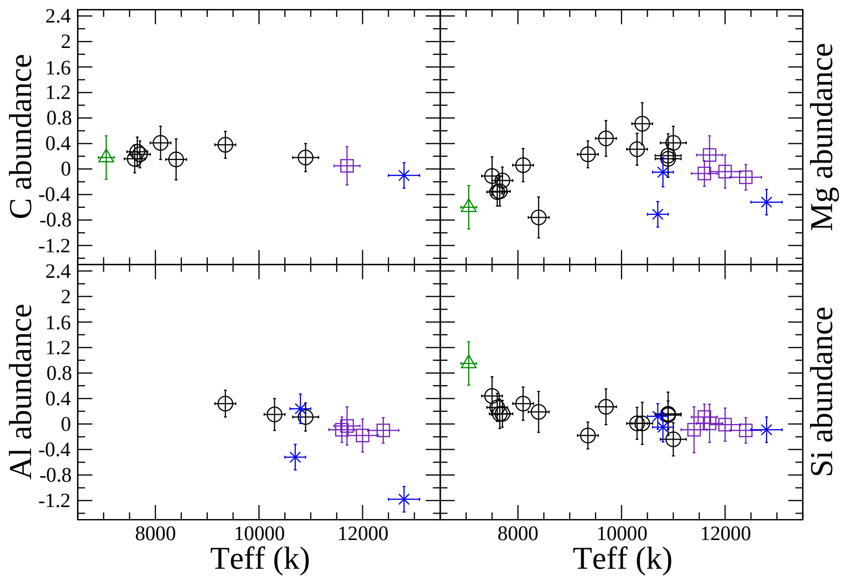

Figure 4.9: Abundances relative to the Sun (Asplund et al. 2005) of C, Mg, Al and Si as a function of $T_{\rm eff}$ for B-type stars (square), A-type stars (circle), F-type stars (triangle) and He-weak stars (cross).

For some elements such as Mg and Fe it is possible to notice a mild correlation of the obtained abundances with $T_{\rm eff}$. In particular for the two mentioned elements,

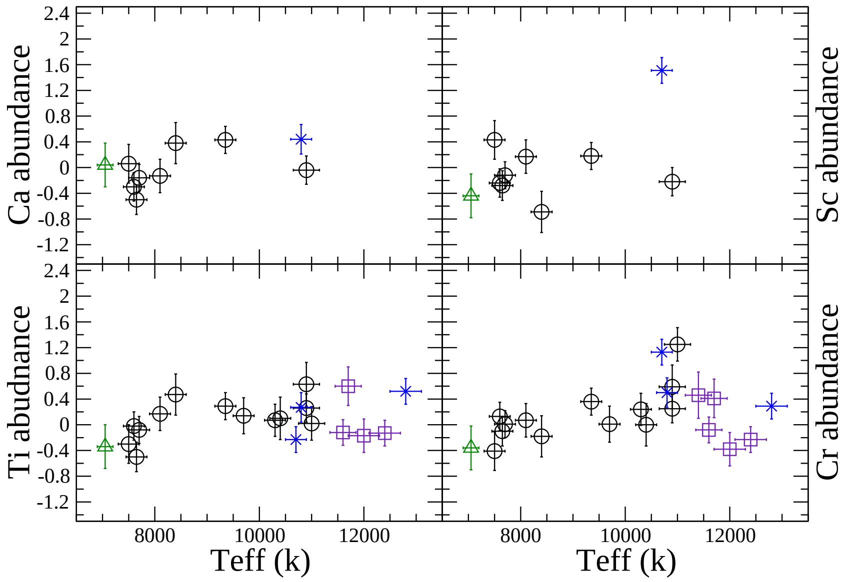

Figure 4.10: Same as Fig. 4.9, but for Ca, Sc, Ti and Cr.

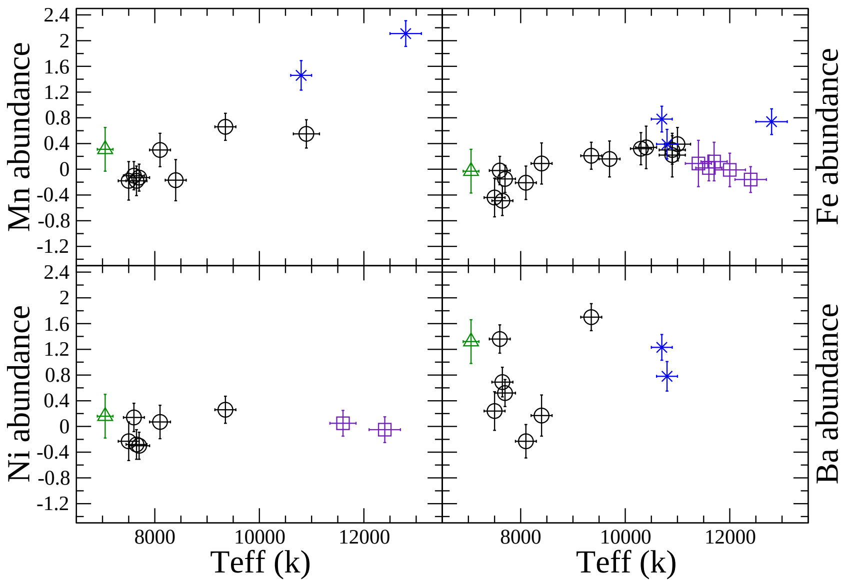

Figure 4.11: Same as Fig. 4.9, but for Mn, Fe, Ni and Ba.

the abundance increases with temperature till $T_{\rm eff} \sim 10500$ K, where it decreases then with increasing temperature.

The trends obtained for Mg and Fe could in principle not be real, but due to other factors, such as $\upsilon_{\rm mic}$, $\log g$ and $\upsilon \sin i$. I exclude that both $\upsilon_{\rm mic}$ and $\log g$

would have produced such trends, since the error bars shown for the abundances take carefully into account the uncertainty on the determination of $\upsilon_{\rm mic}$, and the effect of a log g variation on the abundances is much smaller than what found here. I did not find any clear trend between abundances and $\upsilon \sin i$, as shown in Fig. 4.12, except for a decreasing Ba abundance (diffusion indicator) with increasing $\upsilon \sin i$ up to $\upsilon \sin i$ values of about 150 km s^{-1}, in agreement with predictions by Turcotte & Charbonneau (1993).

I went to look for such correlation in other sample of stars consistently analysed and present in literature. Luck & Heiter (2005) has consistently analysed a sample of 114 stars in the local vicinity, covering the $T_{\rm eff}$ range between 4000 and 7500 K. For the hottest stars of their sample there is no presence of any correlation of the Fe abundance with $T_{\rm eff}$, but their sample above $T_{\rm eff}$ = 6500 K is composed only by four stars. Erspamer & North (2003) consistently analysed the spectra of 140 A- and F-type stars, present in the ELODIE archive, obtaining fundamental parameters and abundances. Fig. 4.13 shows a comparison between the results obtained in NGC 5460 and what published by Erspamer & North (2003) for C, Mg, Ti and Fe.

The comparison reveals a good agreement for both Mg and Fe, although the trends appear less pronounced in the data by Erspamer & North (2003). They plot as well the abundances as a function of $T_{\rm eff}$ but only in the $T_{\rm eff}$ range between 6500 and 7500 K, not enough to show large scale trends. Unfortunately the sample of stars presented by Erspamer & North (2003) did not cover temperatures higher than 10500 K, so that it is not possible to check the presence of the abundance drop visible here.

In literature there are some abundance analysis of open cluster stars and different authors looked for trends between abundances and $T_{\rm eff}$. One of the first abundance analysis of early-type cluster stars was presented by Varenne & Monier (1999), but the range in $T_{\rm eff}$ of their sample of stars was too small to show what I obtained here. Gebran & Monier (2005) presented the Fe abundance obtained in the α Persei open cluster as a function of $T_{\rm eff}$ in a large temperature range, from 7000 to 16000 K. Their plot shows a mild trend that might be similar to what here found, but the number of analysed stars is not large enough, in particular around 10000 K, where I obtain the abundance drop. Gebran & Monier (2008) presented an abundance analysis of early type stars in the Pleiades open cluster. The sample of stars they analysed covers quite uniformly the temperature range between 6500 and 10000 K, but from their data does not appear any trend similar to what obtained here.

With the increase of the effective temperature the hydrogen and helium ionisation zones are shifted more and more towards the surface of the star. As a consequence the convection zones, close to the stellar surface become thinner and less turbulent. But the fact that they become less turbulent does not mean that the atmospheres of normal A- and B-type stars are static. In these kind of stars there are clear signatures of microscopic and macroscopic transports. For example, it is well known that Ba is always overabundant in early-type stars, clear signature of an

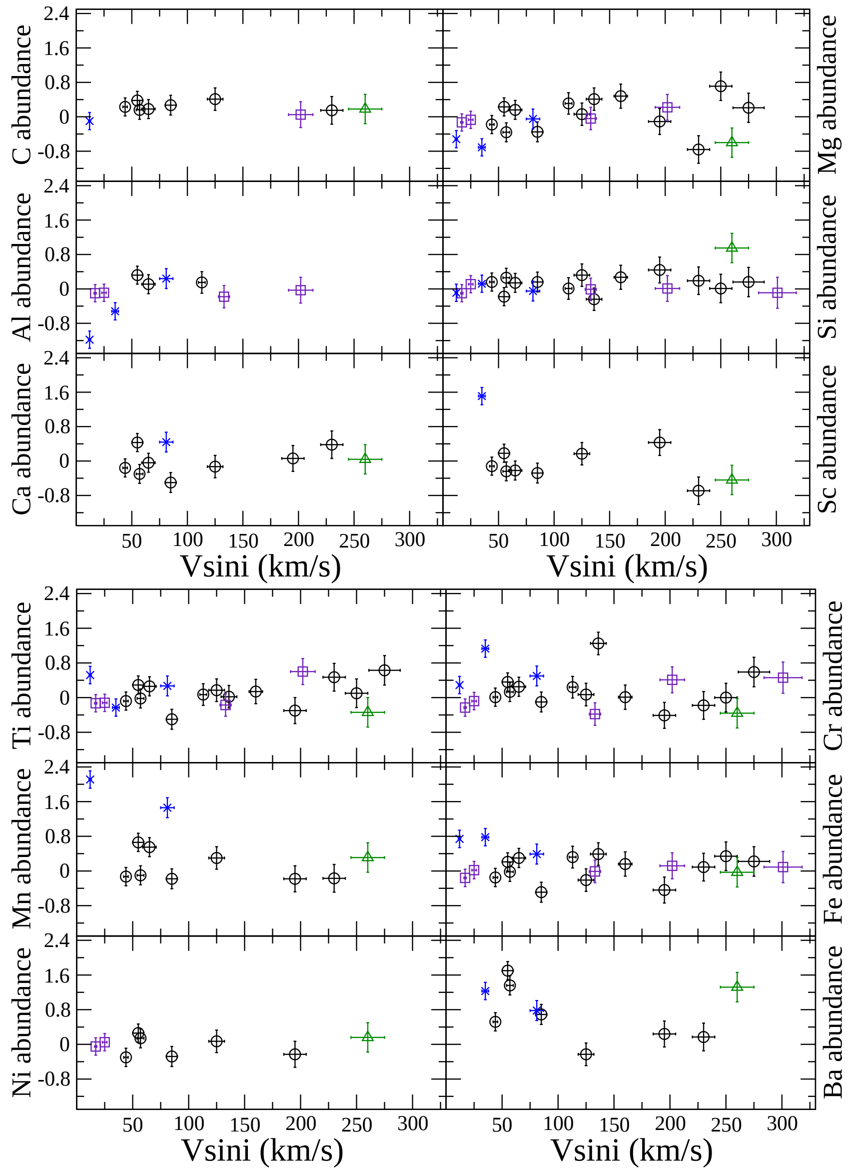

Figure 4.12: Abundances relative to the Sun (Asplund et al. 2005) as a function of $\upsilon \sin i$ for B-type stars (square), A-type stars (circle), F-type stars (triangle) and He-weak stars (cross).

influence of gravitation and radiation (diffusion) even in chemically normal stars. Another example is given by the presence of a correlation between strontium and oxygen or strontium and magnesium, obtained for chemically normal B-type stars by Hempel & Holweger (2003). Where strontium is overabundant, Mg and O are underabundant, in other words, where strontium is radiatively driven outwards, Mg

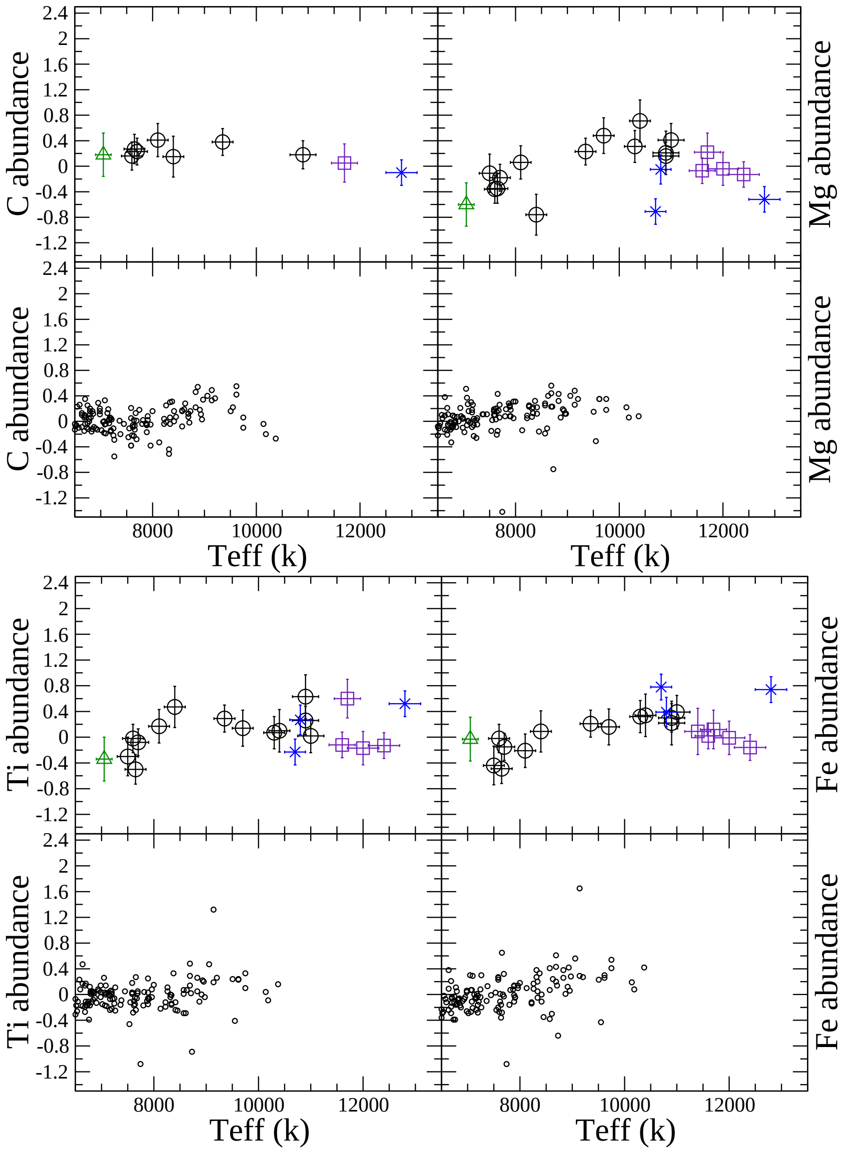

Figure 4.13: Comparison between the results obtained in this work (upper plots with error bars) and by Erspamer & North (2003) (lower plots without error bars). The upper figure shows the comparison for C and Mg, while the lower figure for Ti and Fe. B-type stars are denoted with squares, A-type stars with circles, F-type stars with triangles and He-weak stars with crosses.

and O sink down. For this reason it should not be very surprising that correlations with $T_{\rm eff}$, such as the ones here obtained, are found.

I have to mention that there is also another possibility that would explain at least the increase of the iron abundance with effective temperature. Non-LTE effects for

FeI are known to increase with increasing $T_{\rm eff}$ (Rentzsch-Holm 1996), and the iron abundance given for the cool stars of the sample is essentially given by the FeI lines, dominant in number on the FeII lines. For this reason the increase of the Fe abundance with $T_{\rm eff}$ up to about 8500 K could be due to non-LTE effects. If it would be so, it would then be anyway not straightforward to understand and explain without diffusion the strong decrease of the Fe abundance for the hotter stars, since FeII (the dominant iron ionisation stage for these stars) should not be strongly affected by non-LTE effects at these $T_{\rm eff}$.

The efficiency of diffusion processes is actually reduced by rotation. In particular, simulations carried out by Turcotte & Charbonneau (1993) show that for rotational velocities higher than 125 km s^{-1} the envelope results to be completely mixed. This would suggest that correlation between abundances of diffusion indicator elements (such as Sr, O, Mg, Ba) and $\upsilon \sin i$ should be obtained even for chemically normal star. The problem, in this case, is that $\upsilon \sin i$ represents the projected rotational velocity and not the rotational velocity itself. Correlations between abundance and $\upsilon \sin i$ are not obtained here, except for Ba, one of the diffusion indicators, for which the abundance decreases mildly with $\upsilon \sin i$, up to $\upsilon \sin i$ values of about 150 km s^{-1}, in agreement with what predicted by Turcotte & Charbonneau (1993). Probably a much larger sample of stars, that include some chemically normal low $\upsilon \sin i$ stars could show the presence or not of this effect. It is therefore important to continue with the analysis of the other observed open clusters in such a way to be able to collect a large amount of stars analysed in a consistent way to be able to detect such effects.

4.1.7 Abundances vs. M/M$_\odot$ and fractional age

For each star of the sample I calculated $M/M_\odot$, fractional age (τ) and their uncertainties according to Landstreet et al. (2007) and listed them in Table 4.9. Since I had to deal with several spectroscopic binary stars for which the magnitude of the single components was unknown, I decided to put them as well in Table 4.9, but with slightly higher error bars, that anyway are not realistic. An example is given by the secondary component of HD 123225 for which the derived $M/M_\odot$ is at least 1 solar mass above the real value. Such stars are also highlighted in Table 4.9 so that the reader is aware that the obtained $M/M_\odot$ and τ should not be taken in consideration.

Three stars of the sample (HD 122983, HD 123183 and HD 123225) are included in the work by Landstreet et al. (2007) and there is a good agreement between the obtained $\log L/L_\odot$ and $M/M_\odot$ values. The very small differences are due to the adoption of a different source for the stellar magnitudes. I adopted the magnitudes given by Claria et al. (1993), while Landstreet et al. (2007) adopted the magnitudes published by Claria (1971).

Figure 4.14 shows the abundances of some well sampled elements as a function of stellar mass. The plots show mild trends similar to what obtained with $T_{\rm eff}$, as expected since $T_{\rm eff}$ and $M/M_\odot$ are strictly related.

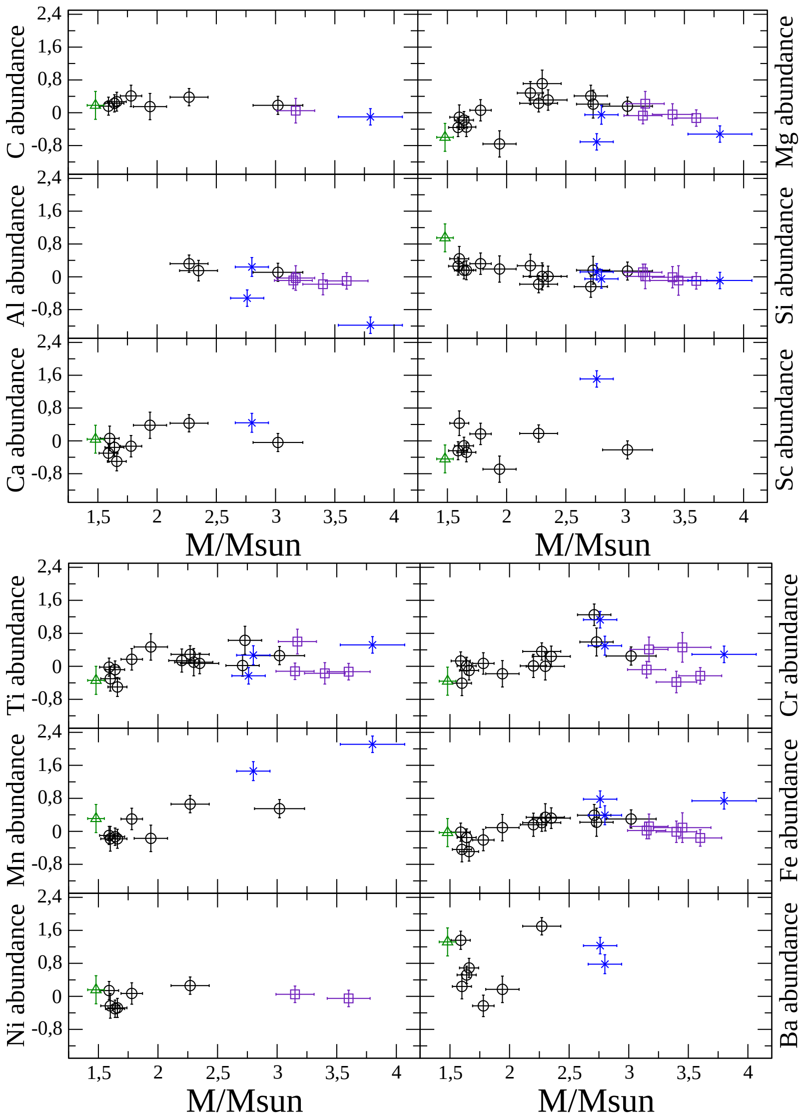

Figure 4.14: Abundances relative to the Sun (Asplund et al. 2005) as a function of $M/M_{\odot}$ for B-type stars (square), A-type stars (circle), F-type stars (triangle) and He-weak stars (cross) of NGC 5460.

4.2 Praesepe

Praesepe (NGC 2632), a nearby intermediate age open cluster ($\log t = 8.85 \pm 0.15$, González-García et al. 2006), is an especially interesting target because it includes a large number of A-type stars, among which are many Am stars. Praesepe is probably the known open cluster with the largest number of Am stars. Furthermore, since the cluster is relatively close to the sun (d = 182 ± 6 pc, van Leeuwen 2007), many of the member A-type stars are bright enough to allow to obtain high resolution spectra with intermediate class telescopes. I analysed spectra of 27 cluster member early-type stars, six of them were observed with the ESPaDOnS spectropolarimeter, four with ELODIE, 16 with SOPHIE and one with the MuSiCoS spectropolarimeter. I personally carried out the observations of fourteen of the sixteen stars observed with SOPHIE.

The results presented in this section of the thesis regarding the Praesepe open cluster are also published in three papers: Fossati et al. (2007), Fossati et al. (2008a) and Fossati et al. (2009a).

4.2.1 Target list

Table 4.10 lists the complete sample of stars observed and analysed in the Praesepe cluster. In the sample eight objects are Am stars, while all the others are chemically normal A-type stars. Seven stars are spectroscopic binaries. Eight stars are present in the δSct variable star catalog by Rodríguez et al. (2000). One star (HD 73993) is present in the Combined General Catalogue of Variable Stars (Samus & Durlevich 2004), but the variability type is listed as "unknown".

HD 73709 was observed with the MuSiCoS spectropolarimeter, now decommissioned and substituted by NARVAL, mounted at the 2-m Bernard Lyot Telescope (TBL) of the Pic du Midi Observatory. I did not include the description of MuSiCoS in Chapter 2 because I performed the abundance analysis of only one archive spectrum that was already used for measurement of the mean longitudinal magnetic field by Shorlin et al. (2002). MuSiCoS, as ESPaDOnS, consists of a table-top cross-dispersed echelle spectrograph fed via a double optical fiber directly from a Cassegrain-mounted polarisation analysis module. MuSiCoS provides a Stokes V, Q or U stellar spectrum from 4500 to 6600 Å with a mean resolving power of 35 000. A more detailed description of the instrument and of the observing procedures are reported by Donati et al. (1999).

All the stars in the sample (including the spectroscopic binaries) were considered as cluster members by several authors: Robichon et al. (1999), Baumgardt et al. (2000), Kharchenko et al. (2004) and Dias et al. (2006). The radial velocities derived for the observed stars, excluding the spectroscopic binaries, confirm the given membership, because they are all compatible with the cluster mean of $34.5\pm0.1\,\mathrm{km\,s^{-1}}$ (Robichon et al. 1999). For several observed spectroscopic binary stars Abt (1970) and Abt & Willmarth (1999) derived the orbit parameters. For all these stars I found a good agreement between the measured υ_{r} and the one calculated with the orbit parameters obtained by Abt (1970) and Abt & Willmarth (1999). The fact that all the observed stars are considered as cluster members confirms the quality of the performed target selection for this cluster.

4.2.2 Results of the abundance analysis

The parameter determination and the abundance analysis were performed as described in Chapter 3, and the set of spectroscopically derived fundamental parameters is shown in Table 4.11

I analysed all the stars in the sample, classified as SB1, as single stars since the secondary does not contribute significantly to the total flux of the spectrum (Budaj 1996; Burkhart & Coupry 1998; Abt & Willmarth 1999; Debernardi et al. 2000).

The obtained abundances for each analysed star are given in Table 4.12 (Am stars and blue straggler), Table 4.13 (F-type stars) and Table 4.14 (A-type stars).

In the following I give some more additional comment for some interesting stars.

HD 72942

The abundance analysis of HD 72942 shows that Ca and Sc are not underabundant and that the Fe-peak elements show an abundance similar to the one of the other normal A-type stars of the cluster. This indicates that the star is a normal A-type stars and not an Am star, as classified by Bond (1972) and given in SIMBAD.

HD 73045

During the abundance determination I noticed an extra broadening of the wings of deep lines, perhaps due to the binarity. To be able to fit these lines I introduced a macroturbulent velocity ($\upsilon_{\rm macro} = 10\,{\rm km\,s^{-1}}$ - obtained fitting several deep lines) to compensate for this effect. The use of the macroturbulence velocity does not lead to any significant abundance change, as expected. In particular the iron abundance calculated without the use of the macroturbulence velocity results to be 0.01 dex lower than the final adopted one.

HD 73174

HD 73174 is an Am star and is the primary component of a quadruple system. For this star, the derived $T_{\rm eff}$ from photometry and from spectroscopy differ by about 700 K and I have no explanation for this effect. For this reason, I keep this star out of the following analysis. Due to the extreme low rotation of this star, it would be probably necessary the analysis of a very high resolution spectrum. In such slowly rotating Am stars, velocity fields (Landstreet 1998) begin to be extremely important for the analysis, but the spectral resolution of ELODIE (R=42 000) is not high enough to allow to take them properly into account.

HD 73666

HD 73666 is an extreme blue straggler (Ahumada & Lapasset 2007) of the Praesepe cluster. The HR diagram (see Sect. 4.2.6) reveals that the star appears to be about 1200 K hotter than the hottest main sequence stars member of the cluster. The mass derived from the HR diagram for HD 73666 is 2.46±0.12 $M_{\odot}$, about 0.5 $M_{\odot}$ more than for the turn-off stars. From $T_{\rm eff}$ and $\log L/L_{\odot}$ I derived a radius of $R/R_{\odot}$ = 2.72±0.12. In Fossati et al. (2009a), with the use of theoretical results on blue straggler formation present in literature, we were able to conclude that HD 73666 was probably formed by physical collision involving at least one binary system, between 5 and 350 Myr (50 Myr if the star is an intrinsic slow rotator) ago. The details of this analysis are presented in Fossati et al. (2009a).

HD 73709

HD 73709 is the primary component of an SB1 quadruple system and was classified as Am by Gray & Garrison (1989), but was found photometrically to be an Ap star by Maitzen & Pavlovski (1987) according to the Δa index (Δa = +0.018 mag). Debernardi et al. (2000), using two ELODIE spectra and observations with the CORAVEL radial velocity scanner, found a magnetic field of 7.5 kG. Shorlin et al. (2002) looked for the presence of such a magnetic field using the LSD technique applied to the same MuSiCoS spectrum here analysed. Their result shows clearly that HD 73709 does not have a significant magnetic field, with the measured value equal to $\langle B_z \rangle = 66 \pm 39$ G. I calculated a synthetic Δa value with respect to the theoretical normality line a_0 determined in Khan & Shulyak (2007, Sect. 3.3.2) and found that Δa = +0.012 mag, which is compatible with the observed value.

4.2.3 Abundances of the Am, A- and F-type stars of the Praesepe cluster

I first grouped all the observed stars according to their spectral classification as F, A and Am stars; Fig. 4.15 shows the mean abundances for each group. The error bars in Fig. 4.15 are the standard deviations from the calculated mean abundances of each group.

The A- and F-type stars show similar abundance patterns, characterised by solar abundances for almost all the elements. The Am stars show the typical abundance pattern characterised by underabundances of C, N, O, Ca and Sc, with a general overabundance of the other elements, in particular of the Fe-peak and heavy elements. As expected, the error bars associated with the abundances of the F-type stars turn out to be comparable to or smaller than those for the A-type stars. It is also possible to see this effect in Figures from 4.19 to 4.21.

I calculated the metallicity of the cluster (Z) from the abundances derived for the F-type stars, excluding HD 73575. This star is close to the TAMS and its Fe abundance differs by 0.27 dex with respect to the mean Fe abundance (0.11±0.03 dex) of the other F-type stars. For this reason I omitted HD 73575 from the determination of the cluster metallicity. The Z value I obtained is 0.015±0.002 dex.

The Z value adopted by several other authors and used to characterise isochrones (see Sect. 4.2.6) is calculated with the approximation shown in Eq. 4.1 and assum-

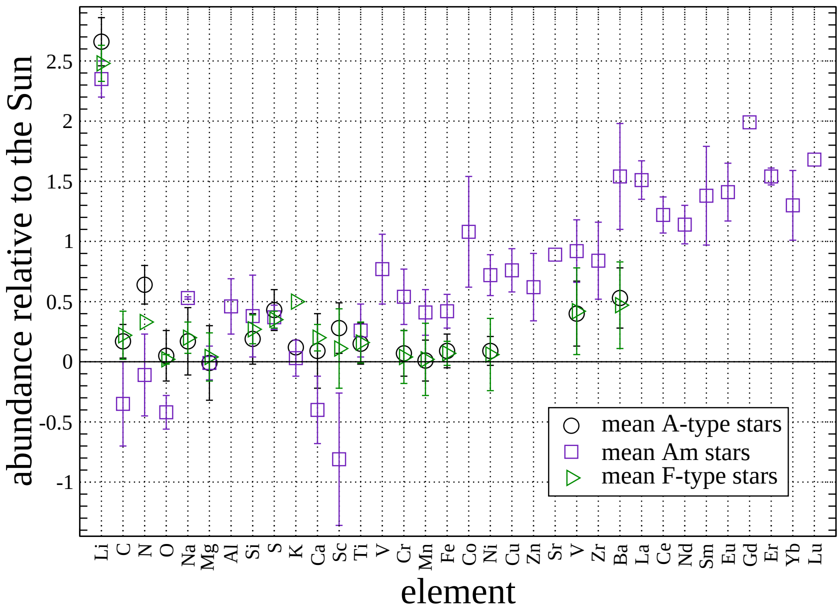

Figure 4.15: Comparison between the mean abundances obtained for Am, A- and F-type stars indicated by an open circle, square and triangle respectively. The error bars are the standard deviations from the calculated mean abundances. In the case of only one measurement, no error bar is shown.

ing $Z_{\odot}$=0.019 dex. I recalculated the Z of the cluster according to this approximation obtaining Z = 0.024±0.002. I derived this value using the mean Fe abundance of all the F-type stars except HD 73575 ([Fe/H]=0.11±0.03 dex).

My estimated metallicity is in agreement with that included in the catalogue of Chen et al. (2003) of [Fe/H]=0.14 dex and with that recently obtained by An et al. (2007) of [Fe/H]=0.11±0.03 dex. An et al. (2007) derived the metallicity from an Fe abundance determination from high resolution spectra of four G-type cluster members.

Normal A-type vs. Am stars

The precision obtained with the abundance analysis allows to distinguish clearly the normal A-type stars and the Am stars. For both of them, the abundances of the Fe-peak elements are different. In normal A-type stars, Fe, Ni, and Cr are solar or slightly overabundant (compared to their solar abundances). In Am stars, these elements are clearly overabundant. In all but one of the stars of the sample, Ba is overabundant. However, the Ba abundance is definitely lower in normal A-type stars than in Am stars. This suggests that Ba may be considered as an additional indicator of Am peculiarities, together with C, N, O, Ca, Sc and the Fe-peak elements.

4.2.4 Li abundance

In the context of radiative diffusion theory, it is interesting to examine the atmospheric abundance of lithium in stars where diffusion is known to be active, like in Am stars. Such studies have been carried out especially by Burkhart & Coupry (1991) and Burkhart et al. (2005). Their conclusion was that, in general, the Li abundance in Am stars is close to the cosmic value ($\log N_{Li}/N_{total} \sim -9.04$ dex), although a small proportion of them are deficient. The normal A-type stars result to have a higher Li abundance ($\log N_{Li}/N_{total} \sim -8.64$ dex), in the $T_{\rm eff}$ range 7000–8500 K (Burkhart & Coupry 1995).

I calculated precise Li abundance only for HD 73045 taking into account hyperfine structure, while for HD 73730 and HD 74656 I give an estimation derived from one line and without hyperfine structure. For other stars it was possible to derive only an upper limit, since the higher $\upsilon \sin i$ values did not allow a more accurate abundance determination. In HD 73666 I did not found any Li line (due to the high $T_{\rm eff}$), while for HD 73709 the MuSiCoS spectrum did not cover the strong Li 6707.761 Å line. The determinations confirm the overabundances (relative to the Sun) for three Am stars. Since for all the other stars I can only derive upper limits, I cannot confirm the overabundances. In Fig. 4.16 I show the absolute Li abundance as a function of $T_{\rm eff}$, in comparison with the values given by Burkhart & Coupry (1995).

Since almost all the Li abundances here derived are upper limits it is difficult to address the behavior of the lithium abundance in the temperature range between 7000 K and 8500 K, but I notice that the abundances appear to be higher than those derived by Burkhart & Coupry (1995) in open clusters. I notice as well the tendency of the normal A-type stars to have a higher Li abundance. The results appear to be more consistent with those derived by North et al. (2007) for field stars.

4.2.5 Are weak magnetic fields present in the Am stars of Praesepe?

If magnetic fields are present in Am stars, this might help explain some of the peculiar properties of these stars, such as slow rotation and the typical Ca/Sc underabundances (Böhm-Vitense 2006).

I decided to use the LSD approach to detect magnetic fields in Am stars since this method is the most precise method currently available, especially for stars with rich line spectra and low $\upsilon \sin i$.

Lanz & Mathys (1993) claimed evidence of magnetic fields in the Am star (o Peg - $T_{\rm eff} = 9550$ K) using the difference of equivalent widths of two FeII lines at 6147.741 Å and 6149.258 Å. I did not try to apply the same method to compare my results to theirs as all of the sharp-lined Am stars in my sample are spectroscopic binaries, and the blending due to the spectral lines of the secondary might well affect the subtle signal of a magnetic field. Another problem is due to the fact that my Am stars are cool Am stars and the FeII line at 6147.741 Å is strongly blended by an FeI line, preventing an accurate equivalent width determination.

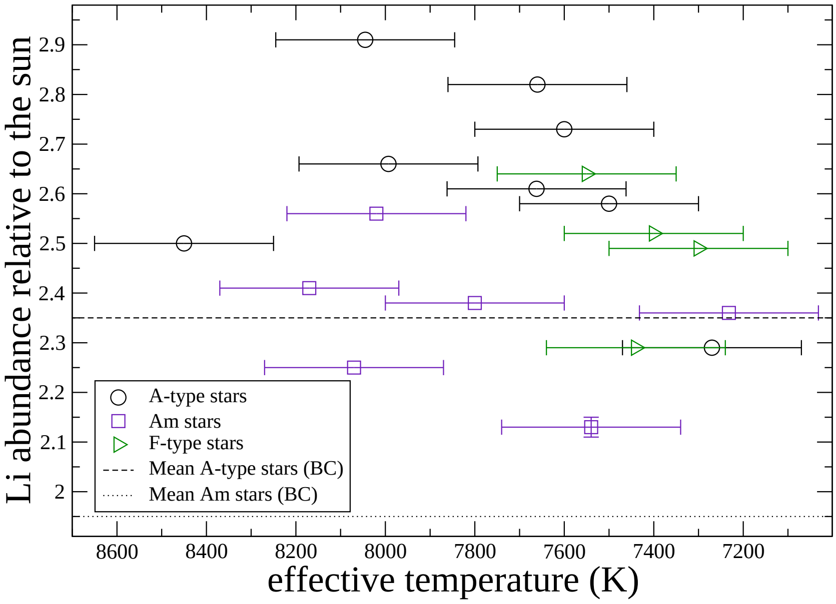

Figure 4.16: Distribution of the Li abundance as a function of the T_{eff}. The dashed line shows the Li abundance value found by Burkhart & Coupry (1995) (BC in the legend) for normal A-type stars. The dotted line shows their Li abundance value for Am stars. The open circles, squares and triangles correspond to the Li abundances of the program A-type, Am and F-type stars respectively.

Shorlin et al. (2002) analysed 25 Am stars with the LSD technique without having found any significant magnetic field signature. These authors concluded that no credible evidence exists for the presence of organised or complex magnetic fields in Am or normal A-type stars.

In this analysis, the three Am stars observed with ESPaDOnS and the one observed with MuSiCoS did not reveal any magnetic field signature in the circular polarised spectra, analysed with the LSD procedure.

The conclusion is that the cool Am stars of Praesepe ($T_{\mathrm{eff}} < 8500$ K) show no evidence of magnetic fields that could explain the well-known phenomena associated with Am stars. These results support and strengthen the conclusion of Shorlin et al. (2002).

Figure 4.17 shows the LSD profile of HD 73045, one of the Am stars observed in circular polarisation. It is clear that no magnetic field was detected.

4.2.6 HR diagram

Using the temperatures determined during the abundance analysis I built the HR diagram of the cluster around the turn-off point (Fig. 4.18). I calculated the luminosity of each star photometrically, adopting the magnitudes in V band given by

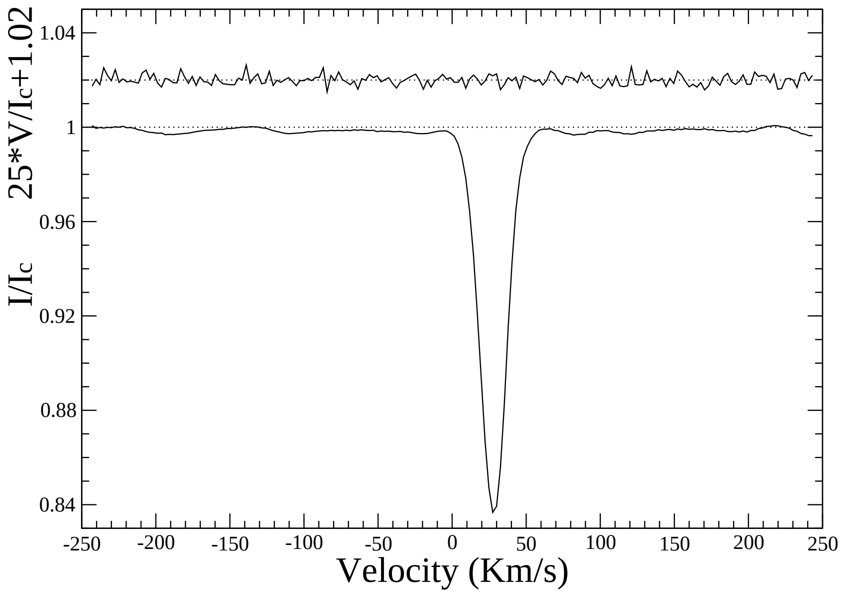

Figure 4.17: LSD profiles for the normalised Stokes *I* and Stokes *V* spectra (from bottom to top) of HD 73045. The Stokes *V* profile is expanded by a factor of 25 and shifted upward of 1.02.

SIMBAD and a cluster distance modulus of 6.30±0.07 mag (van Leeuwen 2007). I used a reddening of 0.009 mag (WEBDA) and the bolometric correction given by Balona (1994). Luminosities are listed in Table 4.15. With a distance modulus uncertainty of 0.07 mag, an uncertainty in the bolometric correction of about 0.07 mag, and a reddening uncertainty of 0.01 mag, I estimate that the typical uncertainty in $M_{\rm bol}$ is about 0.15 mag, corresponding to an uncertainty in $\log L/L_{\odot}$ of about 0.06 dex.

In the diagram I divided the sample into Am stars (crosses) and normal A- and F-type stars (full squares). I denoted also (open squares) the spectroscopic binary stars. I did not correct the luminosities of the spectroscopic binaries, as the only information I have about the secondaries is that their contribution to the analysed spectra is not detected. This suggests that their flux contribution is below about 5%.

The two stars located at the top left and top right of the HR diagram are HD 73666 and HD 73575, respectively. HD 73666 is clearly a blue straggler, while HD 73575 should be just at the TAMS. The maximum age of HD 73666 since becoming a blue straggler is given by the age of the isochrone on which it would be at the turn-off point. This is about 350 Myr. HD 73575 deserves a further comment. It is the most evolved star of the cluster and the position close to the TAMS is consistent with this. This star also shows anomalous chemical composition compared with that of the other normal F-type stars. The position on the HR

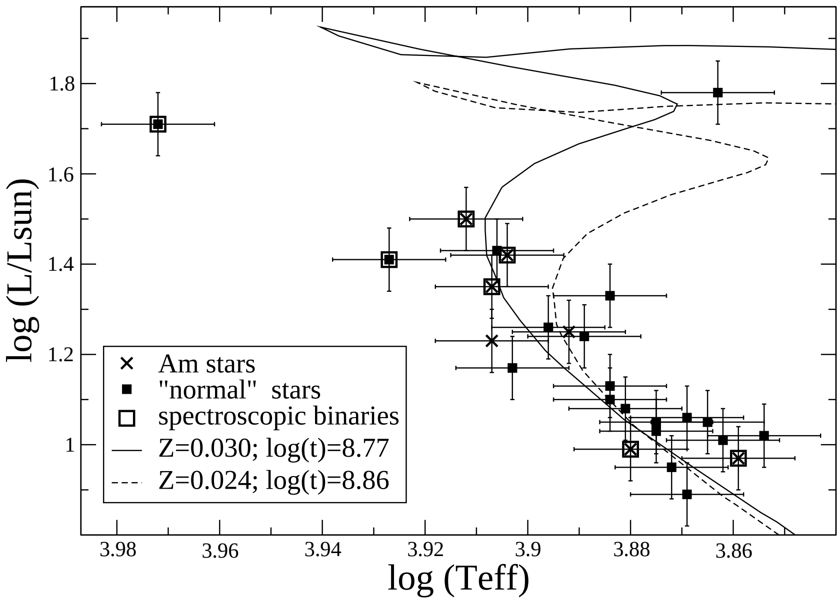

Figure 4.18: Hertzsprung-Russell diagram of the Praesepe cluster. The crosses and filled squares show the position on the HR diagram for the Am and normal A- and F-type stars, respectively. The open squares indicate the spectroscopic binaries (HD 73666 is a speckle binary). I did not correct the luminosity of these stars due to the presence of a companion. This correction is anyway assumed to be less than 0.1 dex. The error bar in luminosity is 0.07 dex. The dashed line shows an isochrone from Girardi et al. (2002) for the age and metallicity given in the literature ($\log t$ = 8.85 dex; Z = 0.024 dex). The solid line shows the isochrone corresponding to my best fit ($\log t$ = 8.77 dex; Z = 0.030 dex).

diagram and the peculiar chemical composition of HD 73575 suggest an unusual evolutionary history.

I adopted isochrones by Girardi et al. (2002) to determine age and metallicity of the cluster using the HR diagram. In Fig. 4.18 I plotted two isochrones: one corresponding to the age and metallicity of the cluster taken from WEBDA ($\log t$ = 8.85 dex; Z = 0.024 dex; dashed line) and the other corresponding to my best fit on the HR diagram ($\log t$ = 8.77 dex; Z = 0.030 dex; solid line).

An et al. (2007) determined the metallicity of the Praesepe cluster by fitting Yale Rotating Evolutionary Code (YREC, Sills et al. 2000) isochrones to the main sequence of the cluster, obtained from Johnson photometry. They derived a metallicity of [Fe/H] = 0.20±0.04 corresponding to Z = 0.030±0.003. This result is in agreement with the results of the fit of isochrones to the sample of stars around the turn-off point.

All the Am stars are on the main sequence. Only HD 73618 and HD 72942 can be considered blue stragglers (Ahumada & Lapasset 2007), taking into account the age and metallicity given in the literature.

4.2.7 Abundances vs. T_{eff} and $\upsilon \sin i$

The abundances of the elements analysed for most of the stars are displayed against T_{eff} and $\upsilon \sin i$ in the left and right panels respectively from Fig. 4.19 to Fig. 4.21. I divided the sample of stars according to their spectral classification: A-type stars (open circles), Am stars (open squares) and F-type stars (open triangles). This division and visualisation will be retained in the following sections.

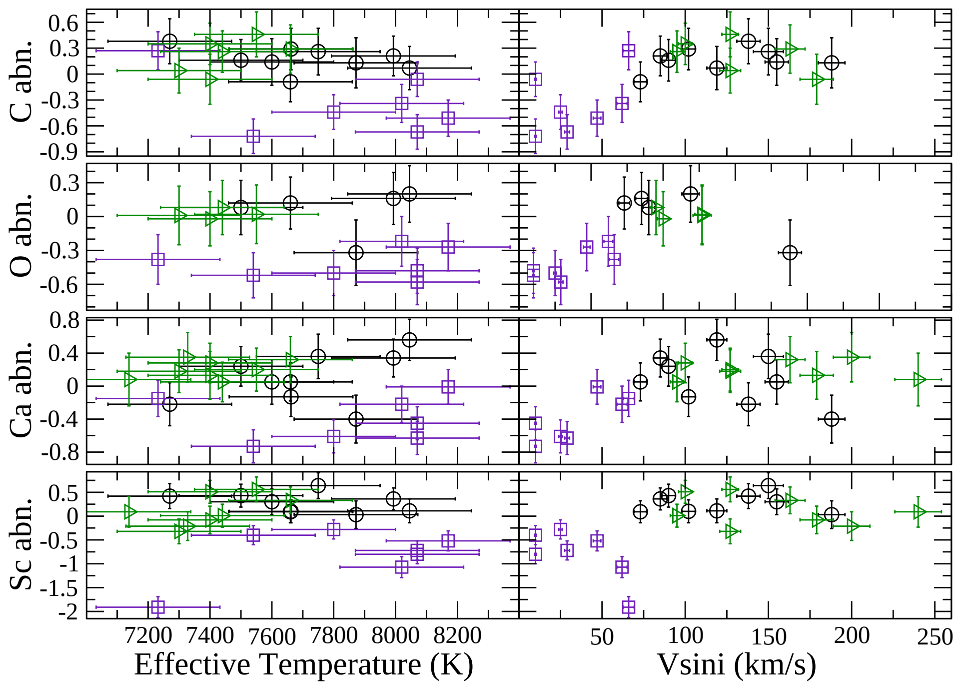

Figure 4.19: Abundances relative to the Sun (Asplund et al. 2005) of C, O, Ca and Sc as a function of T_{eff} and $\upsilon \sin i$ for normal A-type stars (circle), Am stars (square) and normal F-type stars (triangle). A correlation between abundances of C, O, Ca and $\upsilon \sin i$ is found for Am stars; an anticorrelation between Sc abundance and $\upsilon \sin i$ is found for Am stars. For plotting reasons I excluded from the plot HD 72942.

The plots show that the abundances of the F-type stars are less scattered than those obtained for the A-type stars, as expected.

For the normal A- and F-type stars I do not find any clear correlation between abundance and T_{eff} or abundance and $\upsilon \sin i$, except for a hint of correlation between the Mg abundance and T_{eff}. This result is apparently in contrast with what found for NGC 5460. This apparent disagreement can be explained by the large difference in the covered temperature range in the sample of stars collected for the

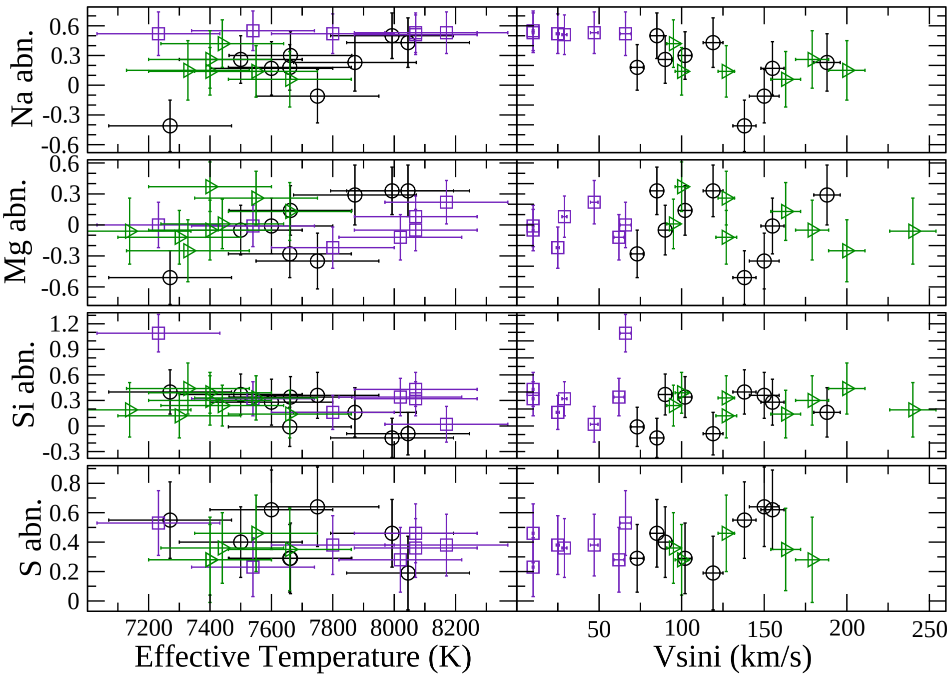

Figure 4.20: Same as in Fig. 4.19 but for Na, Mg, Si and S. No correlation is found.

two open clusters.

For the Am stars, none of the plotted elements, except Y, shows any trend between abundance and $T_{\rm eff}$. Richer et al. (2000) predict mild correlations between abundances of some elements (e.g. Ni) and $T_{\rm eff}$, but probably the temperature range is not large enough to show such correlations.

In Am stars, I find a correlation between abundance and $\upsilon \sin i$ for all peculiar elements, except for scandium and titanium. As described in detail in Sect. 4.2.3, Am stars of the Praesepe cluster show peculiarities mainly for C, O, Ca and Sc (underabundant) and Ti, Cr, Fe, Ni, Y and Ba (overabundant). C, O and Ca show an increasing abundance with $\upsilon \sin i$. The Fe-peak elements, Y, and Ba show a decreasing abundance with $\upsilon \sin i$. Na, Mg, Si and S are not peculiar in Am stars and they do not show any correlation with $\upsilon \sin i$. As a general behavior, the peculiarities decrease with $\upsilon \sin i$, becoming closer and closer to the abundances typical of the normal A- and F-type stars of the cluster. The behavior was recently confirmed by Takeda et al. (2008). Scandium and titanium are exceptions: Ti does not show any clear trend with $\upsilon \sin i$, and Sc shows a trend opposite to that of C, O and Ca, while I would have expected a similar behavior.

Burkhart (1979) derived the abundance anomaly, from the Strömgren m1 index, and $\upsilon \sin i$ values for a sample of well-known Am stars. She suggested a jump in the abundance anomaly for stars with $\upsilon \sin i > 55\,{\rm km\,s^{-1}}$; the results here shown confirm this claim.

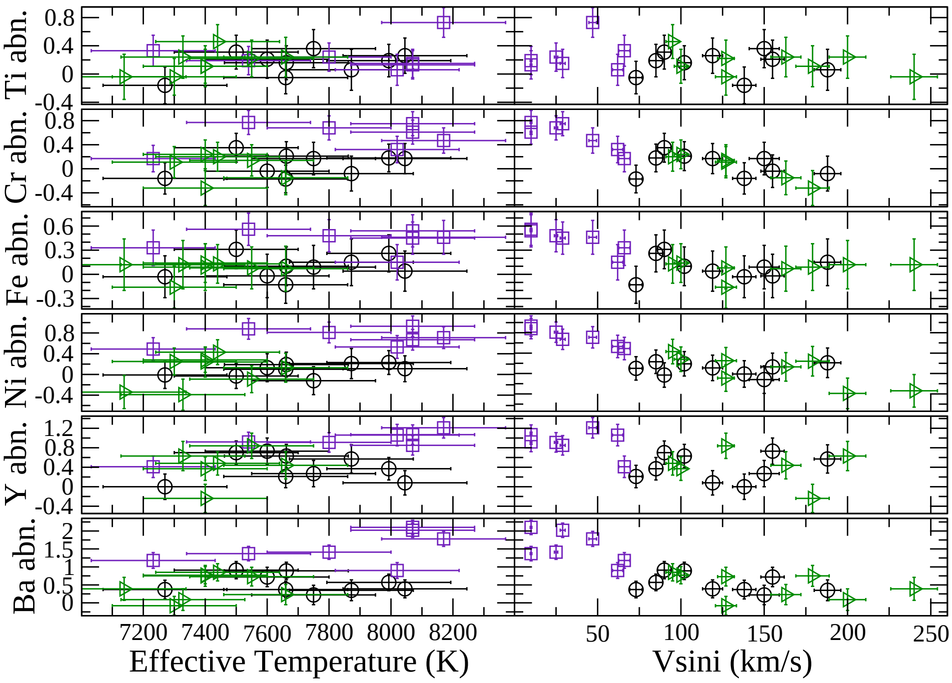

Figure 4.21: Same as in Fig. 4.19 but for Ti, Cr, Fe, Ni, Y and Ba. No correlation is found for Ti. An anticorrelation between Cr, Fe, Ni, Y and Ba abundance and $\upsilon \sin i$ is found for Am stars.

Models by Charbonneau & Michaud (1991) do not predict any strong correlation between element abundances and rotational velocity: "For FmAm stars, it was shown quantitatively that despite the potentially inhibiting effects of meridional circulation on chemical separation, no dependence of abundance anomalies on $\upsilon \sin i$ is expected, for most elements, in the rotational velocity interval characteristic of FmAm stars.". The correlations here obtained between abundance and $\upsilon \sin i$, for the Am stars, are in disagreement with the predictions of Charbonneau & Michaud (1991).

Richer et al. (2000) found that element abundances in model Am stars are dependent only on the depth of the zone mixed by turbulence, thus showing that the abundance anomalies in Am stars depend mainly on the turbulence model.

More recently, Talon et al. (2006) tested rotational mixing models with both the Geneva-Toulouse and Montreal codes. They showed how the predicted surface abundances of FmAm stars should vary as a function of rotational velocity of the star. My findings support their predictions.

4.2.8 Abundances vs. M/M$_\odot$ and fractional age

For the stars in the sample I calculated M/M$_\odot$, fractional age (τ) and their uncertainties according to Landstreet et al. (2007) and listed them in Table 4.15.

I took the abundances of three representative elements (Mg, Ca and Fe) showing, for the Am stars, the three different properties discussed in Sect. 4.2.7. I plot the abundances of these elements as functions of M/M$_\odot$ and display the results in Fig. 4.22.

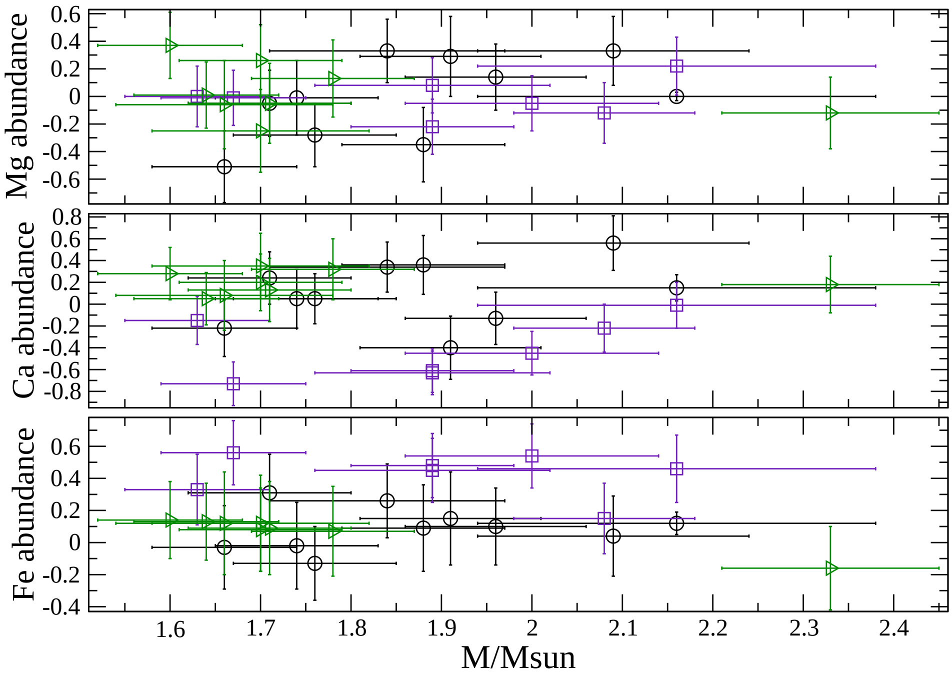

Figure 4.22: Abundances relative to the Sun (Asplund et al. 2005) of Mg, Ca and Fe as a function of the M/M⊙. No correlations are found.

No clear correlation is visible for any of the three plotted elements, for the normal or the Am stars.

Richer et al. (2000) suggest that the abundance anomalies typical of Am stars depend very little on the mass and therefore fractional age of the star (in an open cluster where I assume that all the stars are coeval). This is consistent with the results of this study.

4.2.9 Searching for correlations between abundances

In a sample of seventeen Am stars, Adelman & Unsuree (2007) found significant correlations between the abundances of twelve elements.

The abundances of the elements analysed in most of the stars of the sample are displayed against the Fe abundance in Fig. 4.23 and Fig. 4.24.

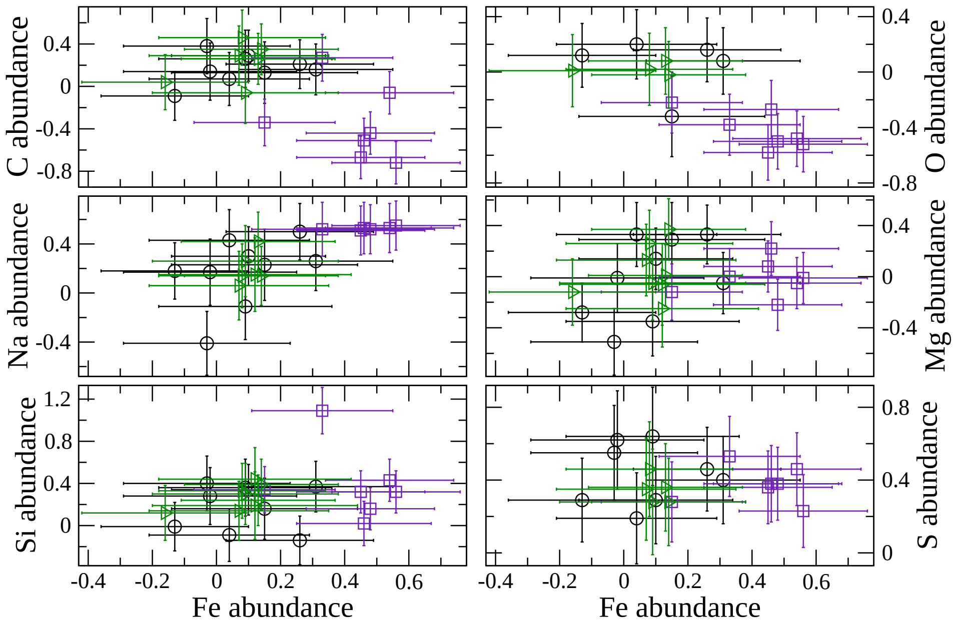

Figure 4.23: Abundances relative to the Sun (Asplund et al. 2005) of C, O, Na, Mg, S and Si as a function of the Fe abundance.

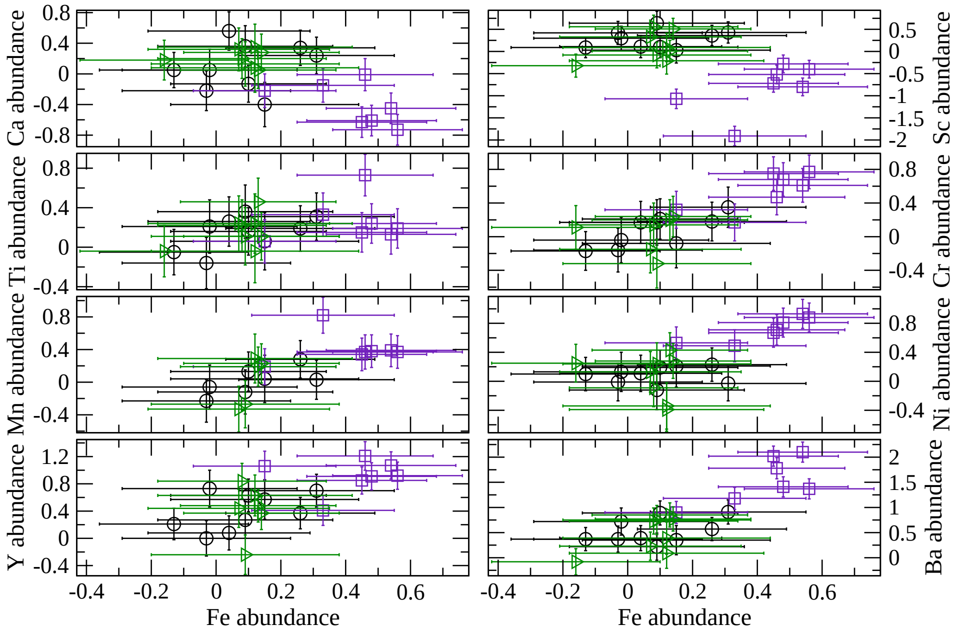

Figure 4.24: Same as in Fig. 4.23 but for Ca, Sc, Ti, Cr, Mn, Ni, Y and Ba.

I do not find any clear correlation between the abundances of any element and Fe for the A- and F-type stars due to the tiny spread in Fe abundance.

In contrast, the Am stars show correlations for all the elements in which a correlation was already found with $\upsilon \sin i$. The Fe abundance is an indicator of Am peculiarities. As I found a correlation between $\upsilon \sin i$ and Am peculiarities, it is not surprising to obtain similar correlations with the Fe abundance.

The correlations found for C and O are in agreement with those found by Savanov (1995) in a sample of seventeen well-known Am stars analysed by different authors. They looked for a correlation between the C abundance and $\upsilon \sin i$, but without any positive result.

From my results it is clear that these correlations are related to those found with $\upsilon \sin i$ in Sect. 4.2.7.

4.2.10 Constraints to the diffusion theory

Underabundances of Sc and/or Ca and overabundances of iron-group elements are qualitatively explained by diffusion theory (see, e.g., the review in the introduction by Alecian (1996) and references therein). In particular, following Alecian (1996), Richer et al. (2000) developed a detailed modeling of the structure and evolution of Am/Fm stars, taking into account atomic diffusion of metals and radiative accelerations for all species in the OPAL opacities.

The results of this work can be used to constrain diffusion models, and I can compare my results with theoretical predictions (Fig. 4.25). For the comparison, I use the mean Am abundances shown in Fig. 4.15.

Figure 14 of Richer et al. (2000) shows the predicted abundances from a diffusion and turbulence model as a function of time and effective temperature. Open circles (reported also in Fig. 4.25) refer to the predicted abundances for 670 Myr old stars, an age that is closely comparable to that one of the Praesepe cluster (~700 Myr, according to González-García et al. 2006). For temperatures around $T_{\rm eff}$ = 8000 K, about the mean temperature of the Am stars of the cluster, the model by Richer et al. (2000) predicts underabundances of -0.3 (relative to the Sun) for C, N and O, of -0.1 for Na, Mg and Ca, solar abundances for Si, S and Ti, overabundances of +0.1 for Al, of +0.3 for Cr and Fe, of +0.4 for Mn, of +0.8 for Ni and +2.3 for Li, within 0.1 dex.

Figure 4.25 shows an agreement for Li, C, N, O, Mg, Al, Si, Ca and Fe-peak elements within 0.1 dex. Discrepancies are instead apparent for Na and S (Sc is not modeled by Richer et al. (2000) because no OPAL data was available for Sc).

Na is the element for which the derived abundance ($\simeq$ 0.5 dex with respect to the solar abundance) has the smallest scatter among the Am stars of the sample. Observations seem definitely to suggest an overabundance of this element which is inconsistent with model predictions of -0.1 dex.

S shows a small scatter in the sample (σ = 0.12 dex). Kamp et al. (2001) analysed the S abundance in the metal poor A-type star λ Boo in LTE and non-LTE. Their analysis shows that the S abundance determined in non-LTE results to

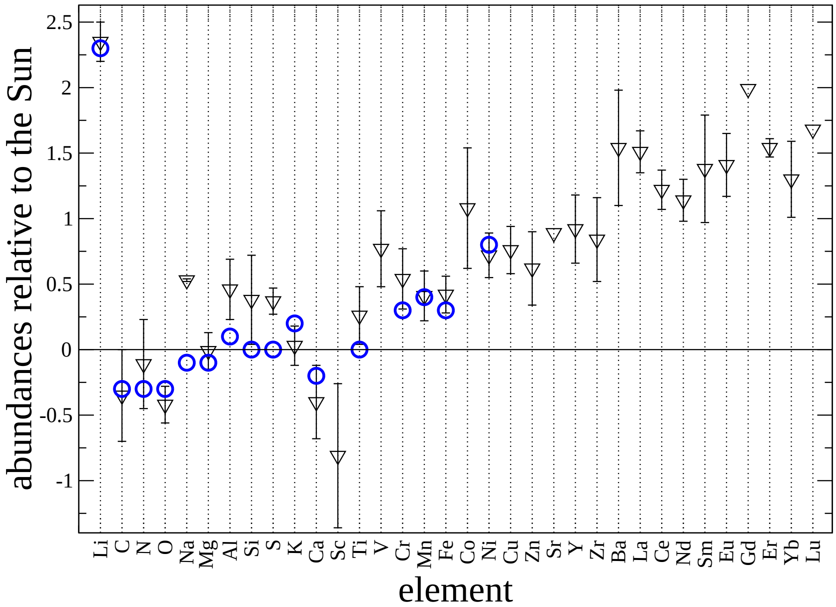

Figure 4.25: The open triangles show the mean Am abundances. The open circles show the predicted abundances displayed in Fig. 14 of Richer et al. (2000).

be lower than the one determined in LTE of 0.1 dex. For metal poor stars non-LTE effects are larger than for normal A-type stars and Am stars. This brings the S abundance ($\simeq +0.35$ dex) to an overabundance (relative to the Sun) of $\geq$0.25 dex, to be compared with a solar abundance predicted by Richer et al. (2000). This apparent discrepancy should be investigated in non-LTE regime.

The results here shown for this cluster indicate that radiative diffusion, combined with turbulent mixing, can account for most of the chemical peculiarities found in Am stars.

Table 4.1: Basic data of the observations for the program stars. For some stars the UCAC catalog name (Dias et al. 2006) was adopted since no other name is given in literature. The second column shows the magnitude of each star in the V_{UCAC} band (Dias et al. 2006). The fourth column indicates the spectrograph used to observe each star (U - UVES; G - GIRAFFE). The fifth column shows the SNR per pixel. For the stars observed with FLAMES/UVES the SNR per pixel is calculated at about 5000 Å. For the stars observed with FLAMES/GIRAFFE the SNR per pixel is calculated for each of the three settings L479/H525/H572 respectively at about 5000 Å, 5200 Å and 5650 Å. SB2 indicates that the object is a double line spectroscopic binary. The spectral types were obtained from SIMBAD or were derived from the automaticaly determined $T_{\rm eff}$ (see text). The latter are denoted with a *. For the SB2 stars, the radial velocity is given in the first line for the primary stars (later denoted as A) and in the second line for the secondary stars (later denoted as B).

Star Name	M_v	Spectral type	Instrument	SNR	υ_r [km s^{-1}]	σ_{υ_r} [km s^{-1}]	Remarks
HD 122983	9.87	B9	G	159/178/213	-24	2	
HD 123097	9.30	B9	G	209/233/275	-20	3	
HD 123182	9.88	B9	G	148/165/195	0	4	
HD 123183	10.11	A0	U	144	-19	7	
HD 123184	9.54	A0	U	195	-15	3	
HD 123201B	9.55	B8	U	199	-20	5	
HD 123202	9.04	B9	G	247/275/323	-19	11	
HD 123225	9.01	B9	U	207	-2	1	SB2
					-53	2	
HD 123226	9.15	B8	G	231/258/306	-12	1	
HD 123269	9.55	B8	G	185/211/243	-20	2	
CD-47 8868	10.66	A0	G	104/116/137	-10	9	
CD-47 8869	10.94	A*	G	96/106/125	-16	5	
CD-47 8879	10.47	A2	G	114/128/151	19	2	SB2
					85	2	
CD-47 8889	10.76	A0	G	99/110/128	-19	4	
CD-47 8905	10.78	A0	G	100/111/131	-18	5	
CD-47 8913	11.17	F*	G	83/92/106	-9	3	
CPD-47 6379	10.17	A0	G	120/134/158	-24	7	
CPD-47 6385	10.46	A0	G	123/135/162	-19	2	
Cl NGC 5460 BB 338	11.80	F*	G	49/55/69	-23	6	SB2
					-23	1	
UCAC 11104969	12.01	F*	G	58/63/76	-17	3	
UCAC 11105038	11.59	A*	G	69/78/94	-20	4	
UCAC 11105083	12.42	F*	G	48/52/65	-19	7	
UCAC 11105106	11.69	A*	G	66/73/82	-16	3	
UCAC 11105144	13.80	G*	G	25/28/37	-16	2	
UCAC 11105150	12.96	F*	G	32/36/45	-20	3	
UCAC 11105152	11.55	A*	G	70/79/93	-23	4	SB2
					-15	1	
UCAC 11105162	13.59	G*	G	27/31/39	-20	3	
UCAC 11105176	11.33	A*	G	78/87/104	-17	5	
UCAC 11105213	11.83	A*	G	62/69/79	-21	3	
UCAC 11105215	13.29	G*	G	31/35/44	-19	3	
UCAC 11105253	13.75	G*	G	24/28/34	-19	2	
UCAC 11105293	12.11	F*	G	58/63/76	-30	4	
UCAC 11105379	11.75	A*	G	65/72/87	-21	2	
UCAC 11105406	12.52	F*	G	48/52/65	-17	7	

Table 4.2: Columns two and three show the stellar proper motion and uncertainty by Dias et al. (2006). while in the fifth and sixth columns by Hog et al. (2000). Column four gives the membership probabilities by Dias et al. (2006). Column seven shows the cluster kinematic (Pkin), photometric (Pph) and positional (Psp) membership probability by Kharchenko et al. (2004). Columns eight and nine list the identification number by Claria et al. (1993) and the membership. The last column shows the adopted cluster membership.

Star name	Prop. motion Dias et al. (2006) [mas/yr]	σ Prop. motion [mas/yr]	Membership Dias et al. (2006) %	Prop. motion Hog et al. (2000) [mas/yr]	σ Proper motion [mas/yr]	Pkin/Pph/Psp Kharchenko et al. (2004)	Claria et al. (1993) ident. #	Memb. Claria et al. (1993)	Adopted memb.
HD 122983	-5.6,-0.8	0.9,1.0	60	-5.3,-0.3	1.1,1.1	0.69/0.66/1	142	m	M
HD 123097	-4.9,-3.1	1.1,1.2	43	-4.6,-2.4	1.2,1.1	0.90/1.00/1	131	m	M
HD 123182	-5.8,-3.2	1.1,1.2	44	-5.7,-3.8	1.2,1.4	0.98/1.00/1	87	m	M
HD 123183	-6.6,0.8	1.3,1.3	58	-6.7,-0.4	1.8,1.8	0.56/0.93/1	86	m	M
HD 123184	-4.9,2.4	0.9,0.9	51	-4.8,-3.7	1.2,1.1	0.63/1.00/1	81	m	M
HD 123201B	-3.6,-5.4	1.3,1.3	20	-5.0,-5.6	1.7,1.7	0.79/1.00/1	85	m	M
HD 123202	-4.0,-1.9	1.0,0.9	57	-4.2,-2.7	1.1,1.1	0.68/1.00/1	79	m	M
HD 123225	-4.9,-2.9	1.2,1.0	52	-6.0,-2.4	1.2,1.3	0.99/1.00/1	55	m	M
HD 123226	-6.3,-4.4	1.2,1.1	31	-5.9,-6.3	1.6,1.5	0.66/1.00/1	61	m	M
HD 123269	-7.1,-2.8	1.0,1.2	44	-7.0,-2.0	1.2,1.2	0.56/1.00/1	31	m	M
CD-47 8868	-6.4,2.8	1.4,2.4	56	-6.3,2.4	1.7,1.6	0.66/1.00/1	141	m	M
CD-47 8869	-4.9,-0.6	1.7,1.4	60	-4.6,0.4	1.7,1.7	0.89/1.00/1	136	m	M
CD-47 8879	-8.5,-2.5	1.4,2.0	36	-9.5,-2.9	1.6,1.6	0.24/1.00/1	124	m	M
CD-47 8889	-6.7,-3.0	1.4,2.2	42	-7.9,-5.1	1.7,1.7	0.64/0.67/1	97	m	M
CD-47 8905	-5.4,-3.2	1.4,1.4	44	-5.2,-3.1	2.1,2.0	0.97/0.64/1	58	m	M
CD-47 8913	-4.4,-3.2	1.9,1.4	43	-3.9,-2.3	2.2,2.1	0.78/0.54/1	34	nm	NM
CPD-47 6379	- , -	- , -	-	- , -	- , -	- / - /-	54	m	M
CPD-47 6385	-5.3,-2.5	1.6,1.4	52	-5.3,-0.2	2.0,1.9	0.91/0.95/1	59	m	M
Cl NGC 5460 BB 338	- , -	- , -	-	- , -	- , -	- / - /-	60	m	M
UCAC 11104969	-6.6,-1.4	2.1,1.7	57	-7.9,-0.6	2.0,2.0	- / - /-	133	m	M
UCAC 11105038	-5.3,-0.2	1.9,1.4	60	-4.8,1.3	1.9,1.9	- / - /-	125	m	M
UCAC 11105083	-3.6,-2.2	2.6,2.4	49	- , -	- , -	- / - /-	127	nm	NM
UCAC 11105106	-7.2,0.4	1.4,1.4	52	-11.1,0.6	2.2,2.2	- / - /-	89	m	M
UCAC 11105144	-5.3,5.0	5.0,5.0	38	- , -	- , -	- / - /-	-	-	NM
UCAC 11105150	-6.0,-0.4	5.0,5.0	69	- , -	- , -	- / - /-	92	nm	NM
UCAC 11105152	-2.2,-0.1	1.4,1.4	48	- , -	- , -	- / - /-	96	m	M
UCAC 11105162	-5.1,-0.6	5.0,5.0	71	- , -	- , -	- / - /-	90	nm	NM
UCAC 11105176	-7.4,-1.0	1.4,2.7	50	-6.6,1.1	2.3,2.2	- / - /-	91	m	M
UCAC 11105213	-3.8,-4.9	2.9,1.4	30	- , -	- , -	- / - /-	94	m	M
UCAC 11105215	-7.3,1.3	5.0,5.0	64	- , -	- , -	- / - /-	93	pm	NM
UCAC 11105253	-5.0,5.0	5.1,5.0	38	- , -	- , -	- / - /-	-	m	NM
UCAC 11105293	-4.4,3.8	1.4,3.8	52	- , -	- , -	- / - /-	-	-	NM
UCAC 11105379	-6.8,2.4	2.1,1.4	56	-5.4,2.1	2.3,2.1	- / - /-	36	m	M
UCAC 11105406	-4.9,-0.4	3.8,4.3	65	- , -	- , -	- / - /-	33	nm	NM

Table 4.3: Atmospheric parameters for the analysed stars of the Praesepe cluster. For $\upsilon_{\rm mic}$ the error bar increases with $\upsilon \sin i$ approximatively from $0.2\,{\rm km\,s^{-1}}$ to $0.9\,{\rm km\,s^{-1}}$. The spectral type here shown are obtained after the whole abundance analysis. He-w and HgMn indicate He-weak and mercury-manganese star, respectively.

Star name	$T_{\rm eff}$ [K]	$\sigma_{T_{\rm eff}}$ [K]	$\log g$ [cgs]	$\sigma_{\log g}$ [cgs]	$\upsilon_{\rm mic}$ [km s^{-1}]	$\upsilon \sin i$ [km s^{-1}]	$\sigma_{\upsilon \sin i}$ [km s^{-1}]	Spectral type
HD 122983	10700	200	4.00	0.15	0.0	35	3	He-w
HD 123097	12000	300	3.96	0.10	0.0	133	5	B9
HD 123182	10800	200	4.25	0.15	0.0	81	6	He-w
HD 123183	10900	250	4.05	0.15	0.0	275	14	A0
HD 123184	10900	250	4.25	0.15	0.0	65	6	A0
HD 123201B	11700	250	3.95	0.15	0.0	202	11	B8
HD 123202	11400	250	3.70	0.15	0.0	301	17	B9
HD 123225A	12800	300	4.00	0.20	0.0	12	1	HgMn
HD 123225B	8000	500	4.00	0.50	2.0	20	2	A*
HD 123226	12400	300	4.04	0.10	0.0	17	1	B8
HD 123269	11600	250	3.94	0.15	0.0	25	2	B8
CD-47 8868	10400	200	4.20	0.15	0.9	250	10	A0
CD-47 8869	8400	200	3.60	0.20	1.2	230	10	A*
CD-47 8879A	11000	500	4.00	0.30	-	26	2	A*
CD-47 8879B	8500	500	4.00	0.30	-	20	2	A*
CD-47 8889	10300	200	4.15	0.15	0.5	113	3	A0
CD-47 8905	9700	200	4.10	0.20	1.6	160	6	A0
CD-47 8913	6300	150	4.20	0.30	0.8	55	5	F*
CPD-47 6379	11000	250	4.30	0.15	1.7	136	7	A0
CPD-47 6385	9350	200	4.12	0.20	1.6	55	5	A0
Cl NGC 5460 BB 338A	7000	500	4.00	0.40	-	140	10	F*
Cl NGC 5460 BB 338B	7000	500	4.00	0.40	-	10	1	F*
UCAC 11104969	7050	150	4.00	0.20	1.4	260	15	F*
UCAC 11105038	7650	200	4.00	0.20	3.4	85	5	A*
UCAC 11105083	6400	150	4.00	0.30	1.2	196	10	F*
UCAC 11105106	7500	200	4.00	0.20	2.5	195	10	A*
UCAC 11105144	5800	150	4.00	0.40	0.4	12	1	G*
UCAC 11105150	6200	150	4.00	0.30	1.0	39	3	F*
UCAC 11105152A	7500	200	4.00	0.40	-	190	10	A*
UCAC 11105152B	7500	200	4.00	0.40	-	10	1	A*
UCAC 11105162	5800	150	4.00	0.40	0.0	35	4	G*
UCAC 11105176	8100	200	4.00	0.20	1.8	125	7	A*
UCAC 11105213	7600	200	4.00	0.20	1.9	57	3	A*
UCAC 11105215	5800	150	4.40	0.40	0.6	80	5	G*
UCAC 11105253	5600	150	4.00	0.40	0.0	26	2	G*
UCAC 11105293	6200	150	4.00	0.30	0.2	90	5	F*
UCAC 11105379	7700	200	4.00	0.20	2.1	44	2	A*
UCAC 11105406	6400	150	4.00	0.30	1.4	157	8	F*

Table 4.4: Abundances ($\log(N_X/N_{tot})$) of the analysed B-type and He-weak stars with the estimated internal errors in units of 0.01 dex, in parenthesis. For comparison, the solar abundances (Asplund et al. 2005) are given in the last column. At.N. gives the Atomic Numbers of the elements. Abundances obtained from just one line have no error (-). The second number in the brackets is the number of lines used to derive the mean abundance.

				B-type stars		Solar
At.N.	Element	HD 123202	HD 123269	HD 123201B	HD 123226	Abundances
2	He		-0.98(-;1)	-1.00(03;6)	-1.02(05;2)	-1.11
6	C			-3.60(-;1)		-3.65
8	O			-3.28(-;1)	-3.41(01;2)	-3.38
12	Mg		-4.58(16;3)	-4.29(10;5)	-4.64(08;3)	-4.51
13	Al		-5.76(-;1)	-5.70(-;1)	-5.77(17;2)	-5.67
14	Si	-4.62(-;1)	-4.42(-;1)	-4.52(01;2)	-4.63(-;1)	-4.53
16	S		-4.45(-;1)		-4.77(17;6)	-4.90
22	Ti		-7.26(25;2)	-6.54(18;5)	-7.27(-;1)	-7.14
24	Cr	-5.94(10;2)	-6.48(13;9)	-5.99(14;4)	-6.63(12;6)	-6.40
26	Fe	-4.50(07;5)	-4.57(16;60)	-4.47(14;20)	-4.75(15;54)	-4.59
28	Ni		-5.76(-;1)		-5.86(-;1)	-5.81
	$T_{\rm eff}$	11400	11600	11700	12400	
	$\log g$	3.70	3.94	3.95	4.04	
	$\upsilon_{\rm mic}$	0.0	0.0	0.0	0.0	
	$\upsilon \sin i$	301	25	202	17	
				He-weak stars		Solar
At.N.	Element	HD 122983	HD 123182	HD 123097	HD 123225A	Abundances
2	He	-2.00(-;1)	-1.48(-;1)	-0.90(-;1)	-2.15(15;6)	-1.11
6	C				-3.75(-;1)	-3.65
8	O	-3.41(-;1)	-3.41(-;1)		-3.17(-;1)	-3.38
10	Ne				-3.87(11;5)	-4.20
12	Mg	-5.22(-;1)	-4.56(01;2)	-4.55(36;3)	-5.03(34;3)	-4.51
13	Al	-6.19(-;1)	-5.43(-;1)	-5.85(-;1)	-6.85(07;2)	-5.67
14	Si	-4.41(-;1)	-4.58(09;2)	-4.54(01;2)	-4.62(13;5)	-4.53
15	P				-4.86(14;20)	-6.68
16	S				-5.30(-;1)	-4.90
17	Cl				-5.10(-;1)	-6.54
20	Ca		-5.29(-;1)			-5.73
21	Sc	-7.48(20;4)				-8.99
22	Ti	-7.37(13;3)	-6.87(08;5)	-7.31(10;2)	-6.62(04;7)	-7.14
24	Cr	-5.27(14;19)	-5.90(23;9)	-6.78(12;2)	-6.11(06;5)	-6.40
25	Mn		-5.19(23;9)		-4.54(21;31)	-6.65
26	Fe	-3.81(12;100)	-4.20(14;60)	-4.60(05;12)	-3.85(13;145)	-4.59
31	Ga				-5.63(32;2)	-9.16
33	As				-4.62(03;2)	-9.75
39	Y		-9.81(-;1)			-9.83
54	Xe				-5.37(21;6)	-9.77
56	Ba	-8.64(-;1)	-9.09(-;1)			-9.87
59	Pr	-7.57(20;3)			-8.35(24;2)	-11.33
60	Nd	-7.43(10;8)				-10.59
80	Hg				-5.98(20;3)	-10.91
	$T_{\rm eff}$	10700	10800	12000	12800	
	$\log g$	4.00	4.25	3.96	4.00	
	$\upsilon_{\rm mic}$	0.0	0.0	0.0	0.0	
	$\upsilon \sin i$	35	81	133	12	

Table 4.5: Abundances ($\log(N_X/N_{tot})$) of part of the analysed A-type cluster member stars with the estimated internal errors in units of 0.01 dex, in parenthesis. For comparison, the solar abundances (Asplund et al. 2005) are given in the last column. At.N. gives the Atomic Numbers of the elements. Abundances obtained from just one line have no error (-). The second number in the brackets is the number of lines used to derive the mean abundance.

				A-type stars			Solar
At.N.	Element	CD-47 8869	CD-47 8905	CD-47 8889	CD-47 8868	CPD-47 6379	Abundances
6	C	-3.50(-;1)					-3.65
12	Mg	-5.27(16;2)	-4.03(11;3)	-4.20(06;3)	-3.80(-;1)	-4.10(28;3)	-4.51
13	Al			-5.52(-;1)			-5.67
14	Si	-4.34(-;1)	-4.26(09;2)	-4.52(17;2)	-4.52(-;1)	-4.77(45;2)	-4.53
20	Ca	-5.35(-;1)					-5.73
21	Sc	-9.68(-;1)					-8.99
22	Ti	-6.67(08;2)	-7.00(28;4)	-7.07(13;3)	-7.04(15;2)	-7.12(22;4)	-7.14
24	Cr	-6.58(11;4)	-6.39(10;4)	-6.16(09;5)	-6.40(25;4)	-5.15(15;4)	-6.40
25	Mn	-6.82(-;1)					-6.65
26	Fe	-4.50(10;15)	-4.43(15;21)	-4.27(17;22)	-4.25(21;13)	-4.20(23;27)	-4.59
56	Ba	-9.70(-;1)					-9.87
	$T_{\rm eff}$	8400	9700	10300	10400	11000	
	$\log g$	3.60	4.10	4.15	4.20	4.30	
	$\upsilon_{\rm mic}$	1.2	1.6	0.5	0.9	1.7	
	$\upsilon \sin i$	230	160	113	250	136	

				A-type stars			Solar
At.N.	Element	UCAC 11105106	UCAC 11105213	UCAC 11105038	UCAC 11105379	UCAC 11105176	Abundances
6	C		-3.49(12;3)	-3.38(14;3)	-3.42(05;3)	-3.24(04;2)	-3.65
11	Na	-6.13(06;2)	-5.69(04;2)	-5.78(03;2)	-5.84(05;2)		-5.87
12	Mg	-4.62(21;4)	-4.87(06;3)	-4.86(07;3)	-4.69(03;3)	-4.45(03;3)	-4.51
14	Si	-4.09(21;2)	-4.27(13;3)	-4.37(15;3)	-4.37(09;3)	-4.21(-;1)	-4.53
16	S		-4.37(-;1)		-4.58(-;1)		-4.90
20	Ca	-5.67(07;8)	-6.03(25;19)	-6.23(09;8)	-5.89(14;15)	-5.86(06;4)	-5.73
21	Sc	-8.56(22;2)	-9.23(09;4)	-9.17(19;3)	-9.11(11;4)	-8.82(11;2)	-8.99
22	Ti	-7.44(14;10)	-7.16(04;13)	-7.64(17;19)	-7.22(05;15)	-6.97(19;7)	-7.14
23	V				-7.76(-;1)		-8.04
24	Cr	-6.81(09;10)	-6.27(15;24)	-6.50(15;16)	-6.39(12;22)	-6.33(08;10)	-6.40
25	Mn	-6.83(08;3)	-6.75(22;5)	-6.83(14;3)	-6.78(12;4)	-6.35(17;3)	-6.65
26	Fe	-5.03(15;54)	-4.61(16;133)	-5.08(13;91)	-4.74(16;129)	-4.80(12;61)	-4.59
28	Ni	-6.04(04;3)	-5.67(16;15)	-6.09(18;9)	-6.11(18;14)	-5.74(16;5)	-5.81
30	Zn	-6.79(-;1)	-7.15(-;1)		-7.75(-;1)		-7.44
39	Y		-9.64(16;3)		-9.87(13;2)		-9.83
56	Ba	-9.63(-;1)	-8.51(16;2)	-9.18(16;2)	-9.35(16;2)	-10.10(-;1)	-9.87
	$T_{\rm eff}$	7500	7600	7650	7700	8100	
	$\log g$	4.00	4.00	4.00	4.00	4.00	
	$\upsilon_{\rm mic}$	2.5	1.9	3.4	2.1	1.8	
	$\upsilon \sin i$	195	57	85	44	125	

Table 4.6: Abundances ($\log(N_X/N_{tot})$) of part of the analysed A-type cluster stars and the F-type cluster stars with the estimated internal errors in units of 0.01 dex, in parenthesis. For comparison, the solar abundances (Asplund et al. 2005) are given in the last column. At.N. gives the Atomic Numbers of the elements. Abundances obtained from just one line have no error (-). The second number in the brackets is the number of lines used to derive the mean abundance.

			A-type stars			Solar
At.N.	Element	UCAC 11104969	CPD-47 6385	HD 123183	HD 123184	Abundances
2	He				-0.90(05;3)	-1.11
6	C	-3.47(-;1)	-3.27(13;5)		-3.47(-;1)	-3.65
8	O			-3.40(11;4)	-3.28(01;3)	-3.38
12	Mg	-5.11(32;2)	-4.28(02;3)	-4.30(16;3)	-4.35(16;5)	-4.51
13	Al		-5.35(-;1)		-5.56(-;1)	-5.67
14	Si	-3.58(-;1)	-4.71(24;2)	-4.37(19;2)	-4.39(10;4)	-4.53
16	S				-4.20(-;1)	-4.90
20	Ca	-5.69(17;4)	-5.30(09;4)		-5.77(-;1)	-5.73
21	Sc	-9.43(-;1)	-8.81(04;3)		-9.21(-;1)	-8.99
22	Ti	-7.48(32;5)	-6.85(13;12)	-6.51(-;1)	-6.88(14;8)	-7.14
24	Cr	-6.76(15;6)	-6.04(09;17)	-5.81(01;2)	-6.15(13;10)	-6.40
25	Mn	-6.34(08;3)	-5.99(03;2)		-6.10(-;1)	-6.65
26	Fe	-4.62(05;12)	-4.38(09;59)	-4.37(22;11)	-4.29(14;57)	-4.59
28	Ni	-5.65(65;5)	-5.55(30;2)			-5.81
38	Sr				-9.34(-;1)	-9.12
39	Y	-8.64(03;2)				-9.83
56	Ba	-8.55(-;1)	-8.17(11;2)			-9.87
	T_{eff}	7050	9350	10900	10900	
	$\log g$	4.00	4.12	4.05	4.25	
	υ_{mic}	1.4	1.6	0.0	0.0	
	$\upsilon \sin i$	260	55	275	65	

Table 4.7: Abundances ($\log(N_X/N_{tot})$) of the analysed non cluster member stars with the estimated internal errors in units of 0.01 dex, in parenthesis. For comparison, the solar abundances (Asplund et al. 2005) are given in the last column. At.N. gives the Atomic Numbers of the elements. Abundances obtained from just one line have no error (-). The second number in the brackets is the number of lines used to derive the mean abundance.

		Non cluster member stars					Solar
At.N.	Element	UCAC 11105253	UCAC 11105144	UCAC 11105215	CD-47 8913	UCAC 11105083	Abundances
6	C				-3.18(-;1)		-3.65
11	Na	-6.07(16;2)	-5.99(01;2)	-6.11(19;2)	-6.07(08;2)	-5.17(18;2)	-5.87
12	Mg	-5.62(17;3)	-6.18(07;3)	-5.31(17;4)	-5.36(-;1)	-4.49(-;1)	-4.51
14	Si	-4.57(14;2)	-4.36(11;3)	-4.18(-;1)	-4.48(-;1)		-4.53
20	Ca	-6.17(22;9)	-6.38(18;9)	-6.30(17;8)	-5.90(13;10)	-5.69(05;5)	-5.73
21	Sc	-9.00(16;3)	-8.76(06;7)	-9.06(-;1)	-8.74(12;6)	-8.10(29;4)	-8.99
22	Ti	-7.54(15;30)	-7.34(14;34)	-7.18(32;39)	-7.17(14;24)	-7.66(27;4)	-7.14
23	V	-8.04(06;3)	-8.06(06;6)	-7.48(35;2)			-8.04
24	Cr	-6.62(15;21)	-6.75(21;32)	-6.57(22;28)	-6.89(13;31)	-6.70(09;7)	-6.40
25	Mn	-6.86(14;5)	-7.09(23;5)	-6.46(08;5)	-6.75(08;4)	-6.67(13;4)	-6.65
26	Fe	-4.85(13;122)	-4.98(24;139)	-4.71(22;142)	-5.00(18;127)	-4.80(21;31)	-4.59
28	Ni	-6.07(21;28)	-5.89(10;29)	-5.75(21;29)	-6.16(20;27)	-5.79(20;6)	-5.81
29	Cu		-8.20(03;2)		-7.93(-;1)		-7.83
30	Zn	-7.25(-;1)	-7.46(-;1)	-6.92(-;1)	-7.71(-;1)	-6.68(-;1)	-7.44
39	Y	-9.21(06;2)	-10.32(02;2)	-9.14(-;1)	-10.07(-;1)		-9.83
56	Ba	-9.91(-;1)	-10.12(18;2)	-9.82(-;1)	-9.67(13;2)	-9.35(-;1)	-9.87
	$T_{\rm eff}$	5600	5800	5800	6300	6400	
	$\log g$	4.00	4.00	4.40	4.20	4.00	
	$\upsilon_{\rm mic}$	0.0	0.4	0.6	0.8	1.2	
	$\upsilon \sin i$	26	12	80	55	196	

Table 4.8: As for Table 4.7, but for other stars not member of NGC 5460.

		Non cluster member stars				Solar
At.N.	Element	UCAC 11105162	UCAC 11105150	UCAC 11105293	UCAC 11105406	Abundances
6	C					-3.65
11	Na	-6.41(05;2)	-5.79(11;2)	-5.53(07;2)	-5.66(06;2)	-5.87
12	Mg	-5.60(12;4)	-5.19(06;3)	-4.46(21;4)	-5.13(15;3)	-4.51
14	Si	-4.48(19;3)	-4.36(13;2)			-4.53
20	Ca	-6.58(07;8)	-6.51(14;8)	-5.57(15;5)	-5.89(14;4)	-5.73
21	Sc	-9.06(16;6)	-8.71(14;5)	-8.52(11;4)	-8.19(22;5)	-8.99
22	Ti	-7.28(14;26)	-7.42(13;28)	-7.56(14;16)	-7.49(15;13)	-7.14
23	V	-8.16(13;5)				-8.04
24	Cr	-6.67(17;27)	-6.66(16;28)	-6.81(16;10)	-6.78(11;14)	-6.40
25	Mn	-6.51(09;4)	-6.50(07;6)	-6.63(11;4)	-6.86(09;4)	-6.65
26	Fe	-5.09(29;156)	-4.98(19;108)	-4.80(19;80)	-4.88(13;46)	-4.59
28	Ni	-5.94(23;37)	-5.89(15;24)	-6.18(15;9)	-6.34(13;7)	-5.81
29	Cu	-8.24(28;2)	-8.22(-;1)			-7.83
30	Zn	-7.47(39;2)	-8.61(-;1)	-9.02(-;1)	-8.30(-;1)	-7.44
39	Y	-9.86(01;2)	-9.82(17;3)	-8.46(01;2)	-9.82(04;2)	-9.83
56	Ba	-10.02(14;2)	-9.66(18;2)	-9.53(11;2)	-9.57(-;1)	-9.87
	$T_{\rm eff}$	5800	6200	6200	6400	
	$\log g$	4.00	4.00	4.00	4.00	
	$\upsilon_{\rm mic}$	0.0	1.0	0.2	1.4	
	$\upsilon \sin i$	35	39	90	157	

Table 4.9: $\log L/L_{\odot}$, $\log T_{\rm eff}$, M/M$_{\odot}$ and fractional age (τ) with associated error bars for the analysed stars of the NGC 5460 open cluster. The last column denotes the spectroscopic binary stars for which $\log L/L_{\odot}$, $M/M_{\odot}$ and *tau* should not be taken into consideration.

Star name	$\log L/L_{\odot}$ dex	Sp.Type	$\log T_{\rm eff}$	$M/M_{\odot}$	$\sigma_{M/M_{\odot}}$	τ	σ_{τ}	Binarity
HD 122983	1.88	He-w	4.029	2.76	0.14	0.37	0.15	
HD 123097	2.25	B9V	4.079	3.40	0.17	0.67	0.27	
HD 123182	1.89	He-w	4.033	2.80	0.14	0.38	0.16	
HD 123183	1.80	A0	4.037	2.73	0.14	0.36	0.15	
HD 123184	2.06	A0	4.037	3.02	0.21	0.48	0.19	
HD 123201B	2.10	B8	4.068	3.17	0.16	0.55	0.22	
HD 123202	2.33	B9V	4.057	3.45	0.24	0.70	0.28	
HD 123225A	2.44	HgMn	4.107	3.80	0.27	0.92	0.37	SB2
HD 123225B	2.11	A	3.903	2.80	0.28	0.38	0.15	SB2
HD 123226	2.35	B8IV	4.093	3.60	0.18	0.79	0.32	
HD 123269	2.11	B8V	4.064	3.15	0.16	0.54	0.22	
CD-47 8868	1.50	A0	4.017	2.30	0.16	0.22	0.09	
CD-47 8869	1.25	A	3.924	1.94	0.14	0.14	0.05	
CD-47 8879A	1.63	A	4.041	2.55	0.18	0.29	0.12	SB2
CD-47 8879B	1.46	A	3.929	2.15	0.15	0.18	0.7	SB2
CD-47 8889	1.47	A0	4.013	2.35	0.16	0.23	0.09	
CD-47 8905	1.41	A0	3.987	2.20	0.11	0.19	0.08	
CPD-47 6379	1.76	A0	4.041	2.71	0.14	0.35	0.14	
CPD-47 6385	1.52	A0	3.971	2.27	0.16	0.21	0.09	
Cl NGC 5460 BB 338A	0.83	F	3.845	1.52	0.11	0.07	0.03	SB2
Cl NGC 5460 BB 338B	0.83	F	3.845	1.52	0.11	0.07	0.03	SB2
UCAC 11104969	0.72	F	3.848	1.48	0.07	0.06	0.03	
UCAC 11105038	0.92	A	3.884	1.66	0.08	0.09	0.04	
UCAC 11105106	0.88	A	3.875	1.60	0.08	0.08	0.03	
UCAC 11105152A	0.95	A	3.875	1.65	0.12	0.09	0.03	SB2
UCAC 11105152B	0.95	A	3.875	1.65	0.12	0.09	0.03	SB2
UCAC 11105176	1.06	A	3.908	1.78	0.09	0.11	0.04	
UCAC 11105213	0.80	A	3.881	1.59	0.08	0.08	0.03	
UCAC 11105379	0.88	A	3.886	1.64	0.08	0.08	0.03	

Table 4.10: Basic datas of the observations for the program stars. The SNR per pixel are calculated at about 5000 Å. The exposure time is in seconds. The HJD indicate the Heliocentric Julian Date at the middle of the exposure. BS indicates the the star is a blue straggler.

HD	HJD	M_v	Spectral Type	Instrument	Resolution	SNR	Exp. Time	Remarks
72757	2454172.336	8.45	F0	SOPHIE	40 000	190	3600	
72846	2454070.737	7.48	A5V	SOPHIE	40 000	210	3600	
72942	2453746.098	7.48	A3V	ESPaDOnS	65 000	350	1600	SB1
74028	2454171.318	7.97	A7V	SOPHIE	40 000	185	3600	δSct
73045	2453745.091	6.82	Am	ESPaDOnS	65 000	290	2400	SB1
74050	2454170.566	7.91	A6Vn	SOPHIE	40 000	160	3600	δSct
74135	2454172.559	8.88	F0	SOPHIE	40 000	120	3600	
73174	2453010.574	7.76	Am	ELODIE	42 000	120	2700	SB1
73175	2454171.406	8.25	F0Vn	SOPHIE	40 000	155	3600	δSct
73345	2454171.363	8.14	A7V	SOPHIE	40 000	188	3600	δSct
73430	2453746.125	8.33	A9V	ESPaDOnS	65 000	220	1800	
73450	2454171.494	8.59	A9V	SOPHIE	40 000	185	3600	δSct
73574	2454171.585	7.75	A8V	SOPHIE	40 000	170	3600	
73575	2453747.116	6.66	F0III	ESPaDOnS	65 000	250	2400	δSct
74587	2454172.468	8.51	A5	SOPHIE	40 000	177	3600	
74589	2454172.379	8.46	F0	SOPHIE	40 000	200	3600	
73618	2453009.612	7.30	Am	ELODIE	42 000	160	3600	SB1
74656	2454170.537	8.04	Am	SOPHIE	75 000	226	2x3600	
73666	2453745.063	6.61	A0V	ESPaDOnS	65 000	660	1600	BS
73709	2451611.473	7.68	Am	MuSiCoS	35 000	120	2400	SB1
73711	2453010.432	7.51	Am	ELODIE	42 000	90	3600	SB1
74718	2454171.538	8.39	A5	SOPHIE	40 000	172	3600	
73730	2453745.123	7.99	Am	ESPaDOnS	65 000	330	2000	
73746	2454172.514	8.72	F0V	SOPHIE	40 000	154	3600	δSct
73798	2454172.424	8.48	F0V	SOPHIE	40 000	190	3600	δSct
73818	2453012.102	8.69	Am	ELODIE	42 000	80	2400	SB1
73993	2454171.450	8.56	F2V	SOPHIE	40 000	134	3600	variable

Table 4.11: Atmospheric parameters for the analysed stars of the Praesepe cluster. The errors on the fundamental parameters are estimated to be 200 K and 0.2 for $T_{\rm eff}$ and $\log g$ respectively. For $\upsilon_{\rm mic}$ the error bar increases with $\upsilon \sin i$ approximatively from 0.2 km s^{-1} to 0.7 km s^{-1}. $\langle B_z \rangle$ indicates the Longitudinal Magnetic Field (measured in Gauss) calculated with the LSD tecnique.

HD	$T_{\rm eff}$ [K]	$\log g$ [cgs]	$\upsilon_{\rm mic}$ [km s^{-1}]	$\upsilon \sin i$ [km s^{-1}]	$\sigma_{\upsilon \sin i}$ [km s^{-1}]	$\upsilon_{\rm r}$ [km s^{-1}]	$\sigma_{\upsilon_{\rm r}}$ [km s^{-1}]	$\langle B_z \rangle$ G
72757	7400	3.60	2.7	179	10	35.8	7.0	-
72846	8040	3.50	2.5	119	6	35.1	7.3	-
72942	8450	3.90	2.4	73	4	39.9	3.4	12 ± 31
73045	7570	4.05	3.6	10	0.5	27.9	0.2	-1 ± 4
73174	8350	4.15	2.9	<5	1	2.9	0.4	-
73175	7660	3.94	2.6	163	9	36.7	5.7	-
73345	7990	3.96	2.6	85	4	34.5	4.4	-
73430	7660	4.02	2.6	73	4	33.7	3.6	1 ± 45
73450	7270	4.20	2.7	138	7	34.5	5.1	-
73574	7660	4.00	2.6	102	4	35.3	4.5	-
73575	7300	2.92	2.7	127	6	33.4	4.5	-215 ± 149
73618	8170	4.00	2.5	47	2	15.1	2.1	-
73666	9380	3.78	1.9	10	0.5	34.1	0.2	6 ± 5
73709	8070	3.78	2.3	10	1	26.7	0.4	-
73711	8020	3.69	2.5	62	3	23.4	3.6	-
73730	8070	3.97	2.6	29	1	36.6	1.5	-12 ± 9
73746	7440	4.08	2.7	95	4	34.2	3.6	-
73798	7330	3.95	2.7	200	11	34.1	5.9	-
73818	7230	3.82	2.8	66	3	22.5	3.6	-
73993	7140	3.92	2.8	240	14	33.6	7.5	-
74028	7750	4.50	2.6	150	9	35.3	7.4	-
74050	7870	3.66	2.6	188	8	36.0	7.8	-
74135	7400	4.00	2.7	100	4	32.5	5.7	-
74587	7500	4.20	2.7	90	4	33.9	4.1	-
74589	7550	4.03	2.7	127	5	34.1	4.7	-
74656	7800	3.99	3.6	25	1	34.1	1.3	-
74718	7600	4.00	2.7	155	7	34.1	5.7	-

Table 4.12: Abundances ($\log(N_X/N_{tot})$) of the analysed Am stars and the blue straggler HD 73666 with the estimated internal errors in units of 0.01 dex, in parenthesis. For comparison, the solar abundances (Asplund et al. 2005) are given in the last column. At.N. gives the Atomic Numbers of the elements. Abundances obtained from just one line have no error (-). Upper limits are denoted by <. The second number in the brackets is the number of lines used to derive the mean abundance.

		Am stars									Solar
At.N.	Element	HD 73818	HD 73045	HD 74656	HD 73711	HD 73730	HD 73709	HD 73618	HD 73174	HD 73666	Abundances
2	He									-1.20(05;2)	-1.11
3	Li	¡-8.63(-;1)	-8.86(02;1)	-8.61(-;1)	¡-8.43(-;1)	-8.74(-;1)		¡-8.58(-;1)	-8.51(02;1)		-10.99
6	C	-3.38(07;3)	-4.37(04;3)	-4.09(-;1)	-3.99(15;4)	-4.32(47;3)	-3.71(26;15)	-4.16(16;2)	-4.08(06;3)	-3.25(03;3)	-3.65
7	N		-4.49(-;1)	-3.98(-;1)		-4.63(-;1)			-4.50(12;2)	-3.67(10;4)	-4.26
8	O	-3.76(-;1)	-3.90(10;2)	-3.88(-;1)	-3.60(04;2)	-3.96(09;4)	-3.86(08;4)	-3.65(04;2)	-3.72(01;3)	-3.06(07;12)	-3.38
11	Na	-5.35(01;2)	-5.32(03;4)	-5.35(01;2)		-5.36(01;2)	-5.34(06;2)	-5.34(03;2)	-5.13(04;2)	-5.47(01;2)	-5.87
12	Mg	-4.51(16;4)	-4.52(04;2)	-4.73(11;3)	-4.63(05;3)	-4.43(06;2)	-4.56(06;4)	-4.29(-;1)	-4.21(05;4)	-4.25(14;6)	-4.51
13	Al		-5.41(01;2)	-5.15(-;1)		-5.37(-;1)	-4.91(16;2)		-5.06(-;1)	-5.34(06;3)	-5.67
14	Si	-3.44(32;2)	-4.21(05;4)	-4.37(-;1)	-4.19(05;2)	-4.21(05;5)	-4.10(06;4)	-4.51(-;1)	-4.08(11;6)	-4.30(01;2)	-4.53
15	P						-5.12(-;1)		-5.23(-;1)		-6.68
16	S	-4.36(26;4)	-4.67(09;2)	-4.52(04;5)	-4.62(-;1)	-4.54(03;4)	-4.44(01;2)	-4.52(13;2)	-4.37(03;4)	-4.47(-;1)	-4.90
18	Ar									-5.10(-;1)	-5.86
19	K		-7.04(-;1)			-6.83(-;1)				-6.49(-;1)	-6.96
20	Ca	-5.88(03;4)	-6.46(04;3)	-6.34(13;3)	-5.95(08;5)	-6.36(03;4)	-6.18(06;6)	-5.74(07;4)	-5.70(08;18)	-5.53(14;6)	-5.73
21	Sc	-10.90(-;1)	-9.39(01;2)	-9.27(-;1)	-10.06(01;2)	-9.71(03;2)	-9.79(01;2)	-9.51(27;2)	-9.44(08;3)	-8.95(06;3)	-8.99
22	Ti	-6.81(30;2)	-6.95(04;5)	-6.90(16;18)	-7.08(04;2)	-6.99(09;8)	-7.01(07;8)	-6.41(01;2)	-6.72(05;18)	-6.86(04;23)	-7.14
23	V		-7.60(-;1)	-7.06(-;1)			-7.16(-;1)		-7.19(05;4)	-7.48(05;2)	-8.04
24	Cr	-6.23(-;1)	-5.63(16;5)	-5.72(10;11)	-6.08(09;3)	-5.65(08;3)	-5.79(13;12)	-5.93(10;2)	-5.69(08;19)	-6.01(07;8)	-6.40
25	Mn	-5.83(-;1)	-6.28(-;1)	-6.27(11;5)	-6.46(13;4)	-6.31(03;3)	-6.26(01;3)	-6.28(-;1)	-6.07(06;8)	-6.32(01;2)	-6.65
26	Fe	-4.26(20;50)	-4.03(04;48)	-4.11(13;74	-4.44(13;22)	-4.14(05;34)	-4.05(11;103)	-4.13(10;37)	-3.88(09;189)	-4.30(07;71)	-4.59
27	Co		-6.47(04;2)	-5.38(-;1)		-6.15(-;1)	-6.16(04;3)		-6.12(12;4)		-7.12
28	Ni	-5.32(14;3)	-4.93(06;8)	-5.00(08;15)	-5.28(02;2)	-5.14(07;7)	-4.88(06;26)	-5.10(15;17)	-4.79(02;22)	-5.53(03;5)	-5.81
29	Cu	-7.29(-;1)	-6.93(-;1)	-6.92(-;1)		-7.12(-;1)			-6.78(-;1)		-7.83
30	Zn		-6.65(-;1)	-6.77(-;1)		-6.82(-;1)	-6.59(-;1)	-7.29(-;1)	-6.42(-;1)		-7.44
38	Sr			-8.23(-;1)							-9.12
39	Y	-9.42(29;2)	-8.91(09;4)	-8.92(11;3)	-8.77(13;4)	-8.98(05;3)	-8.76(08;4)	-8.62(-;1)	-8.50(09;5)	-9.78(-;1)	-9.83
40	Zr		-9.05(01;4)	-8.62(-;1)		-8.51(01;3)	-8.28(-;1)		-8.16(03;4)		-9.45
56	Ba	-8.69(06;2)	-8.50(-;1)	-8.46(23;3)	-8.97(09;2)	-7.85(16;2)	-7.77(10;2)	-8.09(18;3)	-8.02(38;3)	-9.13(04;3)	-9.87
57	La		-9.61(09;2)	-9.22(14;3)		-9.41(-;1)	-9.36(08;3)		-9.26(09;15)		-10.91
58	Ce		-9.26(04;2)	-9.11(08;3)		-9.44(03;3)	-9.14(-;1)		-8.94(15;7)		-10.46
59	Pr								-9.09(-;1)		-11.33
60	Nd		-9.48(03;3)	-9.27(13;5)		-9.66(11;3)	-9.41(04;3)		-9.23(07;9)		-10.59
62	Sm		-9.89(05;4)	-9.89(-;1)			-9.18(07;2)		-9.81(10;4)		-11.03
63	Eu		-10.20(-;1)	-9.89(-;1)		-10.42(-;1)	-9.95(-;1)				-11.52
64	Gd						-8.93(-;1)		-9.30(04;2)		-10.92
68	Er		-9.65(-;1)	-9.53(-;1)			-9.54(-;1)		-9.39(-;1)		-11.11
70	Yb		-9.87(-;1)	-9.46(-;1)							-10.96
71	Lu						-10.30(-;1)		-10.20(-;1)		-11.98
	$T_{\rm eff}$	7230	7570	7800	8020	8070	8070	8170	8350	9380	
	$\log g$	3.82	4.05	3.99	3.69	3.97	3.78	4.00	4.15	3.78	
	$\upsilon_{\rm mic}$	2.8	3.6	3.6	2.5	2.6	2.8	2.5	2.9	1.9	
	$\upsilon \sin i$	66	10	25	62	29	10	47	<5	10	

Table 4.13: As Table 4.12 but for the F-type stars.

					F - type stars				A - type stars		Solar
At.N.	Element	HD 73993	HD 73798	HD 72757	HD 74135	HD 73746	HD 74589	HD 73175	HD 73575	HD 73430	Abundances
3	Li				¡-8.47(-;1)	¡-8.70(-;1)	¡-8.35(-;1)		¡-8.50(-;1)	¡-8.17(-;1)	-10.99
6	C			-3.71(16;2)	-3.30(14;2)	-3.39(-;1)	-3.19(18;2)	-3.36(01;2)	-3.61(-;1)	-3.74(-;1)	-3.65
7	N								-3.93(-;1)	-3.62(16;2)	-4.26
8	O				-3.40(-;1)	-3.30(-;1)	-3.36(-;1)		-3.37(-;1)	-3.26(-;1)	-3.38
11	Na			-5.61(-;1)	-5.73(24;2)	-5.45(13;2)	-5.73(07;2)	-5.81(01;2)		-5.69(06;2)	-5.87
12	Mg	-4.57(-;1)	-4.76(23;2)	-4.56(14;2)	-4.14(09;2)	-4.50(11;5)	-4.25(02;2)	-4.38(07;2)	-4.63(-;1)	-4.79(15;2)	-4.51
14	Si	-4.34(-;1)	-4.09(-;1)	-4.23(06;3)	-4.14(-;1)	-4.29(-;1)	-4.20(-;1)	-4.39(-;1)	-4.41(-;1)	-4.44(04;2)	-4.53
16	S			-4.62(01;2)	-4.62(05;2)	-4.54(05;5)	-4.44(07;2)	-4.55(-;1)		-4.59(-;1)	-4.90
19	K								-6.46(-;1)	-6.84(-;1)	-6.96
20	Ca	-5.65(-;1)	-5.38(15;5)	-5.60(11;6)	-5.45(14;4)	-5.68(16;8)	-5.53(05;7)	-5.41(03;3)	-5.55(08;2)	-5.68(05;3)	-5.73
21	Sc	-8.90(-;1)	-9.20(-;1)	-9.07(-;1)	-8.48(15;4)	-8.98(10;3)	-8.43(25;3)	-8.66(-;1)	-9.31(10;4)	-8.90(10;2)	-8.99
22	Ti	-7.18(-;1)	-6.90(-;1)	-7.03(16;5)	-7.03(09;6)	-6.68(13;3)	-6.92(11;7)	-6.90(15;3)	-7.18(-;1)	-7.19(-;1)	-7.14
24	Cr		-6.64(36;4)	-6.72(08;3)	-6.16(12;3)	-6.20(23;6)	-6.26(20;4)	-6.55(01;2)	-6.29(-;1)	-6.57(11;2)	-6.40
25	Mn		-6.36(-;1)	-6.92(-;1)	-6.42(11;3)	-6.46(01;2)		-6.98(08;2)			-6.65
26	Fe	-4.47(08;6)	-4.47(06;17)	-4.50(08;31)	-4.45(11;60)	-4.46(08;49)	-4.51(11;53)	-4.52(08;14)	-4.75(10;9)	-4.72(12;33)	-4.59
28	Ni	-6.15(-;1)	-6.20(07;2)	-5.57(-;1)	-5.53(10;4)	-5.38(12;5)	-5.90(17;4)	-5.68(05;3)	-5.56(01;2)	-5.71(15;3)	-5.81
39	Y		-9.20(-;1)	-10.07(-;1)	-9.46(-;1)	-9.35(01;2)	-8.99(-;1)	-9.39(-;1)		-9.62(06;2)	-9.83
56	Ba	-9.48(-;1)	-8.78(-;1)	-9.12(06;2)	-9.10(-;1)	-9.02(12;2)	-9.14(-;1)	-9.64(-;1)	-9.95(-;1)	-9.47(-;1)	-9.87
	$T_{\rm eff}$	7140	7330	7400	7400	7440	7550	7660	7300	7660	
	$\log g$	3.92	3.95	3.60	4.00	4.08	4.03	3.94	2.92	4.02	
	$\upsilon_{\rm mic}$	2.8	2.7	2.7	2.7	2.7	2.7	2.6	2.7	2.6	
	$\upsilon \sin i$	240	200	179	100	95	127	163	127	73	

Table 4.14: As Table 4.12 but for the A-type stars.

		A - type stars									Solar
t.N.	Element	HD 73450	HD 74587	HD 74718	HD 73574	HD 74028	HD 74050	HD 73345	HD 72846	HD 72942	Abundances
3	Li	¡-8.70(-;1)	¡-8.41(-;1)	¡-8.26(-;1)	¡-8.38(-;1)			¡-8.33(-;1)	¡-8.08(-;1)	¡-8.49(-;1)	-10.99
6	C	-3.27(-;1)	-3.49(01;2)	-3.51(04;2)	-3.36(18;2)	-3.39(08;2)	-3.52(-;1)	-3.44(12;3)	-3.58(-;1)	-3.85(-;1)	-3.65
7	N									-3.84(-;1)	-4.26
8	O		-3.30(-;1)				-3.70(-;1)	-3.22(01;2)	-3.18(-;1)	-3.58(-;1)	-3.38
11	Na	-6.28(-;1)	-5.61(02;2)	-5.70(14;2)	-5.57(02;2)	-5.98(-;1)	-5.64(13;2)	-5.37(01;2)	-5.44(01;2)		-5.87
12	Mg	-5.02(18;2)	-4.56(08;3)	-4.52(01;2)	-4.37(04;3)	-4.86(08;3)	-4.22(05;4)	-4.18(02;3)	-4.18(08;3)	-4.51(03;4)	-4.51
14	Si	-4.13(-;1)	-4.16(-;1)	-4.25(-;1)	-4.19(-;1)	-4.17(-;1)	-4.37(-;1)	-4.67(-;1)	-4.62(16;2)	-4.67(-;1)	-4.53
16	S	-4.35(-;1)	-4.50(04;2)	-4.28(11;2)	-4.61(02;2)	-4.26(01;2)		-4.44(03;4)	-4.71(04;2)	-4.48(-;1)	-4.90
20	Ca	-5.95(06;4)	-5.49(15;6)	-5.68(02;3)	-5.86(16;5)	-5.37(16;2)	-6.13(06;2)	-5.39(09;6)	-5.17(-;1)	-5.58(12;3)	-5.73
21	Sc	-8.57(14;3)	-8.56(-;1)	-8.69(14;2)	-8.89(02;3)	-8.35(-;1)	-8.96(27;3)	-8.63(07;3)	-8.88(-;1)	-8.88(11;3)	-8.99
22	Ti	-7.30(11;5)	-6.83(16;3)	-6.93(10;5)	-6.98(09;5)	-6.78(-;1)	-7.08(15;5)	-6.95(06;6)	-6.88(03;5)	-6.89(07;2)	-7.14
24	Cr	-6.56(08;3)	-6.05(13;4)	-6.44(20;5)	-6.19(16;3)	-6.23(12;4)	-6.48(10;3)	-6.22(08;2)	-6.23(06;3)	-6.41(16;3)	-6.40
25	Mn	-6.88(-;1)	-6.62(04;2)	-6.71(-;1)	-6.52(02;2)	-6.77(-;1)	-6.61(-;1)	-6.37(-;1)		-6.91(-;1)	-6.65
26	Fe	-4.62(09;15)	-4.28(10;33)	-4.61(11;26)	-4.49(10;30)	-4.50(09;18)	-4.44(13;16)	-4.33(11;61)	-4.55(18;42)	-4.47(07;16)	-4.59
28	Ni	-5.82(16;2)	-5.84(-;1)	-5.68(02;3)	-5.62(08;4)	-5.93(14;3)	-5.60(15;3)	-5.58(11;4)	-5.70(18;2)	-5.57(-;1)	-5.81
39	Y	-9.83(-;1)	-9.13(-;1)	-9.10(-;1)	-9.20(-;1)	-9.56(-;1)	-9.26(-;1)	-9.46(-;1)	-9.75(-;1)	-9.02(16;2)	-9.83
56	Ba	-9.50(02;2)	-8.96(25;2)	-9.15(-;1)	-8.98(04;2)	-9.65(-;1)	-9.52(01;2)	-9.30(06;2)	-9.48(-;1)	-8.97(-;1)	-9.87
	$T_{\rm eff}$	7270	7500	7600	7660	7750	7870	7990	8040	8450	
	$\log g$	4.20	4.20	4.00	4.00	4.50	3.66	3.96	3.50	3.90	
	$\upsilon_{\rm mic}$	2.7	2.7	2.7	2.6	2.6	2.6	2.6	2.5	2.4	
	$\upsilon \sin i$	138	90	155	102	150	188	85	119	73	

Table 4.15: $\log L/L_{\odot}$, $\log T_{\rm eff}$, M/M$_{\odot}$ and fractional age (τ) with associated error bars for the analysed stars of the Praesepe cluster. No fractional age is given for HD 73666 since it is a Blue Straggler.

HD	$\log L/L_{\odot}$ dex	Sp.Type	$\log T_{\rm eff}$	M/M$_{\odot}$	$\sigma_{M/M_{\odot}}$	τ	σ_{τ}
72757	1.06	F0	3.869	1.71	0.09	0.43	0.06
72846	1.43	A5V	3.906	2.09	0.15	0.76	0.11
72942	1.41	A4V	3.927	2.16	0.22	0.53	0.15
73045	0.99	Am	3.880	1.67	0.08	0.40	0.06
73175	1.13	F0V	3.884	1.78	0.09	0.48	0.07
73345	1.17	A7V	3.903	1.84	0.13	0.53	0.08
73430	1.10	A7V	3.884	1.76	0.09	0.47	0.07
73450	1.01	A9V	3.862	1.66	0.08	0.39	0.06
73574	1.33	A8V	3.884	1.96	0.10	0.64	0.10
73575	1.78	F0III	3.863	2.33	0.12	1.02	0.15
73618	1.50	Am	3.912	2.16	0.22	0.84	0.13
73666	1.71	A0	3.972	2.46	0.12		
73709	1.35	Am	3.907	2.00	0.14	0.68	0.10
73711	1.42	Am	3.904	2.08	0.10	0.75	0.11
73730	1.23	Am	3.907	1.89	0.13	0.58	0.09
73746	0.95	F0V	3.872	1.64	0.08	0.38	0.06
73798	1.05	F0V	3.865	1.70	0.12	0.42	0.06
73818	0.97	Am	3.859	1.63	0.08	0.37	0.06
73993	1.02	F2V	3.854	1.66	0.12	0.39	0.06
74028	1.24	A7V	3.889	1.88	0.09	0.57	0.09
74050	1.26	A6V	3.896	1.91	0.10	0.60	0.09
74135	0.89	F0	3.869	1.60	0.08	0.35	0.05
74587	1.03	A5	3.875	1.71	0.09	0.43	0.06
74589	1.05	F0	3.875	1.70	0.09	0.42	0.06
74656	1.25	Am	3.892	1.89	0.09	0.58	0.09
74718	1.08	A5	3.881	1.74	0.09	0.45	0.07

Chapter 5

Discussion and conclusions

I obtained low (FLAMES/GIRAFFE), mid (FLAMES/GIRAFFE) and high (FLAMES/UVES, ELODIE, SOPHIE, FIES, ESPaDOnS) resolution, high SNR spectra of stars in the field of view of ten open clusters, approximately uniformly distributed in logarithmic age. This project is intended to study, for the first time, the correlation between the element abundances of early-type stars and the stellar evolution state, concentrating in particular on the analysis of the obtained abundances in the context of diffusion, looking for correlations between the abundances of the chemical elements and other stellar parameters, such as $T_{\rm eff}$, $\upsilon \sin i$ and stellar mass.

In this thesis I presented the results on an abundance analysis of early-type stars in NGC 5460 and in the Praesepe open cluster. The whole sample of stars has similar $\log g$ and metallicity, only $T_{\rm eff}$ varies between about 6000 K and 12000 K. It is important to notice that I am here looking for star to star variations and not absolute effects, so that the presence of, for example, non-LTE effects (not taken into account in this analysis) do not influence much the results. Non-LTE effects are dependent on the fundamental parameters and on the lines adopted to derive the abundances. As already said, the only difference in fundamental parameters between the various stars is the effective temperature, thus in a not too wide $T_{\rm eff}$ range the non-LTE effects associated to each star can be considered of the same magnitude. A similar consideration is applied to the line selection, since at similar $T_{\rm eff}$ the lines adopted to derive the element abundances were always almost the same (see Chapter 3). The fact that the non-LTE effects are approximately of similar magnitude for stars in a not too wide $T_{\rm eff}$ range allows to compare the element abundances of almost each analysed star between each other without the need of any non-LTE correction.

For this work the knowledge of the cluster membership was of crucial importance and only recently it is possible to determine it with the necessary accuracy for a large number of stars in open clusters' field of view, thanks to several membership catalogs recently published.

The NGC 5460 open cluster was almost completely unknown on the spectroscopic point of view, including the spectral classification of several stars that was here assigned for the first time. For the stars observed in NGC 5460 the determination of the cluster membership was a particularly important and delicate part of the work, since not enough HIPPARCOS data were available and the cluster proper motion is similar to the one of the field stars in the same field of view. For this reason I took into high consideration the photometric membership provided by Claria et al. (1993). The stars were observed with the FLAMES spectrograph at the ESO/VLT and for the analysis I selected stars according to the criteria given in Chapter 4. The analysis was performed in a consistent way, as described in Chapter 3, extracting fundamental parameters and abundances for each star. The sample of analysed stars in NGC 5460 consists of three He-weak stars, five B-type stars, eighteen A-type stars and three F-type stars. The analysis brought also to the discovery of four new double line spectroscopic binary systems and, maybe, one single line spectroscopic binary system (HD 123182).

For the stars observed in the Praesepe cluster the determination of the membership was not a difficult task since Praesepe is a well studied cluster with extremely reliable HIPPARCOS data (van Leeuwen 2007). The selected sample of stars was finally composed of eight Am stars, 11 A-type stars and eight F-type stars. One Am star was not considered in the analysis due to a large uncertainty in the $T_{\rm eff}$ measurement, and HD 73666 was also neglected in the analysis since it is a collisionally formed (Fossati et al. 2009a) blue straggler for which the abundances cannot be considered as proper of stars with the age of the Praesepe cluster. No double line spectroscopic binaries were found due to the performed target selection.

The original approach of this work consists of an *homogeneous* analysis of two *homogeneous* sample of stars that differ mainly in metallicity and age, allowing to minimise systematic errors that can be introduced comparing results obtained by different authors and on stars formed in many different environments.

The sample of stars analysed in NGC 5460 covers a wide range in $T_{\rm eff}$ giving the possibility to look for effects due to different physical processes across the whole center of the main sequence, from early F- to late B-type stars. The sample collected in the Praesepe cluster contains a large number of A-type stars, among which are many Am stars. The collection of several Am stars was then important for the characterisation of this often forgotten class of chemically peculiar stars.

All these considerations allow to proceed combining the two set of stars analysed in both clusters. This operation could lead to big systematic errors if performed with field stars, mainly in respect to the comparison of the abundances. The different metallicity of the two open clusters is an unavoidable bias that can be minimised. If the abundances of the analysed open cluster stars are normalised to the abundances of the original cloud from which the cluster was formed, then it is possible to compare directly the results obtained from the two star's cluster samples. In other words the obtained abundances have to be normalised with the ones obtained from the well mixed G- and late F-type stars, that provide the original metallicity of the cluster. For this reason it is extremely important to have in the sample cool stars, not only for this thesis, but furthermore for the prosecution of the project, since the main goal is the characterisation of the abundance evolution, impossible if systematics, such as the cluster to cluster difference in original metallicity, are present.

In the following I will discuss the results obtained when the combination of the two sample of stars is performed. At first I will concentrate on the obtained distribution of the projected rotational velocity, that is one of the main project goal as presented in Chapter 1, then I will discuss the results obtained after the normalisation of the element abundances to the ones obtained from the cool stars of each of the two samples.

5.1 Distribution of the projected rotational velocity

It is expected that the rotational velocity is increasing with T_{eff}, in particular that it is rather low (less than about $30\,\mathrm{km\,s^{-1}}$) for cooler stars up to the early G-type stars, increasing rapidly (up to about $250\,\mathrm{km\,s^{-1}}$) in the region where F-type stars lay (Wilson 1966; Kraft 1967) and increasing then smoothly with increasing temperature (in this region the upper limit for the rotational velocity is given by the break-up velocity). A complete picture of the rotational velocity distribution along the main sequence is not yet available.

The consistent analysis of all the stars in the sample allows to explore the distribution of the projected angular velocity as a function of stellar parameters such as T_{eff} and mass. Figure 5.1 shows the distribution of the measured stellar $\upsilon \sin i$ for the analysed cluster stars as a function of the effective temperature. This plot shows a steep increase of the projected rotational velocity around 6000 K, as expected (Wilson 1966; Kraft 1967) across the G- and F-type stars. The region between 7000 and 8500 K is better sampled, showing that single early F-type stars are fast rotators, while SB stars show in general (but not always) low $\upsilon \sin i$ values. The region of the late A-type stars is the best sampled one. The $\upsilon \sin i$ distribution in the Praesepe cluster shows a clear distinction between normal and metallic line stars. In particular, there are no normal A-type stars with a low $\upsilon \sin i$. In NGC 5460 among the normal A-type stars (not SB) here analysed there are also objects with a rather low $\upsilon \sin i$, comparable to the one of the Am stars. This could be just a selection effect due to the inclination of the rotation axis, but there could be also another more fascinating explanation: the stars in the Praesepe cluster might tend to have a common inclination of the rotation axis, while for the stars in NGC 5460 the inclination is more random, leading to the presence of single stars with low $\upsilon \sin i$. Figure 5.3 shows the number of stars with T_{eff} between 7000 K and 8500 K in $\upsilon \sin i$ bins of $50\,\mathrm{km\,s^{-1}}$ wide. This plot clearly shows that the stars in NGC 5460 cover uniformly a large $\upsilon \sin i$ range, while the stars observed in the Praesepe open cluster concentrate very much between $\upsilon \sin i$ $50\,\mathrm{km\,s^{-1}}$ and $200\,\mathrm{km\,s^{-1}}$. The number of stars here analysed is anyway not large enough to be able to conclude anything and only with the analysis of the other available open clusters it will be possible to arrive at solid conclusions.

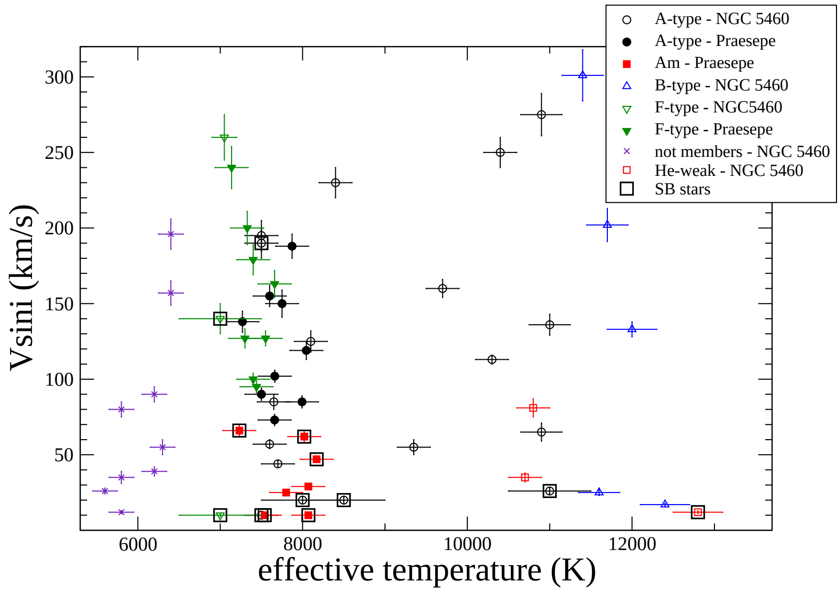

Figure 5.1: Distribution of the measured $\upsilon \sin i$ value for each analysed star as a function of the derived $T_{\rm eff}$. The open symbols denote the stars belonging to NGC 5460, while the filled symbols indicate the stars of the Praesepe open cluster. Upside triangles, circles, downside triangles and squares indicate B-, A-, F-type and chemically peculiar stars respectively. The crosses indicate the non cluster members.

For early A- and late B-type stars ($T_{\rm eff}$ between 9000 K and 13000 K) the sampling is not so well refined as for the cooler stars of the sample, but it still shows that the $\upsilon \sin i$ distribution is rather wide, with both high and low $\upsilon \sin i$ stars. The three hot He-weak stars present rather low $\upsilon \sin i$, as expected, but there are also chemically normal slowly rotating stars. In particular at $T_{\rm eff} \geq 9000$ K, excluding SB and He-weak stars, among twelve objects, four have a $\upsilon \sin i$ below 80 km s^{-1} (two well below 50 km s^{-1}), a ratio of one over three. This is a characteristic that helps to obtain high precision fundamental parameters and abundances, thus a statistically large enough number of these stars could allow to detect more clearly small signatures, like the ones that are searched here.

I divided the sample of stars according to their $\upsilon \sin i$ value in bins of 50 km s^{-1} (e.g. from 0 to 49.9, from 50 to 99.9, etc.). In the sample of stars in the following taken into account, I removed the chemically peculiar stars (expected slow rotators), the SB stars (expected in general slow rotators due the tidal breaking and consequent synchronisation) that being in general slowly rotating would introduce systematic errors. Since I want to analyse stars with spectral type between F and B, I do not take here into account the also the G-type stars. Figure 5.2 shows the number of stars for each bin.

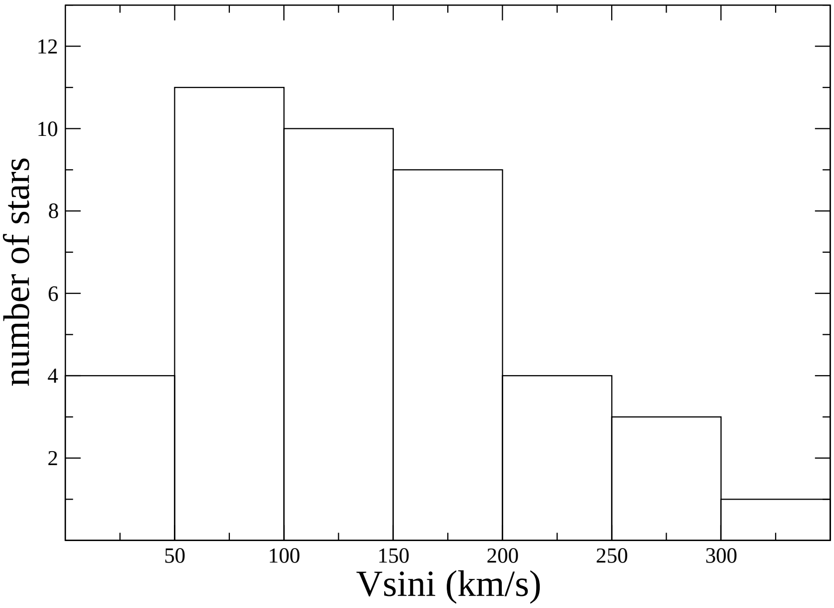

Figure 5.2: Number of stars within an interval of 50 km s^{-1} as a function of $\upsilon \sin i$. The plot does not take into account chemically peculiar stars, SB stars and G-type stars.

A similar analysis, but for a much larger number of field stars, was performed by Abt & Morrel (1995), that for spectral types between F0 and A5 obtained an unimodal distribution with a $\upsilon \sin i$ peak slightly above 150 km s^{-1}. Since the sample of stars here available is particularly dense in this spectral region I decided to produce the same plot shown in Fig. 5.2, but taking into account only stars with spectral types between F0 and A5. The plot is shown in Fig. 5.3.

Figure 5.3 shows a clear peak for $\upsilon \sin i$ values between 100 and 150 km s^{-1}, slightly below the one obtained by Abt & Morrel (1995). It is anyway known that the analysis performed by Abt & Morrel (1995) tend to overestimate $\upsilon \sin i$ for $\upsilon \sin i$ values above 100 km s^{-1} (Royer et al. 2007). On the basis of the correction that has to be given to the data presented by Abt & Morrel (1995), the distributions obtained here and by Abt & Morrel (1995) are in perfect agreement. This is an important result, given the small sample of stars here analysed compared to the one of Abt & Morrel (1995) and a very good sign for the prosecution of the project.

Royer et al. (2007) is probably the reference work on this topic. It is based on $\upsilon \sin i$ catalogs described in Abt & Morrel (1995), Royer et al. (2002a), Royer et al. (2002b) and Abt et al. (2002) of $\upsilon \sin i$ measurements of F-, A- and B-type stars. These sets of $\upsilon \sin i$ measurements were obtained with different spectrographs and methodologies so that a big effort in avoiding systematic errors was given. The result is a consistent catalog of $\upsilon \sin i$ measurements of about 1100 stars with spectral type between F2 and B9.

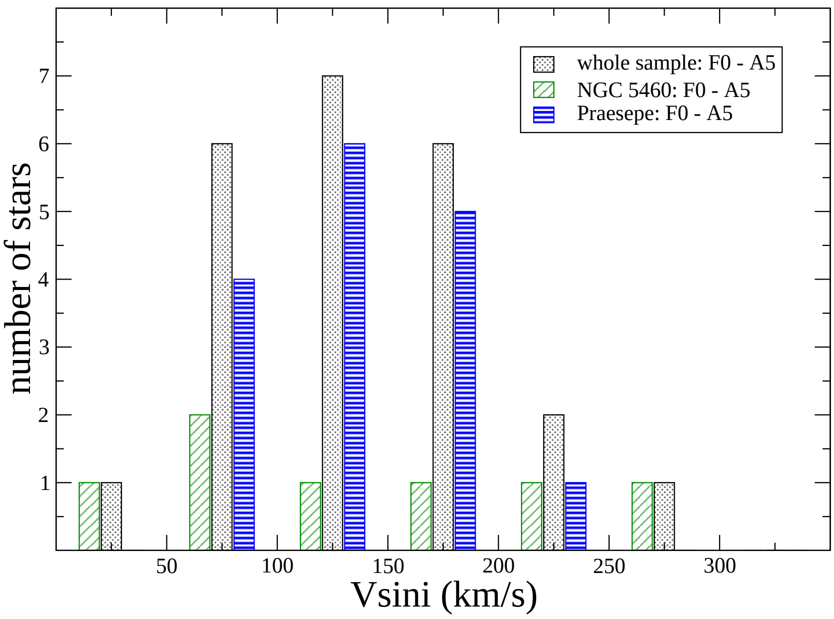

Figure 5.3: Number of stars within an interval of 50 km s^{-1} as a function of $\upsilon \sin i$ for all the stars with spectral type between F0 and A5 for the whole sample of stars (black), considering only the stars in NGC 5460 (green) and in Praesepe (blue). The plot does not take into account chemically peculiar stars, SB stars and G-type stars.

Royer et al. (2007) obtained the following results: a bimodal character of the $\upsilon \sin i$ distribution for stars with spectral type between A2 and B9, a lack of slow rotators ($\upsilon \sin i \leq 70$ km s^{-1}) for spectral types between A9 and A2, a bimodal distribution in the subgroup of stars with spectral types between F2 and F0 and a peak in the $\upsilon \sin i$ distribution at about 200 km s^{-1} for all spectral classes.

The bimodal character of the $\upsilon \sin i$ distribution for stars with spectral type between A2 and B9 can somehow be found here as well, in spite of the small number of stars. Royer et al. (2007) obtained the modes of slow rotators at about 35 km s^{-1} and 60 km s^{-1} respectively for the subgroups of stars with spectral type B9 and A0-A1, while the fast rotation modes at about 190 km s^{-1} and 200 km s^{-1}. The B-type stars analysed in this work are actually B8-B9 stars. Figure 5.1 shows two stars (over five analysed) with a $\upsilon \sin i$ around 25 km s^{-1} and three objects with $\upsilon \sin i$ between about 150 and 300 km s^{-1}, which agrees with the distribution obtained by Royer et al. (2007). I have anyway to mention that the He line profiles of the two slowly rotating B-type stars, HD 123201B and HD 123184, revealed that probably these two objects are actually fast rotators seen pole on. The bimodal distribution obtained for the stars of spectral types A0-A1 is not found in this work, but the sample of stars is very small.

The lack of slow rotators at spectral types between A9 and A2 is difficult to characterise here since the sample is not dense in this region. Anyway the presence of three objects (on about fifteen) with $\upsilon \sin i \leq 70\,\mathrm{km\,s^{-1}}$ has to be mentioned. Also the bimodal distribution for stars of spectral type between F2 and F0 is not here seen.

The peak in the $\upsilon \sin i$ distribution obtained by Royer et al. (2007) at about $200\,\mathrm{km\,s^{-1}}$ is not clearly obtained here. Figure 5.1 would suggest a peak more at $\upsilon \sin i$ about $150\,\mathrm{km\,s^{-1}}$, but again the sample here shown is much smaller than the one presented by Royer et al. (2007).

Systematic errors could be introduced by the geometry of the star, in particular when fast rotators are seen pole-on, since for these objects there is a general underestimation of the $\upsilon \sin i$ and an overestimation of T_{eff}. The analysis here performed will allow to detect these objects (see e.g. HD 123201B and HD 123184 in NGC 5460) and possibly remove or treat them in such a way to minimise systematic effects that they could introduce.

There is anyway the possibility of a common orientation of the inclination axes for stars in the same open cluster. This effect is very difficult to discover since inclination axes can be measured almost only with interferometry or for magnetic stars or for binary stars. Nobody before has ever explored this intriguing effect and the analysis here shown could give the possibility to discover it, if a clear lack of fast or slow rotators is present for a whole sample of stars in a single cluster.

5.2 Diffusion at work

The sample of stars collected for each of the two analysed open clusters differs in respect to the range of the main sequence that is studied (from early G- to late B-type stars for NGC 5460, for early F- and late A-type stars for the Praesepe cluster) and of the chemical peculiarities that are analysed (mainly chemically "normal" stars in NGC 5460 and Am stars in the Praesepe cluster). It is very important to remember here that the two sample of stars are completely homogeneous in respect of both the adopted instrumentation (see Chapter 2) and the performed analysis (see Chapter 3). In Sect. 5.2.1 and Sect. 5.2.2 I summarise the results obtained for each of the two clusters, leaving to Sect. 5.2.3 the discussion of the combined analysis.

5.2.1 NGC 5460

The measurement of the radial velocity of several stars member of NGC 5460 allowed me to derive a reliable mean cluster υ_{r} of $-17.9 \pm 5.2\,\mathrm{km\,s^{-1}}$. This value is in good agreement with what previously published by (Kharchenko et al. 2005, $-12.70 \pm 2.18\,\mathrm{km\,s^{-1}}$,) on the basis of the υ_{r} measurement of only three cluster member stars.

I derived the metallicity of NGC 5460 from the late A-type stars and the only F-type star for which a complete abundance analysis was possible. For the derivation of the metallicity it was not possible to use the G-type stars because they were not cluster members. The resultant metallicity is Z = 0.014±0.003 dex. The cluster metallicity was here derived for the first time. Several authors derived the cluster age ($\log t = 8.20 \pm 0.20$), assuming a solar cluster metallicity, from fitting of theoretical isochrones on the photometrically derived main sequence. Therefore the conclusion that NGC 5460 has a solar metallicity confirms that the previous age determinations were correct.

For each star of the sample I derived photometrically $\log L/L_{\odot}$, from the V magnitudes provided by Claria et al. (1993) and, adopting the $T_{\rm eff}$ values derived for the abundance analysis, built the Hertzsprung-Russell (HR) diagram of the cluster.

I plotted the abundances of the elements analysed in most of the stars of the sample as a function of $T_{\rm eff}$ and $\upsilon \sin i$. For some elements, such as Mg and Fe, I obtained trends between abundance and $T_{\rm eff}$, while no trends were found with $\upsilon \sin i$, except for Ba. In particular the abundance increases up to a $T_{\rm eff}$ value of about 10500 K to rapidly decrease with increasing effective temperatures. I looked for the presence of such abundance trend in literature and I obtained that the increase of the iron abundance with increasing effective temperature is actually obtained also with results by Erspamer & North (2003) who analysed a large sample of F- and A-type stars. Their data do not cover anyway the region were I obtained the abundance drop, so that there is not the possibility to check the presence of this phenomenon.

There is the possibility that these trends are real effects due to diffusion in chemically normal stars, known to be effective at least up to $\upsilon \sin i$ values of about 125 km s^{-1} (Hempel & Holweger 2003; Turcotte & Charbonneau 1993). There is as well the possibility that at least for the iron abundance of the cool stars of the sample the abundance increase with $T_{\rm eff}$ is due to non-LTE effects (Rentzsch-Holm 1996).

I derived M/M$_{\odot}$ and fractional age (τ) for each of the stars of the sample and plotted the abundances as a function of M/M$_{\odot}$. Here I obtained the same trend obtained with $T_{\rm eff}$. This is anyway not surprising due to the correlation between stellar mass and effective temperature.

The three stars observed with FORS1 by Bagnulo et al. (2006) are actually not magnetic chemically peculiar stars. Bagnulo et al. (2006) obtained only marginal or not magnetic field detection for all of them.

For two of the three He-weak stars it was not possible to clearly say if they are for example hot Am or cool HgMn stars, while for the third object, HD 123225, it was possible to perform a detailed abundance analysis that led to the conclusion that this star is a HgMn star. This is also the primary component of an SB2 system where the secondary appears to be an A-type star with solar abundances. Anyway this secondary star is itself a very slowly rotating star, so that there is the possibility that it is itself a chemically peculiar stars, precisely an Am star. It would be of great interest to obtain time resolved high resolution spectra to be able to disentangle the spectra to perform a detailed analysis also of the secondary star. A system composed by a HgMn star and an Am star in an open cluster would be of great help for further observational constraints to diffusion models.

5.2.2 Praesepe

The A- and F-type stars show a similar abundance pattern, close to solar, while the Am stars show the typical Am peculiarities: underabundance of C, N, O Ca, Sc and overabundance of the Fe-peak elements and of the rare earths. The abundance scatter of the Am stars is higher than for the normal stars and, between A- and F-type stars, the F-stars show the smaller scatter, as expected.

I turned my attention to the Li abundance of the sample, obtaining results comparable to those of (Burkhart & Coupry 1995), in open clusters, and North et al. (2007), for field stars.

Some stars of the sample were observed in circular polarisation and the LSD technique was adopted to measure the longitudinal magnetic field. No significant magnetic field signature was found applying the LSD technique to the Am stars, which were observed with ESPaDOnS and MuSiCoS. This leads to the conclusion that peculiar abundances and slow rotation of the Praesepe Am stars cannot be explained by the presence of a magnetic field. But since about all of them are SBs I can conclude that slow rotation, induced by binarity, can lead to the Am chemical peculiarities.

I derived the metallicity of the cluster from the F-type stars of the sample, omitting HD 73575 which is already on the TAMS. The resultant metallicity is Z = 0.015±0.002 dex. To be able to compare this metallicity ([Fe/H] = 0.11±0.03) with that used by other authors I derived Z with the approximation given in Chapter 4 that corresponds to Z = 0.024±0.002 dex, assuming $Z_{\odot}$ = 0.019 dex. This result is in agreement with previous metallicity determinations from abundance analysis of G-type stars by An et al. (2007).

For each star of the sample I derived photometrically $\log L/L_{\odot}$ and, adopting the $T_{\rm eff}$ values derived for the abundance analysis, built the Hertzsprung-Russell (HR) diagram of the cluster around the turn-off point. I then fit isochrones by Girardi et al. (2002) to the HR diagram to derive age and metallicity ($\log t$ = 8.77±0.1 dex; Z = 0.030±0.007 dex). This result is in agreement with that obtained by An et al. (2007) fitting YREC isochrones to a photometrically derived main sequence of the cluster. I confirm the discrepancy in metallicity found by An et al. (2007). Within the errors, my age determination agrees with earlier determinations in the literature ($\log t$ = 8.85±0.15, González-García et al. 2006).

I plotted the abundances of the elements analysed in most of the stars of the sample as a function of $T_{\rm eff}$ and $\upsilon \sin i$. I did not find any clear abundance trend with respect to $T_{\rm eff}$ and $\upsilon \sin i$ for the A- and F-type stars. However, I found several trends between abundances and $\upsilon \sin i$ for Am stars. Correlations are present for the elements that characterise the Am peculiarities. Only Sc and Ti do not show this trend. With increasing $\upsilon \sin i$ the peculiarities tend to weaken, and the abundances approach the mean of the other A- and F-type stars. This is the first real observational evidence of a direct connection between abundance anomalies or diffusion processes and rotational velocity in Am stars.

The trends obtained in this work are in disagreement with those predicted by Charbonneau & Michaud (1991), as according to their models meridional circulation does not affect abundance peculiarities. Recently Richer et al. (2000) and later Talon et al. (2006) calculated diffusion models with a more accurate treatment of the rotational mixing. Their predicted abundances for stars with various rotational velocities are qualitatively in agreement with observed properties of the sample of Am stars. Detailed models, with a full treatment of diffusion and rotational mixing, calculated individually for each Am star of this sample, would be necessary for a more substantial comparison between models and observed abundances.

I derived $M/M_\odot$ and fractional age (τ) for each of the stars of the sample and plotted the abundances as a function of $M/M_\odot$. No correlation was found for any of the three spectral groups considered here, as predicted by Richer et al. (2000).

I searched for correlations between abundances of the elements analysed in most of the stars and the Fe abundance. For normal A- and F-type stars I did not find any correlation, while for Am stars strong correlations are obtained for all the peculiar elements. The behavior of the abundances of the elements which are peculiar in Am stars, as a function of the Fe abundance, is the same as that found for $v \sin i$. I conclude that there is a strong connection between the correlations among the abundances, with the correlations of abundances with $v \sin i$. This is anyway expected since Fe is a peculiarity indicator for Am stars.

For this sample of Am stars I compared the obtained abundances with the predictions of diffusion models by Richer et al. (2000). I obtained an excellent agreement, within the errors, with the predictions for almost all the common elements. Only Na and probably S show a clear discrepancy from the theoretical abundances. Unfortunately, my Na and S abundances do not take into account non-LTE effects that would bring the abundances closer to the predictions (Kamp et al. 2001). A non-LTE abundance determination should be performed, at least for few Am stars, in order to confirm the abundance predictions of these two elements. Richer et al. (2000) did not analyse Sc because it is not present in the OPAL opacity database. Model predictions for this element and for heavy elements are especially important and should be performed.

These results indicate that radiative diffusion, combined with turbulent mixing, can account for most of the chemical peculiarities found in Am stars. More abundance determinations on cluster stars with a variety of ages will help to constrain the physical processes at work in Am stars.

5.2.3 Combined analysis of the two samples of open clusters, and future work

The merging of the results of the two samples of cluster stars has to be performed taking into account the different original metallicity of the two open clusters. The best way would be to obtain the abundance of the maximum number of elements from the G-type stars member of each cluster and then normalise the abundances obtained for the early-type stars on the basis of the ones of the G-type stars.

Unfortunately I do not have spectra of G-type stars member of the two open clusters, so that I assumed that the original metallicity of the cluster is given by the early F- and late A-type stars. A confirmation of the possibility to adopt these abundances as original cluster abundances in first approximation is given by the results obtained for the metallicity of the Praesepe cluster. In this cluster the Fe abundance obtained from the early F-type stars is in perfect agreement with the Fe abundance derived from spectra of G-type stars and published by An et al. (2007).

From Fig. 5.4 to Fig. 5.12 I show the abundances relative to the original cluster metallicity for the most analysed elements: C, Mg, Si, Ca, Sc, Ti, Cr, Fe and Ba. The assumed original cluster metallicity relative to the sun for each mentioned elements for NGC 5460 is: 0.23, -0.33, 0.35, -0.09, -0.17, -0.09, -0.12, -0.18, 0.58 respectively. While for the Praesepe cluster stars the assumed original cluster metallicity is: 0.26, 0.06, 0.29, 0.20, 0.17, 0.19, 0.02, 0.11, 0.54 respectively.

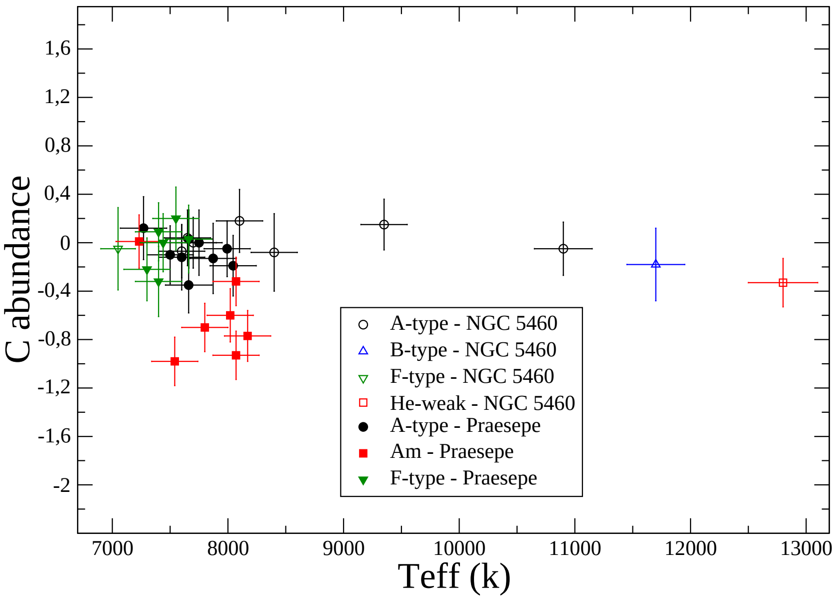

Figure 5.4: Carbon abundances of the analysed stars as a function of the derived $T_{\rm eff}$. The open symbols denote the stars belonging to NGC 5460, while the closed symbols indicate the stars analysed in the Praesepe open cluster. Upside triangles, circles, downside triangles and squares indicate B-, A-, F-type and chemically peculiar stars respectively. The crosses indicate the non cluster members. The abundances of the stars member of the NGC 5460 open cluster were normalised to the original cluster metallicity of 0.23, while for the Praesepe cluster the normalisation was of 0.26.

The abundance trends with $T_{\rm eff}$ visible from Fig. 5.4 to Fig. 5.12 are very similar to the ones shown for the results obtained for NGC 5460, since the Praesepe

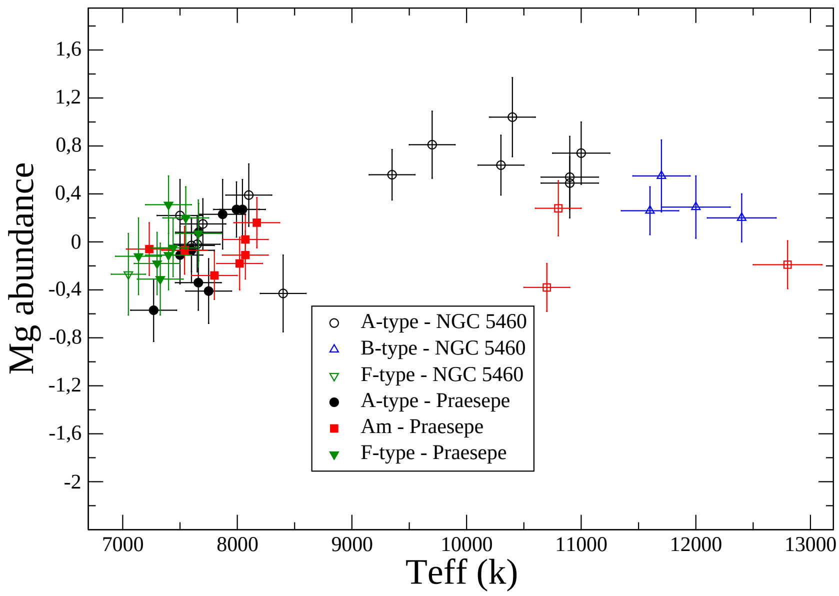

Figure 5.5: Same as Fig. 5.4, but for magnesium. The abundances were normalised to -0.33 and 0.06 for stars belonging to NGC 5460 and the Praesepe cluster respectively.

stars contribute only to the cool side of the plots.

To be able to give observational constraints to diffusion models in respect of the abundance evolution with time it will be useful to subdivide the sample in mass bins. At this stage of the analysis it is not necessary since the comparison between the abundances of clusters with different age could be performed only with two clusters and for one mass bin ($M/M_{\odot} \leq 2$).

Figures from 5.4 to 5.12 show that the abundances of the cool stars of the two samples scatter around zero, since I normalised all the abundances to the mean abundance of these objects. The performed abundance normalisation has advantages and disadvantages. The clear advantage is that the normalisation is based on abundances that were obtained consistently for all the open clusters and for all the stars in each open cluster. In this way it is possible to minimise possible systematic errors introduced by a normalisation based on abundances obtained with different instruments, methodology, atomic parameters, etc. On the other hand the disadvantage is that it is not possible to explore the abundance evolution for the cool stars (F- and late A-type stars). For this reason it will be extremely important for the prosecution of the project to obtain high resolution spectra of cluster member late type stars for each analysed cluster and to analyse them with the same methodology adopted up to now. In this way the normalisation will be really effective to search the kind of effects for which the project is intended.

Clearly the analysis limited to only two open clusters prevents to obtain any

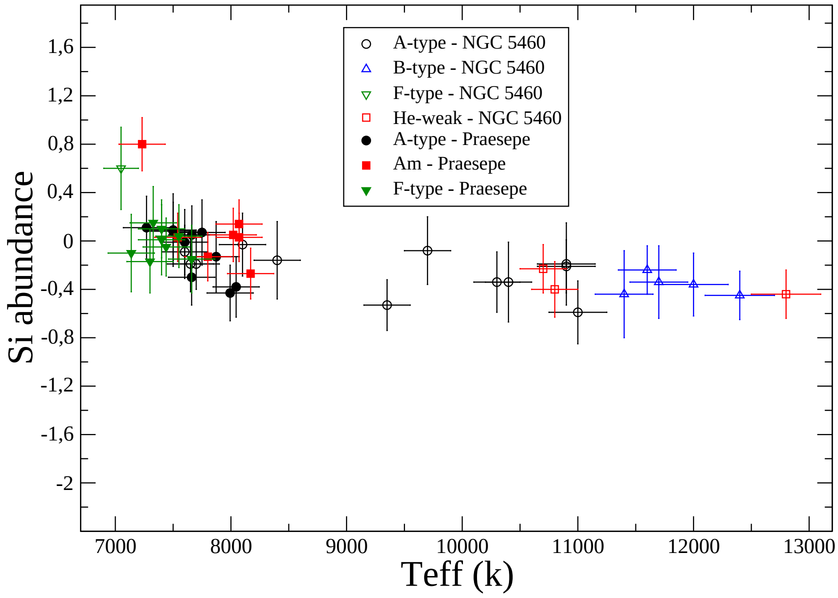

Figure 5.6: Same as Fig. 5.4, but for silicon. The abundances were normalised to 0.35 and 0.29 for stars belonging to NGC 5460 and the Praesepe cluster respectively.

result regarding the abundance evolution with age, but here I show the path to follow for the future analysis.

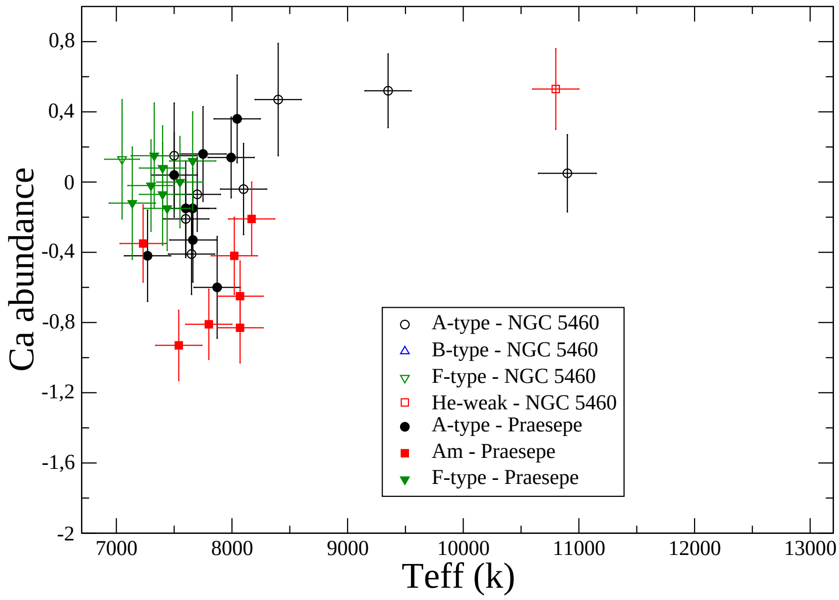

Figure 5.7: Same as Fig. 5.4, but for calcium. The abundances were normalised to -0.09 and 0.20 for stars belonging to NGC 5460 and the Praesepe cluster respectively.

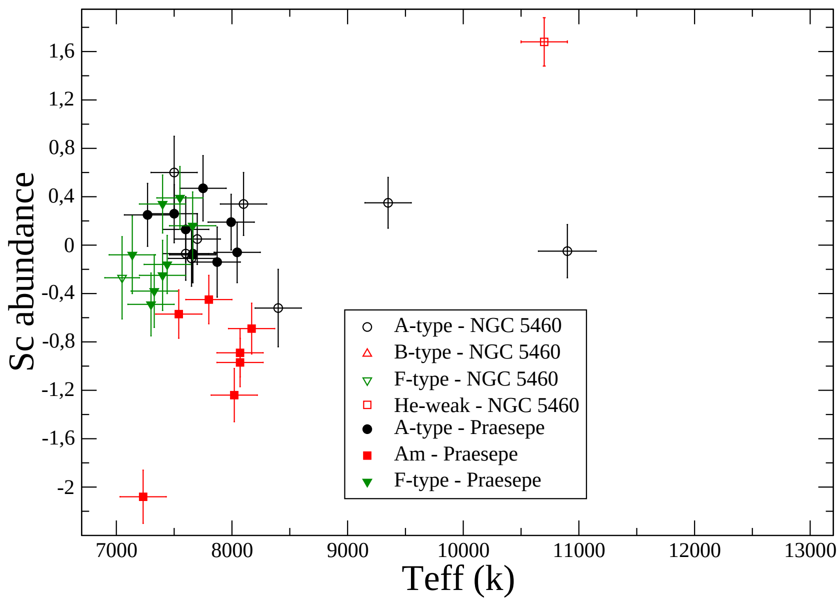

Figure 5.8: Same as Fig. 5.4, but for scandium. The abundances were normalised to -0.17 and 0.17 for stars belonging to NGC 5460 and the Praesepe cluster respectively.

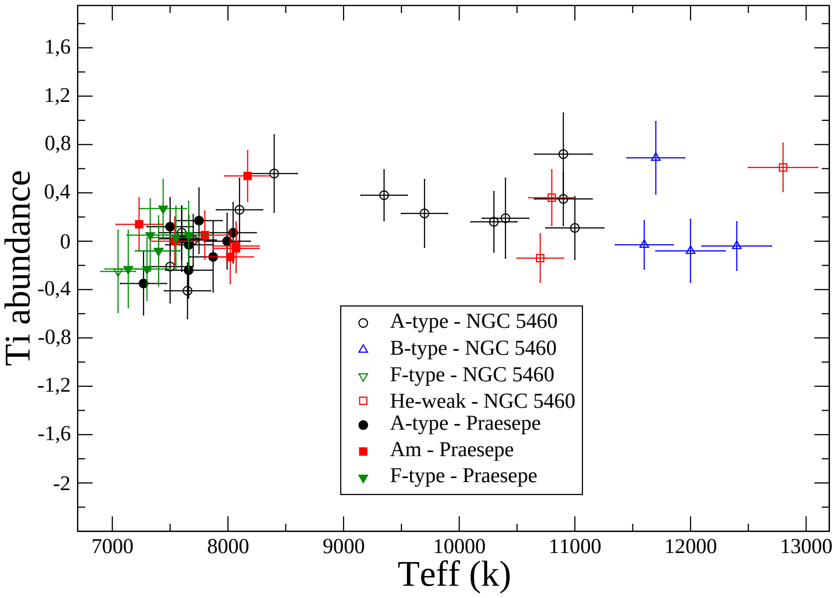

Figure 5.9: Same as Fig. 5.4, but for titanium. The abundances were normalised to -0.09 and 0.19 for stars belonging to NGC 5460 and the Praesepe cluster respectively.

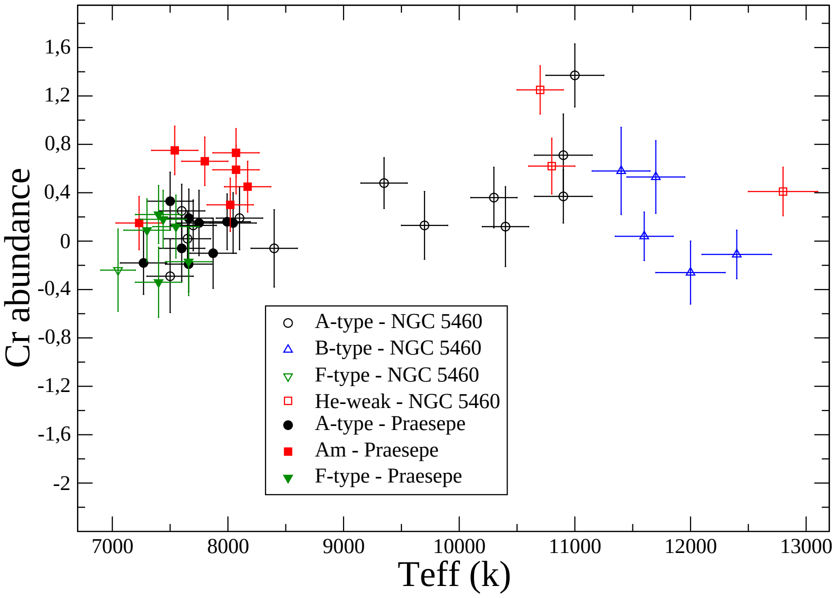

Figure 5.10: Same as Fig. 5.4, but for chromium. The abundances were normalised to -0.12 and 0.02 for stars belonging to NGC 5460 and the Praesepe cluster respectively.

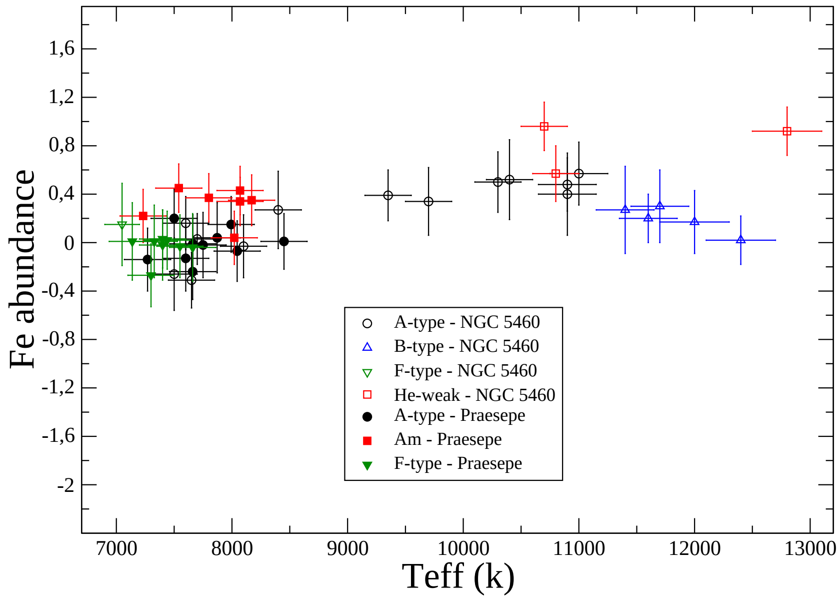

Figure 5.11: Same as Fig. 5.4, but for iron. The abundances were normalised to -0.18 and 0.11 for stars belonging to NGC 5460 and the Praesepe cluster respectively.

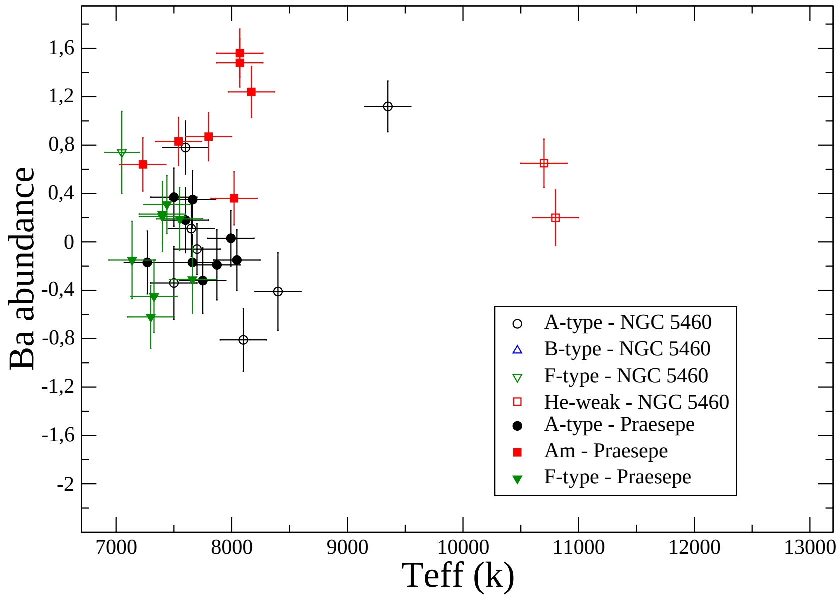

Figure 5.12: Same as Fig. 5.4, but for barium. The abundances were normalised to 0.58 and 0.54 for stars belonging to NGC 5460 and the Praesepe cluster respectively.

Bibliography

Abt, H. A. 1970, ApJS, 19, 387

Abt, H. A. & Morrel, N. I. 1995, ApJS, 99, 135

Abt, H. A., & Willmarth, D. W. 1999, ApJ, 521, 682

Abt, H. A., Levato, H. & Grosso, M. 2002, ApJ, 573, 359

Adelman, S. J. 1988, MNRAS, 230, 671

Adelman, S. J., Pyper, D. M., Shore, S. N., White, R. E. & Warren, Jr., W. H. 1989, A&AS, 81, 221

Adelman, S. J. 1991, MNRAS, 252, 116

Adelman, S. J., Bolcal, C., Kocer, D. & Hill, G. 1991, MNRAS, 252, 329

Adelman, S. J. 1994, MNRAS, 271, 355

Adelman, S. J. 1996, MNRAS, 280, 130

Adelman, S. J., Caliskan, H., Kocer, D. & Bolcal, C. 1997, MNRAS, 288, 470

Adelman, S. J. 1998, MNRAS, 296, 856

Adelman, S. J., Ryabchikova, T. A. & Davydova, E. S. 1998, MNRAS, 297, 1

Adelman, S. J. & Albayrak, B., 1998, MNRAS, 300, 359

Adelman, S. J. 1999, MNRAS, 310, 146

Adelman, S. J., Caliskan, H., Kocer, D., Cay, I. H. & Gokmen Tektunali, H. 2000, MNRAS, 316, 514

Adelman, S. J., Caliskan, H., Kocer, D. et al. 2001, MNRAS, 371, 1078

Adelman, S. J., Pintado, O. I., Nieva, M. F., Rayle, K. E. & Sanders, Jr., S. E. 2002, A&A, 392, 1031

Adelman, S. J., & Unsuree, N. 2007, Baltic Astronomy, 16, 183

Ahumada, J. A., & Lapasset, E. 2007, A&A, 463, 789

Alecian, G. 1996, A&A, 310, 872

Alecian, E., Wade, G. A., Catala, C. et al. 2008, A&A, 481, L99

An, D., Terndrup, D. M., Pinsonneault, M. H., et al. 2007, ApJ, 655, 233

Asplund, M., Grevesse, N., & Sauval, A. J. 2005, in ASP Conf. Ser. 336: Cosmic Abundances as Records of Stellar Evolution and Nucleosynthesis, ed. Thomas G. Barnes III & Frank N. Bash, 25

Bagnulo, S., Landstreet, J.D., Mason, E., et al. 2006, A&A, 450, 777

Bagnulo, S., Landolfi, M., Landstreet, J.D. et al. 2009, PASP, submitted

Balona, L. A. 1994, MNRAS, 268, 119

Balona, L. A., Krisciunas, K. & Cousins, A. W. J. 1994, MNRAS, 270, 905

Barklem, P. S., Piskunov, N. & O'Mara, B. J. 2000, A&AS 142, 467

Barrado, D. & Byrne, P. B. 1995, A&AS, 111, 275

Baumgardt, H., Dettbarn, C., & Wielen, R. 2000, A&AS, 146, 251

Böhm-Vitense, E. 2006, PASP, 118, 419

Bond, H. E. 1972, PASP, 84, 446

Breger, M. 1976, ApJS, 32, 7

Breger, M. 2000, in ASP Conf. Ser. 220: δ Scuti stars (Review), ed. Breger, M., & Montgomery, M., 3

Bruntt, H., De Cat, P., & Aerts, C. 2008, A&A, 478, 487

Budaj, J. 1996, A&A, 313, 523

Burkhart, C. 1979, A&A, 74, 38

Burkhart, C., & Coupry, M. F. 1991, A&A, 249, 205

Burkhart, C., & Coupry, M. F. 1995, Memorie della Societa Astronomica Italiana, 66, 357

Burkhart, C., & Coupry, M. F. 1998, A&A, 338, 1073

Burkhart, C., Coupry, M. F., Faraggiana, R., & Gerbaldi, M. 2005, A&A, 429, 1043

Caliskan, H. & Adelman, S. J. 1997, MNRAS, 288, 501

Caliskan, H., Adelman, S. J., Cay, M. T. et al. 2002, A&A, 394, 187

Canuto, V. M., & Mazzitelli, I. 1992, ApJ, 389, 724

Charbonneau, P. & Michaud, G. 1991, ApJ, 370, 693

Chen, L., Hou, J. L., & Wang, J. J. 2003, AJ, 125, 1397

Clampitt, L. & Burstein, D. 1997, AJ, 114, 699

Claria, J. J. 1971, AJ, 76, 639

Claria, J. J., Lapasset, E. & Bosio, M. A. 1993, A&AS, 99, 1

Debernardi, Y., Mermilliod, J.-C., Carquillat, J.-M., & Ginestet, N. 2000, A&A, 354, 881

Dias, W. S., Assafin, M., Flório, V., Alessi, B. S., & Líbero, V. 2006, A&A, 446, 949

Donati, J.-F., Semel, M., Carter, B. D., Rees, D. E., & Collier Cameron, A. 1997, MNRAS, 291, 658

Donati, J.-F., Catala, C., Wade, G. A., et al. 1999, A&AS, 134, 149

Erspamer, D., & North, P. 2003, A&A, 398, 1121

Folsom, C. P., Wade, G. A, Bagnulo, S., & Landstreet, J. D. 2007, MNRAS, 376, 361

Fossati, L., Bagnulo, S., Monier, R., et al. 2007, A&A, 476, 911

Fossati, L., Bagnulo, S., Landstreet, J, et al. 2008, A&A, 483, 891

Fossati, L., Kolenberg, K., Reegen, P. & Weiss, W. 2008, A&A, 485, 257

Fossati, L., Mochnacki, S., Landstreet, J., Weiss, W. 2009, A&A, submitted

Fossati, L., Ryabchikova, T., Bagnulo, S., et al. 2009, A&A, in press

Fuhrmann, K., Pfeiffer, M., Frank, C., Reetz, J. & Gehren, T. 1997, A&A, 323, 909

Gebran, M. & Monier, R. 2005, Memorie della Societa Astronomica Italiana Supplement, 8, 200

Gebran, M. & Monier, R. 2008, A&A, 483, 567

Girardi, L., Bertelli, G., Bressan, A., et al. 2002, A&A, 391, 195

Glebocki, R., & Stawikowski, A. 2000, Acta Astronomica, 50, 509

González-Garcá, B. M., Zapatero Osorio, M. R., Béjar, V. J. S., et al. 2006, A&A, 460, 799

Gray, R. O., & Garrison, R. F. 1989, ApJS, 70, 623

Gray, D. F. 1992, The observation and analysis of stellar photospheres (Cambridge University Press)

Handler, G. & Shobbrook, R. R. 2002, MNRAS, 333, 251

Handler, G., Balona, L. A., Shobbrook, R. R. et al. 2002, MNRAS, 333, 262

Hauck, B., & Mermilliod, M. 1998, A&AS, 129, 431

Hauck, B., & North, P. 1993, A&A, 269, 403

Hempel, M., & Holweger, H. 2003, A&A, 408, 1065

Hill, G. M., & Landstreet, J. D. 1993, A&A, 276, 142

Hog, E., Fabricius, C., Makarov, V. V. et al. 2000, A&A, 355, L27

Hubrig, S. & Mathys, G. 1996, A&AS, 120, 457

Jamar, C., Macau-Hercot, D., Monfils, A. et al. 1976, Ultraviolet bright-star spectrophotometric catalogue. A compilation of absolute spectrophotometric data obtained with the Sky Survey Telescope (S2/68) on the European Astronomical Satellite TD-1

Kamp, I., Iliev, I. K., Paunzen, E. et al. 2001, A&A, 375, 899

Kamp, I., Martínez-Galarza, J. R., Paunzen, E. et al. 2008, Contributions of the Astronomical Observatory Skalnate Pleso, 38, 147

Khan, S. A., & Shulyak, D. V. 2007, A&A, 469, 1083

Kharchenko, N. V., Piskunov, A. E., Röser, S., Schilbach, E., & Scholz, R.-D. 2004, AJ, 325, 740

Kharchenko, N. V., Piskunov, A. E., Röser, S., Schilbach, E., & Scholz, R.–D. 2005, A&A, 438, 1163

Kobi, D. & North, P. 1990, A&AS, 85, 999

Kocer, D., Adelman, S. J., Caliskan, H., Gulliver, A. F. & Gokmen Tektunali, H. 2003, A&A, 406, 975

Kochukhov, O. 2007, Spectrum synthesis for magnetic, chemically stratified stellar atmospheres, Physics of Magnetic Stars, 109, 118

Kochukhov, O. 2008, Communications in Asteroseismology, 157, 228

Kraft, R. P. 1967, ApJ, 150, 551

Kunzli, M., North, P., Kurucz, R. L. & Nicolet, B. 1997, A&AS, 122, 51

Kupka, F., Piskunov, N. E., Ryabchikova, T. A., Stempels, H. C., & Weiss, W. W. 1999, A&AS, 138, 119

Kurtz, D. W. 1989, MNRAS, 238, 1077

Kurucz, R. L. 1973, Line-Blanketed Model Atmospheres, PhD Thesis, AA(Harvard University)

Kurucz, R. 1993, ATLAS9: Stellar Atmosphere Programs and 2 km/s grid. Kurucz CD-ROM No. 13 (Cambridge: Smithsonian Astrophysical Observatory)

Landstreet, J. D. 1969, PASP, 81, 896

Landstreet, J. D. 1998, A&A, 338, 1041

Landstreet, J. D., Bagnulo, S., Andretta, V., et al. 2007, A&A, 470, 685

Landstreet, J. D., Silaj, J., Andretta, V. et al. 2008, A&A, 481, 465

Lanz, T., & Mathys, G. 1993, A&A, 280, 486

van Leeuwen, F. 2007, Hipparcos, the New Reduction of the Raw Data. Institute of Astronomy, Cambridge University, Cambridge, UK Series: Astrophysics and Space Science Library, Vol. 350 20 Springer Dordrecht

Luck, R. E. & Heiter, U. 2005, AJ, 129, 1063

Maitzen, H. M., & Pavlovski, K. 1987, A&AS, 71, 441

Mermilliod, J.-C., & Paunzen, E. 2003, A&A, 410, 511

Mihalas, D. 1978, Stellar atmospheres, 2nd edition, San Francisco, W. H. Freeman and Co.

Moon, T. T. & Dworetsky, M. M. 1985, MNRAS, 217, 305

Napiwotzki, R., Schoenberner, D. & Wenske, V. 1993, A&A, 268, 653

North, P. & Nicolet, B. 1990, A&A, 228, 78

North, P., Betrix, F., & Besson, C. 2007, EAS Publications Series, 17, 333

Pintado, O. I. & Adelman, S. J. 1993, MNRAS, 264, 63

Piskunov, N. E., Kupka, F., Ryabchikova, T. A., Weiss, W. W., & Jeffery, C. S. 1995, A&AS, 112, 525

Pourbaix, D., Tokovinin, A. A., Batten, A. H., et al. 2004, A&A, 424, 727

Preston, G. W. 1974, ARA&A, 12, 257

Renson, P., Gerbaldi, M., & Catalano, F. A. 1991, A&AS, 89, 429

Rentzsch-Holm, I. 1996, A&A, 312, 966

Richer, J., Michaud, G., & Turcotte, S. 2000, ApJ, 529,338

Robichon, N., Arenou, F., Mermilliod, J.-C., & Turon, C. 1999, A&A, 345, 471

Rodríguez, E., López-González, M. J., & López de Coca, P. 2000, A&AS, 144, 469

Royer, F., Gerbaldi, M., Faraggiana, R. & Gómez, A. E. 2002, A&A, 381, 105

Royer, F., Grenier, S., Baylac, M.-O., Gómez, A. E., & Zorec, J. 2002, A&A, 393, 897

Royer, F., Zorec, J. & Gómez, A. E. 2007, A&A, 463, 671

Rufener, F. 1988, Catalogue of stars measured in the Geneva Observatory photometric system : 4 : 1988, Sauverny: Observatoire de Geneve

Ryabchikova, T. A., Zakharova, L. A. & Adelman, S. J. 1996, MNRAS, 283, 1115

Ryabchikova, T. A., Piskunov, N. E., Stempels, H. C., Kupka, F., & Weiss, W. W. 1999, Phis. Scr., T83, 162

Ryabchikova, T. A., Kochukhov, O., & Bagnulo, S. 2008, A&A, 480, 811

Ryabchikova, T., Fossati, L. & Shulyak, D. 2009, A&A, submitted

Samus, N. N., & Durlevich, O. V. 2004, VizieR Online Data Catalog, 2250

Savanov, I. S. 1995, Astronomy Letters, 21, 684

Schaller, G., Schaerer, D., Meynet, G., & Maeder, A. 1992, A&AS, 96, 269

Shorlin, S. L. S., Wade, G. A., Donati, J.-F., et al. 2002, A&A, 392, 637

Shulyak, D., Tsymbal, V., Ryabchikova, T., Stütz, Ch., & Weiss, W. W. 2004, A&A, 428, 993

Sills, A., Pinsonneault, M. H., & Terndrup, D. M. 2000, ApJ, 534, 335

Stütz, Ch., Bagnulo, S., Jehin, E., et al. 2006, A&A, 451, 285

Stütz, Ch., Nesvacil, N., Fossati, L. & Shulyak, D. 2008, Contributions of the Astronomical Observatory Skalnate Pleso, 38, 457

Takeda, Y., Han, I., Kang, D.-I., Lee, B.-C. & Kim, K.-M. 2008, Journal of Korean Astronomical Society, 41, 83

Talon, S., Richard, O., & Michaud, G. 2006, ApJ, 645, 634

Tsymbal, V. V. 1996, in ASP Conf. Ser. 108, Model Atmospheres and Spectral Synthesis, ed. S. J., Adelman, F., Kupka, & W. W., Weiss, 198

Turcotte, S. & Charbonneau, P. 1993, ApJ, 413, 376

Varenne, O. & Monier, R. 1999, A&A, 351, 247

Wade, G. A., Donati, J.-F., Landstreet, J. D., & Shorlin, S. L. S. 2000, MNRAS, 313, 823

Wilson, S. C. 1966, ApJ, 144, 695

Zacharias, N., Urban, S. E., Zacharias, M. I. et al. 2004, AJ, 127, 3043

Zorec, J. 2004, Rotation and Properties of Be Stars (Invited Review), IAU Symposium, ed. Maeder, A. & Eenens, P., 215, 73

Chapter 6

Acknowledgements, ringraziamenti, Bestätigung

Essendo italiano, avendo sposato una meravigliosa ragazza austriaca e lavorando in ambito internazionale mi tocca scrivere questi ringraziamenti in tre lingue: italiano per gli italiani, tedesco per gli austriaci ed inglese per il resto del mondo.

Beh...e' molto facile sapere con chi cominciare. Questa e' una tesi di dottorato e non sarei mai arrivato fin qui (inteso sia nel tempo che nello spazio) senza l'aiuto di Stefano. Mi ha dato il mio primo lavoro, mi ha procurato un dottorato in un posto meraviglioso (dove tra le altre cose ho conosciuto mia moglie) e mi ha praticamente insegnato un mestiere, cosa che purtroppo la scuola italiana non e' capace di fare. Ti ringrazio davvero di cuore e spero che tu sia contento di come questo tuo primo studente ti sia venuto fuori.
Ich danke Werner für das Vertrauen, das er hat mir in diesen drei Jahren geschenkt hat. Ich hoffe nur, ich habe ihm dieses Vertrauen zrückgeben können.

I can only say thank you to Tanya and John. Together with Stefano they tought me practically everything I have learned during this thesis. My very short visit in Moscow working with Tanya on abundance analysis was incredibly important for the development of this thesis and of my scientific knowledge in general. John is always very patient with me, also when I am asking him very stupid things.

A big thank you goes also to all the persons that helped me during the time of this PhD and in particular Gregg and Oleg. I appreciate also the useful help and discussion I had, have and hope to continue to have with Vadim and Dima.

Hier, in Wien, ich habe eine ganz besondere Person gefunden ("ich habe einen Schatz gefunden ..."): meine Frau Sibylle. Mit ihr habe ich verstanden, was man meint, wenn man sagt: du bist gleichzeitig meine Frau, meine Geliebte und meine Freundin. Danke, dass Du meine Frau, meine Geliebte und meine Freunde bist. Wie Du manchmal sagst ... zusammen koennen wir alles schaffen.

E' la seconda volta che ringrazio i miei genitori in una tesi e non saprei davvero quale altra parola usare se non un immenso e profondo grazie per tutto l'aiuto, il conforto e l'amore che mi hanno dato. Dovrei ringraziarli cento ... mille volte, pero' che non si aspettino che scriva un'altra tesi: questa e quella prima mi sono bastate. Poi viene la mia sorellina, il medico di famiglia, che ha gia' salvato la vita al papa'. Mi sembra sinceramente un buon inizio. Spero che un giorno impari a focalizzare di piu' i suoi pensieri, invece di cambiarli ogni volta che cambia il vento. La Millina non va dimenticata. Purtroppo non posso dedicarle anche questa tesi, e' un documento un po' troppo ufficiale per dedicarlo a qualcuno, pero' e' come se lo fosse. Beatrice ormai e' piu' una sorella che una cugina, va ringraziata soltanto perche' esiste: ci ricorda sempre che bella persona sia stata suo padre e colma un po' il vuoto. Le auguro di essere pero' molto piu' fortunata di lui.

Seit ich vereiratet bin, habe ich auch eine neue Familie, darüberhinaus ein Neffen, zwei wunderbare Nichten und nicht zuletzt Oma und Opa. Ich danke ihnen allen dafür, dass sie mich sofort mit offenem Herzen in die Familie aufgenommen haben.

Un immenso grazie ad Andrea non solo per essere un ottimo amico ed il mio testimone di nozze, ma soprattutto per aver avuto una sera l'idea geniale di andare a bere qualche cosa al bar Italia, dopo l'opera.

Un grazie speciale va anche a Denis, il miglior DJ che si possa sperare di avere ad un matrimonio oltre che un ottimo amico, e Claudia.

Ich danke meinen TT-freunden hier in Wien: Daniel, Herbert, Henning, Gil, Andreas mit der ganzen WUW und BA. Daniel merita un ringraziamento particolare per l'aiuto che mi ha dato in questi anni col tedesco e con la tesi, ma soprattutto per avermi fatto provare davvero una forte emozione cantando al matrimonio. Ich danke auch Karima und Matteo (spero che trovi un po' di serenita'), sie haben mir am Anfang viel geholfen.

Thank you also to all the people working here at the University and with whom I joined this important period of my life.

E' ora il momento di ringraziare i miei amici in Italia. Il CIC, cioe' Nicola, Davide, Roberto, Aldo e Claudio. Anche se viviamo lontani sappiamo sempre di esserci l'uno per gli altri e questo lo trovo davvero meraviglioso. Chiudo ringraziando Anna per avermi davvero spesso aiutato tanto a capirmi, spero di aver fatto altrettanto con lei.

Appendix A

Copyright permissions

Astronomy and Astrophysics
Editor in Chief: C. Bertout

C. Bertout
Observatoire de Paris
61, avenue de l'Observatoire
75014 Paris, France

Tel.: 33 0(1) 43 29 05 41
Fax: 33 0(1) 43 29 05 57
e-mail: aanda.paris@obspm.fr
Web: http://www.aanda.org

merging
Annales d'Astrophysique
Arkiv for Astronomi
Bulletin of the Astronomical Institutes of the Netherlands
Bulletin Astronomique
Journal des Observateurs
Zeitschrift fur Astrophysik
Bulletin of the Astronomical Institutes of Czechoslovakia

Paris, February 26, 2009

Reprint Permission

Material:
Fossati et al. 2008, A&A, 483, 891
Fossati et al. 2007, A&A, 476, 911
Ryabchikova et al., AA/2009/11871 (provided the article is accepted)
Fossati et al., AA/2009/11561 (provided the article is accepted)
The map of the NGC5460 open cluster published by: Kharchenko et al. 2005, A&A, 438, 1163
Figure 1 in: Bagnulo et al. 2006, A&A, 450, 777

To be used in:
PhD thesis, University of Vienna

Permission granted to:
Luca Fossati <fossati@jan.astro.univie.ac.at>

I hold copyright on the material referred to above, and hereby grant permission for its use as requested herewith.

Claude Bertout
A&A Editor-in-Chief

The journal "Contributions of the Astronomical Observatory Skalnaté Pleso" copyright holder Astronomical Institute of the Slovak Academy of Sciences grants permission to Mr. Luca Fossati to reproduce whole or parts of the article specified bellow in his PhD thesis.

Article:

* Author(s): Fossati, L.; Bagnulo, S.; Monier, R.; Khan, S.A.; Kochukhov, O.; Landstreet, J.D.; Wade, G.A.; Weiss, W.W.
* Journal: Contributions of the Astronomical Observatory Skalnaté Pleso, vol. 38, no. 2, p. 123-128.
* Date: 4/2008
* Title: Chemical evolution of A- and B-type stars in open clusters: observed abundances vs. diffusion models. Am stars in the Praesepe cluster
* Pages: 123 -- 128

Richard KOMZIK (rkomzik@ta3.sk)
CAOSP executive editor

Februray 26, 2009

Appendix B

Thesis reference publications

As mentioned at the beginning of this thesis, part of the work here presented was taken from three already published papers for which I am the first author. Here I summarise the work I performed for each of them.

- Fossati, L., Bagnulo, S., Monier, R., Khan, S. A., Kochukhov, O., Landstreet, J.,Wade, G. & Weiss, W. 2007, A&A, 476, 911

For this paper I performed the whole parameter determination and abundance analysis. I have also written the whole paper, besides parts of Sect. 1 and 3. I produced also all Tables and Figures present in the paper.

- Fossati, L., Bagnulo, S., Monier, R., Khan, S. A., Kochukhov, O., Landstreet, J.,Wade, G. & Weiss, W. 2008, Contributions of the Astronomical Observatory Skalnate Pleso, 38, 2, 123

For this paper I performed the whole parameter determination and abundance analysis. I have also written the whole text, Tables and produced the Figure present in the paper.

- Fossati, L., Bagnulo, S., Landstreet, J, Wade, G., Kochukhov, O., Monier, R., Weiss, W., Gebran, M. 2008, A&A, 483, 891

For this paper I performed the whole parameter determination and abundance analysis. I have also written the whole text, Tables and Figures present in the paper. For this publication I have also performed the observing proposal and the following observations.

- Fossati, L., Ryabchikova, T., Bagnulo, S., Alecian, E., Grunhut, J., Kochukhov, O., Wade, G. 2009, A&A, in press

I wrote the whole text and the two figures reproduced in this thesis and taken from this publication.

A&A 476, 911–925 (2007)
DOI: 10.1051/0004-6361:20078320
© ESO 2007

Astronomy & Astrophysics

Late stages of the evolution of A-type stars on the main sequence: comparison between observed chemical abundances and diffusion models for 8 Am stars of the Praesepe cluster⋆

L. Fossati[1], S. Bagnulo[2], R. Monier[3], S. A. Khan[4], O. Kochukhov[5], J. Landstreet[4], G. Wade[6], and W. Weiss[1]

[1] Institut fur Astronomie, Universität Wien, Türkenschanzstrasse 17, 1180 Wien, Austria
e-mail: [fossati;weiss]@astro.univie.ac.at
[2] Armagh Observatory, College Hill, Armagh BT61 9DG, Northern Ireland
e-mail: sba@arm.ac.uk
[3] Groupe de Recherches en Astronomie et Astrophysique du Languedoc, UMR 5024, Université Montpellier II, Place E. Bataillon, 34095 Montpellier, France
e-mail: Richard.Monier@graal.univ-montp2.fr
[4] Department of Physics & Astronomy, University of Western Ontario, London, N6A 3K7, Ontario, Canada
e-mail: [skhan;jlandstr]@astro.uwo.ca
[5] Department of Astronomy and Space Physics, Uppsala University, 751 20, Uppsala, Sweden
e-mail: oleg@astro.uu.se
[6] Physics Dept., Royal Military College of Canada, PO Box 17000, Station Forces, K7K 4B4, Kingston, Canada
e-mail: Gregg.Wade@rmc.ca

Received 20 July 2007 / Accepted 19 September 2007

ABSTRACT

Aims. We aim to provide observational constraints on diffusion models that predict peculiar chemical abundances in the atmospheres of Am stars. We also intend to check if chemical peculiarities and slow rotation can be explained by the presence of a weak magnetic field.

Methods. We have obtained high resolution, high signal-to-noise ratio spectra of eight previously-classified Am stars, two normal A-type stars and one Blue Straggler, considered to be members of the Praesepe cluster. For all of these stars we have determined fundamental parameters and photospheric abundances for a large number of chemical elements, with a higher precision than was ever obtained before for this cluster. For seven of these stars we also obtained spectra in circular polarization and applied the LSD technique to constrain the longitudinal magnetic field.

Results. No magnetic field was detected in any of the analysed stars. HD 73666, a Blue Straggler previously considered as an Ap (Si) star, turns out to have the abundances of a normal A-type star. Am classification is not confirmed for HD 72942. For HD 73709 we have also calculated synthetic Δa photometry that is in good agreement with the observations. There is a generally good agreement between abundance predictions of diffusion models and values that we have obtained for the remaining Am stars. However, the observed Na and S abundances deviate from the predictions by 0.6 dex and ≥0.25 dex respectively. Li appears to be overabundant in three stars of our sample.

Key words. stars: abundances – stars: atmospheres – stars: fundamental parameters – stars: chemically peculiar

1. Introduction

Main sequence A-type stars present spectral peculiarities, usually interpreted as due to peculiar photospheric abundances and abundance distributions which are believed to be produced by the interaction of a large variety of physical processes (e.g. diffusion, magnetic field, pulsation and various kinds of mixing processes).

An interesting problem that has yet to be addressed is how these peculiarities change during main sequence evolution. The chemical composition of field A-type stars have been studied by several authors, e.g. Hill & Landstreet (1993), Adelman et al. (2000). However, it is not straightforward to use the results of these investigations to study how photospheric chemistry evolves during a star's main sequence life. First, the original composition of the cloud from which stars were born is not known and is likely somewhat different for each field star. It is therefore not possible to discriminate between evolutionary effects and differences due to original chemical composition. Secondly, it is difficult to estimate the age of field stars with the precision necessary for such evolutionary studies (for a discussion of this problem see Bagnulo et al. 2006).

From this point of view, A-type stars belonging to open clusters are much more interesting objects. Compared to field stars, A-type stars in open clusters have three very interesting properties:

– they were all presumably born from the interstellar gas with an approximately uniform composition;
– they all have approximately the same age (to within a few Myr);
– their age can be determined much more precisely than for field stars.

⋆ Figures 13–22 and Table 4 are only available in electronic form at http://www.aanda.org

Article published by EDP Sciences and available at http://www.aanda.org or http://dx.doi.org/10.1051/0004-6361:20078320

Few abundance analyses of A-type stars in open clusters have been carried out. Those that have been published have usually focused on a limited numbers of stars.

Varenne & Monier (1999) have determined the abundances of eleven chemical elements for a large sample of stars regularly distributed in spectral type along the main sequence in order to sample the expected masses uniformly. All these stars were analysed in a uniform manner using spectrum synthesis. Stütz et al. (2006) have performed a detailed abundance analysis for five A-type stars of the young open cluster IC 2391. Folsom et al. (2007) have performed a detailed abundance analysis for four Ap/Bp stars and one normal late B-type star of the open cluster NGC 6475.

A goal of this programme is to determine photospheric abundance patterns in A-type star members of clusters of different ages. This is crucial in order to: *i)* investigate the chemical differences between normal and peculiar stars inside the same cluster, *ii)* study the evolution with time of abundance peculiarities by studying clusters of various ages, *iii)* set constraints on the hydrodynamical processes occurring at the base of the convection zone in the non magnetic stars and *iv)* study the effects of diffusion in the presence of a magnetic field for the magnetic (Ap) stars in the cluster. The abundance analysis will be performed in an homogeneous way applying a method described in this first work.

Praesepe (NGC 2632), a nearby intermediate-age open cluster ($\log t = 8.85 \pm 0.15$, González-García et al. 2006), is an especially interesting target because it includes a large number of A-type stars, among which are many Am stars. Furthermore, because the cluster is relatively close to the sun ($d = 180 \pm 10$ pc, Robichon et al. 1999), many of the member A-type stars are bright enough to allow us to obtain high resolution spectra with intermediate class telescopes.

We dedicate this first paper to the Am stars of the Praesepe cluster, searching for magnetic fields in these objects and discussing the differences between "normal"[1] A-type stars and Am stars in the cluster.

We also compare our results with previous works and with theoretical chemical evolution models. In particular we take into account diffusion models by Richer et al. (2000). We want to provide observational constraints to the theory of the evolution of the abundances in normal and chemically peculiar stars. Our detailed abundance analysis could provide information about the turbulence occurring in the outer stellar regions in Am stars with well determined age. In particular, our analysis can give constraints to define the depth of the zone mixed by turbulence, since it is the only parameter characterising turbulence (Richer et al. 2000). A systematic abundance analysis of normal and peculiar stars in clusters could provide information on the origin of the mixing process and show if only turbulence is needed to explain abundance anomalies, or if other hydrodynamical processes occur.

We tackle this problem using new and more precise new-generation spectrographs providing a wider wavelength coverage together with newer analysis codes and procedures (e.g. Least-Squares Deconvolution and synthetic line profile fitting instead of equivalent width measurements).

The observed stars, the instruments employed and the target selection are described in Sect. 2. The data reduction and a discussion of the continuum normalisation are provided in Sect. 2.3. In Sects. 3 and 4 we describe the models and the procedure used to perform the abundance analysis. Our results are summarised in Sect. 5. Discussion and conclusions are given in Sects. 6 and 7 respectively.

[1] We consider as "normal" A-type stars all the A-type stars that are classified neither as Am nor Ap.

2. Observations and data reduction

2.1. Instruments

We observed six stars of the Praesepe cluster using the ESPaDOnS (Echelle SpectroPolarimetric Device for Observations of Stars) spectropolarimeter at the Canada-France-Hawaii Telescope (CFHT) from January 8th to 10th 2006. Spectra were acquired in circular polarisation.

Spectra of an additional four stars were obtained with the ELODIE spectrograph at the Observatoire de Haute Provence (OHP) from January 4th to 6th 2004.

An additional circular polarisation spectrum of HD 73709 was obtained with the MuSiCoS spectropolarimeter at the 2-m Bernard Lyot Telescope (TBL) of the Pic du Midi Observatory on 7 March 2000. The magnetic field derived form this observation has been discussed by Shorlin et al. (2002).

2.1.1. ESPaDOnS

ESPaDOnS consists of a table-top cross-dispersed echelle spectrograph fed via a double optical fiber directly from a Cassegrain-mounted polarization analysis module. In "polarimetric" mode, the instrument can acquire a Stokes *V*, *Q* or *U* stellar spectrum throughout the spectral range 3700 to 10 400 Å with a resolving power of about 65 000. A complete polarimetric observation consists of a sequence of 4 sub-exposures, between which the retarder is rotated by ±90 degrees (Donati et al. 1997; Wade et al. 2000). In addition to the stellar exposures, a single bias spectrum and ThAr wavelength calibration spectrum, as well as a series of flat-field exposures, were obtained at the beginning and end of each night.

2.1.2. ELODIE

ELODIE is a cross-dispersed echelle spectrograph at the 1.93-m telescope at the OHP observatory. Light from the Cassegrain focus is fed into the spectrograph through a pair of optical fibers. Two focal-plane apertures are available (both 2 arcsec wide), one of which is used for starlight and the other can be used for either the sky background or the wavelength calibration lamp, but can also be masked. The spectra cover a 3000 Å wavelength range (3850–6800 Å) with a mean spectral resolution of 42 000. ELODIE was decommissioned in mid-August 2006.

2.1.3. MuSiCoS

MuSiCoS, like ESPaDOnS, consists of a table-top cross-dispersed echelle spectrograph fed via a double optical fiber directly from a Cassegrain-mounted polarization analysis module. MuSiCoS provides a Stokes *V*, *Q* or *U* stellar spectrum from 4500 to 6600 Å with a mean resolving power of 35 000. A more detailed description of the instrument and of the observing procedures are reported by Donati et al. (1999). MuSiCoSwas decomissioned in December 2006.

Table 1. Basic datas of the observations for the program stars.

HD	RA	Dec	HJD	M_v	Spectral type	Instrument	Resolution	*SNR*	Exp. time	Remarks
73430	08 39 03.585	+19 59 59.08 [2]	2 453 746.125	8.33	A9V	ESPaDOnS	65 000	220	1800	
73575	08 39 42.6548	+19 46 42.440 [1]	2 453 747.116	6.66	F0III	ESPaDOnS	65 000	250	2400	δSct variable
73666	08 40 11.4528	+19 58 16.073 [1]	2 453 745.063	6.61	Ap(Si)	ESPaDOnS	65 000	660	1600	SB1, Blue Straggler
72942	08 36 17.4422	+20 20 29.421 [1]	2 453 746.098	7.48	Am	ESPaDOnS	65 000	350	1600	SB?
73045	08 36 48.0033	+18 52 58.111 [1]	2 453 745.091	6.82	Am	ESPaDOnS	65 000	290	2400	SB1
73730	08 40 23.466	+19 50 05.91 [2]	2 453 745.123	7.99	Am	ESPaDOnS	65 000	330	2000	
73618	08 39 56.496	+19 33 10.76 [2]	2 453 009.612	7.30	Am	ELODIE	42 000	160	3600	SB1
73174	08 37 36.995	+19 43 58.48 [2]	2 453 010.574	7.76	Am	ELODIE	42 000	120	2700	SB1, triple system
73711	08 40 18.099	+19 31 55.17 [2]	2 453 010.432	7.51	Am	ELODIE	42 000	90	3600	SB1
73818	08 40 56.935	+19 56 05.47 [2]	2 453 012.102	8.69	Am	ELODIE	42 000	80	2400	SB1
73709	08 40 20.748	+19 41 12.24 [2]	2 451 611.473	7.68	Am	MuSiCoS	35 000	120	2400	SB1, quadruple system

[1] Positions from Perryman et al. (1997); [2]: positions from Hog et al. (1998). The *SNR* are calculated at ~5000 Å in a bin of 0.5 Å. The exposure time is in seconds. With the ESPaDOnS and MuSiCoS instruments we obtained Stokes *I* and *V* spectra, which allowed us to attempt magnetic field detection. With ELODIE we obtained Stokes *I* spectra only. The HJD indicate the Heliocentric Julian Date at the middle of the exposure.

2.2. Target selection

The target selection for the run with the ESPaDOnS spectrograph was performed taking into account previously-published peculiar spectral classifications of the stars, together with their $\upsilon \sin i$ (if any), giving priority to slowly-rotating stars. Data concerning stars of the cluster were collected from the WEBDA database[2] (Mermillod & Paunzen 2003) and the SIMBAD database, operated at CDS, Strasbourg, France.

The stars observed with the ELODIE spectrograph were the bright stars included in the analysis provided by Burkhart & Coupry (1998), to allow a comparison with their work.

The star observed with MuSiCoS was analysed by Shorlin et al. (2002), with the LSD technique, to measure the magnetic field strength.

Four stars of the sample were accepted as cluster members by the HIPPARCOS survey (Robichon et al. 1999) whereas the others have been confirmed as members by different studies, such as those by Kharchenko et al. (2004) and Wang et al. (1995).

The complete sample of stars observed and analysed in this paper is listed in Table 1. Seven of the stars are spectroscopic binaries and one is a δ Scuti star. Of the eleven stars observed, eight were previously classified as Am stars, two as normal A-type stars and one as an Ap (Si) star.

2.3. Data reduction

The ESPaDOnS spectra were reduced using the Libre-ESpRIT package[3].

The ELODIE spectra were automatically reduced by a standard data reduction pipeline described by Baranne et al. (1996).

The MuSiCoS spectrum was reduced according to the procedure described by Wade et al. (2000) and Shorlin et al. (2002).

The sample of stars includes objects with a high $\upsilon \sin i$ (up to $\simeq$130 km s^{-1}) for which the continuum normalisation is a critical reduction procedure. For this reason, all of the spectra were normalised without the use of any automatic continuum fitting procedure. We considered the single echelle orders of the spectra, which were normalised and then merged. It was not possible to determine a correct continuum level short wards of the Hγ line (4340.462 Å), as there were not enough continuum windows in the spectrum at these shorten wavelengths.

[2] `http://www.univie.ac.at/webda`

[3] `www.ast.obs-mip.fr/projets/espadons/espadons.html` – see also Donati et al. (1997).

3. Calculation of model atmospheres

Model atmospheres were calculated with the LTE code LLMODELS (version 8.4), which uses direct sampling of the line opacity (Shulyak et al. 2004), and allows the computation of model atmospheres with individualised (not scaled solar) abundance patterns. This allows us to compute self-consistent model atmospheres that match the actual abundances of chemically peculiar stars and to thereby minimise systematic errors (Khan & Shulyak 2007).

We used the VALD database (Piskunov et al. 1995; Kupka et al. 1999; Ryabchikova et al. 1999) as a source of spectral line data, including lines that originate from predicted levels. We then performed a preselection procedure to eliminate those lines that do not contribute significantly to the line opacity. For this procedure we utilised model atmospheres calculated by ATLAS9 (Kurucz 1993a) with fundamental parameters corresponding to each star in our sample. Because at this stage of the analysis we did not know the photospheric abundances of the sample stars, we employed the Opacity Distribution Function (ODF) tables for solar abundances (Kurucz 1993b). The line selection criterion required that the line-to-continuum opacity ratio at the center of each line, at any atmospheric depth, be greater than 0.05%.

To compute atmosphere models with individual abundance patterns, we used an iterative procedure. The initial model atmosphere was calculated with the solar abundances taken from Asplund et al. (2005). Then, these abundances were modified according to the results of spectroscopic analysis, and a final model atmosphere was iterated.

A logarithmic Rosseland optical depth scale $\log \tau_{\rm ross}$ was adopted as an independent variable of atmospheric depth spanning from +2 to −6.875 and subdivided into 72 layers. Opacities were sampled with a 0.1 Å wavelength step. Since a posteriori we found no magnetic field in the atmospheres of our stars (Sect. 6.1), the excess line blanketing due to a magnetic field (Kochukhov et al. 2005; Khan & Shulyak 2006a,b) was neglected. The value of the microturbulence velocity $\upsilon_{\rm mic}$ was adopted according to the results of the spectroscopic analysis (Sect. 4.2).

Convection was treated according to the CM approach (Canuto & Mazzitelli 1992). It has been argued that CM should be preferred over the MLT approach (Kupka 1996). For example, Smalley & Kupka (1997) showed that the CM models give results that are generally superior to standard MLT ($\alpha = 1.25$) models. Furthermore, to calculate a part of the NEMO model atmosphere grid, Heiter et al. (2002) adopted the free parameter $\alpha = 0.5$ for the MLT approach as it produced results quite similar to those of the CM method. Consequently, we have taken convection (CM approach) into account for the whole set of calculations to ensure correct modelling for lower effective temperatures, as many of the stars analysed in this paper have effective temperatures below 9000 K. To test the importance of the convection treatment on the abundance analysis, as applied to this sample of stars, we performed several numerical tests using model atmospheres calculated with no convection treatment at all. The results revealed differences of about 0.005 dex, clearly within the errors associated with the analysis.

4. Spectral analysis

4.1. High precision search for magnetic field

One of the main goals of our analysis is to search for weak magnetic fields in the Am stars of Praesepe, and to check if the Ap (Si) star HD 73666 has one, since many Ap stars show a strong magnetic field. For these reasons, we observed some Am stars and HD 73666 with the ESPaDOnS spectrograph that provides the opportunity to obtain high resolution spectra in circular polarization. To detect the presence of a magnetic field and to infer the longitudinal magnetic field we used the Least-Squares Deconvolution technique (hereafter LSD). LSD is a cross-correlation technique developed for the detection and measurement of weak polarization signatures in stellar spectral lines. The method is described in detail by Donati et al. (1997) and Wade et al. (2000).

4.2. Atmosphere fundamental parameters

The initial values of the effective temperature ($T_{\rm eff}$), surface gravity ($\log g$) and metallicity of our sample of stars were estimated via Strömgren photometry (Hauck & Mermilliod 1998).

The initial value of the microturbulence velocity ($\upsilon_{\rm mic}$) was determined using the following relation (Pace et al. 2006):

$$\upsilon_{\rm mic} = -4.7 \log (T_{\rm eff}) + 20.9 \ {\rm km\,s^{-1}}. \quad (1)$$

The uncertainties associated with $T_{\rm eff}$, $\log g$ and $\upsilon_{\rm mic}$ determined photometrically and from Eq. (1) are quite large (about 300 K in $T_{\rm eff}$ and 0.25 in $\log g$, due to uncertainties in the photometric measurements and intrinsic scatter in the calibrations). We have adjusted these parameters spectroscopically to get more accurate values for an abundance analysis.

The best value of the effective temperature was estimated using the abundance-$\chi_{\rm excit}$ correlation, calculated fitting the abundances of different selected lines of an element, in the abundance-excitation potential plane. This correlation is sensitive to effective temperature variations. This property allows us to determine the best value of the effective temperature, which we derived by eliminating the abundance-$\chi_{\rm excit}$ correlation. For this step, the abundances were calculated using a modified version (Tsymbal 1996) of the WIDTH9 code (Kurucz 1993a), using equivalenth widths for the more slowly-rotating stars ($\upsilon \sin i < 30$ km s^{-1}), and by fitting line cores (as described in Sect. 4.3) for the rapid rotators.

In a similar way, the best value for $\log g$ was found by eliminating any systematic difference in abundance derived from different ionisation stages of the same chemical element.

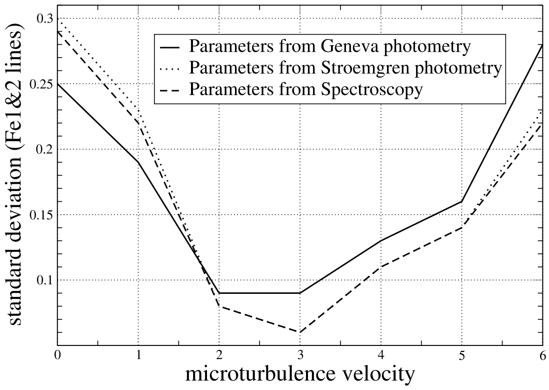

Fig. 1. Standard deviation for Fe I and Fe II lines, selected for HD 73730, as a function of $\upsilon_{\rm mic}$ using fundamental parameters obtained from Geneva photometry (straight line), from Strömgren photometry (dotted line) and from spectroscopy (dashed line).

Finally, for stars with $\upsilon \sin i$ less than 30 km s^{-1}, the $\upsilon_{\rm mic}$ value was determined by eliminating any abundance-equivalent width correlation.

To check the degree of refinement reached with the spectroscopic method, we systematically performed the following check. For each star with $\upsilon \sin i < 30$ km s^{-1} we have performed the abundance analsysis of Fe I and Fe II lines using three different approaches, i.e., by calculating $\log g$ and $T_{\rm eff}$ from (i) Geneva photometry, (ii) from Strömgren photometry, and (iii) with the spectroscopic method outlined above. For each of these three models, we have calculated the abundances of Fe I and Fe II lines for $\upsilon_{\rm mic} = 0, 1, 2, ..., 6$ km s^{-1}. Finally, for each of these 18 sets of $T_{\rm eff}$, $\log g$ and $\upsilon_{\rm mic}$ values, we have calculated the standard deviation from the mean Fe I and Fe II values. In all cases we found that the parameters that we have identified with the method described above are those that minimise the abundance scatter.

In Fig. 1 we give an example of the result of our check, for the Am star HD 73730. The result of the check for all the other stars of the sample is similar to the one shown in Fig. 1.

For faster rotators an insufficient number of unblended lines are available with which to calculate the equivalent width. The more slowly-rotating Am stars of the sample show a mean $\upsilon_{\rm mic}$ value around 2.7 km s^{-1}. For this reason, for fast rotators, we retained the value found using Eq. (1), which was always compatible, within the errors, with 2.7 km s^{-1}.

Following Landstreet (1998) it has been generally adopted that for Am stars $\upsilon_{\rm mic}$ is between 4–5 km s^{-1}. By contrast in the present work we determined values between 2.3–3.1 km s^{-1}, for the slowly rotating stars.

The chemical elements used to determine the fundamental parameters were different for each star, depending mainly on the value of $\upsilon \sin i$, and are described in Sect. 5.

For the lines used to eliminate the correlations discussed above we assumed that non-LTE and stratification effects were negligible (Ryabchikova et al. 2007).

The wavelength range of the ESPaDOnS orders was wide enough to perform a safe continuum normalisation of the Hα and Hβ lines. For the spectra obtained with this instrument it was therefore possible to use these two hydrogen lines to provide an additional constraint on the fundamental parameters. In particular, for effective temperatures less than 8000 K, the wings of the Hydrogen lines are very sensitive to the effective temperature. On the other hand, at higher effective temperatures the wings are particularly sensitive to $\log g$. We did not use the hydrogen lines of the spectra obtained with ELODIE and MuSiCoS because the wavelength ranges of the orders containing the Hα and Hβ lines were too narrow to include the entire line profile.

The spectroscopic procedure of refining the fundamental parameters reduces the errors of $T_{\rm eff}$ and $\log g$ to typically 200 K and 0.2, respectively, while the estimated error for $\upsilon_{\rm mic}$ is around 0.2 km s^{-1}. These errors are estimated taking into account different noise sources, including continuum normalisation errors and uncertainty in the convective model. The errors associated with the effective temperature and $\log g$ have been confirmed by a fit of the Hα and Hβ line profiles using the models calculated with the parameters obtained from the estimated errors.

In some cases a star's high rotational velocity prevented us from recovering $T_{\rm eff}$ and $\log g$ spectroscopically with good precision. In these cases we ultimately adopted an average of parameters determined spectroscopically and those obtained via Strömgren photometry.

For the spectra obtained with the ELODIE spectrograph we also attempted to check for the presence of a magnetic field by looking for a correlation between the abundance derived from each line and its Landé factor. We also conducted a search for magnetically-split lines (e.g. Fe II line at 6149.258 Å) in spectra of the very slowest rotators. In fact, for $\upsilon \sin i$ more than a few km s^{-1} this method cannot be used for detecting typical Ap-star magnetic fields. For the spectra obtained with the ESPaDOnS spectrograph we used the LSD technique to measure the velocity-resolved Stokes V profile and the longitudinal magnetic field.

With the correct fundamental parameters, we determined the best value of $\upsilon \sin i$ fitting it on the Fe I lines at 5434.524 Å and 5576.089 Å. We chose these two Fe I lines because their broadening parameters are well known and are not affected by magnetic field broadening, since their Landé factor is close to 0. The estimated error on $\upsilon \sin i$ is about 5%.

The radial velocity, in km s^{-1}, was determined by performing the median of the results obtained by fitting several lines of the observed spectrum to a synthetic one.

4.3. Element abundance analysis

Once we had obtained the best values for the fundamental parameters, we determined the final elemental abundances by direct fitting of the observed spectra with synthetic models. We synthesised the model spectra with Synth3 (Kochukhov 2006) and fit the cores of selected lines to get a value of the abundance associated with each line. We then calculated the mean and the relative standard deviation for each analysed element. The line core fitting was performed with the "Lispan" and "ATC" codes (written by Ch. Stütz) together with Synth3. The only free parameter in the line core fitting procedure is the abundance of the line. The fitting procedure and the determination of the abundances was performed iteratively in order to obtained a better determination of the abundances for blended lines. The error associated with the derived abundance of each element is the standard deviation from the mean abundance of the selected lines of that element. These errors do not take into account the uncertainties of the fundamental parameters and of the adopted model atmosphere. To have an idea of these uncerteinties, we have calculated the abundances of Fe, Ti and Ni for HD 73730 with five different models varing $T_{\rm eff}$ of $\pm$200 K and $\log g$ of $\pm$0.2 dex from the adopted model. We found a variation of less than 0.2 dex for Fe, 0.1 dex for Ti and 0.1 for Ni due to the temperature varation. We did not find any significant abundance change varing $\log g$. The uncertainty in temperature is probably the main error source on our abundances.

The lines used to synthesise the spectra and selected to calculate the abundances for the various elements were extracted from the VALD database.

The number of selected lines depends on the $\upsilon \sin i$ value found for each star. We also checked the $\log gf$ value of each selected line using the solar spectrum. Lines in the synthetic spectrum of the Sun showing large deviations from the observed solar spectrum were rejected from the selection. For some elements (e.g. Co, Cu and Zn) we derived the abundance from one line. This does not mean that only one line is present in the spectrum, but that only one line was selected to derive the chemical abundance. Other lines of the same element are present, but they were not selected because they are either too much blended or their $\log gf$ value appeared to be in error based on the solar spectrum.

For the elements which were not analysed we assumed solar abundances from Asplund et al. (2005).

4.4. Non-LTE effects

Some potassium lines were visible in the ESPaDOnS spectra (because of the extension of the spectra into the far red), making possible the calculation of the abundance of this element. In particular the K I line at 7698.974 Å was detected and was largely unblended in the spectra of most stars. Unfortunately, this element presents strong non-LTE effects; for this reason the K abundances derived here are reported only as upper limits. The He, O and Na lines were selected in such a way to reduce as much as possible non-LTE effects. For He, we selected lines in the blue region; for O, lines in the red region; and for Na, we used the Na I doublet at 5682.633–5688.205 Å, which is known to be essentially uneffected by non-LTE effects (Ryabchikova, private communication). For all the other elements that present important non-LTE effects (e.g. C, N, Al, S, Y, Ba), the abundances derived here should be considered as upper limits (Baumueller & Gehren 1997; Kamp et al. 2001; Przybilla et al. 2006, and references therein). However at present day it is not known how large are the deviations from LTE for normal A-type stars and Am stars for the various elements. More non-LTE analysis should be performed for this type of star. Since our sample of stars has similar fundamental parameters (mainly $\log g$ and metallicity) the non-LTE effects associated to each star should be of the same magnitude. This allows us to compare the stars of our sample with each other.

5. Results

We have organised our sample of program stars according to their literature classification as normal A-type stars (HD 73430, HD 73575), Blue Stragglers (HD 73666 – Ap(Si) star) and Am stars (HD 72942, HD 73045, HD 73730, HD 73618, HD 73174, HD 73711, HD 73818, HD 73709).

Table 2 lists the initial and final set of fundamental parameters obtained for each program star.

The derived abundances are illustrated in Figs. 13 to 22, and reported in Table 3.

In the following sections we comment on individual stars, devoting special attention to the elements that characterise the peculiarities of each star.

Table 2. Initial and final atmospheric fundamental parameters for the analysed stars of the Praesepe cluster. The initial fundamental parameters are derived from photometry, the final with spectroscopy. The errors on the fundamental parameters are estimated to be 200 K, 0.2 km s^{-1}and 0.2 for $T_{\rm eff}$, $\upsilon_{\rm mic}$ and $\log g$ respectively. The estimated error on $\upsilon \sin i$ is about 5%. The $\upsilon_{\rm r}$ is given in km s^{-1}. $\langle B_z \rangle$ indicate the Longitudinal Magnetic Field (measured in Gauss) calculated with the LSD tecnique. BS: Blue Straggler.

	initial set			final set							
HD	$T_{\rm eff}$ [K]	$\log g$ [cgs]	$\upsilon_{\rm mic}$ [km s^{-1}]	$T_{\rm eff}$ [K]	$\log g$ [cgs]	$\upsilon_{\rm mic}$ [km s^{-1}]	$\upsilon_{\rm macro}$ [km s^{-1}]	$\upsilon \sin i$ [km s^{-1}]	$\upsilon_{\rm r}$ [km s^{-1}]	$\langle B_z \rangle$ G	comments
73 430	7790	3.95	2.6	7660	4.02	2.6	0	73	33.7	1 ± 45	normal
73 575	7435	3.46	2.7	7300	2.92	2.7	0	127	33.4	–215 ± 149	normal
73 666	9429	3.84	2.2	9382	3.78	1.9	0	10	34.1	6 ± 5	SB1; BS; close to normal
72 942	8237	3.80	2.5	8450	3.90	2.4	0	73	39.9	12 ± 31	SB?; between normal & Am
73 045	7470	4.09	2.7	7570	4.05	3.6	10	10	27.9	–1 ± 4	SB1; Am
73 730	8009	3.83	2.5	8070	3.97	2.6	0	29	36.6	–12 ± 9	Am
73 618	8091	3.81	2.5	8170	4.00	2.5	0	47	15.1	–	SB1; Am
73 174	7600	4.20	2.0	8350	4.15	2.9	0	<5	2.9	–	SB1; Am
73 711	8269	3.95	2.5	8020	3.69	2.5	0	62	23.4	–	SB1; Am
73 818	7232	3.82	2.8	7232	3.82	2.8	0	66	22.5	–	SB1; Am
73 709	8063	3.79	2.5	8070	3.78	2.3	0	10	26.7	–	SB1; Am

5.1. Normal A-type stars

5.1.1. HD 73430

This is the slower rotator ($\upsilon \sin i = 73$ km s^{-1}) of the two normal A-type stars studied. The LSD profile (Fig. 2) shows symmetric rotational broadening, and does not show any particular features; the analysis gives a longitudinal magnetic field of $\langle B_z \rangle = 1 \pm 45$ G.

The effective temperature was determined so as to cancel any dependence of abundance versus excitation potential for Fe I. The $\log g$ was calculated imposing equilibrium between the Fe I and Fe II abundances. The values for $T_{\rm eff}$ and $\log g$ found in this way were then averaged with the values found with the photometry. The $T_{\rm eff}$ was then checked and found consistent with the Hα and Hβ profiles, very sensitive to effective temperature at $T_{\rm eff} < 8000$ K.

We find that C and O are solar and N is overabundant, as is observed for the other normal A-type star of our sample, HD 73575 (see Sect. 5.1.2). This differs from the Am stars, in which these elements are usually observed to be underabundant. We note that Asplund et al. (2005) have significantly reduced the solar abundances of C, N and O, so all comparisons with the Sun of previous A-star studies regarding these elements may need to be revised. Ca, Sc, Ti, Cr, Fe and Ni are solar within the errors, allowing us to confirm the previous classification of HD 73430 as a normal A-type star.

5.1.2. HD 73575

This is the faster rotator ($\upsilon \sin i = 127$ km s^{-1}) of the two normal A-type stars. HD 73575 is present in the catalog of Rodriguez et al. (2000) of δ Scuti variable stars. The Stokes I LSD profile (Fig. 3) shows remarkable structure that may well be due to pulsation. No magnetic field was detected ($\langle B_z \rangle = -215 \pm 149$ G).

The very high $\upsilon \sin i$ resulted in a relatively small number of metal lines with which to tune the fundamental parameters. The effective temperature was also determined by fitting the Hα and Hβ line profiles, which were then combined with the values obtained with the photometry. The $\log g$ was determined by imposing equilibrium between different ionisation stages (Fe I and Fe II). Due to the very high rotational velocity, the errors on the fundamental parameters are estimated to be similar to the photometric ones.

HD 73575 shows all the properties of normal A-type stars of the cluster (e.g. C and O solar with N overabundant; Fe underabundant), except for Sc, which appears to be slightly underabundant.

5.2. The blue straggler HD 73666

HD 73666 is the hottest star of the sample and the only Blue Straggler present in the cluster, according to Andrievsky (1998). It is also included in the "New Catalogue of Blue Stragglers in Open Clusters" by Ahumada & Lapasset (2007). The photospheric chemistry of this star has been previously investigated by several authors (Andrievsky 1998; Burkhart & Coupry 1998), but their results, the iron abundances for example, vary wildly ([Fe/H] = +0.1, +0.5 respectively). These discrepancies are probably due to the narrow wavelength ranges available to those investigators.

The result of the application of the LSD technique is shown in Fig. 4. The derived longitudinal magnetic field is $\langle B_z \rangle = 6 \pm 5$ G.

This star is the primary component of a close binary system (SB1), as is the case for many other Blue Stragglers (Leonard 1996), and the flux coming from the secondary star is negligible, as previously checked by Burkhart & Coupry (1998), so the star was analysed ignoring the presence of the secondary.

The sharp lines ($\upsilon \sin i = 10$ km s^{-1}) allowed for a detailed abundance analysis. The microturbulence velocity and $T_{\rm eff}$ were determined respectively by eliminating the abundance-equivalent width and abundance-excitation potential correlations, using Fe I, Fe II and Ti II lines. The $\log g$ value was obtained using the equilibrium between Fe I and Fe II, and finally by looking for the best fit of the profile for the Hα and Hβ line wings (very sensitive to $\log g$ at $T_{\rm eff} > 8000$ K). The resulting $\log g$ is the average of the values obtained with the two methods.

For the adopted model, Mg I and Mg II deviate noticeably from the ionisation equilibrium condition. Their abundances are −3.98 and −4.35 respectively. The same behavior was found for Ca I and Ca II with abundances of −5.65 and −5.41 respectively. These features of the Mg and Ca abundances explain the high value of the associated errors.

Abt (1985) classified this star as Ap (Si). The signature of this kind of star is a strong silicon overabundance. However, it can be seen in Table 3 and Fig. 15 that the Si abundance is not much higher than the solar abundance of this element. Also

Table 3. Abundances ($\log(N_X/N_{tot})$) of the program stars with the estimated internal errors in units of 0.01 dex, in parenthesis. For comparison, the solar abundances (Asplund et al. 2005) are given in the last column. At.N. gives the Atomic Numbers of the elements. Abundances obtained from just one line have no error (−). Upper limits are denoted by <.

		"Normal" A-type stars		Blue Straggler	Am stars								Solar
At.N.	Element	HD 73430	HD 73575	HD 73666	HD 72942	HD 73045	HD 73730	HD 73618	HD 73174	HD 73711	HD 73818	HD 73709	Abundances
2	He			−1.20(05)									−1.11
3	Li	<−8.17(−)	<−8.50(−)		<−8.49(−)	−8.86(02)	−8.74(−)	<−8.58(−)	−8.51(02)	<−8.43(−)	<−8.63(−)		−10.99
6	C	<−3.74(−)	<−3.61(−)	<−3.25(03)	<−3.85(−)	<−4.37(04)	<−4.32(47)	<−4.16(16)	<−4.08(06)	<−3.99(15)	<−3.38(07)	<−3.71(26)	−3.65
7	N	<−3.62(16)	<−3.93(−)	<−3.67(10)	<−3.84(−)	<−4.49(−)	<−4.63(−)		<−4.50(12)				−4.26
8	O	−3.26(−)	−3.37(−)	−3.06(07)	−3.58(−)	−3.90(10)	−3.96(09)	−3.65(04)	−3.72(01)	−3.60(04)	−3.76(−)	−3.86(08)	−3.38
11	Na	−5.69(06)		−5.47(01)		−5.32(03)	−5.36(01)	−5.34(03)	−5.13(04)		−5.35(01)	−5.34(06)	−5.87
12	Mg	−4.79(15)	−4.63(−)	−4.25(14)	−4.51(03)	−4.52(04)	−4.43(06)	−4.29(−)	−4.21(05)	−4.63(05)	−4.51(16)	−4.56(06)	−4.51
13	Al			<−5.34(06)		<−5.41(01)	<−5.37(−)		<−5.06(−)			<−4.91(16)	−5.67
14	Si	−4.44(04)	−4.41(−)	−4.30(01)	−4.67(−)	−4.21(05)	−4.21(05)	−4.51(−)	−4.08(11)	−4.19(05)	−3.44(32)	−4.10(06)	−4.53
15	P								−5.23(−)			−5.12(−)	−6.68
16	S	<−4.59(−)		<−4.47(−)	<−4.48(−)	<−4.67(09)	<−4.54(03)	<−4.52(13)	<−4.37(03)	<−4.62(−)	<−4.36(26)	<−4.44(01)	−4.90
18	Ar			−5.10(−)									−5.86
19	K	<−6.84(−)	<−6.46(−)	<−6.49(−)		<−7.04(−)	<−6.83(−)						−6.96
20	Ca	−5.68(05)	−5.55(08)	−5.53(14)	−5.58(12)	−6.46(04)	−6.36(03)	−5.74(07)	−5.70(08)	−5.95(08)	−5.88(03)	−6.18(06)	−5.73
21	Sc	−8.90(10)	−9.31(10)	−8.95(06)	−8.88(11)	−9.39(01)	−9.71(03)	−9.51(27)	−9.44(08)	−10.06(01)	−10.90(−)	−9.79(01)	−8.99
22	Ti	−7.19(−)	−7.18(−)	−6.86(04)	−6.89(07)	−6.95(04)	−6.99(09)	−6.41(01)	−6.72(05)	−7.08(04)	−6.81(30)	−7.01(07)	−7.14
23	V			−7.48(05)		−7.60(−)			−7.19(05)			−7.16(−)	−8.04
24	Cr	−6.57(11)	−6.29(−)	−6.01(07)	−6.41(16)	−5.63(16)	−5.65(08)	−5.93(10)	−5.69(08)	−6.08(09)	−6.23(−)	−5.79(13)	−6.40
25	Mn			−6.32(01)	−6.91(−)	−6.28(−)	−6.31(03)	−6.28(−)	−6.07(06)	−6.46(13)	−5.83(−)	−6.26(01)	−6.65
26	Fe	−4.72(12)	−4.75(10)	−4.30(07)	−4.47(07)	−4.03(04)	−4.14(05)	−4.13(10)	−3.88(09)	−4.44(13)	−4.26(20)	−4.05(11)	−4.59
27	Co					−6.47(04)	−6.15(−)		−6.12(12)			−6.16(04)	−7.12
28	Ni	−5.71(15)	−5.56(01)	−5.53(03)	−5.57(−)	−4.93(06)	−5.14(07)	−5.10(15)	−4.79(02)	−5.28(02)	−5.32(14)	−4.88(06)	−5.81
29	Cu					−6.93(−)	−7.12(−)		−6.78(−)		−7.29(−)		−7.83
30	Zn					−6.65(−)	−6.82(−)	−7.29(−)	−6.42(−)			−6.59(−)	−7.44
39	Y	<−9.62(06)		<−9.78(−)	<−9.02(16)	<−8.91(09)	<−8.98(05)	<−8.62(−)	<−8.50(09)	<−8.77(13)	<−9.42(29)	<−8.76(08)	−9.83
40	Zr					−9.05(01)	−8.51(01)		−8.16(03)			−8.28(−)	−9.45
56	Ba	<−9.47(−)	<−9.95(−)	<−9.13(04)	<−8.97(−)	<−8.50(−)	<−7.85(16)	<−8.09(18)	<−8.02(38)	<−8.97(09)	<−8.69(06)	<−7.77(10)	−9.87
57	La					−9.61(09)	−9.41(−)		−9.26(09)			−9.36(08)	−10.91
58	Ce					−9.26(04)	−9.44(03)		−8.94(15)			−9.14(−)	−10.46
59	Pr								−9.09(−)				−11.33
60	Nd					−9.48(03)	−9.66(11)		−9.23(07)			−9.41(04)	−10.59
62	Sm					−9.89(05)			−9.81(10)			−9.18(07)	−11.03
63	Eu					−10.20(−)	−10.42(−)					−9.95(−)	−11.52
64	Gd								−9.30(04)			−8.93(−)	−10.92
68	Er					−9.65(−)			−9.39(−)			−9.54(−)	−11.11
70	Yb					−9.87(−)							−10.96
71	Lu								−10.20(−)			−10.3(−)	−11.98
	T_{eff}	7660	7300	9382	8450	7570	8070	8170	8350	8020	7232	8070	
	$\log g$	4.02	2.92	3.78	3.90	4.05	3.97	4.00	4.15	3.69	3.82	3.78	
	υ_{mic}	2.6	2.7	1.9	2.4	3.6	2.6	2.5	2.9	2.5	2.8	2.3	
	υ_{macro}	0.0	0.0	0.0	0.0	10.0	0.0	0.0	0.0	0.0	0.0	0.0	
	$\upsilon \sin i$	73	127	10	73	10	29	47	<5	62	66	10	

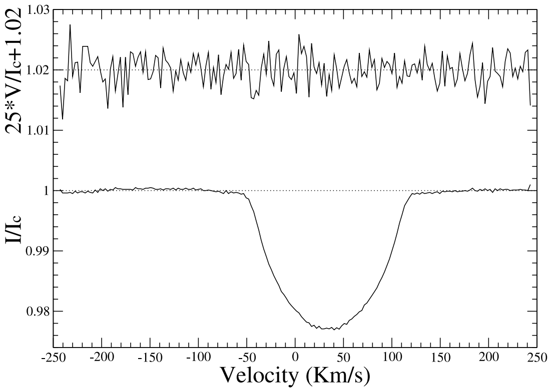

Fig. 2. LSD profiles for the normalised Stokes *I* and Stokes *V* spectra (*from bottom to top*) of HD 73430. The Stokes *V* profile is expanded by a factor of 25 and shifted upward of 1.02.

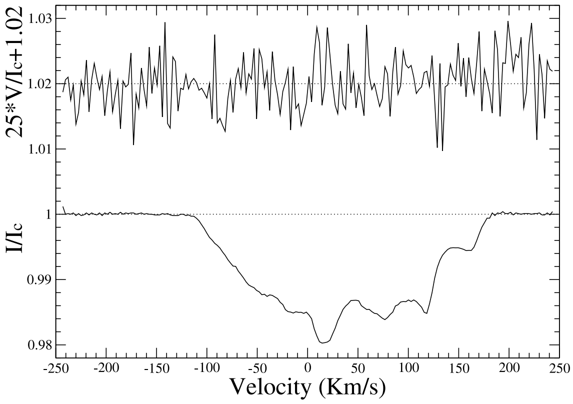

Fig. 3. LSD profiles for the normalised Stokes *I* and *V* (*from bottom to top*) spectra of the δ Scuti star HD 73575. The Stokes *V* profile is expanded by a factor of 25 and shifted upward of 1.02.

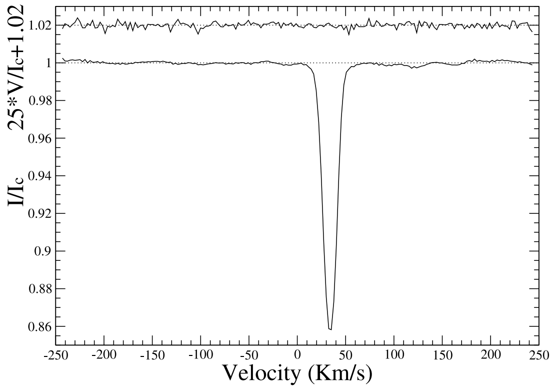

Fig. 4. LSD profiles for the normalised Stokes *I* and *V* (*from bottom to top*) spectra for the Blue Straggler HD 73666. The Stokes *V* profile is expanded by a factor of 25 and shifted upward of 1.02.

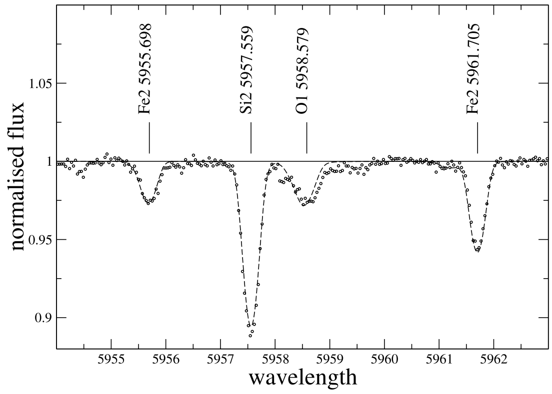

Fig. 5. Portion of the spectrum of HD 73666. The dots show the observation, the dashed line shows the synthetic spectrum. The weak blended lines are omitted.

Ap (Si) stars are magnetic, and the very high precision of the longitudinal field diagnosis effectively rules out the presence of any organised magnetic field. Figure 5 shows one of the selected Si lines. If HD 73666 was an Ap(Si) star, we would expect this line to be much stronger, compared to the surrounding Fe lines. Andrievsky (1998) cataloged this star as an Am star, but Ca is slightly overabundant while Sc is solar. C, N and O are overabundant and, as it is possible to see in Fig. 10, these overabundances are typical of the normal A-type stars of the Praesepe cluster. These results allow us to conclude that HD 73666 is neither an Ap nor an Am star.

5.3. Am stars

In this section we analyse the stars of the sample classified as Am stars in previous works. According to Preston (1974) a star in the temperature range of 7000−10 000 K is classified as Am (CP1) if Ca and/or Sc are underabundant and the heavy metals are overabundant. Am stars nearly always show low values of $\upsilon \sin i$, tipically less than 100 km s^{-1}.

5.3.1. HD 72942

The LSD profile for HD 72942 is symmetric and rotationally broadened, as is illustrated in Fig. 6. The magnetic analysis of the LSD profiles gives a value of the longitudinal magnetic field of $\langle B_z \rangle = 12 \pm 31$ G.

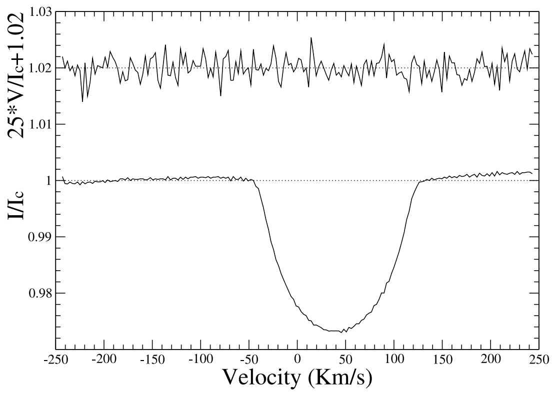

Fig. 6. LSD profiles of the normalised Stokes *I* and *V* (*from bottom to top*) spectra of HD 72942. The Stokes *V* profile is expanded by a factor of 25 and shifted upward of 1.02.

$T_{\rm eff}$ was set using Ti II and Fe I lines. The $\log g$ value was estimated using the equilibrium between the Fe I and Fe II abundances and fitting the Hα and Hβ line profiles.

The large error associated with the Y abundance is due to the poor determination of the line parameters and to the unknown non-LTE effects associated with each line. It was not possible to derive the K abundance from the K I line at 7698.974 Å because the line was blended by a telluric line.

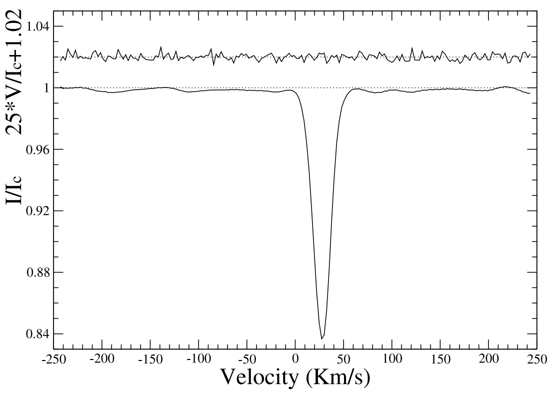

Fig. 7. LSD profiles for the normalised Stokes *I* and *V* (*from bottom to top*) spectra of HD 73045. The Stokes *V* profile is expanded by a factor of 25 and shifted upward of 1.02.

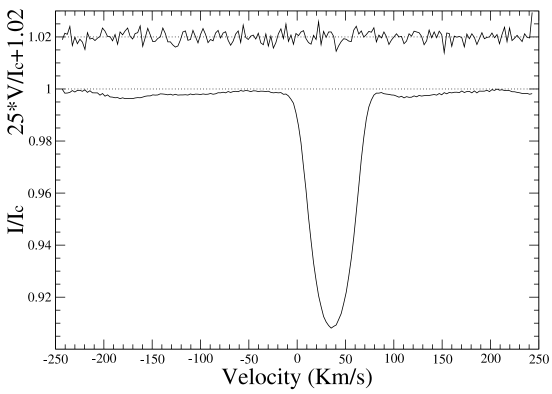

Fig. 8. LSD profiles of the normalised Stokes *I* and *V* (*from bottom to top*) spectra of HD 73730. The Stokes *V* profile is expanded by a factor of 25 and shifted upward of 1.02.

Ca and Sc are not underabundant, indicating that HD 72942 is probably not an Am star. However, the Fe abundance is similar to that observed in the metallic stars of the sample.

HD 72942 is not known to be a spectroscopic binary and is neither a classical Am star nor a normal A-type star (Sect. 6.2). The calculated radial velocity is rather high as compared to those of the other members and to the mean of the cluster. See also the discussion in Sect. 6.2.

5.3.2. HD 73045

HD 73045 is the primary component of an SB1 binary system (Debernardi et al. 2000). It exhibits a low projected rotational velocity ($\upsilon \sin i = 10\,\mathrm{km\,s^{-1}}$).

The LSD profiles of the Stokes *I* and *V* spectra are shown in Fig. 7. The magnetic field analysis provided a longitudinal magnetic field of $\langle B_z \rangle = -1 \pm 4$ G.

The secondary star does not contribute significantly to the lines of the spectrum, according to Debernardi et al. (2000) and Budaj (1996), so we have analysed the system as a single star. During our abundance determination we noticed an extra broadening of the wings of deep lines, perhaps due to the binarity. To be able to fit these lines we introduced a macroturbulence velocity ($\upsilon_{\mathrm{macro}} = 10$ km s^{-1} – obtained fitting several deep lines) to compensate for this effect. The use of the macroturbulence velocity does not lead to any significant abundance change, as expected. In particular the Iron abundance calculated without the use of the macroturbulence velocity results to be 0.01 dex lower than the final adopted one. The microturbulence velocity and the effective temperature were established using Fe I, Fe II and Ni I unblended lines, using the method described previously. The $\log g$ value was obtained imposing the ionisation equilibrium condition for Fe. The determined T_{eff} was then checked with the Hα and Hβ line wings.

HD 73045 is a typical Am star as Ca and Sc are underabundant and the Fe-peak elements are overabundant, as are the rare earth elements. C, N and O are underabundant, typical of all the Am stars of the sample. For the Cu I line at 5105.537 Å, Co I line at 5342.695 Å and Co I line at 5352.045 Å we applied a hyperfine structure correction, but the $\upsilon \sin i$ was too high to produce any detectable difference in the line broadening.

5.3.3. HD 73730

HD 73730 is an Am star with an intermediate rotational velocity ($\upsilon \sin i = 29\,\mathrm{km\,s^{-1}}$).

The LSD profiles for the Stokes *I* and Stokes *V* spectra are shown in Fig. 8. No magnetic field was detected from the LSD profiles. The calculated longitudinal magnetic field was $\langle B_z \rangle = -12 \pm 9$ G.

We obtained the fundamental parameters (υ_{mic}, T_{eff}, and $\log g$) using only Fe I and Fe II lines, since the $\upsilon \sin i$ did not allow us to select a sufficient number of unblended lines with good line parameters for any other element. Since we had the possibility to use only Fe I and Fe II lines, we also used the values of the $\log g$ obtained from the fitting of the Hα and Hβ line profiles.

The $\upsilon \sin i$ and the non-binarity allowed us to perform a precise abundance analysis for many elements – in fact only C shows a large error bar. This is probably due to the small number of selected C lines, all of which present non-LTE effects. The underabundances of Ca and Sc confirm that HD 73730 is an Am star. Also C, N and O are underabundant, as is the case for the other Am stars of the sample.

The $\upsilon \sin i$ is sufficiently large to hide any hyperfine structure broadening.

5.3.4. HD 73618

HD 73618 is the primary component of an SB1 binary system in which the flux of the secondary star does not significantly influence the total flux spectrum, according to Mason et al. (1993). For this star, as for all the others observed with the ELODIE spectrograph, we do not have a Stokes *V* LSD profile since the instrument did not support a polarimetric mode. So we checked for the presence of a magnetic field with the correlation between abundance and Landé factor for Fe I. This method allows the detection of magnetic fields stronger than about 1−2 kG (Stütz et al. 2006). We did not find any detectable magnetic field for HD 73618. To obtain the T_{eff} and the $\log g$ we used Fe I and Fe II lines. The fitting of the Hα and Hβ lines was not applied because their wings were broader than the wavelength range of the respective orders of the spectrograph. Since the $\upsilon \sin i$ is too high to get equivalent widths for enough unblended Fe I lines, we used the υ_{mic} calculated with Eq. (1).

Only Sc is underabundant, while Ca is solar. C and O are underabundant, as we have found for the other Am stars of the sample. Also, the Fe-peak elements show a behavior typical of this type of star. This confirms the previous classification of HD 73618. Because of the lower resolution of the ELODIE spectrograph with respect to the ESPaDOnS spectrograph, the errors associated with the abundances turn out to be higher than those calculated for the other stars described above.

This star is included, as a Blue Straggler, in the catalogue by Ahumada & Lapasset (2007). Andrievsky (1998) analysed this star in his paper on Blue Stragglers in the Praesepe cluster, but he did not define it as a true Blue Straggler, since in the colour−magnitude diagram it does not lie outside the cluster's main sequence. Our sample of stars is too small to allow us to generate a trustworthy colour−magnitude diagram based on spectroscopic temperatures. For this reason we are not able to confirm either the classification of Ahumada & Lapasset (2007) or that of Andrievsky (1998).

5.3.5. HD 73174

HD 73174 is the primary component of a triple SB1 system (Debernardi et al. 2000) and is the slowest rotator of the program stars, with $\upsilon \sin i < 5$ km s^{-1}. The spectrum was obtained with the ELODIE spectrograph with a mean resolution of 45 000, not sufficient to allow an accurate measurement of the $\upsilon \sin i$ of this star.

Debernardi et al. (2000) obtained the masses of the three components of the system (2 $M_{\odot}$; 0.68 $M_{\odot}$; 0.63 $M_{\odot}$). Knowing the age of the cluster (González-García et al. 2006, $\log(t) = 8.85$) it was possible to estimate the effective temperatures and the radii of the three stars comprising the system. Using the evolutionary mass models of Schaller et al. (1992), we estimated the effective temperature and the radius of the primary component (8375 K and 2.22 $R_{\odot}$ respectively). From plots on evolutionary models of cool stars of Gray (1992) we estimated the effective temperature and the radii of the other two components: 4557 K and 0.68 $R_{\odot}$ for the secondary and 4300 K and 0.65 $R_{\odot}$ for the third component. Since the presence of the third component is not certain we have not taken this star into account in our analysis. The radius ratio between the primary and the secondary star turns out to be $R_1/R_2 = 3.26$. We assumed a $\upsilon_{\rm mic}$ of 2 km s^{-1} for both the stars and a $\log g$ of 4.2 and of 4.4 for the primary and the secondary respectively. We calculated a model atmosphere for each of the two stars, using the parameters just described, and produced a synthetic spectrum for each of the two stars to check how much flux in the observed intensity spectrum is due to the secondary component. As it is possible to see in Fig. 9, the flux coming from the secondary star is negligible with respect to that of HD 73174. For this reason we analysed the system as a single one. The error bars on these inferred fundamental parameters could be very high since the error bars on the mass determination are unknown.

The low $\upsilon \sin i$ allowed us to perform a very detailed abundance analysis and the errors associated with the various elements are for this reason quite low, even if the signal to noise ratio and the resolution were not optimal.

C, N, O and Sc are underabundant while Ca is almost solar, as was found for HD 73618. For this reason we confirm the previous classification of this star. Only Ba shows a large error bar. This is probably due to the strong difference in depth of the selected lines and to the different influence that the non-LTE effects have on each of these lines.

We took into account the hyperfine structure correction for the following lines: Co I at 5342.695 Å and 5352.045 Å, Cu I at 5105.537 Å, Mn I at 6021.819 Å and Zn I at 4722.153 Å. The

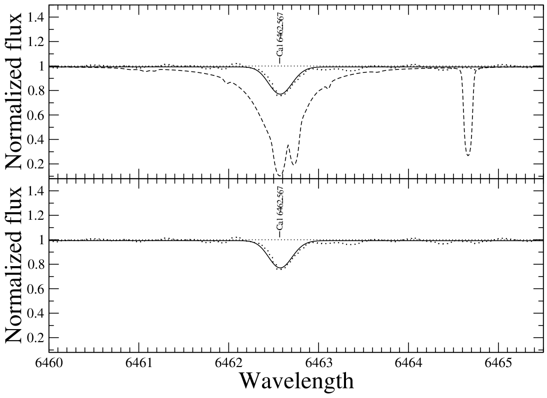

Fig. 9. Comparison between the incoming flux from the two components of the HD 73174 system. In the *upper panel* the dotted thick line is the observed (normalised) spectrum, while the solid and the dashed lines are the synthetic spectra of the primary and the secondary star respectively. These two synthetic spectra are calculated with the parameters described in the text and with solar abundances. In the *lower panel* we show with the dotted thick line the observed and normalised spectrum and with the straight line the resultant synthetic spectrum after the application of the calculated radius ratio ($R_1/R_2 = 3.26$).

abundance correction from HFS observed for all of these lines is smaller than 0.03 dex, much less than our typical errors.

We have to comment the difference of about 700 K between the $T_{\rm eff}$ derived from Strömgren photometry and from spectroscopy. We are not able to explain the reason for this dicrepancy. Probably, give concerning the very low $\upsilon \sin i$ of this star, a spectrum taken with a much higher resolution could solve this puzzle.

5.3.6. HD 73711

The ELODIE spectrum of this Am star has unfortunately a low *SNR* (Table 1) and a quite high $\upsilon \sin i$ (62 km s^{-1}), making the abundance analysis more difficult and less precise. HD 73711 is also the primary component of an SB1 system. The abundances of this star were previously analysed by Burkhart & Coupry (1998) who considered the spectrum as that of a single star.

We have used Fe I and Fe II lines to calculate the $T_{\rm eff}$ and $\log g$, while $\upsilon_{\rm mic}$ was calculated with Eq. (1). As with all the other ELODIE spectra we were not able to use the Hα and Hβ lines to determine the parameters. We have not found any detectable magnetic field with the abundance-Landé factor correlation for Fe I lines.

We confirm the previous classification of HD 73711, as Ca and Sc are underabundant, like C and O, as occurs for all the Am stars of the sample. The errors associated with the abundances are below 0.15 dex in spite of the high $\upsilon \sin i$ and the low *SNR*; only the error associated with the C abundance reaches 0.15 dex, probably due to the small number of selected lines used to calculate the final abundance, which were analysed without taking into account non-LTE effects.

5.3.7. HD 73818

The spectrum of the Am star HD 73818 has the lowest *SNR* of the whole sample. This fact, combined with the rather high $\upsilon \sin i$ (66 km s^{-1}), made the abundance analysis very difficult and imprecise. This is the primary star of an SB1 system. We analysed this spectrum as a single star, as suggested by Burkhart & Coupry (1998).

We tried to calculate $T_{\rm eff}$ and $\log g$ using Fe I and Fe II lines, applying the method described in Sect. 4.2, but we were never able to converge to two final values. For this reason we adopted the fundamental parameters calculated with the photometry. The $\upsilon_{\rm mic}$ was calculated using Eq. (1).

The abundances of many elements show large errors, mainly those elements for which non-LTE effects should be taken into account. The error associated with the Fe abundance is quite high in comparison to all other stars of the sample. This example illustrates the importance of a high *SNR* to be able to perform an accurate abundance analysis that starts with a spectroscopic determination of the fundamental parameters.

Ca and Sc are underabundant, confirming in this way the previous classification. Only the C abundance is higher than expected for an Am star of the Praesepe cluster.

5.3.8. HD 73709

HD 73709 is the primary star of an SB1 quadruple system (Abt & Willmarth 1999). The low $\upsilon \sin i$ allowed a good determination of the elemental abundances; only the moderate resolution of MUSICOS decreased the quality of our results.

This star was classified as Am by Gray & Garrison (1989), but was found photometrically to be an Ap star by Maitzen & Pavlovski (1987) according to the Δa index (Δa = +0.018 mag). Debernardi et al. (2000), using two ELODIE spectra and observations with the CORAVEL radial velocity scanner, found a magnetic field of 7.5 kG. Shorlin et al. (2002) looked for the presence of such a magnetic field using the LSD technique applied to the same MuSiCoS spectrum we analyse here. Their result shows clearly that HD 73709 does not have a significant magnetic field, with the measured value equal to $\langle B_z \rangle$ = 66 ± 39 G.

We calculated a synthetic Δa value with respect to the theoretical normality line a_0 determined by Khan & Shulyak (2007, Sect. 3.3.2) and found that Δa = +0.012 mag, which is compatible with the observed value.

As mentioned before, this star is the main component of a quadruple system. We ruled out that the third or fourth components could contribute significantly to the light since they appear to be much less massive than the other components. The ratio between the masses of the primary and secondary component is $M_2/M_1 \geq 0.27$ (Abt & Willmarth 1999). For HD 73174 we employed a value of $M_2/M_1 \geq 0.35$ (Abt & Willmarth 1999) and in that case our test demonstrated that the flux coming from the secondary star was negligible with respect to the primary for a radius ratio lower than two (Sect. 5.3.5). For this reason we arrived immediately at the same conclusion as for HD 73174 – that the contribution of the secondary to the observed spectrum is negligible.

The $\upsilon_{\rm mic}$ and $T_{\rm eff}$ were established using Fe I, Fe II and Ni I unblended lines. The $\log g$ was set imposing the ionisation equilibrium condition for Fe I and Fe II. The fitting of the Hα and Hβ lines was not applied to obtained the fundamental parameters, for the same reason as for the ELODIE spectrograph.

O, Ca and Sc are underabundant, confirming in this way the previous classification. C and Al show large error bars (≥0.15 dex), probably due to the fact that non-LTE effects were not taken into account.

6. Discussion

6.1. Are weak magnetic fields present in the Am stars of Praesepe?

If magnetic fields are present in Am stars, this might help explain some of the peculiar properties of these stars, such as slow rotation and the typical Ca/Sc underabundances (Böhm-Vitense 2006).

We decided to use the LSD approach to detect magnetic fields in Am stars since this method is the most precise method currently available, especially for stars with rich line spectra and low $\upsilon \sin i$. As explained in Sect. 4.2 we have also looked for magnetic fields using other techniques, but these methods have resulted in substantially higher upper limits.

Lanz & Mathys (1993) have claimed evidence of magnetic fields in the Am star *o* Peg ($T_{\rm eff} = 9550$) using the difference of equivalent widths of two Fe II lines at 6147.741 Å and 6149.258 Å. We did not try to apply the same method to compare our results to theirs as all of the sharp-lined Am stars in our sample are spectroscopic binaries, and the blending due to the spectral lines of the secondary might well affect the subtle signal of a magnetic field. Another problem is due to the fact that our Am stars are cool Am stars and the Fe II line at 6147.741 Å is strongly blended by an Fe I line, preventing an accurate equivalent width determination.

Shorlin et al. (2002) analysed 25 Am stars with the LSD technique without finding any significant magnetic field signature. These authors concluded that no credible evidence exists for the presence of organised or complex magnetic fields in Am or normal A-type stars.

In our study, the three Am stars observed with ESPaDOnS and the one observed with MuSiCoS did not reveal any magnetic field signature in the circular polarized spectra, analysed with the LSD procedure. We also tried to detect the presence of potential magnetic fields in the other Am stars, observed with ELODIE, using the method described in Sect. 4.2. For all of them it was not possible to detect any magnetic field.

Our conclusion is that the cool Am stars of Praesepe ($T_{\rm eff} < 8500$ K) show no evidence of magnetic fields that could explain the well-known phenomena associated with Am stars. This result supports and strengthens the conclusion of Shorlin et al. (2002).

6.2. Normal vs. Am stars

In Fig. 10 and in Table 3 we show the final adopted abundances for all of the program stars. The precision obtained with the abundance analysis allows us to distinguish two groups among the A-type stars of Praesepe: the normal A-type stars and the Am stars. For the two kinds of star analysed in this paper, the abundances of the Fe-peak elements are different. In normal A-type stars, Fe, Ni, and Cr are solar or slightly underabundant (compared to their solar abundances). In Am stars, these elements are slightly overabundant. In all but one of the stars of our sample, Ba is overabundant. However, the Ba abundance is definitely lower in normal A-type stars than in Am stars. This suggests that Ba may be considered as an additional indicator of Am peculiarities, together with C, N, O, Ca, Sc and the Fe-peak elements.

The abundance pattern found for HD 72942 deserves further comment. Bidelman (1956) classified HD 72942 as Am. Our abundance analysis shows some features common to the Am stars, like underabundances of C and O and an

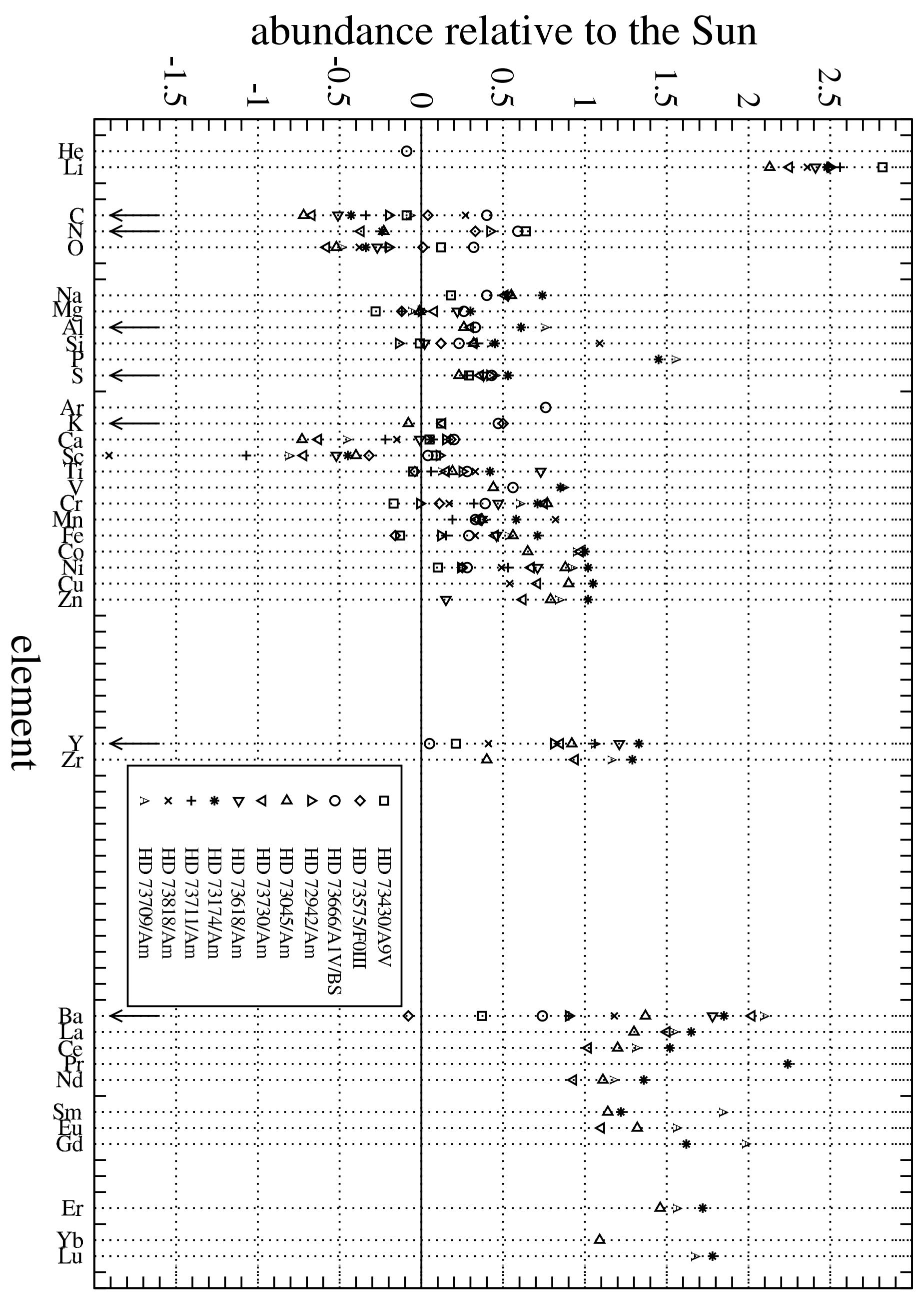

Fig. 10. Elemental abundances relative to the Sun for the program stars. The solar abundances are taken from Asplund et al. (2005). In order to show a more readable Figure, the errors (Table 3) are omitted. Arrows show elements affected by non-LTE effects.

overabundance of Fe, and some others in common with normal A-type stars, like overabundance of N, Ca and Sc and a low Ba abundance. For these reasons we believe that HD 72942 has a chemical composition between the normal A-type stars and the Am stars. The high observed radial velocity of this star may be indicative of undetected binarity.

The remaining Am stars represent a fairly homogeneous sample.

6.3. Constraints to the diffusion theory

Underabundances of Sc and/or Ca and small overabundances of Iron-group elements are qualitatively explained by diffusion theory (see, e.g., the review in the introduction by Alecian (1996) and references therein). In particular, following Alecian (1996), Richer et al. (2000) developed a detailed modeling of the structure and evolution of Am/Fm stars, taking into account atomic diffusion of metals and radiative accelerations for all species in the OPAL opacities.

The results of this work can be used to constrain diffusion models, and we can compare our results with theoretical predictions. For the comparison, we use the abundances of HD 73730 (Fig. 11) since it is the star among those that are not binary with the lowest $\upsilon \sin i$, which favors the abundance analysis. Furthermore, the elemental abundances of this star are also representative of the homogeneous group of Am stars of the Praesepe cluster as listed in Sect. 6.2.

Figure 14 of Richer et al. (2000) shows the predicted abundances from a diffusion and turbulence model as a function of time and effective temperature. Open circles (reported also in Fig. 11) refer to the predicted abundances for 670 Myr old stars, an age that is closely comparable to that one of the Praesepe cluster (~700 My, according to González-García et al. 2006). For temperatures around $T_{\rm eff} = 8000$ K, the temperature of HD 73730, the model by Richer et al. (2000) predicts

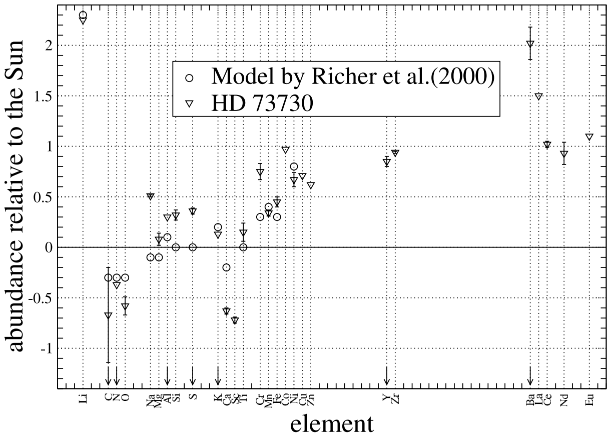

Fig. 11. The open triangles show the abundances derived for HD 73730. The open circles show the predicted abundances displayed in Fig. 14 of Richer et al. (2000). Arrows show elements affected by non-LTE effects

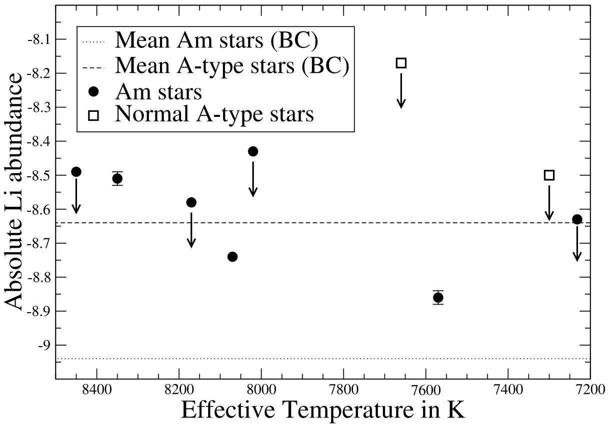

Fig. 12. Distribution of the Li abundance as a function of the $T_{\rm eff}$. The dashed line shows the Li abundance value found by Burkhart & Coupry (1995) (BC in the legend) for normal A-type stars. The dotted line shows their Li abundance value for Am stars. The open squares and the closed circles correspond to the Li abundances of the program normal A-type stars and Am stars respectively. The upper limit values are indicated with an arrow.

underabundances of −0.3 (relative to the Sun) for C, N and O, of −0.1 for Na, Mg and Ca, solar abundances for Si, S and Ti, overabundances of +0.1 for Al, of +0.3 for Cr and Fe, of +0.4 for Mn, of +0.8 for Ni and +2.3 for Li, within 0.1 dex.

Our Fig. 10 (see also Table 3) shows an agreement for Li, C, N, O, Mg, Al, Si, Ca and Fe-peak elements within 0.1 dex. Discrepancies are apparent for Na and S (Sc was not modeled by Richer et al. (2000) because no OPAL data was available for Sc).

Na is the element for which the derived abundance (≃0.5 dex with respect to the solar abundance) has the smallest scatter among the Am stars of our sample. Observations seems definitely to suggest an overabundance of this element which is inconsistent with model predictions of −0.1 dex.

S shows a small scatter in our sample (σ = 0.12 dex). Kamp et al. (2001) analysed the S abundance in the metal poor A-type star λ Boo in LTE and non-LTE. Their analysis shows that the S abundance determined in non-LTE is lower than that determined in LTE by 0.1 dex. For metal poor stars non-LTE effects are larger than for normal A-type stars and Am stars. This brings our S abundance (≃+0.35 dex) to an overabundance (relative to the Sun) of ≥0.25 dex, as compared with a solar abundance predicted by Richer et al. (2000). This apparent discrepancy should be investigated in non-LTE regime.

6.4. Lithium abundance

In the context of radiative diffusion theory, it is interesting to examine the atmospheric abundance of lithium in stars where such a mechanism is known to be present, like in Am stars. Such studies have been carried out especially by Burkhart & Coupry (1991) and Burkhart et al. (2005). Their conclusion was that, in general, the Li abundance in Am stars is close to the cosmic value ($\log N_{\rm Li}/N_{\rm total} \sim -9.04$ dex), although a small proportion of them are Li deficient. The normal A-type stars appear to have a higher Li abundance ($\log N_{\rm Li}/N_{\rm total} \sim -8.64$ dex), in the $T_{\rm eff}$ range 7000−8500 K (Burkhart & Coupry 1995).

We have calculated precise Li abundances for HD 73045 and for HD 73174 taking into account hyperfine structure, while for HD 73730 we give an estimation derived from one line and without hyperfine structure. For other stars it was possible to derive only an upper limit, since the higher $\upsilon \sin i$ values did not allow a more accurate abundance determination. In HD 73666 we have not found any Li line, while for HD 73709 the MuSiCoS spectrum did not cover the strong Li 6707.761 Å line. Our determinations confirm the overabundances (relative to the Sun) for three Am stars. Since for the normal A-type stars and the other Am stars we can only derive upper limits, we cannot confirm the overabundances. In Fig. 12 we show the absolute Li abundance as a function of $T_{\rm eff}$, in comparison with the values given by Burkhart & Coupry (1995). Our sample is not large enough to address the behavior of the lithium abundance in the temperature range between 7000 K and 8500 K, but we notice that the abundances appear to be higher than those derived by Burkhart & Coupry (1995) in open clusters. We cannot confirm the tendancy of the normal A-type stars to have a higher Li abundance. Our results appear to be more consistent with those derived by North et al. (2007) for field stars.

6.5. Comparison with previous abundance determinations

In the past years, some of the stars belonging to our sample were analysed by different authors: Hui-Bon-Hoa et al. (1997), Hui-Bon-Hoa & Alecian (1998), Andrievsky (1998) and Burkhart & Coupry (1998).

In Table 4 (available only in the online version) we compare our final abundances with those obtained by other authors. The abundances coming from other papers were converted to our $\log N_{\rm el}/N_{\rm total}$ scale, using the solar abundances taken as reference in each paper.

As explained in Sect. 4.2, our $T_{\rm eff}$ and $\log g$ were determined spectroscopically, while the other authors derived these parameters from photometry. All the measurements are in perfect agreement considering the associated errors. This shows that for normal A-type stars and for Am stars the fundamental parameters, derived from photometry, are not too far from a more precise determination given by the spectroscopy. For some stars, the microturbulence velocity appears to differ for different authors. It is notable that the our $\upsilon_{\rm mic}$ and that derived by Hui-Bon-Hoa & Alecian (1998) for the slow rotator HD 73174 are in good agreement. This agreement is due probably to the similar methods used to derive it (see Hui-Bon-Hoa & Alecian 1998).

Taking into account a default error of 0.2 dex for the abundances without an individual error, inspection of Table 4 reveals a good agreement between our work and the previous ones. Only Li, Sc, Ba and Eu show some deviations. The deviation associated with the Sc abundance occurs because of the difficulty to calculate this abundance for Am stars in which Sc is underabundant, showing only shallow lines. Concerning the Ba and Eu discrepancies, they could be due to a different line selection with different non-LTE effects associated with the Ba lines and a different weight given to the blended Eu lines, selected to determine the abundances. We are not able to find a clear reason of the discrepancies for the Li abundances.

We believe that our determination of the fundamental parameters and of the elemental abundances are affected by smaller external errors than those of the other authors. We state this based on the wider wavelength range available, on the use of better and more carefully-checked line parameters, on the more reliable atmospheres models used and finally on the methodology used to determine the abundances (fitting of the line profile instead of using equivalent widths).

7. Conclusions

We have obtained high resolution, high *SNR* spectra for eleven A-type stars belonging to the nearby intermediate-age Praesepe open cluster. For seven stars of the sample the spectra were also obtained in circular polarization.

Eight stars of the sample were previously classified as Am stars, two as normal A-type stars and one as an Ap (Si) star. We have calculated the fundamental parameters and performed a detailed abundance analysis for each star of the sample. For the stars observed in circular polarization we have used the LSD technique to measure the longitudinal magnetic field.

No significant magnetic field signature was found applying the LSD technique to the Am stars, which were observed with ESPaDOnS and MuSiCoS. This leads us to the conclusion that peculiar abundances and slow rotation of the Praesepe Am stars cannot be explained by the presence of a magnetic field. But since nearly all of them are SBs we can conclude that slow rotation, induced by binarity, can lead to the Am chemical peculiarities.

Fundamental parameters and elemental abundances were derived by adjusting synthetic spectra to the observed ones. The model atmospheres were computed by means of the 8.4 version of the LLMODELS code, without taking into account non-LTE corrections, using atomic line data extracted from the VALD database. Synthetic spectra were produced with Synth3 (Kochukhov 2006).

The abundance analysis shows that the Blue Straggler HD 73666, previously classified Ap (Si) star, is a normal A-type star. This star does not show any magnetic field nor peculiarity. We confirm the membership and the classification of the two normal A-type stars HD 73430 and HD 73575. HD 72942 cannot be confirmed either as member of the cluster or as an Am star. For all the other Am stars classification is confirmed.

For this sample of Am stars we have compared our abundances with the predictions of diffusion models by Richer et al. (2000). We obtained an excellent agreement, within the errors, with the predictions for almost all the common elements. Only Na and probably S show a clear discrepancy from the theoretical abundances. Unfortunately, our Na and S abundances do not take into account non-LTE effects that would bring the abundances closer to the predictions of theory (Kamp et al. 2001). A non-LTE abundance determination should be performed, at least for a few Am stars, in order to confirm the abundance predictions of these two elements. Richer et al. (2000) did not analyse Sc because it is not present in the OPAL opacity database. Model predictions for this element and for heavy elements are especially important and should be performed.

Finally, we have turned our attention to the Li abundance of the sample, obtaining results comparable to those of Burkhart & Coupry (1995), in open clusters, and North et al. (2007), for field stars.

Our results indicate that radiative diffusion, combined with turbulent mixing, can account for most of the chemical peculiarities found in Am stars. More abundance determinations on cluster stars with a variety of ages will help to constrain the physical processes at work in A and Am stars.

Acknowledgements. We are deeply indebted to Tanya Ryabchikova for her close and accurate supervision of the abundance analysis. L.F. and O.K. have received support from the Austrian Science Foundation (FWF project P17980-N2). S.K., J.D.L. and G.A.W. acknowledge support from the Natural Science and Engineering Council of Canada (NSERC). G.A.W. acknowledges support from the Department of National Defence Academic Research Programme (DND-ARP). This paper was based on observations obtained using the ESPaDOnS spectropolarimeter at the Canada-France-Hawaii Telescope (Canada), the ELODIE spectrograph at the Observatoire de Haute Provence (France) and the MuSiCoS spectropolarimeter at the Bernard Lyot Telescope (France).

References

Abt, H. A. 1985, ApJ, 294, L103
Abt, H. A., & Willmarth, D. W. 1999, ApJ, 521, 682
Adelman, S. J., Caliskan, H., Kocer, D., Cay, I. H., & Gokmen Tektunali, H. 2000, MNRAS, 316, 514
Ahumada, J. A., & Lapasset, E. 2007, A&A, 463, 789
Alecian, G. 1996, A&A, 310, 872
Andrievsky, S. M. 1998, A&A, 334, 139
Asplund, M., Grevesse, N., & Sauval, A. J. 2005, in Cosmic Abundances as Records of Stellar Evolution and Nucleosynthesis, ed. T. G. Barnes III, & F. N. Bash, ASP Conf. Ser., 336, 25
Bagnulo, S., Landstreet, J. D., Mason, E., et al. 2006, A&A, 450, 777
Baranne, A., Queloz, D., Mayor, M., et al. 1996, A&AS, 119, 373
Baumueller, D., & Gehren, T. 1997, A&A, 325, 1088
Bidelman, W. P. 1956, PASP, 68, 318
Böhm-Vitense, E. 2006, PASP, 118, 419
Budaj, J. 1996, A&A, 313, 523
Burkhart, C., & Coupry, M. F. 1991, A&A, 249, 205
Burkhart, C., & Coupry, M. F. 1995, Mem. Soc. Astron. It., 66, 357
Burkhart, C., & Coupry, M. F. 1998, A&A, 338, 1073
Burkhart, C., Coupry, M. F., Faraggiana, R., & Gerbaldi, M. 2005, A&A, 429, 1043
Canuto, V. M., & Mazzitelli, I. 1992, ApJ, 389, 724
Debernardi, Y., Mermilliod, J.-C., Carquillat, J.-M., & Ginestet, N. 2000, A&A, 354, 881
Donati, J.-F., Semel, M., Carter, B. D., Rees, D. E., & Collier Cameron, A. 1997, MNRAS, 291, 658
Donati, J.-F., Catala, C., Wade, G. A., et al. 1999, A&AS, 134, 149
Folsom, C. P., Wade, G. A, Bagnulo, S., & Landstreet, J. D. 2007, MNRAS, 376, 361
González-Garcá, B. M., Zapatero Osorio, M. R., Béjar, V. J. S., et al. 2006, A&A, 460, 799
Gray, D. F. 1992, The observation and analysis of stellar photospheres (Cambridge University Press)
Gray, R. O., & Garrison, R. F. 1989, ApJS, 70, 623
Hauck, B., & Mermilliod, M. 1998, A&AS, 129, 431
Heiter, U., Kupka, F., van't Veer-Menneret, C., et al. 2002, A&A, 392, 619
Hill, G. M., & Landstreet, J. D. 1993, A&A, 276, 142
Hog, E., Kuzmin, A., Bastian, U., et al. 1998, A&A, 335, 65
Hui-Bon-Hoa, A., & Alecian, G. 1998, A&A, 332, 234
Hui-Bon-Hoa, A., Burkhart, C., & Alecian, G. 1997, A&A, 323, 901
Kamp, I., Iliev, I. K., Paunzen, E. et al. 2001, A&A, 375, 899
Khan, S. A., & Shulyak, D. V. 2006, A&A, 448, 1153
Khan, S. A., & Shulyak, D. V. 2006, A&A, 454, 933
Khan, S. A., & Shulyak, D. V. 2007, A&A, 469, 1083
Kharchenko, N. V., Piskunov, A. E., Röser, S., Schilbach, E., & Scholz, R.-D. 2004, AJ, 325, 740
Kochukhov, O. 2006, in Magnetic Stars, ed. I. I. Romanyuk, & D. O. Kudryavtsev, in press
Kochukhov, O., Khan, S., & Shulyak, D. V. 2005, A&A, 433, 671

Kupka, F. 1996, in Stellar Surface Structure, ed. K. G. Strassmeier, & J. L. Linsky, IAU Symp., 176, 557
Kupka, F., Piskunov, N. E., Ryabchikova, T. A., Stempels, H. C., & Weiss, W. W. 1999, A&AS, 138, 119
Kurucz, R. 1993a, ATLAS9: Stellar Atmosphere Programs and 2 km s^{-1} grid. Kurucz CD-ROM No. 13 (Cambridge: Smithsonian Astrophysical Observatory)
Kurucz, R. 1993b, Opacities for Stellar Atmospheres: Abundance Sampler. Kurucz CD-ROM No. 14 (Cambridge: Smithsonian Astrophysical Observatory)
Landstreet, J. D. 1998, A&A, 338, 1041
Lanz, T., & Mathys, G. 1993, A&A, 280, 486
Leonard, P. J. T. 1996, ApJ, 470, 521
Maitzen, H. M., & Pavlovski, K. 1987, A&AS, 71, 441
Mason, B. D., Hartkopf, W. I., McAllister, H. A., & Sowell, J. R. 1993, AJ, 106, 637
Mermilliod, J.-C., & Paunzen, E. 2003, A&A, 410, 511
North, P., Betrix, F., & Besson, C. 2007, EAS Publ. Ser., 17, 333
Pace, G., Recio-Blanco, A., Piotto, G., & Momany, Y. 2006, A&A, 452, 493
Perryman, M. A. C., Lindegren, L., Kovalevsky, J., et al. 1997, A&A, 323, 49
Piskunov, N. E., Kupka, F., Ryabchikova, T. A., Weiss, W. W., & Jeffery, C. S. 1995, A&AS, 112, 525
Preston, G. W. 1974, ARA&A, 12, 257
Przybilla, N., Butler, K., Becker, S. R., & Kudritzki, R. P. 2006, A&A, 445, 1099
Richer, J., Michaud, G., & Turcotte, S. 2000, ApJ, 529,338
Robichon, N., Arenou, F., Mermilliod, J.-C., & Turon, C. 1999, A&A, 345, 471
Rodriguez, E., Lopez-Gonzalez, M. J., & Lopez de Coca, P. 2000, A&AS, 144, 469
Ryabchikova, T. A., Piskunov, N. E., Stempels, H. C., Kupka, F., & Weiss, W. W. 1999, Phis. Scr., T83, 162
Ryabchikova, T. A., Kochukhov, O., & Bagnulo, S. 2007, A&A, submitted
Schaller, G., Schaerer, D., Meynet, G., & Maeder, A. 1992, A&AS, 96, 269
Shorlin, S. L. S., Wade, G. A., Donati, J.-F., et al. 2002, A&A, 392, 637
Shulyak, D., Tsymbal, V., Ryabchikova, T., Stütz, Ch., & Weiss, W. W. 2004, A&A, 428, 993
Smalley, B., & Kupka, F. 1997, A&A, 328, 349
Stütz, Ch., Bagnulo, S., Jehin, E., et al. 2006, A&A, 451, 285
Tsymbal, V. V. 1996, in Model Atmospheres and Spectral Synthesis, ed. S. J. Adelman, F. Kupka, & W. W. Weiss, ASP Conf. Ser., 108, 198
Varenne, O., & Monier, R. 1999, A&A, 351, 247
Wade, G. A., Donati, J.-F., Landstreet, J. D., & Shorlin, S. L. S. 2000, MNRAS, 313, 823
Wang, J. J., Chen, L., Zhao, J. H., & Jiang, P. F. 1995, A&AS, 113, 419

Online Material

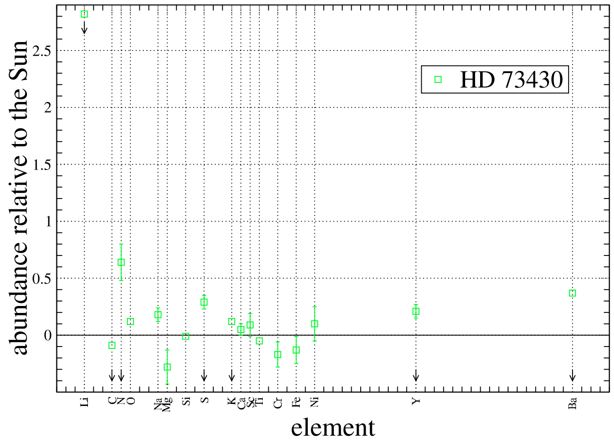

Fig. 13. Elemental abundances relative to the Sun for HD 73430. The solar abundances are taken from Asplund et al. (2005). Arrows show elements affected by non-LTE effects. Errors are given in Table 3.

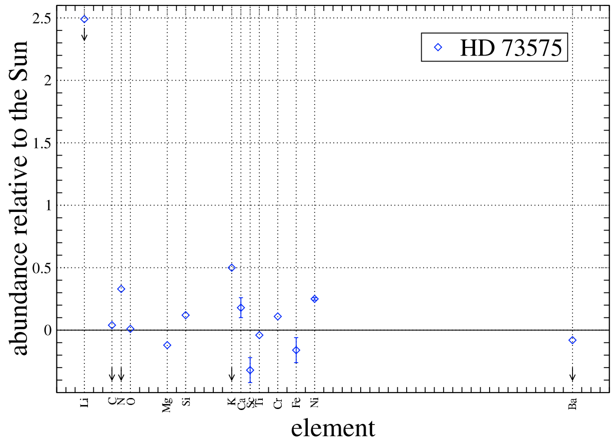

Fig. 14. As for Fig. 13 for HD 73575.

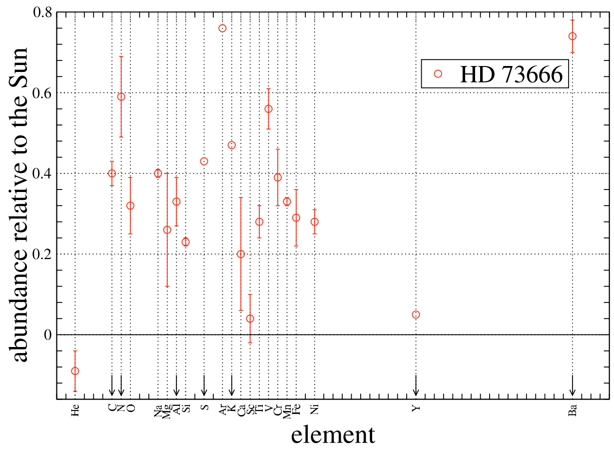

Fig. 15. As for Fig. 13 for HD 73666.

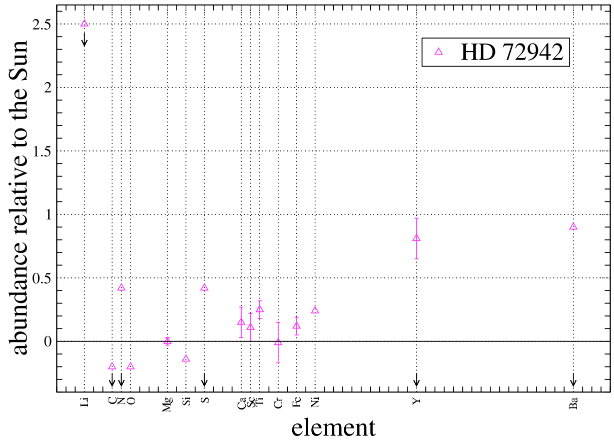

Fig. 16. As for Fig. 13 for HD 72942.

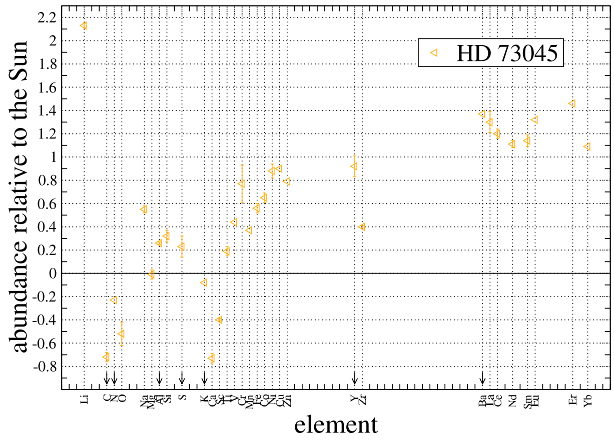

Fig. 17. As for Fig. 13 for HD 73045.

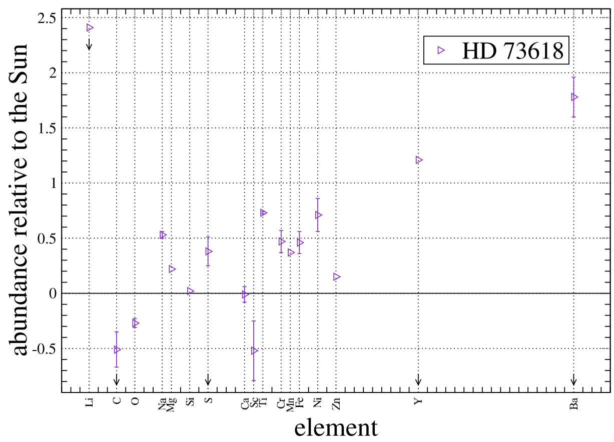

Fig. 18. As for Fig. 13 for HD 73618.

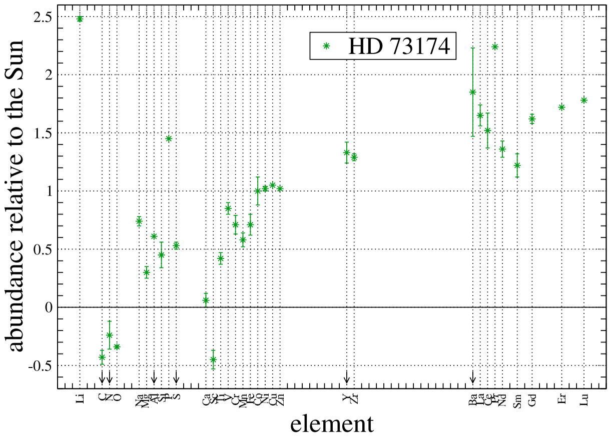

Fig. 19. As for Fig. 13 for HD 73174.

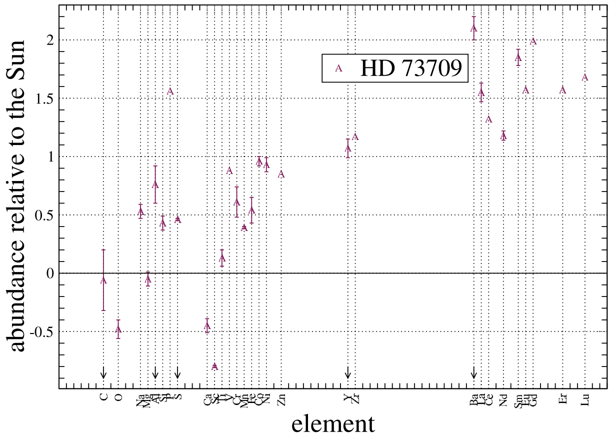

Fig. 22. As for Fig. 13 for HD 73709.

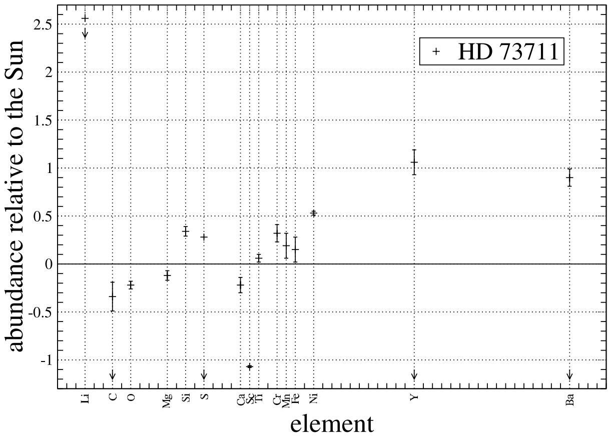

Fig. 20. As for Fig. 13 for HD 73711.

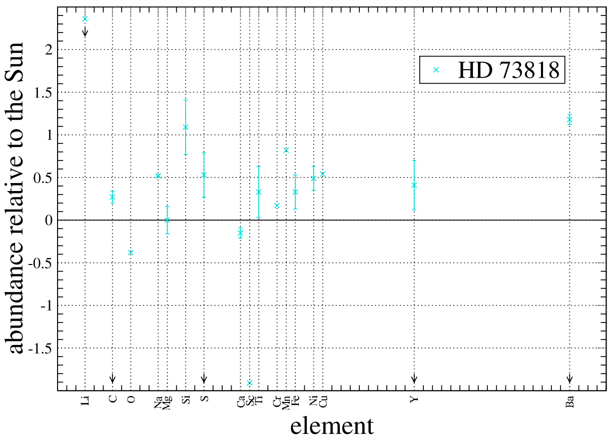

Fig. 21. As for Fig. 13 for HD 73818.

Table 4. The table shows the comparison between the abundances described in this paper and those derived by other authors for the common stars. We compare also the fundamental parameters. HBA: Hui-Bon-Hoa et al. (1997); HA: Hui-Bon-Hoa & Alecian (1998); A: Andrievsky (1998); BC: Burkhart & Coupry (1998); TW: this work.

	$T_{\rm eff}$	$\log g$	$\upsilon \sin i$	$\upsilon_{\rm mic}$	He	Li	C	O	Na	Mg	Al
HD 73666											
A	9600	3.80	30	3.0	−1.05(−)		−3.59(−)	−3.37(−)	−5.41(−)		
BC	9500	−	−	4.5		<−8.59(−)					
TW	9382	3.78	10	1.9	−1.20(05)	−	<−3.25(03)	−3.06(07)	−5.47(01)		
HD 72942											
HA	8130	3.80	70	2.0						−4.38(−)	
BC	8300	−	−	4.5		<−8.74(−)					
TW	8450	3.90	73	2.4		<−8.49(−)				−4.51(03)	
HD 73045											
HBA	7520	4.27	10	3.5						−4.31(−)	
BC	7500	−	−	4.5		−9.04(−)					−5.44(−)
TW	7570	4.05	10	3.6		−8.86(02)				−4.52(04)	<−5.41(01)
HD 73730											
HA	8020	3.90	32	4.0						−4.67(−)	
BC	8020	−	−	4.5		−9.04(−)					−5.64(−)
TW	8070	3.97	29	2.6		−8.74(−)				−4.43(06)	<−5.37(−)
HD 73618											
HBA	8060	3.87	60	3.0						−3.93(−)	
A	8050	4.00	60	3.0			−3.89(−)	−3.77(−)	−5.71(−)		
BC	8100	−	−	4.5		−8.94(−)					−5.29(−)
TW	8170	4.00	47	2.5		<−8.58(−)	<−4.16(16)	−3.65(04)	−5.34(03)	−4.29(−)	−
HD 73174											
HA	8090	4.00	<10	2.8						−4.40(−)	
BC	8090	−	−	4.5		−9.04(−)					−5.34(−)
TW	8350	4.15	<5	2.9		−8.51(02)				−4.21(05)	<−5.06(−)
HD 73711											
BC	8290	−	−	4.5		<−8.64(−)					
TW	8020	3.69	62	2.5		<−8.43(−)					
HD 73818											
BC	7230	−	−	4.5		−8.99(−)					
TW	7230	3.82	66	2.8		<−8.63(−)					
HD 73709											
HBA	8060	3.95	20	3.5						−4.39(−)	
BC	8080	−	−	4.5		−8.64(−)					−5.14(−)
TW	8070	3.78	10	2.3		−				−4.56(06)	<−4.91(16)

	Si	S	Ca	Sc	Cr	Mn	Fe	Ni	Ba	Eu
HD 73666										
A	−4.89(−)		−5.68(−)				−4.44(−)		−9.31(−)	
BC		−4.64(−)	−5.24(−)				−3.94(−)			−10.04(−)
TW	−4.30(01)	<−4.47(−)	−5.53(14)				−4.30(07)		<−9.13(04)	−
HD 72942										
HA			−6.09(−)	−9.05(−)	−6.40(−)		−4.59(07)	−5.09(−)		
BC		−4.54(−)					−4.29(−)			
TW		<−4.48(−)	−5.58(12)	−8.88(11)	−6.41(16)		−4.47(07)	−5.57(−)		
HD 73045										
HBA			−6.22(27)	−9.87(−)	−5.67(−)		−3.95(14)	−4.99(−)		
BC	−4.29(−)	−4.94(−)					−4.17(−)	−5.09(−)		−10.54(−)
TW	−4.21(05)	<−4.67(09)	−6.46(04)	−9.39(01)	−5.63(16)		−4.03(04)	−4.93(06)		−10.20(−)
HD 73730										
HA			−6.24(−)	−10.54(−)	−6.06(−)		−4.35(06)	−5.14(−)		
BC	−4.39(−)	−4.64(−)					−4.14(−)	−5.34(−)		−10.74(−)
TW	−4.21(05)	<−4.54(03)	−6.36(03)	−9.71(03)	−5.65(08)		−4.14(05)	−5.14(07)		−10.42(−)
HD 73618										
HBA			−5.70(−)	−10.53(−)	−5.92(−)		−4.08(20)	−4.93(−)		
A	−4.69(−)	−4.51(−)	−5.78(−)			−6.75(−)	−4.24(−)	−5.49(−)	−9.21(−)	
BC	−4.14(−)	−4.74(−)					−4.01(−)			
TW	−4.51(−)	<−4.52(13)	−5.74(07)	−9.51(27)	−5.93(10)	−6.28(−)	−4.13(10)	−5.10(15)	<−8.09(18)	
HD 73174										
HA			−6.07(07)	−10.52(−)	−6.09(−)		−4.27(16)	−5.20(−)		
BC	−4.34(−)	−4.74(−)					−4.22(−)	−5.24(−)		−10.54(−)
TW	−4.08(11)	<−4.37(03)	−5.70(08)	−9.44(08)	−5.69(08)		−3.88(09)	−4.79(02)		−
HD 73711										
BC		−4.64(−)					−3.94(−)			
TW		<−4.62(−)					−4.44(13)			
HD 73818										
BC							−4.34(−)			
TW							−4.26(20)			
HD 73709										
HBA			−5.92(17)	−10.20(−)	−5.72(−)		−3.96(17)	−4.76(−)		
BC	−4.24(−)	−4.54(−)					−4.04(−)	−5.04(−)		−10.24(−)
TW	−4.10(06)	<−4.44(01)	−6.18(06)	−9.79(01)	−5.79(13)		−4.05(11)	−4.88(06)		−9.95(−)

2008CoSka..38..123F

Contrib. Astron. Obs. Skalnaté Pleso **38**, 123 – 128, (2008)

Chemical evolution of A– and B–type stars in open clusters: observed abundances vs. diffusion models

Am stars in the Praesepe cluster

L. Fossati[1], S. Bagnulo[2], R. Monier[3], S.A. Khan[4], O. Kochukhov[5], J.D. Landstreet[4], G.A. Wade[6] and W.W. Weiss[1]

[1] *Institut für Astronomie, Universität Wien,*

[2] *Armagh Observatory, College Hill, Armagh BT61 9DG, Northern Ireland.*

[3] *Groupe de Recherches en Astronomie et Astrophysique du Languedoc UMR 5024, Université Montpellier II, France.*

[4] *Department of Physics & Astronomy, University of Western Ontario, London, N6A 3K7, Ontario, Canada.*

[5] *Department of Astronomy and Space Physics, Uppsala University, Uppsala, Sweden.*

[6] *Physics Dept., Royal Military College of Canada, PO Box 17000, Station Forces, K7K 4B4, Kingston, Canada.*

Received: November 30, 2007; Accepted: December 15, 2007

Abstract. We have decided to address the problem of how abundances and peculiarities change during main sequence evolution. We have setup a program to measure the atmospheric abundance patterns from tens of A–type star members of clusters of different ages, and compare the results with theory predictions. In this paper we present the overall project and we focus on the results obtained for a sample of Am stars of the Praesepe cluster ($\log t = 8.85 \pm 0.15$; González–García *et al.*, 2006). We have obtained spectra for eight Am stars, two normal A–type stars and one blue straggler, that are probable members of the Praesepe cluster. For all of these stars we have determined fundamental parameters and photospheric abundances for a large number of chemical elements. For seven stars we also obtained spectra in circular polarisation and applied the LSD technique to measure the mean longitudinal magnetic field. We have found good agreement between abundance predictions of diffusion models and measured abundances, except for Na and S. Li appears to be overabundant in three stars of our sample. No magnetic field was detected in any of the analysed stars.

Key words: stars: abundances – stars: atmospheres – stars: fundamental parameters – stars: chemically peculiar

© Astronomical Institute of the Slovak Academy of Sciences • Provided by the NASA Astrophysics Data System

2008CoSka..38..123F

1. A high–resolution spectroscopic survey of A–type stars in open clusters

The chemical composition of field A–type stars have been studied by several authors, e.g. Hill and Landstreet (1993), Adelman *et al.* (2000). It is not straightforward to use the results of these works to study how chemical elements evolve during the life of the star on the main sequence. This because the original composition of the cloud from which stars were born is unknown and it is not possible to discriminate between evolutionary effects, and differences due to the original chemical composition. Furthermore, it is difficult to estimate the age of field stars with good accuracy, as demonstrate in Bagnulo *et al.* (2006).

Our goal is to determine abundance patterns in A–type star members of clusters of different ages. This is crucial to investigate the chemical differences between normal and peculiar stars inside the same cluster, to study the evolution with time of abundance peculiarities by studying clusters of various ages, to set constraints on the hydrodynamical processes occurring at the base of the convection zone in the non magnetic stars and to study the effects of diffusion in chemically peculiar stars (Fm/Am/Ap/Bp) of the cluster.

We have performed a large observational campaign obtaining high–resolution spectroscopy of a large number of early–type stars in a sample of ten open clusters of homogeneously distributed in age from $\log t = 6.8$ to $\log t = 8.9$. We have performed the observations with the use of five different spectrographs: FLAMES at the ESO VLT, FIES at the Nordic Optical Telescope (NOT), ELODIE and SOPHIE at the Observatoire de Haute–Provence (OHP), and ESPaDOnS at the CFHT. The observed clusters and the instrument used for the observations are listed in Table 1. The chemically peculiar stars of each cluster have already been searched for magnetic field in a previous FORS1 survey (Bagnulo *et al.*, 2006).

We dedicate this first paper to the Am stars of the Praesepe cluster.

2. Observations and analysis of the Am stars of the Praesepe cluster

We observed six stars of the Praesepe cluster using the ESPaDOnS (Echelle SpectroPolarimetric Device for Observations of Stars) spectropolarimeter ($R \sim 65\,000$) at the Canada-France-Hawaii Telescope (CFHT), in polarimetric mode. Spectra of other four stars were obtained with the ELODIE spectrograph ($R \sim 42\,000$) at the Observatoire de Haute Provence (OHP). An additional spectrum was obtained with the MuSiCoS spectropolarimeter ($R \sim 35\,000$) at the 2-m Bernard Lyot Telescope (TBL) of the Pic du Midi Observatory, in polarimetric mode. The spectra were reduced with the pipelines provided for each instrument. The continuum normalisation was performed without the use of any automatic continuum fitting procedure.

© Astronomical Institute of the Slovak Academy of Sciences • Provided by the NASA Astrophysics Data System

2008CoSka..38..123F

Table 1. Open clusters already observed for the survey. The second and third columns give the distance modulus, in magnitudes, and age of the cluster, in $\log t$. The last column shows which instrument (and telescope) were used to obtain the spectra of the stars.

Cluster	Distance Modulus mag.	$\log t$ dex.	Instrument
NGC 6193	11.8	6.8	FLAMES (VLT)
NGC 6383	10.9	6.9	FLAMES (VLT)
NGC 6250	10.8	7.4	FLAMES (VLT)
IC 4665	8.3	7.6	FIES (NOT)
NGC 6405	8.9	8.0	FLAMES (VLT)
NGC 3114	10.0	8.1	FLAMES (VLT)
NGC 5460	9.4	8.2	FLAMES (VLT)
NGC 7092	7.6	8.4	FIES (NOT)
NGC 6633	8.4	8.6	FLAMES (VLT)
M 44 / Praesepe	6.4	8.9	SOPHIE & ELODIE (1.93–m T) ESPaDOnS (CFHT)

The complete sample of stars observed and analysed in this work, together with the adopted set of fundamental parameters are listed in Table 2. Model atmospheres were calculated with the LTE code LLMODELS (Shulyak *et al.*, 2004). We used the VALD database (Piskunov *et al.*, 1995; Kupka *et al.*, 1999; Ryabchikova *et al.*, 1999) as source of spectral line parameters. Convection was treated according to the CM approach (Canuto, Mazzitelli 1992). The fundamental parameters ($T_{\rm eff}$, $\log g$, $\upsilon_{\rm mic}$) were derived spectroscopically using lines of Fe–peak elements and with fitting of Hydrogen lines. Once otained the fundamental parameters, the elemental abundances were derived with direct fitting of the synthetic spectra on the observation. We have synthesised the spectra with Synth3 (Kochukhov, 2006) and fit the core of selected lines to obtain an abundance value for each line. The adopted abundance of a chemical element is the mean of the abundances of the single lines of each element. More details are given in Fossati *et al.* (2007).

We have divided our sample of stars according to the spectral classification given in letterature: normal A–type stars, the blue straggler HD 73666 and Am stars (see Table 2).

2.1. Normal A–type stars

The LSD profile of the normal A–type stars of the cluster (HD 73430 and HD 73575) do not show any magnetic field signature, as it is possible to see in Table 2.

© Astronomical Institute of the Slovak Academy of Sciences • Provided by the NASA Astrophysics Data System

2008CoSka..38..123F

Table 2. Adopted spectroscopic atmospheric fundamental parameters for the analysed stars of the Praesepe cluster. The errors on the fundamental parameters are estimated to be 200 K, 0.2 $\mathrm{km\,s^{-1}}$and 0.2 for $T_{\rm eff}$, $\upsilon_{\rm mic}$ and $\log g$ respectively. The estimated error on $\upsilon \sin i$ is about 5%. The $\upsilon_{\rm r}$ is given in $\mathrm{km\,s^{-1}}$. $\langle B_z \rangle$ indicate the longitudinal magnetic field (measured in Gauss) calculated with the LSD tecnique. The spectral classification is given taking into account our results.

HD	Spectral type	$T_{\rm eff}$ [K]	$\log g$ [cgs]	$\upsilon_{\rm mic}$ [$\mathrm{km\,s^{-1}}$]	$\upsilon \sin i$ [$\mathrm{km\,s^{-1}}$]	$\upsilon_{\rm r}$ [$\mathrm{km\,s^{-1}}$]	$\langle B_z \rangle$ G
73430	A9V	7660	4.02	2.6	73	33.7	1 ± 45
73575	F0III	7300	2.92	2.7	127	33.4	-215 ± 149
73666	A1V	9382	3.78	1.9	10	34.1	6 ± 5
72942	A3V	8450	3.90	2.4	73	39.9	12 ± 31
73045	Am	7570	4.05	3.6	10	27.9	-1 ± 4
73730	Am	8070	3.97	2.6	29	36.6	-12 ± 9
73618	Am	8170	4.00	2.5	47	15.1	–
73174	Am	8350	4.15	2.9	<5	2.9	–
73711	Am	8020	3.69	2.5	62	23.4	–
73818	Am	7232	3.82	2.8	66	22.5	–
73709	Am	8070	3.78	2.3	10	26.7	–

2.2. The Blue Straggler HD 73666

The blue straggler HD 73666 is the hottest star of the cluster and is included in the "New Catalogue of Blue Stragglers in Open Clusters" by Ahumada, Lapasset (2007). This star was classified as normal A1V by Conti *et al.* (1965), as Ap (Si) star by Abt (1985) and as Am star by Andrievsky (1998).

HD 73666 does not show a Si overabundance and magnetic field, as it is for Ap (Si) stars or a Ca/Sc underabundance, as in Am stars. These results bring to the conclusion that HD 73666 is neither an Ap nor an Am star.

2.3. Am stars

The LSD analysis of the Am stars of our sample has not provided any longitudinal magnetic field detection. Our conclusion is that cool Am stars ($T_{\rm eff}$<8500 K) do not have magnetic field that could explain well–known phenomena associated to Am stars, like slow rotation.

The abundance analysis of HD 72942 shows that this star is a normal A–type star and not an Am star. Also membership and/or non-binarity are confirmed. For normal A–type stars and Am stars, the abundances of the Fe–peak elements are different. In normal A–type stars, Fe, Ni, and Cr are solar or slightly underabundant (compared to solar abundances). In Am stars, these elements are slightly overabundant. The Am stars show the characteristic Ca/Sc underabundance together with an underabundance of C, N and O. In all but one stars of our sample, Ba is overabundant, but Ba abundance is definitely lower in nor-

© Astronomical Institute of the Slovak Academy of Sciences • Provided by the NASA Astrophysics Data System

2008CoSka..38..123F

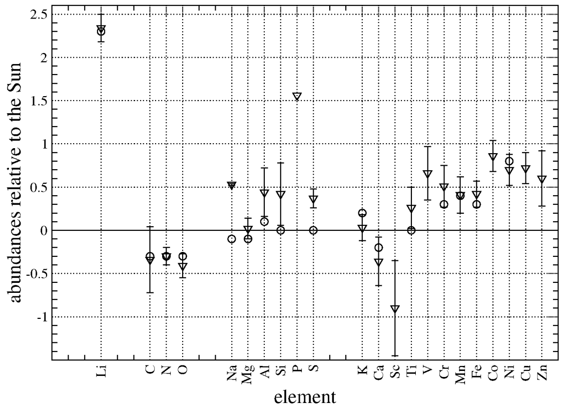

Figure 1. Comparison between the mean abundances of the Am stars of our sample (open triangles) and predicted abundances (open circles) by Richer *et al.* (2000). The derived abundances are relative to the Sun (Asplund *et al.*, 2005). The error bars are the standard deviation from the mean abundance.

mal A–type star than in Am stars. This suggests that Ba may be considered as a further indicator for Am peculiarities, together with C, N, O, Ca, Sc and Fe-peak elements.

3. Comparison with diffusion models

Underabundances of Sc and/or Ca and little overabundances of iron-group elements are qualitatively explained by diffusion theory (see, e.g., the review in the introduction by Alecian, 1996 and references therein).

The results of our abundance analysis can be used to constrain diffusion models. We can also compare our results with theoretical predictions. For the comparison we have calculated the mean abundances of the Am stars for the analysed elements till Zn and taken predicted abundances from Figure 14 of Richer *et al.* (2000). The comparison is shown in Fig. 1.

Fig. 1 shows an agreement for Li, C, N, O, Mg, Al, Si, Ca and Fe–peak elements within 0.1 dex. Discrepancies are apparent for Na and S (Sc was not modeled by Richer *et al.* (2000) because no OPAL data were available for Sc).

Na is the element for which the derived mean abundance ($\simeq 0.5$ dex with respect to the solar abundance) has the smallest scatter, among the Am stars of our sample. Observations seem definitely to suggest an overabundance of this element which is inconsistent with a model prediction of -0.1 dex.

Also S shows a small scatter in our sample ($\sigma = 0.11$ dex). Kamp *et al.* (2001) determined the S abundance in the metal poor A–type star λ Boo in LTE and non-LTE. Their analysis shows that the S abundance determined in

© Astronomical Institute of the Slovak Academy of Sciences • Provided by the NASA Astrophysics Data System

2008CoSka..38..123F

non-LTE is lower than the one determined in LTE by 0.1 dex. For metal poor stars non-LTE effects are larger than for normal A–type stars and Am stars. This brings our S abundance ($\simeq +0.35$ dex) to an overabundance (relative to the Sun) of $\geq$0.25 dex, compared with a solar abundance predicted by Richer *et al.*, (2000). This apparent discrepancy should be investigated in non-LTE regime.

Acknowledgements. We are deeply indebted to Tanya Ryabchikova for her close and accurate supervision of the abundance analysis. LF and OK have received support from the Austrian Science Foundation (FWF project P17890-N2). SK, JDL and GAW acknowledge support from the Natural Science and Engineering Council of Canada (NSERC). GAW acknowledges support from the Department of National Defense Academic Research Programme (DND-ARP).

References

Abt, H.A.: 1985, *Astrophys. J., Lett.* **294**, L103

Adelman, S.J., Caliskan, H., Kocer, D., Cay, I.H., Gokmen Tektunali, H.: 2000, *Mon. Not. R. Astron. Soc.* **316**, 514

Ahumada, J.A., Lapasset, E.: 2007, *Astron. Astrophys.* **463**, 789

Alecian, G.: 1996, *Astron. Astrophys.* **310**, 872

Andrievsky, S.M.: 1998, *Astron. Astrophys.* **334**, 139

Asplund, M., Grevesse, N., Sauval, A.J.: 2005, in *The Solar chemical composition*, eds.: T.G. Barnes III and F.N. Bash, ASP, San Francisco, 25

Bagnulo, S., Landstreet, J.D., Mason, E., Andretta, V., Silaj, J., Wade, G.A.: 2006, *Astron. Astrophys.* **450**, 777

Canuto, V.M., Mazzitelli, I.: 1992, *Astrophys. J.* **389**, 724

Conti, P.S., Wallerstein, G., Wing, R.F.: 1965, *Astrophys. J.* **142**, 999

Fossati, L., Bagnulo, S., Monier, R., Khan, S.A., Kochukhov, O., Landstreet, J., Wade, G., Weiss, W.: 2007, *Astron. Astrophys.* **476**, 911

González-Garcá, B.M., Zapatero Osorio, M.R., Béjar, V.J.S., Bihain, G., Barrado Y. Navascués, D., Caballero, J.A., Morales-Calderón, M.: 2006, *Astron. Astrophys.* **460**, 799

Hill, G.M., Landstreet, J.D.: 1993, *Astron. Astrophys.* **276**, 142

Kamp, I., Iliev, I.K., Paunzen, E., Pintado, O.I., Solano, E., Barzova, I.S.: 2001, *Astron. Astrophys.* **375**, 899

Kochukhov, O.: 2006, in *Physics of Magnetic stars*, eds.: I.I. Romanyuk and D.O. Kudryavtsev, SAO, Nizhnij Arkhyz, 109

Kupka, F., Piskunov, N.E., Ryabchikova, T.A., Stempels, H.C., Weiss, W.W.: 1999, *Astron. Astrophys., Suppl. Ser.* **138**, 119

Piskunov, N.E., Kupka, F., Ryabchikova, T.A., Weiss, W.W., Jeffery, C.S.: 1995, *Astron. Astrophys., Suppl. Ser.* **112**, 525

Richer, J., Michaud, G., Turcotte, S.: 2000, *Astrophys. J.* **529**, 338

Ryabchikova, T.A., Piskunov, N.E., Stempels, H.C., Kupka, F., Weiss, W.W.: 1999, *Phys. Scr.* **83**, 162

Shulyak, D., Tsymbal, V., Ryabchikova, T., Stütz, Ch., Weiss, W.W.: 2004, *Astron. Astrophys.* **428**, 993

© Astronomical Institute of the Slovak Academy of Sciences • Provided by the NASA Astrophysics Data System

A&A 483, 891–902 (2008)
DOI: 10.1051/0004-6361:200809467
© ESO 2008

Astronomy & Astrophysics

The effect of rotation on the abundances of the chemical elements of the A-type stars in the Praesepe cluster⋆,⋆⋆

L. Fossati[1], S. Bagnulo[2], J. Landstreet[3], G. Wade[4], O. Kochukhov[5], R. Monier[6], W. Weiss[1], and M. Gebran[7]

[1] Institut für Astronomie, Universität Wien, Türkenschanzstrasse 17, 1180 Wien, Austria
e-mail: [fossati;weiss]@astro.univie.ac.at
[2] Armagh Observatory, College Hill, Armagh BT61 9DG, Northern Ireland
e-mail: sba@arm.ac.uk
[3] Department of Physics & Astronomy, University of Western Ontario, London, N6A 3K7, Ontario, Canada
e-mail: jlandstr@astro.uwo.ca
[4] Physics Dept., Royal Military College of Canada, PO Box 17000, Station Forces, K7K 4B4, Kingston, Canada
e-mail: Gregg.Wade@rmc.ca
[5] Department of Physics and Astronomy, Uppsala University, 751 20, Uppsala, Sweden
e-mail: oleg@astro.uu.se
[6] Laboratoire Universitaire d'Astrophysique de Nice, Universite de Nice Sophia-Antipolis, Parc Valrose, 06000 Nice, France
e-mail: Richard.MONIER@unice.fr
[7] Groupe de Recherche en Astronomie et Astrophysique du Languedoc, UMR 5024, Université Montpellier II, Place Eugène Bataillon, 34095 Montpellier, France
e-mail: Marwan.Gebran@graal.univ-montp2.fr

Received 28 January 2008 / Accepted 21 March 2008

ABSTRACT

Aims. We study how chemical abundances of late B-, A-, and early F-type stars evolve with time, and we search for correlations between the abundance of chemical elements and other stellar parameters, such as effective temperature and $\upsilon \sin i$.

Methods. We observed a large number of B-, A-, and F-type stars belonging to open clusters of different ages. In this paper we concentrate on the Praesepe cluster ($\log t = 8.85$), for which we have obtained high-resolution, high signal-to-noise ratio spectra of sixteen normal A- and F-type stars and one Am star, using the SOPHIE spectrograph of the Observatoire de Haute-Provence. For all the observed stars, we derived fundamental parameters and chemical abundances. In addition, we discuss another eight Am stars belonging to the same cluster, for which the abundance analysis had been presented in a previous paper.

Results. We find a strong correlation between the peculiarity of Am stars and $\upsilon \sin i$. The abundance of the elements underabundant in Am stars increases with $\upsilon \sin i$, while it decreases for the overabundant elements. Chemical abundances of various elements appear correlated with the iron abundance.

Key words. stars: abundances – stars: atmospheres – stars: fundamental parameters – stars: chemically peculiar

1. Introduction

In stellar astrophysics, the study of the atmospheres of A- and B-type stars plays a very special role. The atmospheres of these stars display a variety of different phenomena, such as the presence of large and relatively simple magnetic fields, strong surface convection, pulsation, diffusion of chemical elements, and various kinds of mixing processes from small-scale turbulence to global circulation currents. These general physical processes are almost certainly active in the atmospheres (and interiors) of stars other than the main sequence A- and B-type stars, but in more subtle ways. Because of the easily visible effects found in A- and B-type stars, these stars provide unique access to the invisible interior processes. To fully understand the actual role of all these physical phenomena, it is very important to seek constraints from the observations, in particular to perform a detailed study of a large number of stars of different ages and peculiarity types.

For this project, it is very interesting to study stars that are cluster members, rather than selecting targets in the field, because of two very compelling reasons. First, we can assume that all cluster members have approximately the same original chemical composition and age. Therefore, when we analyse the chemical abundances of stars belonging to the same cluster, we can assume that we are studying objects that are different only by their initial mass, rotational velocity, magnetic field strength and binarity. Second, the age of stars belonging to open clusters can be determined with much higher accuracy than for objects in the field, especially for stars that are young enough that less than half of their life in the main sequence has elapsed (for a discussion of the star's age determination see Bagnulo et al. 2006). Therefore, we carried out two large observational campaigns. With FORS1 at the ESO VLT and with ESPaDOnS at the Canada-France-Hawaii Telescope (CHFT) we made a

⋆ Based on observations made at the Observatoire de Haute-Provence.
⋆⋆ Figures 13 to 16 are only available in electronic form at http://www.aanda.org

survey of magnetic A- and B-type stars in open clusters, to search for links between magnetic fields and stellar evolution. The results of this campaign are described by Bagnulo et al. (2006); Landstreet et al. (2007, 2008). In the framework of this observational campaign, we obtained also high-resolution spectroscopy of a large number of early-type stars in about ten open clusters of different ages. The clusters are approximately uniformly distributed in logarithmic age from $\log t = 6.8$ to $\log t = 8.9$, and the spectra have been obtained using five different spectrographs: FLAMES at the ESO VLT, FIES at the Nordic Optical Telescope (NOT), ELODIE and SOPHIE at the Observatoire de Haute-Provence (OHP), and ESPaDOnS at the CFHT.

In a previous paper (Fossati et al. 2007, hereafter referred to as Paper I), we started the analysis of the Praesepe cluster, presenting the observations and the results of the abundance analysis of eight Am and three normal A- and F-type stars. In this work we complete the study of the Praesepe cluster by presenting observations of 16 additional normal A- and early F-type stars, and an additional Am star. These new observations were obtained with the SOPHIE spectrograph at the Observatoire de Haute-Provence. Because of the large sample of analysed stars, we are able to make a sensitive search for correlations between the abundances of the chemical elements and other stellar parameters, such as the effective temperature $T_{\rm eff}$ and projected rotational velocity $\upsilon \sin i$.

This Paper is organised as follows. In Sect. 2 we describe the criteria that we adopted for target selection, which were used both for the entire observational campaign, and for the specific observations of the Praesepe cluster presented in this paper. Details about observations of the Praesepe cluster and data reduction are given in Sect. 3. In Sect. 4 we compare spectra of a reference star obtained with two different instruments that we used in our observational campaign: the SOPHIE spectrograph and the ESPaDOnS spectropolarimeter. In Sect. 5 we describe the procedure used to perform the abundance analysis, and we present the results obtained for the early-type stars of the Praesepe cluster observed with the SOPHIE spectrograph. In Sect. 6 we consider the abundances of chemical elements for the stars studied in Paper I and for the stars studied in this work. We search for correlations between chemical element abundances and effective temperature, $\upsilon \sin i$, $M/M_{\odot}$ and fractional age (τ – fraction of main sequence lifetime completed). In Sect. 7 we summarise our conclusions.

2. Target selection

For target selection in the overall programme, we assigned the highest priority to the most probable cluster members that were already known to be chemically peculiar (Am, Ap, HgMn stars) and/or to show slow rotation (typically $\upsilon \sin i < 50$ km s^{-1}). For this purpose we followed a standard procedure to select the stars to observe and to assign their priority.

The first step was to identify the most probable cluster members by checking the membership probabilities given by Robichon et al. (1999) and Baumgardt et al. (2000) obtained from HIPPARCOS data, by Kharchenko et al. (2004) and by Dias et al. (2006). We considered as probable members of the cluster every star with a kinematic and photometric membership probability higher than 0.14 (Kharchenko, private communication) in the case of the Kharchenko et al. (2004) catalogue, or a membership probability higher than 10% for the Dias et al. (2006) catalogue.

We searched then for information about the spectral type, magnitude, $\upsilon \sin i$, binarity, variability, chemical peculiarities, magnetic field and radial velocity for each star considered a probable member of the cluster. We collected information from SIMBAD[1] (scanning also the different references mentioned therein), VIZIER[2] (using a combination of several keywords – binaries:cataclysmic, binaries:eclipsing, binaries:spectroscopic, multiple_stars, open_clusters, positional_data, proper_motions, rotational_velocities, spectral_classification, spectrophotometry, spectroscopy, stars:early-type, stars:late-type, stars:peculiar, stars:variable – in a range of 10 arcsec around the position of each star) and the WEBDA[3] database (Mermilliod & Paunzen 2003). We looked also for additional information about each star in articles by Glebocki & Stawikowski (2000) and Royer et al. (2002) for $\upsilon \sin i$ measurements, Rodríguez et al. (2000) for δSct pulsations, the SB9 catalogue (Pourbaix et al. 2004) for information about a possible binarity and Renson et al. (1991) for chemical peculiarities.

We searched then for archival high resolution spectra in several archives (e.g. the ESO archive[4] and the ELODIE archive[5]), in order to avoid a duplication of observational effort, in case some stars had already been observed with high resolution spectroscopy. Almost no pre-existing spectra were found.

Of the sample obtained with this procedure, we kept only the stars with spectral types between F5 (to avoid too long an exposure time on a single object) and B5 (to avoid strong stellar winds), giving a higher rank to peculiar stars and slow rotators. From the sample we removed stars already known to be SB2 systems, unless they had already been extensively observed using high-resolution spectroscopy.

3. Observations and data reduction

We observed seventeen stars of the Praesepe cluster using the SOPHIE spectrograph at the Observatoire de Haute-Provence (OHP) during two runs, from December 1st to 2nd 2006 and from March 10th to 12th 2007.

SOPHIE is a cross-dispersed échelle spectrograph mounted at the 1.93-m telescope at the OHP. The spectrograph is fed from the Cassegrain focus through a pair of optical fibers, one of which is used for starlight and the other can be used for either the sky background or the wavelength calibration lamp, but can also be masked. The spectra cover the wavelength range 3872–6943 Å. The instrument allows observations either with medium spectral resolution ($R \sim 40\,000$) or with high spectral resolution ($R \sim 75\,000$). Since for most of the stars of our sample no precise $\upsilon \sin i$ measurements were available, we decided to observe all of them in high resolution mode.

The spectra were automatically reduced using the SOPHIE pipeline, adapted from the HARPS software designed by Geneva Observatory. A detailed description of the pipeline is available on the SOPHIE web page[6].

From our spectra we found that almost all of the stars have high rotational velocity ($\upsilon \sin i \geq 30$ km s^{-1}). For these objects the continuum normalisation is a critical reduction procedure that cannot be performed with an automatic fitting procedure. We therefore rectified the continua of these stars manually. Even

[1] http://simbad.u-strasbg.fr/simbad/sim-fid
[2] http://vizier.u-strasbg.fr/viz-bin/VizieR
[3] http://www.univie.ac.at/webda/
[4] http://archive.eso.org/
[5] http://atlas.obs-hp.fr/elodie/
[6] http://www.obs-hp.fr/www/guide/sophie/sophie-eng.html

Table 1. Basic data of the observations for the analysed stars.

HD	HJD	M_v	Spectral type	SNR	Exp. time	Remarks
72757	2454172.336	8.45	F0	190	3600	
72846	2454070.737	7.48	A5V	210	3600	
73175	2454171.406	8.25	F0Vn	155	3600	δSct
73345	2454171.363	8.14	A7V	188	3600	δSct
73450	2454171.494	8.59	A9V	185	3600	δSct
73574	2454171.585	7.75	A8V	170	3600	
73666	2454070.682	6.61	A1V	326	1800	speckle binary
73746	2454172.514	8.72	F0V	154	3600	δSct
73798	2454172.424	8.48	F0V	190	3600	δSct
73993	2454171.450	8.56	F2V	134	3600	variable
74028	2454171.318	7.97	A7V	185	3600	δSct
74050	2454170.566	7.91	A6Vn	160	3600	δSct
74135	2454172.559	8.88	F0	120	3600	
74587	2454172.468	8.51	A5	177	3600	
74589	2454172.379	8.46	F0	200	3600	
74656	2454170.537	8.04	Am	226	2 × 3600	sum of two exposures
74718	2454171.538	8.39	A5	172	3600	

The SNR are calculated at ~5500 Å in a bin of 0.5 Å. The exposure time is in seconds. The HJD indicate the Heliocentric Julian Date at the middle of the exposure.

with manual rectification, it was not possible to determine a correct continuum level shortwards of the Hγ line (4340.462 Å), since there were not enough continuum windows in the spectra, due to the crowding of spectral lines when $\upsilon \sin i$ is high.

It is well known how important it is to reach a high signal-to-noise ratio (SNR) to be able to carry out an abundance analysis of rapidly rotating stars (Hill & Landstreet 1993). For two stars (HD 73798 and HD 73993) the SNR was too low, so we re-binned the spectra to increase the SNR, at the expense of spectral resolution.

The complete sample of stars observed and analysed in this paper is listed in Table 1. In the sample, one object is an Am star, while the others are normal stars with spectral types between F2 and A1. Seven stars of our sample are present in the δSct variable star catalog of Rodríguez et al. (2000). One star (HD 73993) is present in the Combined General Catalogue of Variable Stars (Samus & Durlevich 2004), but the variability type is listed as "unknown". HD 73666 is the only known binary star present in our sample, as we removed all SB2 stars from the selected target stars, as explained in Sect. 2.

4. SOPHIE vs. ESPaDOnS

The observational material employed in this large project has been obtained with different instruments at different telescopes. Since the homogeneity of the analysis is of crucial importance, in this section we compare spectra of a reference star obtained with two different spectrographs to demonstrate the homogeneity of our data.

HD 73666 was previously analysed in Paper I. The star was also used as reference star by Ryabchikova et al. (2008). Here we compare the spectra of HD 73666 obtained with ESPaDOnS (analysed in Paper I) and with SOPHIE. ESPaDOnS was mounted at the Canada-France-Hawaii Telescope (CFHT) in 2005 and SOPHIE at the Observatoire de Haute-Provence (OHP) in 2006. The two instruments have similar mean resolving power, 65 000 and 75 000 respectively. ESPaDOnS is also adapted for spectropolarimetric observations, while SOPHIE for radial velocity observations. Here we compare the spectra of the reference star obtained with the two instruments.

In Figs. 13 and 14 (available online) we show a direct comparison between the ESPaDOnS and SOPHIE spectra for HD 73666 around the He multiplet at ~4471.5 Å and the strong Fe II line at 5018.440 Å respectively. No significant differences are present apart from those due to the small difference of spectral resolution, visible mainly in the cores of the strong lines.

HD 73666 was first detected as a binary star with speckle interferometry by Hartkopf & McAlister (1984), and was observed and analysed further by McAlister et al. (1987). Mason et al. (1993), who collected all available interferometric measurements and concluded that HD 73666 "shows little orbital motion". Radial velocity measurements are reported by Abt (1970), Conti et al. (1974), Abt & Willmarth (1999) and Madsen et al. (2002). All these authors give radial velocities compatible with the cluster mean of 34.5 ± 0.0 km s^{-1} (Robichon et al. 1999). The spectra plotted in Figs. 13 and 14 have been corrected only for the terrestrial radial velocity; nevertheless, no radial velocity difference is visible from the comparison of the two spectra, in agreement with results from previous authors.

5. Model atmosphere and abundance analysis

Model atmospheres were calculated with the LTE code LLMODELS, which uses direct sampling of the line opacities (Shulyak et al. 2004) and makes it possible to compute model atmospheres with an individualised abundance pattern. We adopted the VALD database (Piskunov et al. 1995; Kupka et al. 1999; Ryabchikova et al. 1999) as the source of spectral line data, including lines originating from predicted levels. We carried out a preselection procedure to eliminate all lines that do not contribute significantly to the line opacity. This was done by requiring that the line-to-continuum opacity ratio at the centre of each included line be greater then 0.05%. Convection was treated according to the CM approach (Canuto & Mazzitelli 1992).

The initial values of the fundamental atmospheric parameters ($T_{\rm eff}$ and $\log g$) were derived from Strömgren (Hauck & Mermilliod 1998) and Geneva (Mermilliod & Paunzen 2003) photometry, using calibrations from Napiwotzki et al. (1993) and Kunzli et al. (1997) respectively.

Table 2. Atmospheric parameters for the analysed stars of the Praesepe cluster.

HD	Strömgren photometry $T_{\rm eff}$ [K]	log g [cgs]	Geneva photometry $T_{\rm eff}$ [K]	log g [cgs]	Final set $T_{\rm eff}$ [K]	log g [cgs]	$\upsilon_{\rm mic}$ [km s^{-1}]	$\upsilon \sin i$ [km s^{-1}]	$\sigma_{\upsilon \sin i}$ [km s^{-1}]	$\upsilon_{\rm r}$ [km s^{-1}]	$\sigma_{\upsilon_{\rm r}}$ [km s^{-1}]
72757	7330	3.81			7400	3.60	2.7	179	10	35.8	7.0
72846	8187	3.85	8146	4.12	8045	3.50	2.5	119	6	35.1	7.3
73175	7735	3.94	7506	4.22	7660	3.94	2.6	163	9	36.7	5.7
73345	7779	3.92	7865	4.43	7993	3.96	2.6	85	4	34.5	4.4
73450	7271	3.77	7455	4.26	7270	4.20	2.7	138	7	34.5	5.1
73574	7659	3.90	7733	4.36	7662	4.00	2.6	102	4	35.3	4.5
73746	7390	4.01	7236	4.16	7440	4.08	2.7	95	4	34.2	3.6
73798	7355	3.80	7301	4.11	7328	3.95	2.7	200	11	34.1	5.9
73993	7124	3.74	7153	4.11	7138	3.92	2.8	240	14	33.6	7.5
74028	7517	3.65	7772	4.34	7750	4.50	2.6	150	9	35.3	7.4
74050	7767	3.78	7722	4.19	7872	3.66	2.6	188	8	36.0	7.8
74135			7016	4.22	7400	4.00	2.7	100	4	32.5	5.7
74587			7246	4.15	7500	4.20	2.7	90	4	33.9	4.1
74589	7581	4.04			7550	4.03	2.7	127	5	34.1	4.7
74656			7517	4.11	7800	3.99	3.6	25	1	34.1	1.3
74718	7599	3.99	7453	4.21	7600	4.00	2.7	155	7	34.1	5.7

Columns two to five show the fundamental parameters derived from Strömgren and Geneva photometry. The sixth and seventh columns show the final adopted parameters derived from spectroscopy.

The adopted $T_{\rm eff}$ and log g were derived spectroscopically, as explained in detail in Paper I. We almost always used Fe lines for this purpose, as the generally high $\upsilon \sin i$ of the analysed stars did not provide a suitable number and variety of lines of other elements. The microturbulent velocity ($\upsilon_{\rm mic}$) was determined spectroscopically, from Fe and Ti II lines, for HD 74656 only; this was possible because of its low $\upsilon \sin i$. For all other stars we adopted $\upsilon_{\rm mic}$ computed from the relation (Pace et al. 2006):

$$\upsilon_{\rm mic} = -4.7 \log(T_{\rm eff}) + 20.9 \text{ km s}^{-1}. \quad (1)$$

There is no significant difference between adopting the $\upsilon_{\rm mic}$ given by Eq. (1) and assuming a fixed value of 2.7 km s^{-1}. We notice that $\upsilon_{\rm mic}$ obtained for the Am star HD 74656 is significantly larger than 2.7 km s^{-1}. Whether this is also the case for other stars of the sample cannot be tested with the available data.

Radial velocity ($\upsilon_{\rm r}$) and $\upsilon \sin i$, in km s^{-1}, were determined by computing the median of the results obtained by synthetic fitting of several individual lines in the observed spectrum. We derived error bars for these quantities for each analysed star using the standard deviation of the derived values. The error bar associated with $\upsilon_{\rm r}$ is strongly dependent on $\upsilon \sin i$, ranging from about 1 km s^{-1} for slow rotators, up to about 8 km s^{-1} for the fast rotators. The error bars in $\upsilon \sin i$ are about 5% or 3 km s^{-1}, whichever is larger.

Table 2 reports the fundamental parameters obtained for each star of the sample from photometry and spectroscopy. The parameters adopted for abundance analysis are those obtained from spectroscopy.

We tested the fundamental parameters adopted for the abundance analysis with spectrophotometry from Clampitt & Burstein (1997) for 5 stars of the sample. We used Atlas9 models and the fundamental parameters adopted for the abundance analysis to compute the fluxes for comparison with the spectrophotometry. The fluxes were normalised to the flux at 5560 Å. An example of the comparison is shown in Fig. 1. We found good agreement, within the error bars of the fundamental parameters, for all the stars for which spectrophotometry was available.

The synthetic line spectrum was produced with the synthesis code Synth3 (Kochukhov 2006). In each spectrum we fit the cores of selected lines of each ion to obtain a value of the abundance associated with each line. The adopted abundance of that ion is then defined to be the mean of the abundances obtained from the selected lines. The error bars associated with the mean abundances are the standard deviations, and they do not include uncertainties in fundamental parameters (see below). The abundances and their standard error bars are given in Table 3.

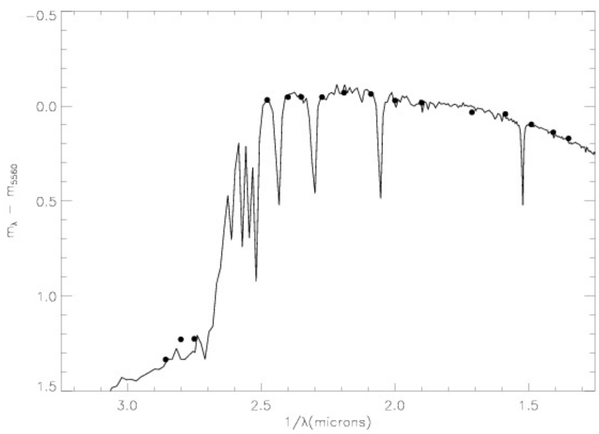

Fig. 1. Comparison between spectrophotometry from Clampitt & Burstein (1997) and normalised fluxes at 5560 Å with the fundamental parameters adopted for the abundance analysis of the star HD 73345.

The line data required for our analysis were extracted from the VALD database. Line parameters of the lines selected for the fundamental parameter derivation and abundance analysis were checked by synthesising these lines in the solar spectrum taken from the National Solar Observatory Atlas[7]. The lines for which we found a discrepancy between the observed and synthesised solar spectrum were rejected.

The typical number of lines selected for the analysis varied according to the rotational velocity of the analysed star. The Fe abundance was always determined on the basis of the largest number of lines, in comparison with other elements. The number of lines used to derive the abundance of each element is given in

[7] http://www.coseti.org/natsolar.htm

Table 3. Abundances ($\log(N_X/N_{tot})$) of the observed stars.

					"Normal" A−type stars					Solar
At.N.	Element	HD 72846	HD 73345	HD 73450	HD 73574	HD 74028	HD 74050	HD 74587	HD 74718	abundances
3	Li	<−8.08(−; 1)	<−8.33(−; 1)	<−8.70(−; 1)	<−8.38(−; 1)			<−8.41(−; 1)	<−8.26(−; 1)	−10.99
6	C	−3.58(−; 1)	−3.44(12; 3)	−3.27(−; 1)	−3.36(18; 2)	−3.39(08; 2)	−3.52(−; 1)	−3.49(01; 2)	−3.51(04; 2)	−3.65
8	O	−3.18(−; 1)	−3.22(01; 2)				−3.70(−; 1)	−3.30(−; 1)		−3.38
11	Na	−5.44(01; 2)	−5.37(01; 2)	−6.28(−; 1)	−5.57(02; 2)	−5.98(−; 1)	−5.64(13; 2)	−5.61(02; 2)	−5.70(14; 2)	−5.87
12	Mg	−4.18(08; 3)	−4.18(02; 3)	−5.02(18; 2)	−4.37(04; 3)	−4.86(08; 3)	−4.22(05; 4)	−4.56(08; 3)	−4.52(01; 2)	−4.51
14	Si	−4.62(16; 2)	−4.67(−; 1)	−4.13(−; 1)	−4.19(−; 1)	−4.17(−; 1)	−4.37(−; 1)	−4.16(−; 1)	−4.25(−; 1)	−4.53
16	S	−4.71(04; 2)	−4.44(03; 4)	−4.35(−; 1)	−4.61(02; 2)	−4.26(01; 2)		−4.50(04; 2)	−4.28(11; 2)	−4.90
20	Ca	−5.17(−; 1)	−5.39(09; 6)	−5.95(06; 4)	−5.86(16; 5)	−5.37(16; 2)	−6.13(06; 2)	−5.49(15; 6)	−5.68(02; 3)	−5.73
21	Sc	−8.88(−; 1)	−8.63(07; 3)	−8.57(14; 3)	−8.89(02; 3)	−8.35(−; 1)	−8.96(27; 3)	−8.56(−; 1)	−8.69(14; 2)	−8.99
22	Ti	−6.88(03; 5)	−6.95(06; 6)	−7.30(11; 5)	−6.98(09; 5)	−6.78(−; 1)	−7.08(15; 5)	−6.83(16; 3)	−6.93(10; 5)	−7.14
24	Cr	−6.23(06; 3)	−6.22(08; 2)	−6.56(08; 3)	−6.19(16; 3)	−6.23(12; 4)	−6.48(10; 3)	−6.05(13; 4)	−6.44(20; 5)	−6.40
25	Mn		−6.37(−; 1)	−6.88(−; 1)	−6.52(02; 2)	−6.77(−; 1)	−6.61(−; 1)	−6.62(04; 2)	−6.71(−; 1)	−6.65
26	Fe	−4.55(18; 42)	−4.33(11; 61)	−4.62(09; 15)	−4.49(10; 30)	−4.50(09; 18)	−4.44(13; 16)	−4.28(10; 33)	−4.61(11; 26)	−4.59
28	Ni	−5.70(18; 2)	−5.58(11; 4)	−5.82(16; 2)	−5.62(08; 4)	−5.93(14; 3)	−5.60(15; 3)	−5.84(−; 1)	−5.68(02; 3)	−5.81
39	Y	−9.75(−; 1)	−9.46(−; 1)	−9.83(−; 1)	−9.20(−; 1)	−9.56(−; 1)	−9.26(−; 1)	−9.13(−; 1)	−9.10(−; 1)	−9.83
56	Ba	−9.48(−; 1)	−9.30(06; 2)	−9.50(02; 2)	−8.98(04; 2)	−9.65(−; 1)	−9.52(01; 2)	−8.96(25; 2)	−9.15(−; 1)	−9.87
	T_{eff}	8045	7993	7270	7662	7750	7872	7500	7600	
	$\log g$	3.50	3.96	4.20	4.00	4.50	3.66	4.20	4.00	
	υ_{mic}	2.5	2.6	2.7	2.6	2.6	2.6	2.7	2.7	
	$\upsilon \sin i$	119	85	138	102	150	188	90	155	
					F−type stars				Am star	Solar
At.N.	Element	HD 72757	HD 73175	HD 73746	HD 73798	HD 73993	HD 74135	HD 74589	HD 74656	abundances
3	Li			<−8.70(−; 1)			<−8.47(−; 1)	<−8.35(−; 1)	−8.61(−; 1)	−10.99
6	C	−3.71(16; 2)	−3.36(01; 2)	−3.39(−; 1)			−3.30(14; 2)	−3.19(18; 2)	−4.09(−; 1)	−3.65
7	N								−3.98(−; 1)	−4.26
8	O			−3.30(−; 1)			−3.40(−; 1)	−3.36(−; 1)	−3.88(−; 1)	−3.38
11	Na	−5.61(−; 1)	−5.81(01; 2)	−5.45(13; 2)			−5.73(24; 2)	−5.73(07; 2)	−5.35(01; 2)	−5.87
12	Mg	−4.56(14; 2)	−4.38(07; 2)	−4.50(11; 5)	−4.76(23; 2)	−4.57(−; 1)	−4.14(09; 2)	−4.25(02; 2)	−4.73(11; 3)	−4.51
13	Al								−5.15(−; 1)	−5.67
14	Si	−4.23(06; 3)	−4.39(−; 1)	−4.29(−; 1)	−4.09(−; 1)	−4.34(−; 1)	−4.14(−; 1)	−4.20(−; 1)	−4.37(−; 1)	−4.53
16	S	−4.62(01; 2)	−4.55(−; 1)	−4.54(05; 5)			−4.62(05; 2)	−4.44(07; 2)	−4.52(04; 5)	−4.90
20	Ca	−5.60(11; 6)	−5.41(03; 3)	−5.68(16; 8)	−5.38(15; 5)	−5.65(−; 1)	−5.45(14; 4)	−5.53(05; 7)	−6.34(13; 3)	−5.73
21	Sc	−9.07(−; 1)	−8.66(−; 1)	−8.98(10; 3)	−9.20(−; 1)	−8.90(−; 1)	−8.48(15; 4)	−8.43(25; 3)	−9.27(−; 1)	−8.99
22	Ti	−7.03(16; 5)	−6.90(15; 3)	−6.68(13; 3)	−6.90(−; 1)	−7.18(−; 1)	−7.03(09; 6)	−6.92(11; 7)	−6.90(16; 18)	−7.14
23	V								−7.06(−; 1)	−8.04
24	Cr	−6.72(08; 3)	−6.55(01; 2)	−6.20(23; 6)	−6.64(36; 4)		−6.16(12; 3)	−6.26(20; 4)	−5.72(10; 11)	−6.40
25	Mn	−6.92(−; 1)	−6.98(08; 2)	−6.46(01; 2)	−6.36(−; 1)		−6.42(11; 3)		−6.27(11; 5)	−6.65
26	Fe	−4.50(08; 31)	−4.52(08; 14)	−4.46(08; 49)	−4.47(06; 17)	−4.47(08; 6)	−4.45(11; 60)	−4.51(11; 53)	−4.11(13; 74)	−4.59
27	Co								−5.38(−; 1)	−7.12
28	Ni	−5.57(−; 1)	−5.68(05; 3)	−5.38(12; 5)	−6.20(07; 2)	−6.15(−; 1)	−5.53(10; 4)	−5.90(17; 4)	−5.00(08; 15)	−5.81
29	Cu								−6.92(−; 1)	−7.83
30	Zn								−6.77(−; 1)	−7.44
38	Sr								−8.23(−; 1)	−9.12
39	Y	−10.07(−; 1)	−9.39(−; 1)	−9.35(01; 2)	−9.20(−; 1)		−9.46(−; 1)	−8.99(−; 1)	−8.92(11; 3)	−9.83
40	Zr								−8.62(−; 1)	−9.45
56	Ba	−9.12(06; 2)	−9.64(−; 1)	−9.02(12; 2)	−8.78(−; 1)	−9.48(−; 1)	−9.10(−; 1)	−9.14(−; 1)	−8.46(23; 3)	−9.87
57	La								−9.22(14; 3)	−10.91
58	Ce								−9.11(08; 3)	−10.46
60	Nd								−9.27(13; 5)	−10.59
62	Sm								−9.89(−; 1)	−11.03
63	Eu								−9.89(−; 1)	−11.52
68	Er								−9.53(−; 1)	−11.11
70	Yb								−9.46(−; 1)	−10.96
	T_{eff}	7400	7660	7440	7328	7138	7400	7550	7800	
	$\log g$	3.60	3.94	4.08	3.95	3.92	4.00	4.03	3.99	
	υ_{mic}	2.7	2.6	2.7	2.7	2.8	2.7	2.7	3.6	
	$\upsilon \sin i$	179	163	95	200	240	100	127	25	

The estimated internal error (in parenthesis) is in units of 0.01 dex. The internal error associated with the derived abundance of each element is the standard deviation from the mean abundance of the selected lines of that element. For comparison, the solar abundances (Asplund et al. 2005) are given in the last column. At.N. gives the Atomic Numbers of the elements. Abundances obtained from just one line have no error (−; 1). Upper limits are denoted by <. The second number in the brackets is the number of lines used to derive the mean abundance.

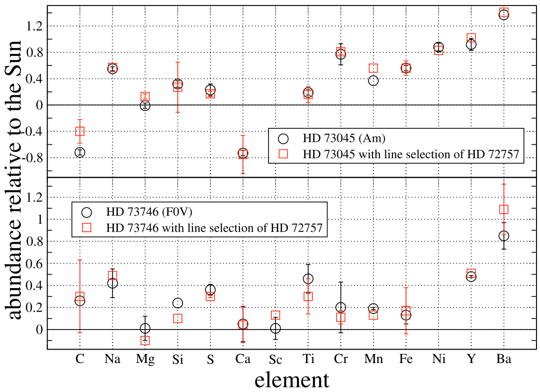

Fig. 2. Comparison between the abundances derived for HD 73045 ($\upsilon \sin i$ = 10 km s^{-1} – open circles in *the upper panel*) and HD 73746 ($\upsilon \sin i$ = 95 km s^{-1} – open circles in *the lower panel*) adopting a proper line selection and the lines used to determine the abundances of HD 72757 ($\upsilon \sin i$ = 179 km s^{-1} – open squares in both panels).

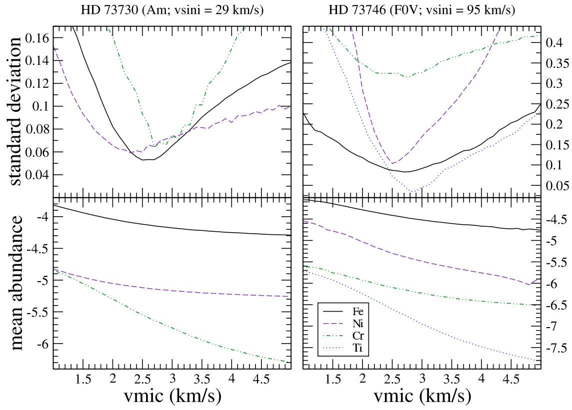

Fig. 3. *The upper panels* show the variation of the standard deviation from the mean abundance of Fe, Ni, Cr and Ti as a function of $\upsilon_{\rm mic}$, for HD 73730 ($\upsilon \sin i$ = 29 km s^{-1}) and HD 73746 ($\upsilon \sin i$ = 95 km s^{-1}). *The lower panels* show the variation of the mean abundance as a function of $\upsilon_{\rm mic}$.

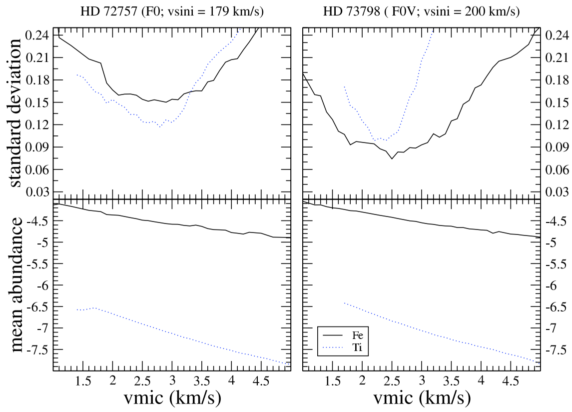

Fig. 4. As for Fig. 3, but for HD 72757 ($\upsilon \sin i$ = 179 km s^{-1}) and HD 73798 ($\upsilon \sin i$ = 200 km s^{-1}).

Table 3, following the (internal) standard deviation associated with each measured abundance.

For all the elements that were not analysed we adopted the solar abundance from Asplund et al. (2005). (This fact enters into the model atmosphere computaion, and in the normalisation of the results expressed according to the total number of nuclei per unit volume $N_{\rm tot}$.)

The high $\upsilon \sin i$ of some of the analysed stars resulted in a different and smaller selection of lines compared to the line list employed for slower rotators. We checked if this is a source of systematic error by performing the abundance analysis of HD 73045 ($\upsilon \sin i$ = 10 km s^{-1} – analysed in Paper I) and HD 73746 ($\upsilon \sin i$ = 95 km s^{-1}) adopting the line list used for HD 72757 ($\upsilon \sin i$ = 179 km s^{-1}). The results of this test, illustrated in Fig. 2, show that no systematic errors are introduced by the difference in selected lines.

The high rotational velocity of many of the analysed stars results in a line list dominated by strong and saturated lines. These lines are more sensitive to $\upsilon_{\rm mic}$ variations than shallow lines. For this reason the uncertainties of the adopted $\upsilon_{\rm mic}$, $T_{\rm eff}$, and $\log g$ values need to be considered to obtain a realistic estimate of the error bars associated with the derived element abundances.

In Paper I we have shown the results of two tests performed on slowly rotating stars. They show i) how the standard deviation from the mean Fe abundance changes for $\upsilon_{\rm mic}$ = 0, 1, 2, ..., 6 km s^{-1}, adopting fundamental parameters derived from photometry and spectroscopy and ii) the uncertainties introduced in the abundances of Fe, Ti and Ni by varying effective temperature and $\log g$ by ±200 K and ±0.2 dex respectively. Our tests show that the spectroscopic parameters are comparable or better than the photometric parameters. Furthermore, the tests show a variation of less than 0.2 dex in abundance due to the temperature variation. No significant abundance change was found varying when $\log g$. However, the $\upsilon_{\rm mic}$ value and its associated uncertainty increase their importance for rapidly rotating stars, and for this reason we performed the following additional test. For four stars with different $\upsilon \sin i$ values (HD 73730, $\upsilon \sin i$ = 29 km s^{-1} – HD 73746, $\upsilon \sin i$ = 95 km s^{-1}– HD 72757, $\upsilon \sin i$ = 179 km s^{-1} – HD 73798, $\upsilon \sin i$ = 200 km s^{-1}) we performed the abundance analysis of selected Fe, Ni, Cr and Ti lines for assumed $\upsilon_{\rm mic}$ varying from 1 to 5 km s^{-1} in steps of 0.1 km s^{-1}. We plotted then in Figs. 3 and 4 the variation of the standard deviation from the mean abundance (upper panel) and the mean abundance itself (lower panel) as a function of $\upsilon_{\rm mic}$.

Figures 3 and 4 show that the adopted $\upsilon_{\rm mic}$ value (2.7 km s^{-1} for all the stars taken into account in this test) obtained with Eq. (1) is reasonable at every rotational velocity. The only exception is for the Am stars, for which slightly larger values of $\upsilon_{\rm mic}$ are obtained for those stars for which this quantity is directly derived. Taking into account the different best $\upsilon_{\rm mic}$ values obtained from different elements, and the dispersion of the standard deviation as a function of $\upsilon_{\rm mic}$, the uncertainty that we assign to $\upsilon_{\rm mic}$, for the rapid rotators, is 0.7 km s^{-1}. The lower panels of Figs. 3 and 4 allow us to derive directly the abundance uncertainty given the uncertainty of $\upsilon_{\rm mic}$ for each element. We used Fe as a standard element to derive the abundance standard error, since it is the element with the highest number of selected lines. An error bar of 0.7 km s^{-1} in $\upsilon_{\rm mic}$ produces an uncertainty of element abundance increasing from 0.1 dex for the slow rotators, to 0.2 dex for the rapid rotators. The error bar on the element abundance is dominated by the uncertainty of $T_{\rm eff}$ for the slow rotators, while the uncertainty in $\upsilon_{\rm mic}$ becomes increasingly important for larger $\upsilon \sin i$. Assuming that $T_{\rm eff}$ and $\upsilon_{\rm mic}$ are completely uncorrelated, the resultant abundance error bar for the rapidly rotating stars is given by standard error propagation theory, which leads to an uncertainty of about 0.3 dex. In conformity with this analysis, we assume an abundance error bar increasing linearly with $\upsilon \sin i$ from 0.2 dex to 0.3 dex at a $\upsilon \sin i$ value of 200 km s^{-1}.

Another source of uncertainty that is dependent on $\upsilon \sin i$ is due to the continuum normalisation. To quantify this uncertainty we performed the following test. We derived the abundance of the Fe II line at 5325.6 Å for HD 73746 ($\upsilon \sin i$ = 95 km s^{-1}), HD 72757 ($\upsilon \sin i$ = 179 km s^{-1}) and HD 73798 ($\upsilon \sin i$ = 200 km s^{-1}) with the adopted normalised observed spectrum and with the spectrum multiplied/divided by 0.99. In this way we increased/decreased the continuum level of 1%, that we estimate to be a reasonable uncertainty. The difference between the abundances obtained in this way is increasing with $\upsilon \sin i$ from about 0.1 dex for HD 73746, to about 0.2 dex for the two faster rotators. We believe that in most cases this error bar is an upper limit since the line by line abundance analysis method, used in this work, allows a very careful line selection that rejects all the lines for which the continuum level looks uncertain. Under the assumption of no systematic errors in the continuum normalisation, this uncertainty is decreasing with an increase of the number of selected lines. If for some lines the continuum level is too low, for some others it would be too high, leading to an increase of the dispersion, but not to an abundance variation.

An example of the spectrum of a rapidly rotating star and the synthetic spectrum obtained after the complete abundance analysis is shown in Fig. 16 (available online).

For all the rapid rotators in our sample, we were able to obtain only an upper limit on the abundance of Li, because the high $\upsilon \sin i$ values did not allow us to detect the Li line. Only the Li abundance of HD 74656 may be considered as a real estimate, although even this value is uncertain because it was derived only from one blended line.

We confirm the membership in Praesepe of all the stars of our sample, because the υ_r measurements are all compatible with the cluster mean of 34.5 ± 0.0 km s^{-1} (Robichon et al. 1999). For none of the analysed stars we found any evidence of binarity. These considerations confirm the quality of our target selection (which were selected for membership and non-binarity).

We confirm the Am classification of HD 74656. In Fig. 15 (available online) the mean abundances for the Am stars analysed in Paper I are compared with the abundances obtained for HD 74656. The comparison shows a good agreement between the two abundance patterns.

6. Discussion

In this section we discuss the results obtained considering both samples of stars: those analysed in this work, and those from Paper I. In the sample of stars from Paper I, we did not includ results for HD 73666 (Blue Straggler), HD 72942 (probable non-member) and HD 73174, for which the derived $T_{\rm eff}$ from Strömgren photometry and from spectroscopy differ by about 700 K and no explanation was found in Paper I. For this reason we decided not to consider this object in our final analysis of the cluster.

6.1. Abundances of the A- and F-type stars of the Praesepe cluster

The stars were first grouped according to their classifications as F, A and Am stars; Fig. 5 shows the mean abundances for each group. The error bars in Fig. 5 are the standard deviations from the calculated mean abundances of each group.

The A- and F-type stars show similar abundance patterns, characterised by solar abundances for almost all the elements. The Am stars show the typical abundance pattern characterised

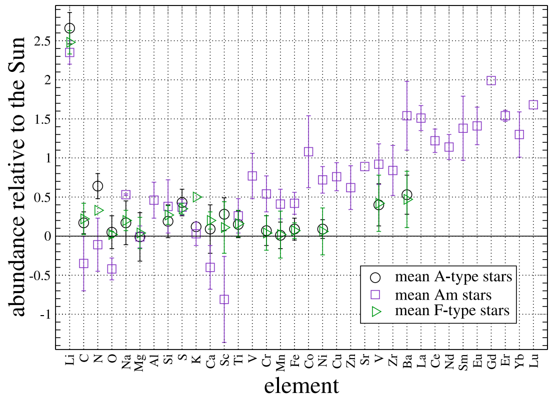

Fig. 5. Comparison between the mean abundances obtained for Am, A- and F-type stars indicated by an open circle, square and triangle respectively. The error bars are the standard deviations from the calculated mean abundances. In the case of only one measurement, no error bar is shown. A- and F-type stars show a similar abundance pattern. The Am stars show the typical peculiar abundance pattern described in detail in Paper I.

by underabundances of C, N, O, Ca and Sc, with a general overabundance of the other elements. As expected, the error bars associated with the abundances of the F-type stars turn out to be comparable to or smaller than those for the A-type stars. It is also possible to see this effect in figures from 7 to 9.

We calculated the metallicity of the cluster (Z) from the abundances derived for the F-type stars, excluding HD 73575. This star is close to the TAMS and its Fe abundance differs by 0.27 dex with respect to the mean Fe abundance (0.11 ± 0.03 dex) of the other F-type stars. For this reason we omitted HD 73575 from the determination of the cluster metallicity. The Z value we obtain is 0.015 ± 0.002 dex.

The Z value adopted by several other authors and used to characteris isochrones (see Sect. 6.2) is calculated with the following approximation:

$$Z_{\rm cluster} \simeq 10^{([{\rm Fe/H}]_{\rm Fstars} - [{\rm Fe/H}]_{\odot})} \cdot Z_{\odot}, \quad (2)$$

assuming $Z_{\odot}$ = 0.019 dex. We recalculated the Z of the cluster according to this approximation obtaining Z = 0.024 ± 0.02. We derived this value using the mean Fe abundance of all the F-type stars except HD 73575 ([Fe/H] = 0.11 ± 0.03 dex).

Our estimated metallicity is in agreement with that included in the catalogue of Chen et al. (2003) of [Fe/H] = 0.14 dex and with that recently obtained by An et al. (2007) of [Fe/H] = 0.11 ± 0.03 dex. An et al. (2007) derived the metallicity from an Fe abundance determination from high resolution spectra of four G-type cluster members.

6.2. HR diagram

Using the spectroscopic temperatures determined to perform the abundance analysis we built the Hertzsprung-Russell (HR) diagram of the cluster around the turn-off point (Fig. 6). We calculated the luminosity of each star photometrically, adopting the magnitudes in V band given by SIMBAD and a cluster distance modulus of 6.30 ± 0.07 mag (van Leeuwen 2007). We used a reddening of 0.009 mag (WEBDA) and the bolometric correction given by Balona (1994). Luminosities are listed in Table 4. With a distance modulus uncertainty of 0.07 mag, an uncertainty in the bolometric correction of about 0.07 mag, and a reddening uncertainty of 0.01 mag, we estimate that the typical uncertainty

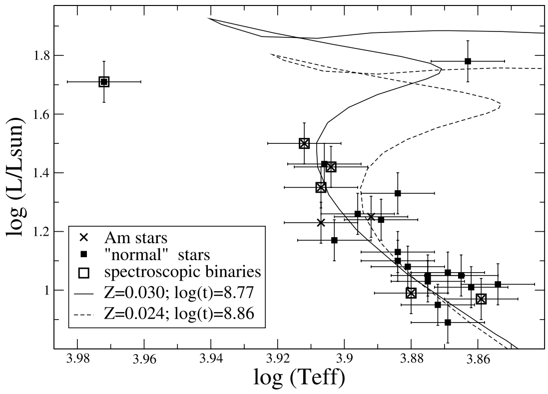

Fig. 6. Hertzsprung-Russell diagram of the Praesepe cluster. The crosses and filled squares show the position on the HR diagram for the Am and normal A- and F-type stars, respectively. The open squares indicate the spectroscopic binaries. We did not correct the luminosity of these stars due to the presence of a companion, but we assume it less than 0.1 dex. The error bar in luminosity is 0.07 dex. The dashed line shows an isochrone from Girardi et al. (2002) for the age and metallicity given in the literature ($\log t$ = 8.85 dex; Z = 0.024 dex). The solid line shows the isochrone corresponding to our best fit ($\log t$ = 8.77 dex; Z = 0.030 dex).

in $M_{\rm bol}$ is about 0.15 mag, corresponding to an uncertainty in $\log L/L_\odot$ of about 0.06 dex.

In the diagram we divided our sample into Am stars (crosses) and normal A- and F-type stars (full squares). We denoted also (open squares) the spectroscopic binary stars. We did not correct the luminosities of the spectroscopic binaries, as the only information we have about the secondaries is that their contribution to the analysed spectra is not detected (Paper I). This suggests that their flux contribution is below about 5%.

The two stars located at the top left and top right of the HR diagram are HD 73666 and HD 73575, respectively. Both have already been analysed in detail in Paper I. HD 73666 is clearly a Blue Straggler, while HD 73575 should be just at the TAMS, if the stars are cluster members (membership given by HIPPARCOS and confirmed in Paper I). HD 73575 deserves a further comment. It is the most evolved star of the cluster and the position close to the TAMS is consistent with this. This star also shows anomalous chemical composition compared with that of the other normal F-type stars. The position on the HR diagram and the peculiar chemical composition of HD 73575 suggest an unusual evolutionary history.

We adopted isochrones by Girardi et al. (2002) to determine age and metallicity of the cluster using the HR diagram. In Fig. 6 we plotted two isochrones: one correspoding to the age and metallicity of the cluster taken from WEBDA ($\log t$ = 8.85 dex; Z = 0.024 dex; dashed line) and the other corresponding to our best fit on the HR diagram ($\log t$ = 8.77 dex; Z = 0.030 dex; solid line).

An et al. (2007) determined the metallicity of the Praesepe cluster by fitting Yale Rotating Evolutionary Code (YREC, Sills et al. 2000) isochrones to the main sequence of the cluster, obtained from Johnson photometry. They derived a metallicity of [Fe/H] = 0.20 ± 0.04 corresponding to Z = 0.030 ± 0.003. This result is in agreement with the results of our fits of isochrones to our sample of stars around the turn-off point.

All the Am stars are on the main sequence. Only HD 73618 (the hottest main sequence star in Fig. 6) can be considered a Blue Straggler (Ahumada & Lapasset 2007), taking into account the age and metallicity given in the literature.

6.3. Abundances vs. $T_{\rm eff}$ and $\upsilon \sin i$

The abundances of the elements analysed for most of the stars are displayed against $T_{\rm eff}$ and $\upsilon \sin i$ in the left and right panels respectively from Figs. 7 to 9. We divided the sample of stars according to their spectral classification: A-type stars (open circles), Am stars (open squares) and F-type stars (open triangles). This division and visualisation will be retained in the following sections.

The plots show that the abundances of the F-type stars are less scattered than those obtained for the A-type stars, as expected.

For the normal A- and F-type stars we do not find any clear correlation between abundance and $T_{\rm eff}$ or abundance and $\upsilon \sin i$. This result confirms the prediction of Charbonneau & Michaud (1991).

For the Am stars, none of the plotted elements, except Y, shows any trend between abundance and $T_{\rm eff}$. Richer et al. (2000) predict mild correlations between abundances of some elements (e.g. Ni) and $T_{\rm eff}$, but probably our temperature range is not large enough to show such correlations.

In Am stars, we find a strong correlation between abundance and $\upsilon \sin i$ for all peculiar elements, except for scandium and titanium. As described in detail in Paper I, Am stars of the Praesepe cluster show peculiarities mainly for C, O, Ca and Sc (underabundant) and Ti, Cr, Fe, Ni, Y and Ba (overabundant). C, O and Ca show an increasing abundance with $\upsilon \sin i$. The Fe-peak elements, Y, and Ba show a decreasing abundance with $\upsilon \sin i$. Na, Mg, Si and S are not peculiar in Am stars and they do not show any correlation with $\upsilon \sin i$. As a general behavior, the peculiarities decrease with $\upsilon \sin i$, becoming closer and closer to the abundances typical of the normal A- and F-type stars of the cluster. Scandium and titanium are exceptions: Ti does not show any clear trend with $\upsilon \sin i$, and Sc shows a trend opposite to that of C, O and Ca, while we would have expected a similar behavior.

Burkhart (1979) derived the abundance anomaly, from the Strömgren m1 index, and $\upsilon \sin i$ values for a sample of well-known Am stars. She suggested a jump in the abundance anomaly for stars with $\upsilon \sin i > 55$ km s^{-1}; our results confirm this claim.

Models by Charbonneau & Michaud (1991) do not predict any strong correlation between element abundances and rotational velocity: "For FmAm stars, it was shown quantitatively that despite the potentially inhibiting effects of meridional circulation on chemical separation, no dependence of abundance anomalies on $\upsilon \sin i$ is expected, for most elements, in the rotational velocity interval characteristic of FmAm stars". The correlations here obtained between abundance and $\upsilon \sin i$, for the Am stars, are in clear disagreement with the predictions of Charbonneau & Michaud (1991).

Richer et al. (2000) found that element abundances in model Am stars are dependent only on the depth of the zone mixed by turbulence, thus showing that the abundance anomalies in Am stars depend mainly on the turbulence model.

More recently, Talon et al. (2006) tested rotational mixing models with both the Geneva-Toulouse and Montreal codes. They showed how the predicted surface abundances of FmAm stars should vary as a function of rotational velocity of the star. Our findings support their predictions.

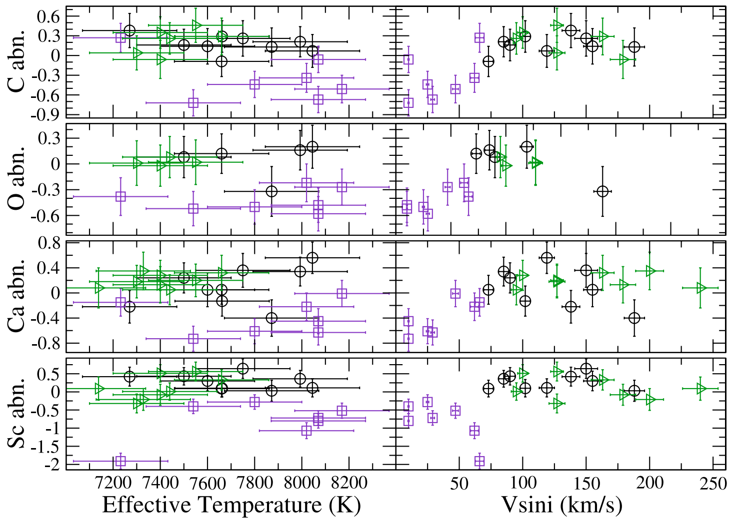

Fig. 7. Abundances relative to the Sun (Asplund et al. 2005) of C, O, Ca and Sc as a function of $T_{\rm eff}$ and $\upsilon \sin i$ for normal A-type stars (circle), Am stars (square) and normal F-type stars (triangle). A correlation between abundances of C, O, Ca and $\upsilon \sin i$ is found for Am stars; an anticorrelation between Sc abundance and $\upsilon \sin i$ is found for Am stars.

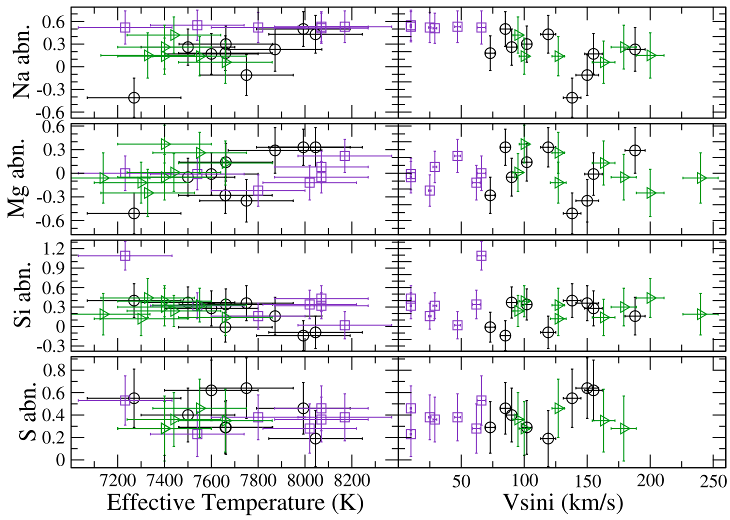

Fig. 8. Same as in Fig. 7 but for Na, Mg, Si and S. No correlation is found.

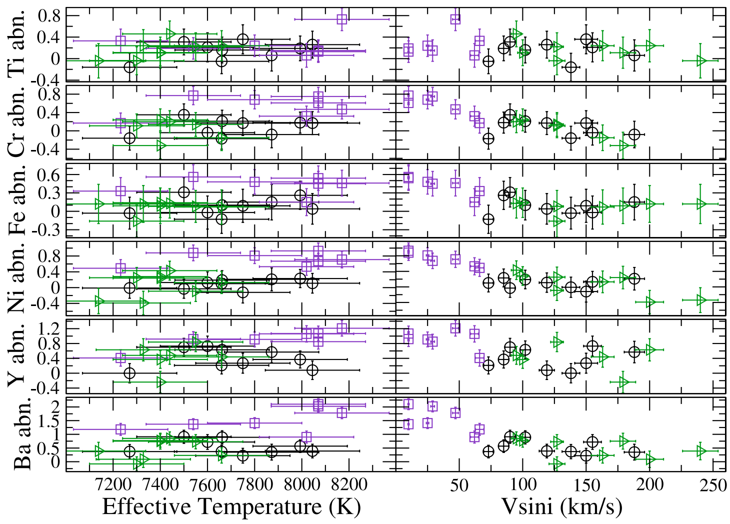

Fig. 9. Same as in Fig. 7 but for Ti, Cr, Fe, Ni, Y and Ba. No correlation is found for Ti. An anticorrelation between Cr, Fe, Ni, Y and Ba abundance and $\upsilon \sin i$ is found for Am stars.

6.4. Abundances vs. $M/M_\odot$ and fractional age

For the stars in our sample we calculated $M/M_\odot$, fractional age (τ) and their uncertainties according to Landstreet et al. (2007) and listed them in Table 4.

We took the abundances of three representative elements (Mg, Ca and Fe) showing, for the Am stars, the three different properties discussed in Sect. 6.3. We plot the abundances of these elements as functions of $M/M_\odot$ and display the results in Fig. 10.

No clear correlation is visible for any of the three plotted elements, for the normal or the Am stars.

Richer et al. (2000) suggest that the abundance anomalies typical of Am stars depend very little on the mass and therefore

Table 4. $\log L/L_\odot$, $\log T_{\rm eff}$, $M/M_\odot$ and fractional age (τ) with associated error bars for the analysed stars of the Praesepe cluster.

HD	$\log L/L_\odot$ dex	Sp.type	$\log T_{\rm eff}$	$M/M_\odot$	$\sigma_{M/M_\odot}$	τ	σ_τ
72757	1.06	F0	3.869	1.71	0.09	0.43	0.06
72846	1.43	A5V	3.906	2.09	0.15	0.76	0.11
73045	0.99	Am	3.880	1.67	0.08	0.40	0.06
73175	1.13	F0V	3.884	1.78	0.09	0.48	0.07
73345	1.17	A7V	3.903	1.84	0.13	0.53	0.08
73430	1.10	A7V	3.884	1.76	0.09	0.47	0.07
73450	1.01	A9V	3.862	1.66	0.08	0.39	0.06
73574	1.33	A8V	3.884	1.96	0.10	0.64	0.10
73575	1.78	F0III	3.863	2.33	0.12	1.02	0.15
73618	1.50	Am	3.912	2.16	0.22	0.84	0.13
73666	1.71	A0	3.972	2.46	0.12		
73709	1.35	Am	3.907	2.00	0.14	0.68	0.10
73711	1.42	Am	3.904	2.08	0.10	0.75	0.11
73730	1.23	Am	3.907	1.89	0.13	0.58	0.09
73746	0.95	F0V	3.872	1.64	0.08	0.38	0.06
73798	1.05	F0V	3.865	1.70	0.12	0.42	0.06
73818	0.97	Am	3.859	1.63	0.08	0.37	0.06
73993	1.02	F2V	3.854	1.66	0.12	0.39	0.06
74028	1.24	A7V	3.889	1.88	0.09	0.57	0.09
74050	1.26	A6V	3.896	1.91	0.10	0.60	0.09
74135	0.89	F0	3.869	1.60	0.08	0.35	0.05
74587	1.03	A5	3.875	1.71	0.09	0.43	0.06
74589	1.05	F0	3.875	1.70	0.09	0.42	0.06
74656	1.25	Am	3.892	1.89	0.09	0.58	0.09
74718	1.08	A5	3.881	1.74	0.09	0.45	0.07

No fractional age is given for HD 73666 since it is a Blue Straggler.

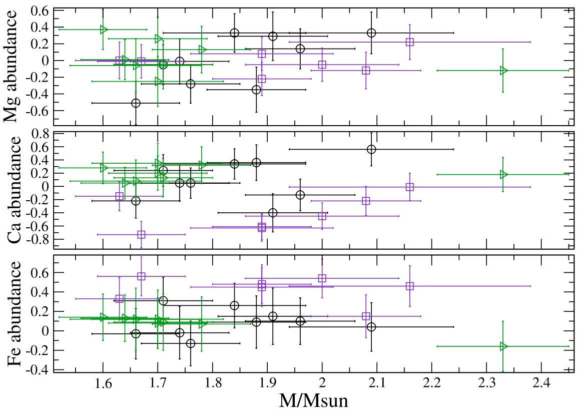

Fig. 10. Abundances relative to the Sun (Asplund et al. 2005) of Mg, Ca and Fe as a function of the $M/M\odot$. No correlations are found.

fractional age of the star. This is consistent with the results of this study.

6.5. Searching for correlations between abundances

In a sample of seventeen Am stars, Adelman & Unsuree (2007) found significant correlations between the abundances of twelve elements.

The abundances of the elements analysed in most of the stars of our sample are displayed against the Fe abundance in Figs. 11 and 12.

We do not find any clear correlation between the abundances of any element and Fe for the A- and F-type stars due to the tiny spread in Fe abundance.

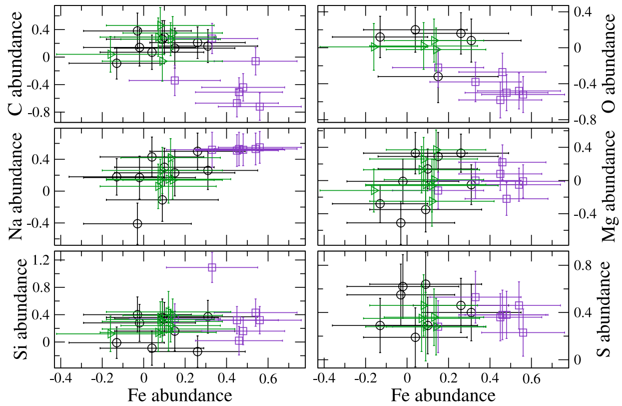

Fig. 11. Abundances relative to the Sun (Asplund et al. 2005) of C, O, Na, Mg, S and Si as a function of the Fe abundance.

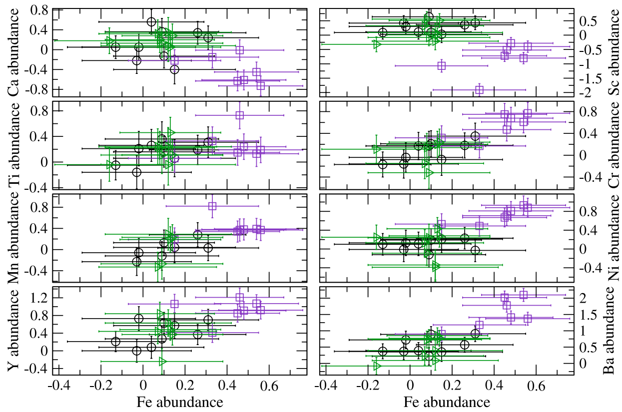

Fig. 12. Same as in Fig. 11 but for Ca, Sc, Ti, Cr, Mn, Ni, Y and Ba.

In contrast, the Am stars show correlations for all the elements in which a correlation was already found with $\upsilon \sin i$. The Fe abundance is an indicator of Am peculiarities. As we found a correlation between $\upsilon \sin i$ and Am peculiarities, it is not surprising to obtain similar correlations with the Fe abundance.

The correlations found for C and O are in agreement with those found by Savanov (1995) in a sample of seventeen well-known Am stars analysed by different authors. They looked for a correlation between the C abundance and $\upsilon \sin i$, but without any positive result.

From our results it is clear that these correlations are related to those found with $\upsilon \sin i$ in Sect. 6.3.

7. Conclusions

We obtained high resolution, high SNR spectra for seventeen F- and A-type stars of the Praesepe open cluster, with the SOPHIE spectrograph at OHP. One of these stars (HD 74656) was classified as Am star.

We calculated the fundamental parameters and performed a detailed abundance analysis for all the stars of the sample, confirming the previous classification, as chemically peculiar, of the Am star HD 74656.

The stars we observed were selected using a standard procedure that will be adopted for future analysis of other open clusters. All the selected stars of the sample shown in Table 1 are confirmed members of the cluster and among them there are no known binaries (except HD 73666). This shows the quality of the selection procedure, since membership and non-binarity were required for the selection.

To be able to discuss general properties of the cluster we added to our sample of stars those considered in Paper I. Of the stars analysed in Paper I we did not include HD 73666 (Blue Straggler), HD 72942 (not a confirmed member) and HD 73174 (important uncertainties in $T_{\rm eff}$). The sample of stars analysed in Paper I and in this work contains all the known cluster members with a spectral type between F2 and A1 and not SB2. This removes any bias that could have been introduced by an inappropriate target selection.

We divided our final sample of stars according to their spectral classification, taken from WEBDA, and derived the mean abundance pattern for three groups of stars: A-, F-type and Am. The A- and F-type stars show a similar abundance pattern, close to solar, while the Am stars show the typical Am peculiarities described in Paper I. The abundance scatter of the Am stars is higher than for the normal stars and, between A- and F-type stars, the F-stars show the smaller scatter, as expected.

We derived the metallicity of the cluster from the F-type stars of our sample, omitting HD 73575 which is already on the TAMS. The resultant metallicity is $Z = 0.015 \pm 0.002$ dex. To be able to compare our metallicity ([Fe/H] = 0.11 ± 0.03) with that used by other authors we derived Z with the approximation given by Eq. (2) that corresponds to $Z = 0.024 \pm 0.002$ dex, assuming $Z_{\odot} = 0.019$ dex. This result is in agreement with previous metallicity determinations from abundance analysis of G-type stars by An et al. (2007).

For each star of the sample we derived photometrically $\log L/L_{\odot}$ and, adopting the spectroscopic temperatures derived for the abundance analysis, built the Hertzsprung-Russell (HR) diagram of the cluster around the turn-off point. We fit isochrones by Girardi et al. (2002) to our HR diagram to derive age and metallicity ($\log t = 8.77 \pm 0.1$ dex; $Z = 0.030 \pm 0.007$ dex). This result is in agreement with that obtained by An et al. (2007) fitting YREC isochrones to a photometrically-derived main sequence of the cluster. We confirm the discrepancy in metallicity found by An et al. (2007). Within the errors, our age determination agrees with earlier determinations in the literature ($\log t = 8.85 \pm 0.15$, González-García et al. 2006).

We plotted the abundances of the elements analysed in most of the stars of our sample as a function of $T_{\rm eff}$ and $\upsilon \sin i$. We did not find any clear abundance trend with respect to $T_{\rm eff}$ and $\upsilon \sin i$ for the A- and F-type stars. However, we found several trends between abundances and $\upsilon \sin i$ for Am stars. Correlations are present for the elements that characterise the Am peculiarities. Only Sc and Ti do not show this trend. With increasing $\upsilon \sin i$ the peculiarities tend to weaken, and the abundances approach the mean of the other A- and F-type stars. This is the first real observational evidence of a direct connection between abundance anomalies or diffusion processes and rotational velocity in Am stars.

The Praesepe cluster could be peculiar in this sense because it contains a high number of Am stars. This fact, combined with the advanced age of the cluster, makes it possible to have many Am stars close to the turn-off point. Since diffusion is a slow process, in this cluster, more than in others, the peculiarities are evident and well-characterised by correlations between abundance anomalies and rotational velocity. Similar relationhips may be less obvious in younger clusters. It will clearly be of interest to check this possibility.

The trends obtained in this work are in disagreement with those predicted by Charbonneau & Michaud (1991), as according to their models meridional circulation does not not affect abundance peculiarities. Recently Richer et al. (2000) and later Talon et al. (2006) calculated diffusion models with a more accurate treatment of the rotational mixing. Their predicted abundances for stars with various rotational velocities are qualitatively in agreement with observed properties of our sample of Am stars. Detailed models, with a full treatment of diffusion and rotational mixing, calculated individually for each Am star of our sample, would be necessary for a more substantial comparison between models and observed abundances.

We derived $M/M_{\odot}$ and fractional age (τ) for each of the stars of our sample and plotted the abundances as a function of $M/M_{\odot}$. No correlation was found for any of the three spectral groups considered here, as predicted by Richer et al. (2000).

We searched for correlations between abundances of the elements analysed in most of the stars and the Fe abundance. For normal A- and F-type stars we did not find any correlation, while for Am stars strong correlations are obtained for all the peculiar elements. The behavior of the abundances of the elements which are peculiar in Am stars, as a function of the Fe abundance, is the same as that found for $\upsilon \sin i$. We conclude that there is a strong connection between the correlations among the abundances, with the correlations of abundances with $\upsilon \sin i$.

Acknowledgements. We thank Tanya Ryabchikova for important help and advice given during this investigation. LF and OK have received support from the Austrian Science Foundation (FWF project P17890-N2). J.D.L. and G.A.W. acknowledge support from the Natural Science and Engineering Council of Canada (NSERC). G.A.W. acknowledges support from the Department of National Defence Academic Research Programme (DND-ARP). This paper is based on observations obtained using the SOPHIE spectrograph at the Observatoire de Haute Provence (France). We acknowledge also the OPTICON programme (Ref. number: 2007/011) for the financial support given to the observing run.

References

Abt, H. A. 1970, ApJS, 19, 387
Abt, H. A., & Willmarth, D. W. 1999, ApJ, 521, 682
Adelman, S. J., & Unsuree, N. 2007, Balt. Astron., 16, 183
Ahumada, J. A., & Lapasset, E. 2007, A&A, 463, 789
An, D., Terndrup, D. M., Pinsonneault, M. H., et al. 2007, ApJ, 655, 233
Asplund, M., Grevesse, N., & Sauval, A. J. 2005, in Cosmic Abundances as Records of Stellar Evolution and Nucleosynthesis, ed. T. G. Barnes III, & F. N. Bash, ASP Conf. Ser., 336, 25
Bagnulo, S., Landstreet, J. D., Mason, E., et al. 2006, A&A, 450, 777
Baumgardt, H., Dettbarn, C., & Wielen, R. 2000, A&AS, 146, 251
Balona, L. A. 1994, MNRAS, 268, 119
Burkhart, C. 1979, A&A, 74, 38
Burkhart, C., & Coupry, M. F. 1998, A&A, 338, 1073
Canuto, V. M., & Mazzitelli, I. 1992, ApJ, 389, 724
Charbonneau, P., & Michaud, G. 1991, ApJ, 370, 693
Chen, L., Hou, J. L., & Wang, J. J. 2003, AJ, 125, 1397
Clampitt, L., & Burstein, D. 1997, AJ, 114, 699
Conti, P. S., Hensberge, G., van den Heuvel, E. P. J., & Stickland, D. J. 1974, A&A, 34, 393
Dias, W. S., Assafin, M., Flório, V., Alessi, B. S., & Líbero, V. 2006, A&A, 446, 949
Fossati, L., Bagnulo, S., Monier, R., et al. 2007, A&A, 476, 911
Girardi, L., Bertelli, G., Bressan, A., et al. 2002, A&A, 391, 195
Glebocki, R., & Stawikowski, A. 2000, Acta Astron., 50, 509
González-Garcá, B. M., Zapatero Osorio, M. R., Béjar, V. J. S., et al. 2006, A&A, 460, 799
Hartkopf, W. I., & McAlister, H. A. 1984, PASP, 96, 105
Hauck, B., & Mermilliod, M. 1998, A&AS, 129, 431
Hill, G. M., & Landstreet, J. D. 1993, A&A, 276, 142
Kharchenko, N. V., Piskunov, A. E., Röser, S., Schilbach, E., & Scholz, R.-D. 2004, AJ, 325, 740

Kochukhov, O. 2006, in Magnetic Stars, ed. I. I. Romanyuk, & D. O. Kudryavtsev, in press
Kunzli, M., North, P., Kurucz, R. L., & Nicolet, B. 1997, A&AS, 122, 51
Kupka, F., Piskunov, N. E., Ryabchikova, T. A., Stempels, H. C., & Weiss, W. W. 1999, A&AS, 138, 119
Landstreet, J. D., Bagnulo, S., Andretta, V., et al. 2007, A&A, 470, 685
Landstreet, J. D., Silaj, J., Andretta, V., et al. 2008, A&A, 481, 465
van Leeuwen, F. 2007, Hipparcos, the New Reduction of the Raw Data, Institute of Astronomy, Cambridge University, Cambridge, UK Series: Astrophysics and Space Science Library (Dordrecht: Springer), 350, 20
Madsen, S., Dravins, D., & Lindegren, L. 2002, A&A, 381, 446
Mason, B. D., Hartkopf, W. I., McAlister, H. A., & Sowell, J. R. 1993, AJ, 106, 637
McAlister, H. A., Hartkopf, W. I., Hutter, D. J., & Franz, O. G. 1987, AJ, 93, 688
Mermilliod, J.-C., & Paunzen, E. 2003, A&A, 410, 511
Napiwotzki, R., Schoenberner, D., & Wenske, V. 1993, A&A, 268, 653
Pace, G., Recio-Blanco, A., Piotto, G., & Momany, Y. 2006, A&A, 452, 493
Piskunov, N. E., Kupka, F., Ryabchikova, T. A., Weiss, W. W., & Jeffery, C. S. 1995, A&AS, 112, 525
Pourbaix, D., Tokovinin, A. A., Batten, A. H., et al. 2004, A&A, 424, 727
Renson, P., Gerbaldi, M., & Catalano, F. A. 1991, A&AS, 89, 429
Richer, J., Michaud, G., & Turcotte, S. 2000, ApJ, 529,338
Robichon, N., Arenou, F., Mermilliod, J.-C., & Turon, C. 1999, A&A, 345, 471
Rodríguez, E., López-González, M. J., & López de Coca, P. 2000, A&AS, 144, 469
Royer, F., Grenier, S., Baylac, M.-O., Gómez, A. E., & Zorec, J. 2002, A&A, 393, 897
Ryabchikova, T. A., Piskunov, N. E., Stempels, H. C., Kupka, F., & Weiss, W. W. 1999, Phys. Scr., T83, 162
Ryabchikova, T. A., Kochukhov, O., & Bagnulo, S. 2008, A&A, 480, 811
Samus, N. N., & Durlevich, O. V. 2004, VizieR Online Data Catalog, 2250
Savanov, I. S. 1995, Astron. Lett., 21, 684
Shulyak, D., Tsymbal, V., Ryabchikova, T., Stütz, Ch., & Weiss, W. W. 2004, A&A, 428, 993
Sills, A., Pinsonneault, M. H., & Terndrup, D. M. 2000, ApJ, 534, 335
Talon, S., Richard, O., & Michaud, G. 2006, ApJ, 645, 634
Tassoul, J.-L., & Tassoul, M. 1982, ApJS, 49, 317

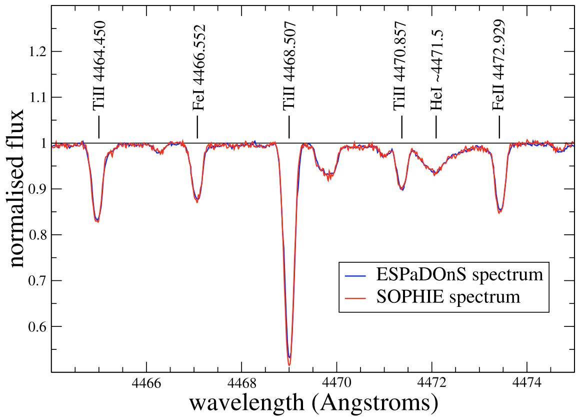

Fig. 13. Comparison between the spectra of HD 73666 obtained with the ESPaDOnS spectropolarimeter (blue line) and the SOPHIE spectrograph (red line) in the region of the He I multiplet at ~4471.5 Å. No difference is visible between the two spectra, apart the one due to the different spectral resolution of the two instruments.

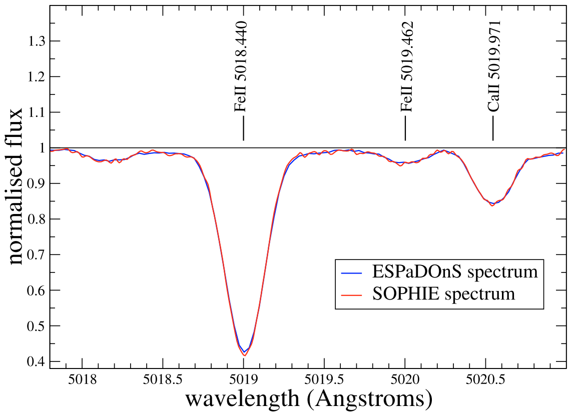

Fig. 14. Same as for Fig. 13, but in the region of the strong Fe II line at 5018.440 Å.

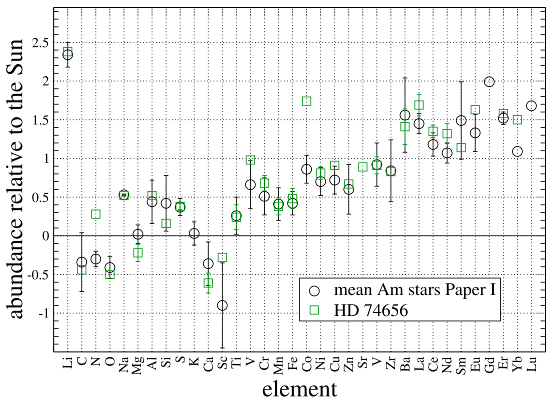

Fig. 15. Comparison between the mean abundance of the Am stars analysed in Paper I and the Am star HD 74656. This plot confirms the Am classification of this star.

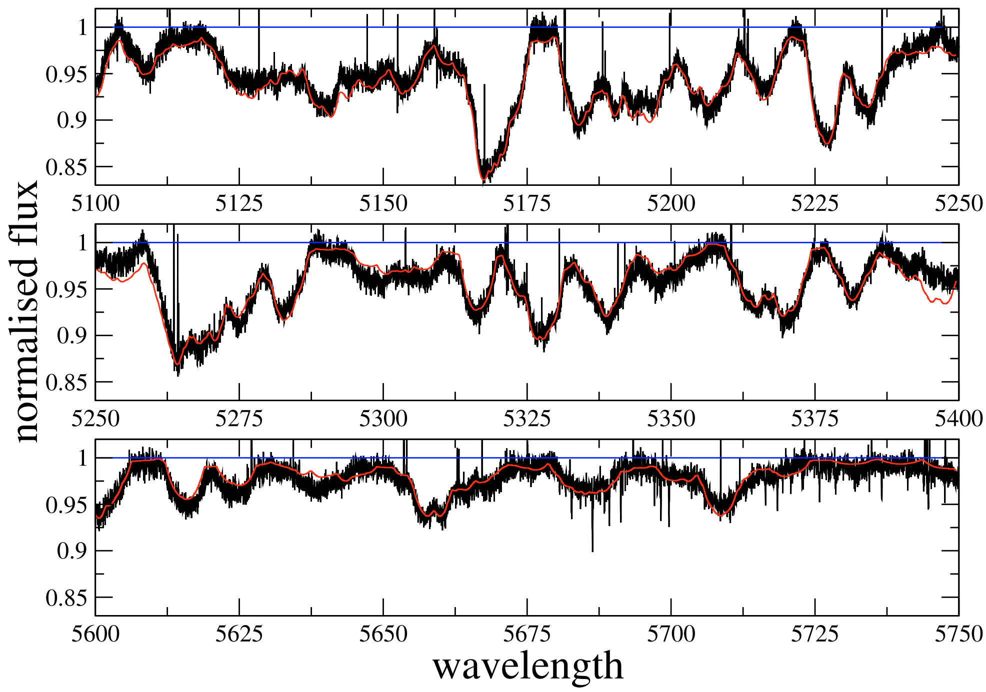

Fig. 16. Portion of the spectrum of HD 72757 ($\upsilon \sin i$ = 179 km s^{-1}) and the synthetic spectrum after the complete abundance analysis in black and red respectively.

Appendix C

Curriculum Vitae and publication list

Luca Fossati

Curriculum Vitae et Studiorum

Personal details

Born in Mortara (Italy), 15 November 1979

Married with no children

Contact addresses

Institut fuer Astronomie der Universitaet Wien
Tuerkenschanzstrasse 17, 1180, Vienna, Austria
Tel. 00431427751873

Porzellangasse 11/73, 1090, Vienna, Austria
Tel. 00436763386700

E-mail: fossati@astro.univie.ac.at

Educational details

Present: PhD student at Universitaet Wien, Instituet fuer Astronomie. Title of the thesis: "A detailed abundance analysis of early-type stars in open clusters: constraints to diffusion models". Supervisors: Prof. Werner Weiss, Dr. Stefano Bagnulo

December 2004: Graduation in Physics with specialisation in Astrophysics, with 110/110, Università degli studi di Pavia. Title of the thesis: "Studio di variabili Cefeidi in IC 1613" (Study of Cepheids variables in IC 1613). Supervisors: Prof. Bruno Bertotti, Dr Luciano Mantegazza

October 1998: Admission in the Borromeo College of Pavia

June 1998: Graduation at Liceo Scientifico B. Cairoli of Vigevano with 60/60

Languages

Italian: mother tongue. Fluent in English and German. Good knowledge of Spanish.

Employment History

January 2006 – present: student researcher at Universitaet Wien with a grant of the Austrian Science Foundation (FWF)

April 2005 – August 2005: short term studentship at ESO-Chile

Awards

February 1995: De Magistris scholarship for scientific activities

Membership of professional bodies

Co-Editor of Ap Newsletter (www.astro.univie.ac.at/apn)

Member of the Vienna Atomic Line Database (VALD) team (ams.astro.univie.ac.at/~vald/)

Teaching experience

Winter semester 2008: Teaching assistant for the course “Astronomische Spektroscopie” at Universitaet Wien

May 1996 – present: Yearly lecturer at classes of the last year at Liceo Scientifico B. Cairoli, on invitation of Prof. Gianna Pagani

May 1996 – present: Invited speaker at the yearly *Science Week* presented at Liceo Scientifico B. Cairoli

September 2003- March 2005: Guest speaker and guide at the Brera Observatory, Merate for visiting groups

Scientific interests

High resolution spectroscopy and chemical abundance analysis of stellar atmospheres

Spectropolarimetry and imaging polarimetry

Photometry of crowded fields

Technical expertise

Good knowledge of C and shell programming language

Good knowledge of the tools of the Virtual Observatory (VO)

Conversant with a broad range of software packages for data reduction, plotting, typesetting, etc... such as IRAF, xmgrace, gnuplot, latex, etc...

Participations in congresses, workshops, meetings

“Spectroscopy and Spectropolarimetry of A and B-type Stars: Research Tools, Techniques and Goals” Armagh, Northern Ireland, 18 – 22 February 2008,
Contributed talk: *Stellar parameter determination and abundance analysis*
Contributed talk: *Archives and Virtual Observatory*
Contributed talk: *Metallic line stars*

“CP#AP Workshop” Vienna, Austria, 10 – 14 September 2007,
Contributed talk: *Chemical evolution of A- and B-type stars in open cluster: observed abundances vs. diffusion models, Am stars in the Praesepe cluster*

"Non-LTE line formation for trace elements in stellar atmospheres” Nice, France, 30 July – 4 August 2007

Seminars

Explaining the Praesepe blue straggler HD 73666, Armagh Observatory, Northern Ireland (9 October 2008)

Visits to other institutes

Armagh Observatory: four times in the last two years

Moscow Institute for Astronomy (INASAN): august 2006

ESO – Santiago: april – august 2005

Awarded telescope time

LASILLA / REM - *A and B-type stars in open clusters: links between rotational velocity, magnetic field and stellar evolution*. Observations performed with REM. Awarded 120 hrs. in service mode **(P.I.;** responsible for **target selection and OB preparation)**

ESO VLT 079.D-0178(A) - *Observing the chemical evolution of early-type stars in open clusters.* Observations performed with FLAMES. Awarded 14 hrs. in service mode (co-I; responsible for **target selection and OB preparation**)

NOT / FIES – *Chemical signatures of A-type stars in open clusters*. August 2007, 5 nights awarded in visitor mode for observations with FIES (co-I; responsible for **target selection**)

OHP / SOPHIE – *Chemical composition of A-type stars in the Praesepe cluster: a clue to t heir evolutionary* status. March 2007, 4 nights awarded in visitor mode for observations with SOPHIE (**P.I.;** responsible for **target selection and observer**)

List of publications

Publications in refereed journals

– Ryabchikova, T., **Fossati, L.**, Shulyak, D., 2009, Improved fundamental parameters and LTE abundances of the solar-type pulsator HD 49933, A&A, (submitted)

– Bagnulo S., Landolfi M., Landstreet J., Landi Degl'Innocenti E., **Fossati, L.**, Sterzik M. , 2009, *Optical polarimetry with retarder waveplate and beam splitter devices*, PASP, (submitted)

– **Fossati, L.**, Mochnacki, S., Landstreet, J., Weiss, W., 2009, *Explaining the blue straggler HD 73666*, A&A, (submitted)

– **Fossati, L.**, Ryabchikova T., Bagnulo S., Alecian E., Grunhut J., Kochukhov O., Wade G., 2009, *The chemical abundance analysis for normal early A- and late B-type main sequence stars* , A&A, (accepted)

– Kallinger, T., Gruberbauer, M., Guenther, D.B., **Fossati, L.**, Weiss W. W. 2009, *The nature of p-modes and granulation in HD 49933*, A&A, (in press), arXiv:0811.4686

– **Fossati, L.**, Kolenberg, K., Regen, P., Weiss, W., 2008, *Abundance analysis of seven delta Scuti Stars*, A&A, 485, 257

– **Fossati, L.**, Bagnulo, S., Landstreet, J., Wade, G., Kochukhov, O., Monier, R., Weiss, W., Gebran, M., 2008, *The effect of rotation on the abundances of the chemical elements of the A-type stars in the Praesepe cluster*, A&A, 483, 891

- Landstreet J.D., Silaj J., Andretta V., Bagnulo S., Berdyugina S., Donati J.-F., **Fossati L.**, Petit P., Silvester J., Wade G.A., 2008, *Searching for links between magnetic fields and stellar evolution III. Measurement of magnetic field in open cluster Ap stars with ESPaDOnS*, A&A, 481, 465

- **Fossati L.**, Bagnulo S., Monier R., Khan S.A., Kochukhov O., Landstreet J.D., Wade G., Weiss W. , 2007, *Late stages of the evolution of A-type stars in the main sequence: comparison between observed chemical abundances and diffusion models for 8 Am stars of the Praesepe cluster*, A&A, 476, 911

- Landstreet, J. D., Bagnulo, S., Andretta, V., **Fossati, L.**, Mason, E., Silaj, J., Wade, G. A., 2007, *Searching for links between magnetic fields and stellar evolution: II. The evolution of magnetic fields as revealed by observations of Ap stars in open clusters and associations*, A&A, 470, 685

- Antonello, E., **Fossati, L.**, Fugazza, D., Mantegazza, L., Gieren, W. 2005, *Variable stars in nearby galaxies. VII. P-L relation in the BVRI bands of Cepheids in IC 1613*, A&A, 445, 901

Other publications

- Heiter, U. , Barklem, P., **Fossati, L.**, Kildiyarova, R., Kochukhov, O., Kupka, F., Obbrugger, M., Piskunov, N., Plez, B., Ryabchikova, T., Stempels, H. C., Stutz, Ch., Weiss, W. W. 2008, *VALD – an atomic and molecular database for astrophysics*, Journal of Physics, Conference series ASOS9, 130, 012011

- Ryabchikova, T., Kildiyarova, R., Piskunov, N., Heiter, U., **Fossati, L.**, Weiss, W.W., 2008, *A comparative analysis of the laboratory and theoretical transition probabilities of the Fe-peak elements for a new release of VALD*, Journal of Physics, Conference series ASOS9, 130, 012017

- Bagnulo, S., Landstreet, J., Wade, G., **Fossati, L.**, 2008, *Measurements and modelling of magnetic fields of chemically peculiar stars*, in CP#Ap Workshop, eds. J. Ziznovsky, J. Zverko, E. Paunzen, M. Netopil, Contribut. Astr. Obs. Skalnat Pleso, 38, 201

- Landstreet, J., Bagnulo, S., Andretta, V., **Fossati, L.**, Mason, E., Silaj, J., Wade, G., 2008, *Evolution of global magnetic fields in main sequence A and B stars*, in CP#Ap Workshop, eds. J. Ziznovsky, J. Zverko, E. Paunzen, M. Netopil, Contribut. Astr. Obs. Skalnat Pleso, 38, 391

- **Fossati, L.**, Bagnulo, S., Monier, R., Khan, S.A., Kochukhov, O., Landstreet, J., Wade, G., Weiss, W., 2008, *Chemical evolution of A- and B-type stars in open clusters: observed abundances vs. diffusion models. Am stars in the Praesepe cluster*, in CP#Ap Workshop, eds. J. Ziznovsky, J. Zverko, E. Paunzen, M. Netopil, Contribut. Astr. Obs. Skalnat Pleso, 38, 123

- Stuetz, Ch., Nesvacil, N., **Fossati, L.**, Shulyak, D., 2008, *On the quality of stellar atmosphere parameters and abundances derived from spectroscopy*, in CP#Ap Workshop, eds. J. Ziznovsky, J. Zverko, E. Paunzen, M. Netopil, Contribut. Astr. Obs. Skalnat Pleso, 38, 457

- **Fossati L.**, Bagnulo S., Mason E., Landi Degl'Innocenti E., 2006, *Standard stars for linear polarization observed with FORS1*, ASP Conference Series of "The Future of Photometric, Spectrophotometric and Polarimetric Standardization", Blankenberge (Belgium), 364, 503

- Landi Degl'Innocenti E., Bagnulo S., **Fossati L.**, 2006, *Polarimetric Standardization*, ASP Conference Series of "The Future of Photometric, Spectrophotometric, and Polarimetric Standardization", Blankenberge (Belgium), 364, 495

- Antonello, E., **Fossati, L.**, Fugazza, D., Mantegazza, L., Gieren, W. 2005, *The P-L relation in the BVRI bands for Cepheids in IC 1613*, Memorie Della Societa' Astronomica Italiana, 77, 259